

LOCKHEED MARTIN ENERGY RESEARCH LIBRARIES



3 4456 0515328 6

ORNL-5258

## Results from Irradiation of Vented GCFR Fuel Rods in the GB-9 and GB-10 Capsule Experiments

A. W. Longest  
J. A. Conlin

OAK RIDGE NATIONAL LABORATORY

CENTRAL RESEARCH LIBRARY

CIRCULATION SECTION

4500N ROOM 175

**LIBRARY LOAN COPY**

DO NOT TRANSFER TO ANOTHER PERSON

If you wish someone else to see this  
report, send in name with report and  
the library will arrange a loan.

UCN 7969 13 9-77

**OAK RIDGE NATIONAL LABORATORY**  
OPERATED BY UNION CARBIDE CORPORATION · FOR THE DEPARTMENT OF ENERGY

Printed in the United States of America. Available from  
National Technical Information Service  
U.S. Department of Commerce  
5285 Port Royal Road, Springfield, Virginia 22161  
Price: Printed Copy \$9.25; Microfiche \$3.00

This report was prepared as an account of work sponsored by an agency of the United States Government. Neither the United States Government nor any agency thereof, nor any of their employees, contractors, subcontractors, or their employees, makes any warranty, express or implied, nor assumes any legal liability or responsibility for any third party's use or the results of such use of any information, apparatus, product or process disclosed in this report, nor represents that its use by such third party would not infringe privately owned rights.

ORNL-5258  
Dist. Category UC-77

Contract No. W-7405-eng-26

ENGINEERING TECHNOLOGY DIVISION

RESULTS FROM IRRADIATION OF VENTED GCFR FUEL RODS  
IN THE GB-9 AND GB-10 CAPSULE EXPERIMENTS

A. W. Longest  
J. A. Conlin

Date Published: September 1978

Prepared by the  
OAK RIDGE NATIONAL LABORATORY  
Oak Ridge, Tennessee 37830  
operated by  
UNION CARBIDE CORPORATION  
for the  
DEPARTMENT OF ENERGY

LOCKHEED MARTIN ENERGY RESEARCH LIBRARIES



3 4456 0515328 6



## CONTENTS

	<u>Page</u>
ACKNOWLEDGMENTS . . . . .	vii
ABSTRACT . . . . .	1
1. INTRODUCTION . . . . .	3
2. IRRADIATION FACILITY DESCRIPTION . . . . .	8
3. GB-9 EXPERIMENT DESCRIPTION . . . . .	13
3.1 Fuel Rod . . . . .	13
3.2 Capsule . . . . .	13
3.3 Gas Systems . . . . .	17
4. GB-9 DESIGN ANALYSES . . . . .	21
4.1 Predicted Power Distributions . . . . .	21
4.2 Predicted Temperature Distributions . . . . .	23
4.3 Thermocouple-to-Cladding-Hot-Side Temperature Corrections . . . . .	24
4.4 Predicted Fission-Gas Release Fractions . . . . .	31
5. GB-9 IRRADIATION CONDITIONS AND GENERAL OPERATING PROCEDURE . . . . .	34
6. RESULTS FROM IRRADIATION TESTING OF CAPSULE GB-9 . . . . .	37
6.1 Description of Initial Startup . . . . .	37
6.2 Effluent Sweep Line Activity . . . . .	39
6.3 Steady-State Fission-Gas Release vs Irradiation Time . . . . .	47
6.4 Fission-Gas Release During Slow Pressure Cycling . . . . .	56
6.5 Correlation of Effluent Sweep Line Activity Data and Sweep-Gas Sample Data . . . . .	60
6.6 Fission-Gas Release vs Charcoal Trap Temperature . . . . .	62
6.7 Fission-Gas Release vs Fuel-Rod Power and Temperature . . . . .	66

	<u>Page</u>
6.8 Fission-Product Decay Heating in Charcoal Trap . . . . .	69
6.9 Iodine Deposition in Charcoal Trap . . . . .	72
6.10 Fission-Gas Release vs Sweep Pressure . . . . .	72
6.11 Neutron Radiography . . . . .	72
7. GB-9 POSTIRRADIATION DISASSEMBLY AND EXAMINATION . . . . .	74
8. GB-10 EXPERIMENT DESCRIPTION . . . . .	81
8.1 Fuel Rod . . . . .	81
8.2 Capsule . . . . .	83
8.3 Gas Systems . . . . .	85
9. GB-10 DESIGN ANALYSES . . . . .	97
9.1 Predicted Power Distributions . . . . .	97
9.2 Predicted Temperature Distributions . . . . .	100
9.3 Comparison of GB-9 and GB-10 Predicted Power Levels . . . . .	106
9.4 Thermocouple-to-Cladding-Hot-Side Temperature Corrections . . . . .	106
9.5 Predicted Fission-Gas Release Fractions . . . . .	109
10. GB-10 IRRADIATION CONDITIONS AND GENERAL OPERATING PROCEDURE . . . . .	114
11. RESULTS FROM IRRADIATION TESTING OF CAPSULE GB-10 . . . . .	119
11.1 Description of Initial Startup . . . . .	122
11.2 Thermal Operating History . . . . .	124
11.3 Fuel-Rod Internal Gas-Flow Conductance vs Irradiation Time . . . . .	129
11.3.1 Flow Conductance of Sweep Lines and Charcoal Trap . . . . .	130
11.3.2 Partial Plugging of BB Line . . . . .	131
11.3.3 Flow Conductance of Fuel and Blanket Regions . . . . .	134

	<u>Page</u>
11.4 Steady-State Fission-Gas Release vs Irradiation Time and Operating Pressure . . . . .	143
11.5 Stable Noble Gas Release Measurements . . . . .	154
11.6 Fission-Gas Release Behavior During Startup and Shutdown . . . . .	156
11.7 Tritium-Monitoring Experiments . . . . .	157
11.8 Fission-Product Decay Heating in Charcoal Trap . . . . .	159
11.9 Iodine-Deposition Measurements . . . . .	160
11.10 Deposition of Long-Lived Activity in Effluent Sweep System . . . . .	167
11.11 Neutron Radiography . . . . .	169
12. GB-10 POSTIRRADIATION DISASSEMBLY AND PRELIMINARY EXAMINATION . . . . .	174
13. DISCUSSION OF UNCERTAINTIES IN GB-9 AND GB-10 DATA . . . . .	176
13.1 Measured Quantities . . . . .	176
13.1.1 Temperatures . . . . .	176
13.1.2 Pressures . . . . .	177
13.1.3 Flow Rates . . . . .	177
13.1.4 Fission-Gas Release Rates . . . . .	177
13.2 Calculated Quantities . . . . .	181
13.2.1 Fuel-Rod Power Levels and Cladding Temperatures . . . . .	181
13.2.2 Fuel Burnup . . . . .	182
13.2.3 Fission-Gas Birth Rates . . . . .	183
13.2.4 Fission-Gas Release-Rate-to-Birth-Rate Ratios . . . . .	186
13.3 Abnormal Occurrences . . . . .	187

	<u>Page</u>
14. STORAGE OF GB-9 AND GB-10 RECORDS . . . . .	189
15. CONCLUSIONS . . . . .	190
REFERENCES . . . . .	192
APPENDIX A. SUMMARY OF DATA FOR AS-BUILT FUEL ROD IN ORR IRRADIATION CAPSULE GB-10 . . . . .	195
APPENDIX B. EVALUATION OF GB-10 THERMAL OPERATING DATA . . . . .	199

## ACKNOWLEDGMENTS

The GB-9 and GB-10 experiments required considerable effort from many persons at Oak Ridge National Laboratory, General Atomic Company, and Argonne National Laboratory, and it would be difficult to properly acknowledge everyone who made an important contribution to the success of these experiments. The authors wish to thank all those who participated in the planning, design, fabrication, operation, analyses, report preparations, or postirradiation examination studies associated with these experiments. In particular, the authors wish to acknowledge the efforts of the following individuals:

Oak Ridge National Laboratory

E. Allen, R. A. Bradley, E. D. Clemmer, J. H. Coobs, D. A. Costanzo, C. W. Cunningham, J. W. Cunningham, V. A. Emert, J. F. Emery, W. K. R. Finnell, R. B. Fitts, R. M. Flanders, Uri Gat, C. R. Hyman, P. R. Kasten, H. T. Kerr, E. M. King, E. L. Long, Jr., H. J. Metz, M. E. Pruitt, J. B. Ruble, J. D. Sease, R. L. Senn, L. J. Shersky, K. R. Thoms, T. N. Tiegs, B. Van Horn, C. A. Wallace, A. A. Walls, J. R. Walton, Diana L. Wood, L. B. Yeatts, Jr.

General Atomic Company

N. L. Baldwin, G. Buzzelli, R. J. Campana, B. D. Epstein, P. W. Flynn, S. Langer, J. R. Lindgren, R. H. Simon, A. F. Weinberg

Argonne National Laboratory

S. Greenberg, L. A. Neimark, R. V. Strain

RESULTS FROM IRRADIATION OF VENTED GCFR FUEL RODS IN THE  
GB-9 and GB-10 CAPSULE EXPERIMENTS

A. W. Longest      J. A. Conlin

ABSTRACT

Two gas-cooled fast breeder reactor (GCFR) vented-and-pressure-equalized fuel rods were tested in the GB-9 and GB-10 instrumented thermal-flux capsule experiments at Oak Ridge National Laboratory (ORNL) in support of fuel development for the GCFR. The test rods were similar in that each was a shortened [ $\sim 40$  cm ( $\sim 15.7$  in.) long] mock-up of the GCFR vented-and-pressure-equalized fuel rod with a mixed-oxide fuel column, a short [ $\sim 5$  cm ( $\sim 2$  in.) long] upper blanket region of depleted  $UO_2$  pellets, and a charcoal trap region above the blanket region. The experiments were designed to yield basic information on the fission-product release and transport behavior and general rod performance to be expected in the reference GCFR vented-element system. This report describes the design and presents the results obtained from each of these closely related experiments. A discussion of the known uncertainties in the data of both experiments is included so that the information may be applied in the GCFR and other applications.

The test rods were connected to a high-pressure [6.9-MPa gage (1000-psig)], high-purity helium sweep system with provisions for monitoring fission products in the effluent stream and measuring flow conductances of the sweep lines and portions of the fuel rod being swept at any given time. The GB-9 rod had sweep lines that permitted flow across the top of the rod or through the charcoal trap. The GB-10 sweep line connections permitted flow through all three main regions of the rod (fuel, upper blanket, and trap), either individually or in combination. The normal flow mode in each experiment was with flow directed across the top of the rod, which simulated normal venting of fission products from a GCFR rod. A GCFR leaking-rod condition was simulated when the flow was directed into the bottom and out of the top of the GB-10 rod. In each experiment, the flow of sweep gas was maintained whenever the fuel rod was at power.

The GB-9 rod was operated 471 days at power from April 1970 to November 1971 at one nominal fuel rod linear-power level of 48.6 kW/m (14.8 kW/ft) (nominal cladding-OD temperature of 685°C) to a fuel burnup of 62 MWd/kg heavy metal. The GB-10 rod was operated 972 days at power from August 1972 to August 1976 at three successive nominal linear-power levels of 39.4, 44.3, and 48.6 kW/m (12, 13.5, and 14.8 kW/ft) (nominal cladding-OD temperatures of 565, 630, and 685°C) to a fuel burnup of 112 MWd/kg heavy metal. The temperature level of the upper blanket and charcoal trap of each rod was controlled by electrical heaters to give 300°C trap temperature, typical of the GCFR rod. Trap temperature, rod power, and sweep pressure [normally 6.9 MPa gage (1000 psig)] were varied in special tests to determine the dependence of fission-product release on these parameters.

The fuel rods performed well in these experiments, and the measurements, many of which were the first of a kind, indicate that the vented-and-pressure-equalized fuel rod should remain a primary candidate design for the GCFR. Fission-gas release from the oxide fuel matrix, somewhat lower than predicted, was obtained for radioactive isotopes with half-lives as short as 16-sec  $^{140}\text{Xe}$  and as long as 12-day  $^{131\text{m}}\text{Xe}$ . Detailed information on the gas-phase transport of the fission gases through the main regions of the rod and the dependence on sweep pressure in the range 1.4-6.9 MPa gage (200-1000 psig) was obtained. Fission-gas release from the top of the rod under the normal venting mode of operation was fairly insensitive to charcoal trap temperature in the range 200-400°C, but very sensitive to fuel-region temperature changes and temperature profile changes over the fuel region. No significant burst-type releases of the radioactive fission gases were detected upon shutdowns and startups; instead, these gases were released continuously during irradiation at fractional release levels up to about 30% for the longer-lived isotopes such as 5.27-day  $^{133}\text{Xe}$ . Iodine deposition measurements, radiation surveys, trap decay heat measurements, and postirradiation gamma scans all indicated that escape of volatile fission products through the upper blanket region of the GCFR rod should be insignificant under normal venting conditions. GB-10 measurements of internal gas-flow conductance

revealed that a severe flow constriction at power developed late in the irradiation, but it was relieved each time a shutdown or large power reduction occurred. Other measurements included neutron radiography and tritium-monitoring experiments.

Keywords — fuel rod, GCFR, thermal, thermocouple, monitoring, fission, irradiation, capsule, release rate, birth rate, fission gas, volatile fission products, xenon, krypton, iodine, tritium, linear power, cladding temperature, flow conductance, capsule, neutron flux, helium sweep, pressure.

---

## 1. INTRODUCTION

A series of fuel-rod irradiation tests have been conducted at Oak Ridge National Laboratory (ORNL) in support of fuel development for the gas-cooled fast breeder reactor (GCFR). The GCFR is being developed at General Atomic Company (GAC) with support from the Energy Research and Development Administration (ERDA)<sup>\*</sup> and a number of electric utility companies. The fuels-irradiation program for the GCFR consists of both thermal- and fast-flux testing in capsule and loop experiments. Thermal-flux tests are being performed at ORNL in a series of capsule tests in the Oak Ridge Research Reactor (ORR) poolside facility. These tests, supported by ERDA, represent the cooperative efforts of GAC, ORNL, and Argonne National Laboratory (ANL).

Two fuel-rod concepts for the GCFR have been investigated in the ORNL thermal-flux tests during the last 10 years: (1) a sealed fuel rod and (2) a vented-and-pressure-equalized fuel rod. Earlier tests (1965 to 1970) of 19 fuel rods of the sealed type indicated this concept to be a feasible backup design; however, cladding temperatures and dimensions must be carefully specified and controlled to ensure that localized

---

<sup>\*</sup>The functions of the Energy Research and Development Administration have since been transferred to the Department of Energy.

cladding collapse does not occur under the high coolant pressures [9.0 MPa (1300 psig)] in the GCFR.<sup>1</sup> During the last 6 years, emphasis has been on the testing of fuel rods of the vented-and-pressure-equalized concept, the reference GCFR fuel-rod design.

In the GCFR vented-fuel-element concept, the top of each fuel rod is vented through an annular charcoal trap, as shown in Fig. 1, and a helium purification system to the inlet side of the main coolant circulators, as shown in Fig. 2. The small pressure differential developed by circulation of the helium coolant keeps the gas pressure inside the rods slightly below the 9.0-MPa (1300-psig) coolant pressure outside the rods. The design and operation of this venting system, called the pressure-equalization system (PES), have been described by Campana.<sup>2</sup>

The individual GCFR stainless-steel-clad fuel rods have a 113-cm-long (44.5-in.) fuel region of (U,Pu)O<sub>2</sub> pellets, 45-cm-long (18-in.) upper and lower blanket regions of UO<sub>2</sub> pellets, and a 7.6-cm-long (3-in.) charcoal trap at the upper end of the rod. The rod traps, which operate at the inlet coolant temperature of about 300°C, form the first stage of the fission-product trapping system. Their main purpose is to remove or delay the release of volatile fission products (Br, I, Cs) should they escape in significant quantities through the upper blanket region. Large releases of the volatile fission products could impose undesirable heat loads on the remainder of the trapping system.

Two shortened prototypes of the GCFR vented fuel rod have been tested in the ORNL thermal-flux test program during the last 6 years. These fuel rods were tested in succession in NaK-filled irradiation capsules that provided for control of a small pressure differential across the cladding and thermocouple monitoring of cladding temperatures. The two capsules, designated GB-9 and GB-10, had the same basic design. In each case, the fuel rod was designed primarily by GAC, and the capsule and associated gas systems were designed primarily by ORNL. Most of the postirradiation examination work on the GB-9 fuel rod was done at ANL, although some work was done at both ORNL and GAC. Irradiation of capsule GB-10 was successfully completed on Aug. 1, 1976, and its postirradiation examination is under way.

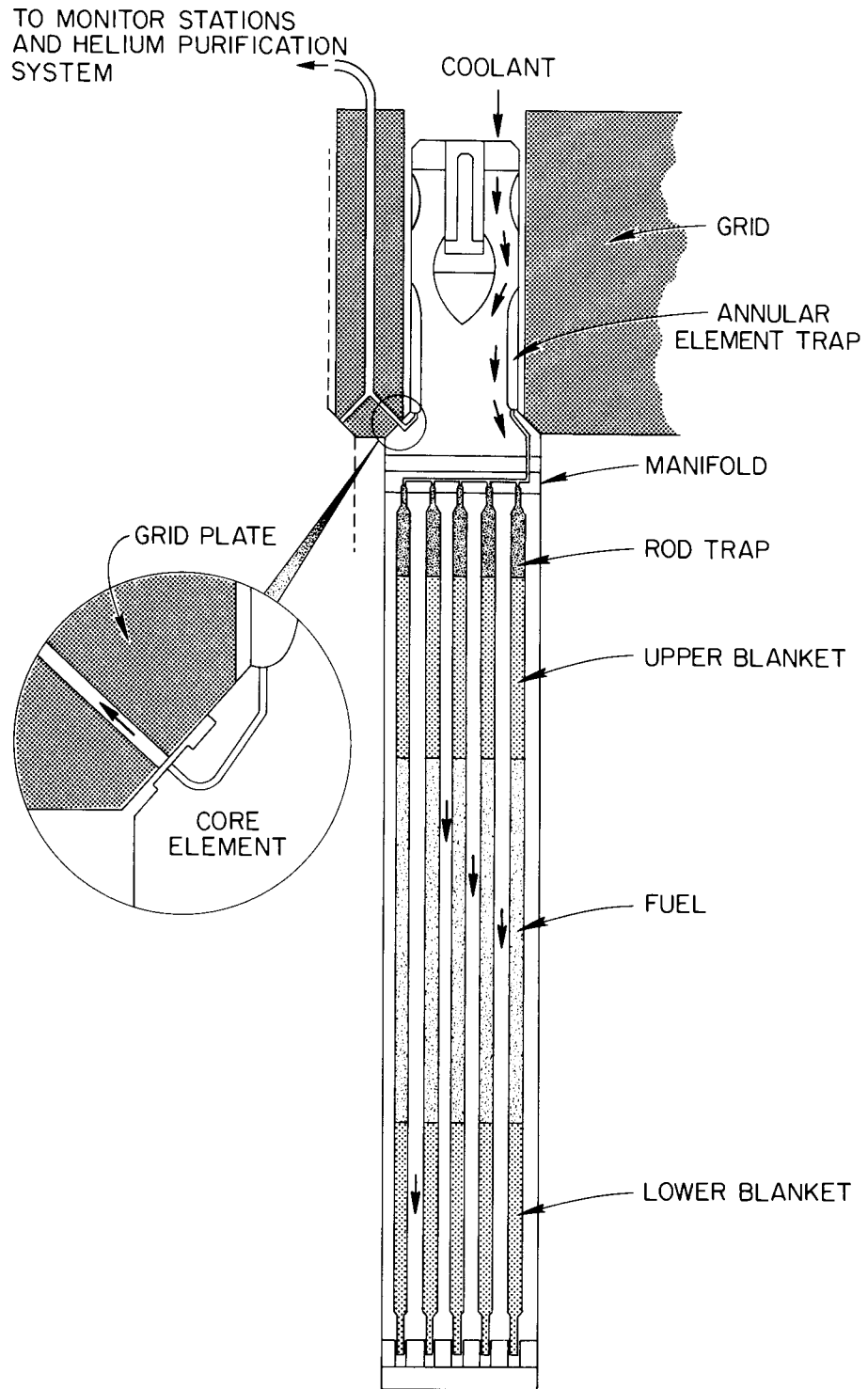


Fig. 1. GCFR vented fuel element.

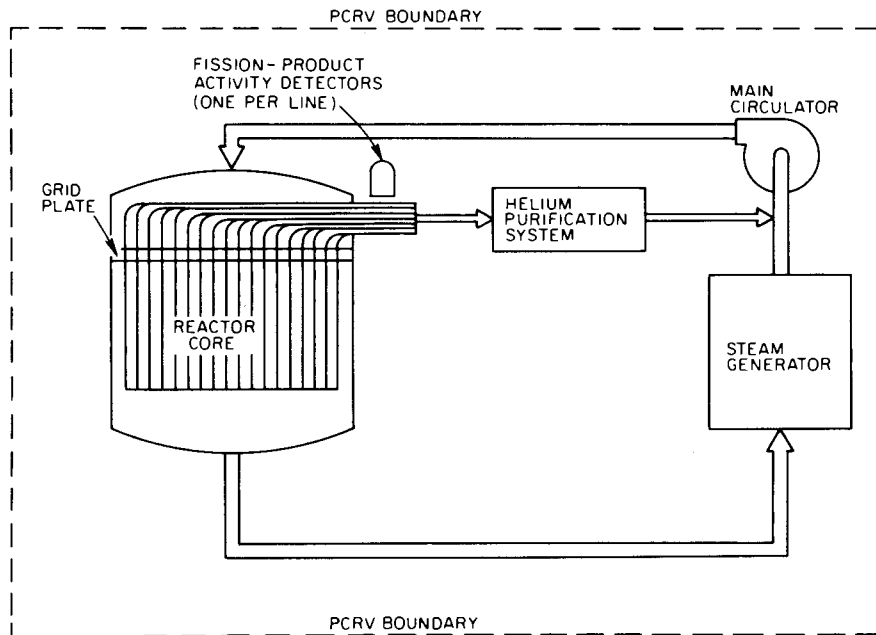


Fig. 2. Concept of the GCFR pressure-equalization-system loop relative to the primary loop.

Capsules GB-9 and GB-10 were designed to provide the data needed for an initial evaluation of the overall performance of the GCFR vented-and-pressure-equalized fuel rod. In order to simulate and study various aspects of the vented-fuel-rod concept in these tests, the interior of the fuel rod in each capsule was connected to a 6.9-MPa gage (1000-psig) helium sweep system which was instrumented to provide continuous monitoring of fission-product release from the rod. The sweep system was designed with many features analogous to the GCFR pressure-equalization-system design.

The GB-9 and GB-10 capsules are unique in that they were designed to provide direct measurements of fission-product release rates from an operating fast breeder reactor fuel rod. The fission-product release data obtained in these experiments are being used in important applications in both the GCFR and the liquid-metal fast breeder reactor (LMFBR) development programs. This is possible because the GCFR and LMFBR fuel-rod materials and operating conditions are similar in many respects.

The experimental data are being used in many aspects of the GCFR pressure-equalization-system design and in computer models for predicting fast breeder reactor fuel performance.

Many results from the GB-9 (formerly designated 04-P9) and GB-10 experiments have been reported previously.<sup>3-18</sup> The intent of this report is to review and present, in one place, the pertinent information obtained from both of the closely related experiments, to the extent of ORNL's involvement in the ORNL-GAC-ANL cooperative effort. Thus, the information presented is primarily the results obtained during the irradiations. The experiment design, results obtained from operation, and ORNL's portion of the postirradiation examination is presented first for the GB-9 capsule and then for the GB-10 capsule. After the data from both experiments are presented and discussed, conclusions we have reached regarding the performance of the GCFR vented fuel rods are given.

## 2. IRRADIATION FACILITY DESCRIPTION

The GB-9 and GB-10 irradiations were conducted in the Oak Ridge Research Reactor (ORR) poolside facility,<sup>19</sup> where in each case the capsule position was adjusted to maintain controlled cladding temperatures or fission rates during the irradiation. The general arrangement of the poolside irradiation facilities with respect to the reactor is shown in Fig. 3.

The ORR is a 30-MW light-water-cooled and -moderated research reactor. A typical layout of the ORR core and the associated poolside irradiation facility positions is shown in Fig. 4. The core consists of a 9 by 7 array of plate-type fuel elements, beryllium reflector elements, shim rods, and experimental facilities. The fuel elements are approximately 7.6 by 7.6 by 81 cm (3 by 3 by 32 in.), but the active fuel height is 61 cm (24 in.). The arrangement of the elements may change from time to time depending on various experimental needs. The reactor is operated on a cycle of 8 weeks, with refueling shutdowns of approximately 4-6 hr duration every 10 to 14 days. End-of-cycle shutdowns are usually 5 to 6 days in duration.

The GB-9 and GB-10 capsules were both irradiated in the ORR poolside position P7-A (see Fig. 4). In each case, the capsule position was adjustable over a 51-cm (20-in.) span from the reactor face, and when fully retracted, the capsule operated at less than 10% of design power.

Estimates of the peak unperturbed neutron flux and the peak gamma heating rate in the P7-A poolside position as a function of distance from the reactor face are shown in Figs. 5 and 6, respectively. The approximate axial shape of the unperturbed neutron flux in the P7-A position at a point 3.8 cm (1.5 in.) from the reactor face is shown in Fig. 7. The axial shape of the gamma heating rate was assumed to be about the same at this distance from the reactor face. Variations in the flux level in the facility occur with changes in core and experimental configurations and in burnup distribution in the reactor fuel elements. Also, there is a change in the axial flux shape associated with the upward movements of the reactor control rods within a given fuel loading.

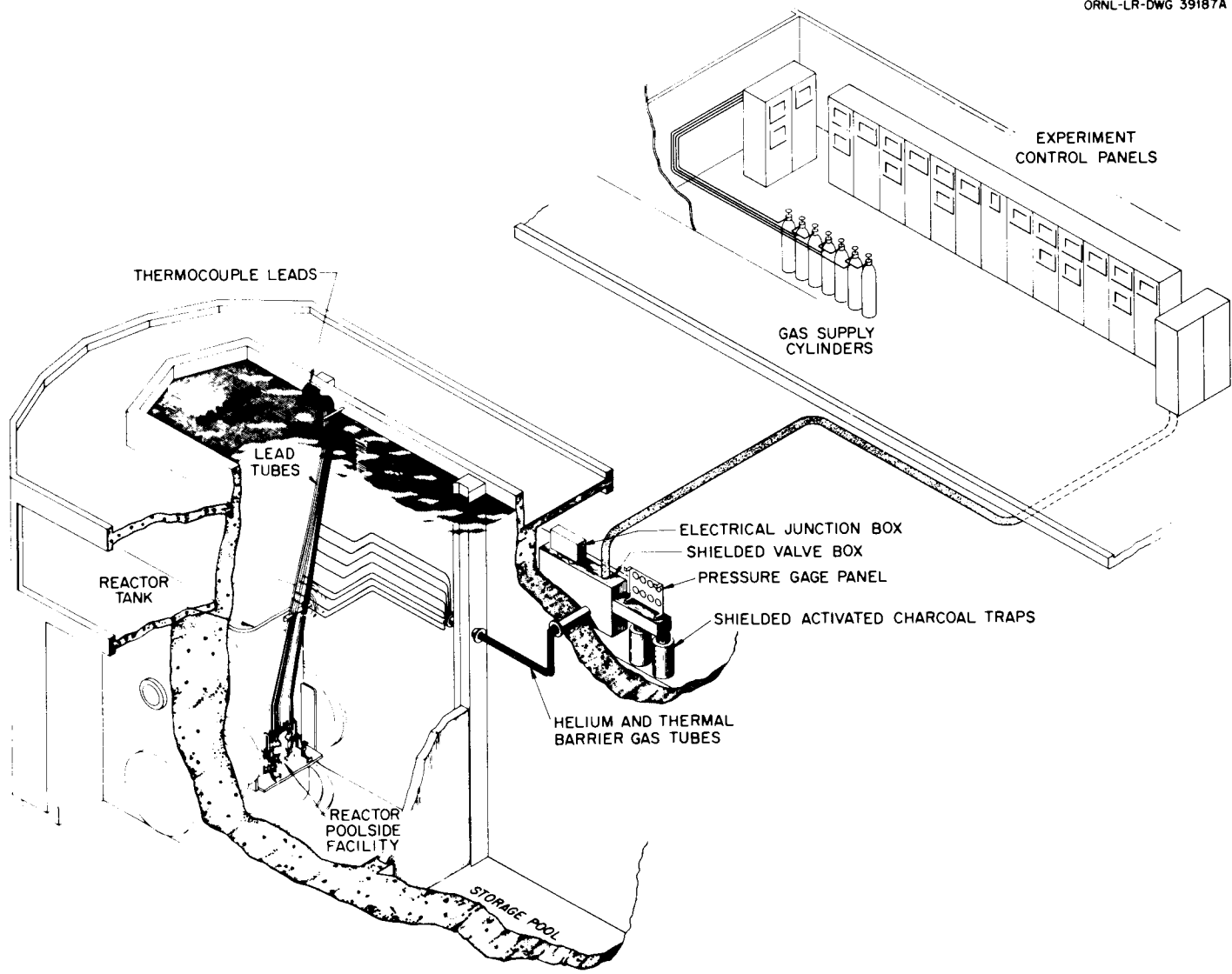


Fig. 3. General arrangement of poolside irradiation facilities in the ORR.

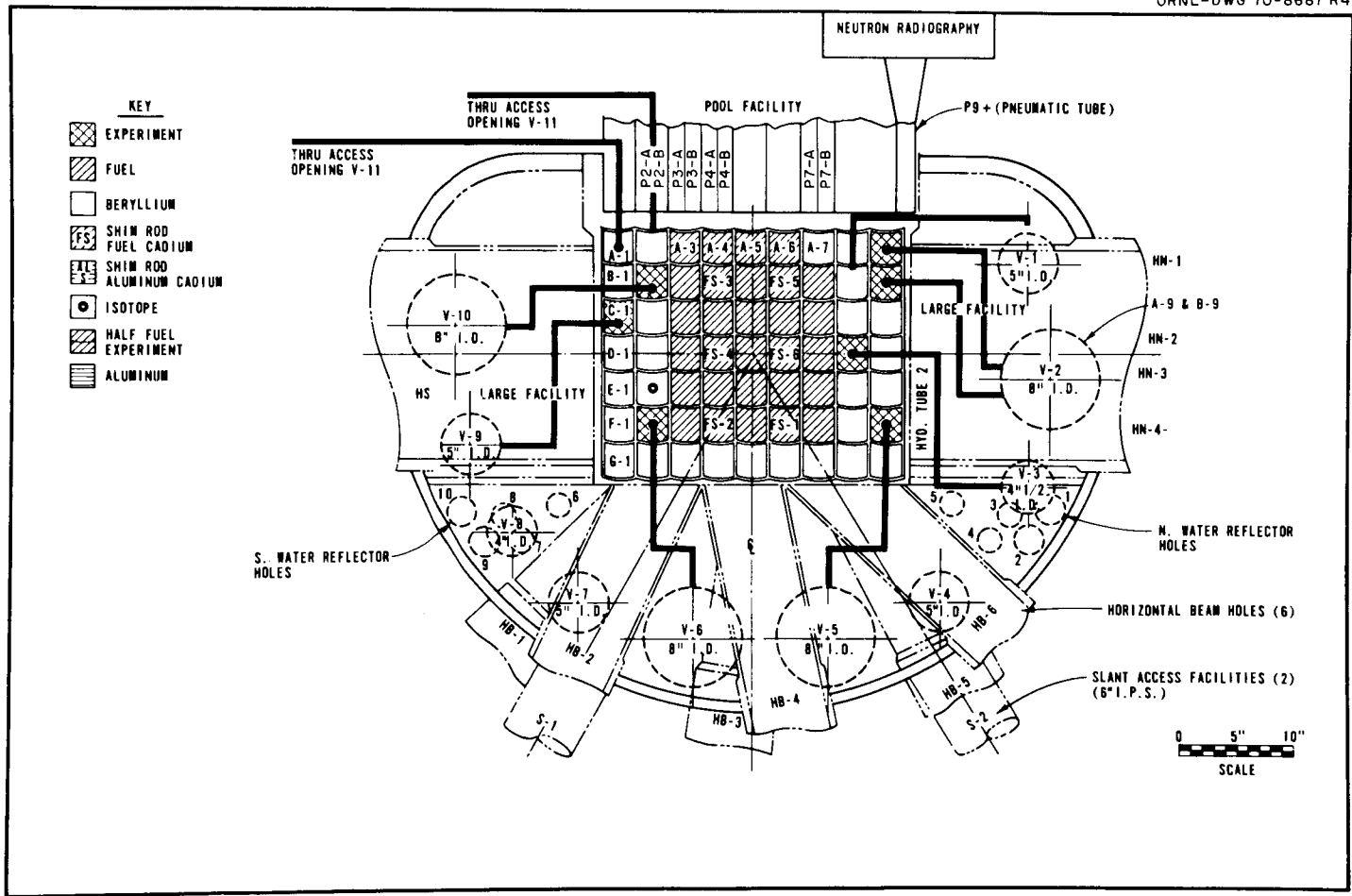


Fig. 4. Cross section of ORR showing typical fuel-loading and experimental facilities.

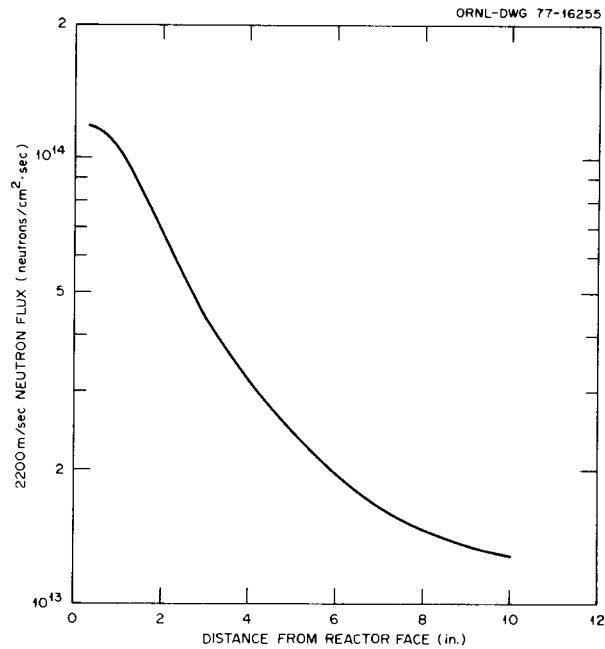


Fig. 5. Estimated peak unperturbed neutron flux in ORR poolside position P7-A (1 in. = 2.54 cm).

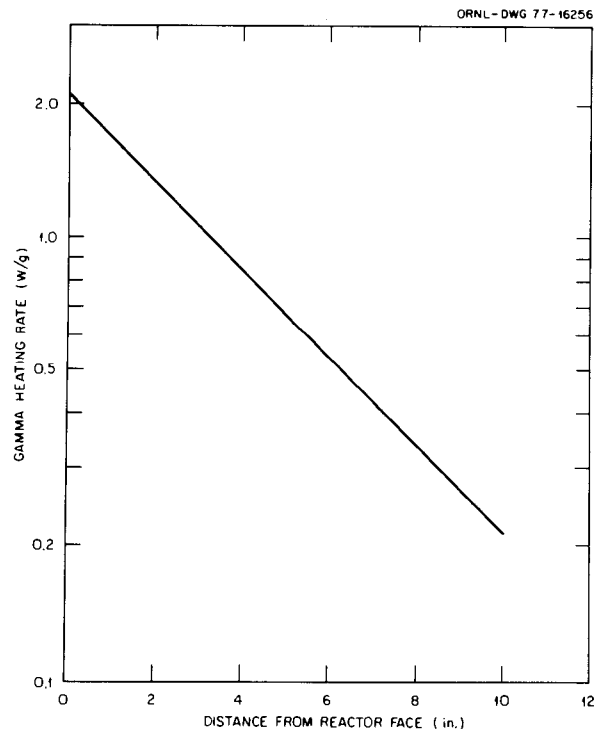


Fig. 6. Estimated peak gamma heating rate in ORR poolside position P7-A (1 in. = 2.54 cm).

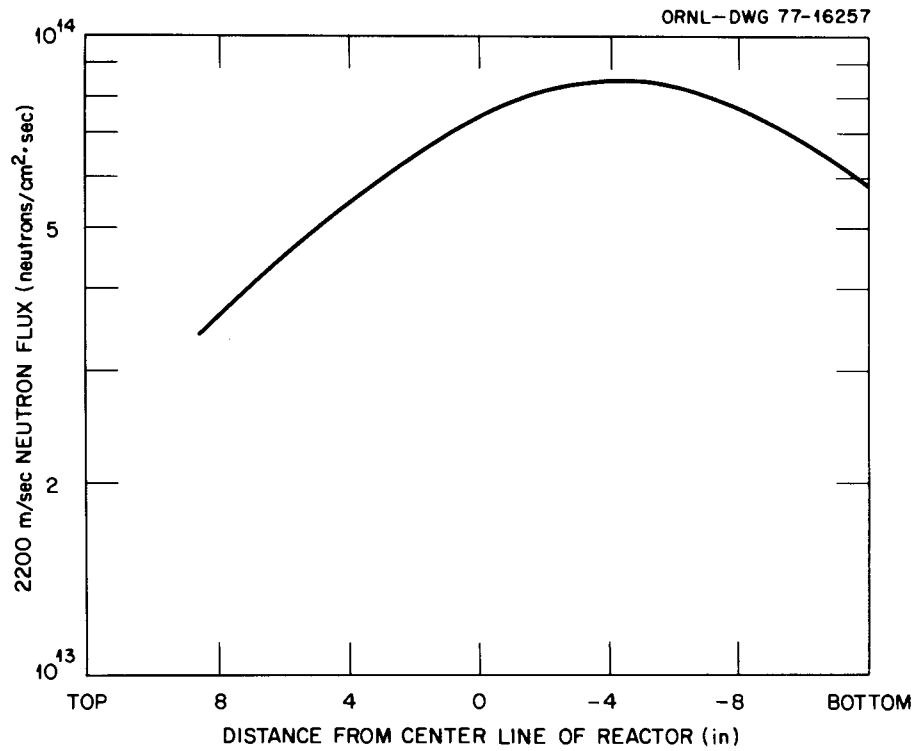


Fig. 7. Estimated axial profile of the unperturbed neutron flux in ORR poolside position P7-A at 3.8 cm (1.5 in.) from the reactor face (1 in. = 2.54 cm).

### 3. GB-9 EXPERIMENT DESCRIPTION

The GB-9 experiment was a thermal-flux irradiation test of a vented GCFR-type fuel rod in which measurements of fission-gas release were made during irradiation. The purpose of the test was to study the performance and adequacy of the vented-and-pressure-equalized fuel rod and its fission-product trap at maximum GCFR ratings.<sup>20</sup>

#### 3.1 Fuel Rod

The design of the GB-9 fuel rod is shown in Fig. 8. The type 316 stainless steel rod was essentially a shortened mock-up of a GCFR vented-and-pressure-equalized fuel rod with a 25-cm (9.9-in.) fuel column, a 4.8-cm (1.9-in.) upper blanket region of depleted UO<sub>2</sub> pellets, and a 8.1-cm-long (3.2-in.) charcoal trap above the blanket region. The fuel column consisted of 32 annular solgel-derived (U<sub>0.88</sub>,Pu<sub>0.12</sub>)O<sub>1.988</sub> test fuel pellets (9% enriched uranium) at a stack smear density of 85% of theoretical and 4 partially enriched UO<sub>2</sub> half-pellets. The UO<sub>2</sub> half-pellets, 2 at each end of the fuel column, had enrichments designed to reduce power-peaking at the ends of the test fuel.

The fuel rod was built with three gas lines entering the top end plug; two of the lines terminated at the top of the charcoal trap and the third line terminated at the bottom of the trap. Thermocouples were located in the fission-product trap at two axial positions.

The void volume inside the fuel rod (from bottom end plug to top end plug) was approximately 4.8 cm<sup>3</sup> (0.29 in.<sup>3</sup>), about one-half of which was below the charcoal trap.

A summary of as-built data for the fuel rod is given in Table 1.

#### 3.2 Capsule

A cross section of capsule GB-9 showing the fuel rod inside the capsule is shown in Fig. 9. The capsule consisted of two concentric containment tubes with a small annular leak-detecting area between them. The fuel rod was centered within a 1.9-cm-OD (0.74-in.) by 1.13-cm-ID (0.445-in.) Zircaloy-2 sleeve which fitted inside the primary stainless

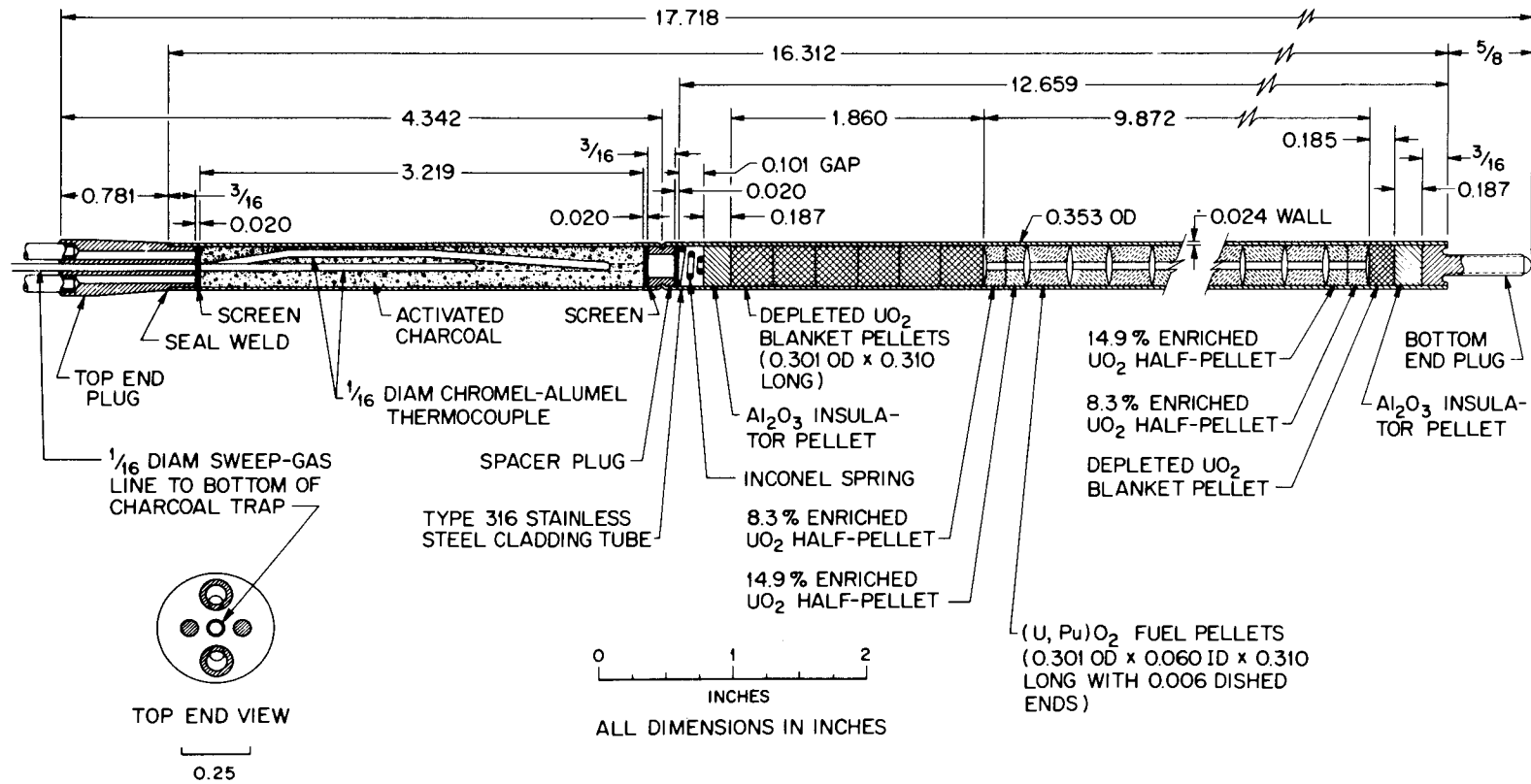


Fig. 8. Gas-cooled fast breeder reactor fuel-rod specimen in ORR capsule GB-9 (1 in. = 2.54 cm).

Table 1. Summary of as-built data for fuel rod of ORR capsule GB-9<sup>a</sup>

Fuel-rod designation	GA-20
Rod type	Vented with integral charcoal trap
Cladding	
Material	Type 316 stainless steel
Outside diameter, in.	0.3535
Wall thickness, in.	0.0245
Ratio of outside to inside diameters	1.161
Length, in.	16.312
Fuel	
Pellet dimensions	
Outside diameter, in.	0.301
Inside diameter, in.	0.060
Length (U,Pu)O <sub>2</sub> , in.	0.273-0.319
Length UO <sub>2</sub> , in.	0.148-0.162
End dish depth, in.	0.006
Total fuel stack height, in. <sup>b</sup>	9.872
(U,Pu)O <sub>2</sub> pellets	
Material	(U,Pu)O <sub>2</sub> , solgel-derived
Number of pellets	32
Composition, %	
UO <sub>2</sub>	88
<sup>235</sup> U enrichment	9
PuO <sub>2</sub>	12 <sup>c</sup>
Oxygen-to-metal ratio	1.983-1.992
Density, % theoretical	91-92
BET surface area, m <sup>2</sup> /g	<0.05
(U,Pu)O <sub>2</sub> stack height, in.	9.240
Stack smear density of (U,Pu)O <sub>2</sub> pellets, % theoretical	85
UO <sub>2</sub> power-peak-reducing half-pellets adjacent to (U,Pu)O <sub>2</sub> at each end	
Material	UO <sub>2</sub>
Number of pellets	4
UO <sub>2</sub> inner pellets (one at each end)	
Enrichment, %	14.9
Oxygen-to-metal ratio	2.004
Density, % theoretical	91-92
UO <sub>2</sub> outer pellets (one at each end)	
Enrichment, %	8.3
Oxygen-to-metal ratio	2.005
Density, % theoretical	90
Blanket pellets	
Pellet material	UO <sub>2</sub>
Enrichment, % (depleted)	0.22
Number of pellets	6
Outside diameter, in.	0.301
Length, in.	0.321-0.328
Stack height, in.	1.959
Oxygen-to-metal ratio	2.004
Density, % theoretical	88-90
Fission-product trap <sup>d</sup>	
Material	Activated coconut charcoal
Manufacturer	Barnebey Cheney
Bed length, in.	3.22

<sup>a</sup> 1 in. = 2.54 cm; 1 m = 3.28 ft.

<sup>b</sup> Includes the (U,Pu)O<sub>2</sub> and the low-enrichment UO<sub>2</sub> half-pellets.

<sup>c</sup> Pu isotopic composition: <sup>239</sup>Pu, 88.7%; <sup>240</sup>Pu, 9.97%; <sup>241</sup>Pu, 1.23%; <sup>242</sup>Pu, 0.101%.

<sup>d</sup> Held between 30- and 40-mesh, type 316 stainless steel screens.

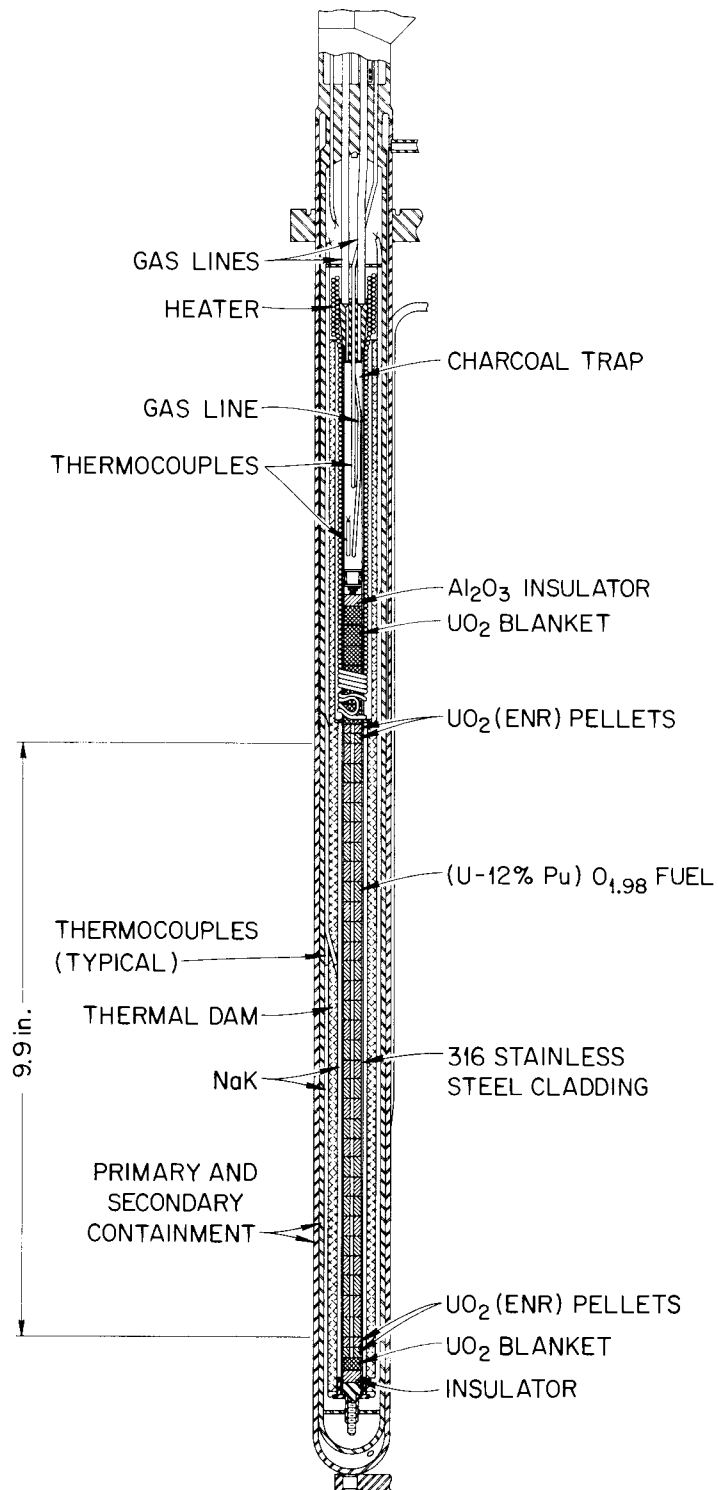


Fig. 9. GCFR-ORR capsule GB-9 (1 in. = 2.54 cm).

steel tube wall. The volume inside the primary tube was filled with NaK to a level above the fuel rod. Heat generated in the rod was thus transferred radially through a NaK annulus, the Zircaloy-2 sleeve, an outer NaK annulus, and across the containment tubes to the ORR pool water. The Zircaloy sleeve served as a holder for the fuel-region thermocouples which were staked into place with their junctions at the inside diameter of the sleeve. The Zircaloy sleeve also served as a thermal barrier (compared to NaK) and reduced the tendency for thermal convection in the NaK volume. In addition to the two thermocouples inside the fuel-rod trap, ten 0.16-cm-diam (1/16-in.) Chromel-Alumel thermocouples were located at various axial positions along the length of the capsule to monitor cladding temperatures.

Cladding temperatures in the region of the charcoal trap (normally operated at 300°C) were controlled with the aid of electrical heaters. Two 0.16-cm-diam (1/16-in.) heaters wrapped into a coil extended from a point above the trap to the lower end of the depleted UO<sub>2</sub> upper blanket region. A tapered helium gap [0.027 to 0.036 cm thick (0.010 to 0.014 in.)] between the primary and secondary containment tubes was used opposite the trap and blanket regions to reduce the required heater power to about 1.5 kW. Either heater alone could have maintained the desired temperature if the other heater had failed. The heaters were of ungrounded, double-ended design, each consisting of a single 24-gauge Nichrome V resistance wire with a 24-gauge nickel lead wire heliarc-welded to each end. The entire length of resistance wire and lead wire was surrounded by compacted MgO inside the stainless steel sheath.

### 3.3 Gas Systems

Provisions were made for a gas sweep to pass across the top of the fuel rod so that fission-gas release rates could be determined during the irradiation. The sweep and cladding external gas systems used for capsule GB-9 are shown in Fig. 10. The GB-9 fuel rod was connected to the 6.9-MPa gage (1000-psig) high-purity helium sweep system by means of the three gas lines entering the top end plug of the rod. Two of the lines were used as inlet lines; one terminated at the top of the

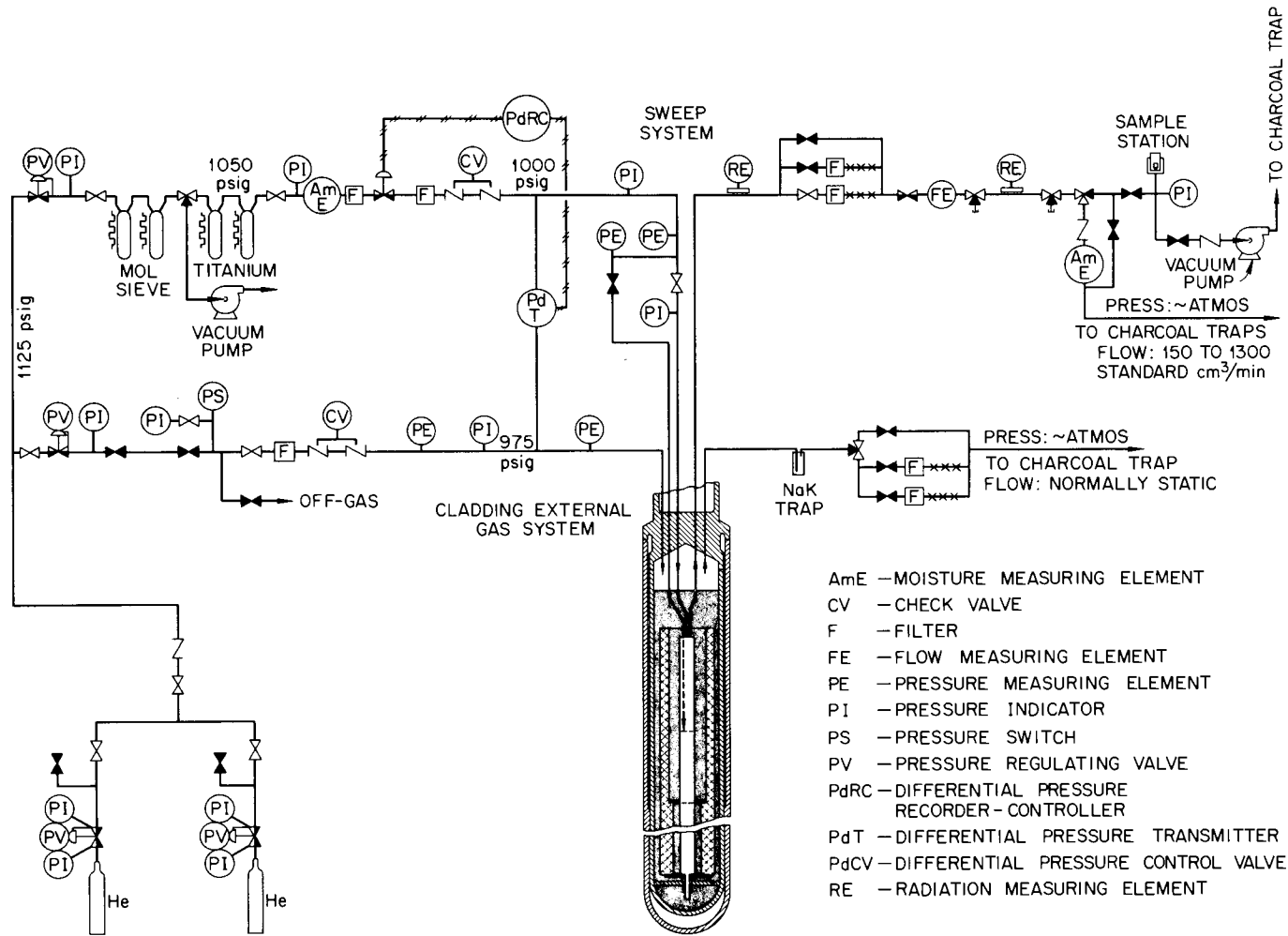


Fig. 10. GCFR-ORR capsule GB-9 sweep and cladding external gas systems (1 psi = 6895 Pa; 1 cm<sup>3</sup> = 0.061 in.<sup>3</sup>).

charcoal trap and the other terminated at the bottom of the charcoal trap. The third line, which connected to the top of the charcoal trap, was used as the sweep effluent line. With this arrangement, the fission-gas release could be monitored with the sweep flowing either across the top of the trap, which was the normal case, or with the sweep flowing upward through the trap (when the inlet flow was transferred to the supply line that goes to the bottom of the trap). In the latter case, the gaseous effluent from the blanket region was swept through the charcoal. Calculations at GAC indicated that the sorption holdup times for krypton and xenon in the charcoal trap were only about 10 to 15 sec when the trap was operating at 300°C and the sweep flow rate through the trap was 1300 cm<sup>3</sup> STP/min (normally used during sweep-gas sampling).

Flow through the sweep system was regulated by adjusting the downstream flow resistance with a needle valve. Flow restrictors were employed immediately upstream of the needle valve to limit the flow rate out of the system to a maximum value. An automatic pressure differential control valve was used to adjust the inlet sweep flow rate as required to maintain the sweep pressure 0.17 MPa (25 psig) above the pressure in the normally static 6.7-MPa gage (975-psig) cladding external gas system. The automatic sweep-pressure-control system normally maintained the pressure differential within ±0.7 kPa (±0.1 psi) of the set point while operating at constant flow rates between 100 and 1300 cm<sup>3</sup> STP/min and within 10 kPa (1.5 psi) of the set point while making flow-rate changes. Good control of sweep pressure was essential to obtaining meaningful fission-gas release data from the experiment, since release was to be measured under steady-state, constant-pressure conditions (where release was expected to be controlled by diffusional delay processes in the rod) and during slow pressure transients.<sup>20</sup>

Analyzed helium was used as the sweep gas and was passed through room-temperature molecular sieve traps and then through 625°C titanium sponge traps before going to the capsule. The molecular sieve traps were expected to remove trace quantities of H<sub>2</sub>O and CO<sub>2</sub>, and the 625°C titanium traps were expected to remove any O<sub>2</sub> present. Two moisture probes were located in the sweep system, one in the sweep supply downstream of the cleanup traps and the other downstream of the capsule.

Provisions for monitoring fission-gas release consisted of a sweep effluent gas-sampling station and two radiation monitors on the effluent sweep line. Gas samples could be taken for determination of isotopic release rates using gamma ray spectrometry. The effluent sweep line activity was monitored continuously by the radiation monitors (ionization chambers), one located on the high-pressure section of the line and the other located on the low-pressure section near the gas-sample withdrawal point (see Fig. 10).

The length of the effluent sweep line from the fuel rod to the gas-sample withdrawal point was about 30 m (100 ft). However, the sweep-gas transient time was minimized to permit analyses for short-lived fission gases by using heavy-wall tubing with a 0.69-mm (0.027-in.) ID over the high-pressure section of the line.

#### 4. GB-9 DESIGN ANALYSES

Detailed design analyses of the fuel and cladding behavior, the power and temperature distributions in the fuel rod, and the fission-product behavior were made at GAC and reported in the planning document for the capsule GB-9 test.<sup>20</sup> ORNL supplied some of the input for those analyses and was responsible for the design of the remainder of the system. Design analyses made at ORNL included a general thermal analysis of the capsule, gas systems flow and pressure-drop analyses, shielding analyses, and hazards evaluation. No attempt will be made to describe all of these analyses in the present report; instead, only the background information needed for presentation and discussion of the experimental results will be given. This information, consisting of predicted power distributions, predicted temperature distributions, thermocouple-to-cladding-hot-side temperature corrections, and predicted fission-gas release fractions, is given in the subsections below.

##### 4.1 Predicted Power Distributions

The predicted power distributions<sup>20</sup> in the fuel rod reflected the strong depression of the thermal flux by the fuel and also the angular variation resulting from the capsule being located in a rather steep flux gradient in the ORR poolside facility. The computed, normalized  $R-\theta$  power distribution at the beginning of life (BOL) is shown in Fig. 11. The predicted variation in the radial power distribution as burnup produces preferential depletion of fuel is indicated in Fig. 12.

Results of an analysis of power peaking at the ends of the fuel column are shown in Fig. 13, where relative axial power distributions are given for three different  $UO_2$ -buffer-pellet enrichment designs. The enrichments chosen for the study were those for  $UO_2$  pellets that were readily available at the time. The power distribution obtained with the 8.3%  $UO_2$  (half-pellet adjacent to blanket) and 14.9%  $UO_2$  (half-pellet adjacent to fuel), shown by the top curve in Fig. 13, was selected for the GB-9 rod.

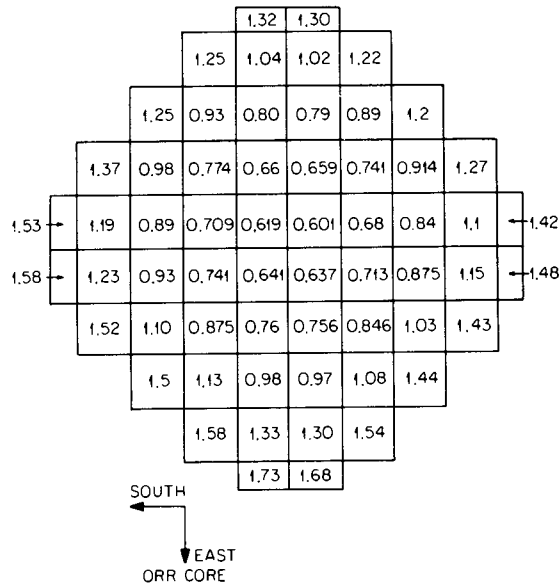


Fig. 11. X-Y coordinate plot of the normalized power distribution in the fuel of capsule GB-9.

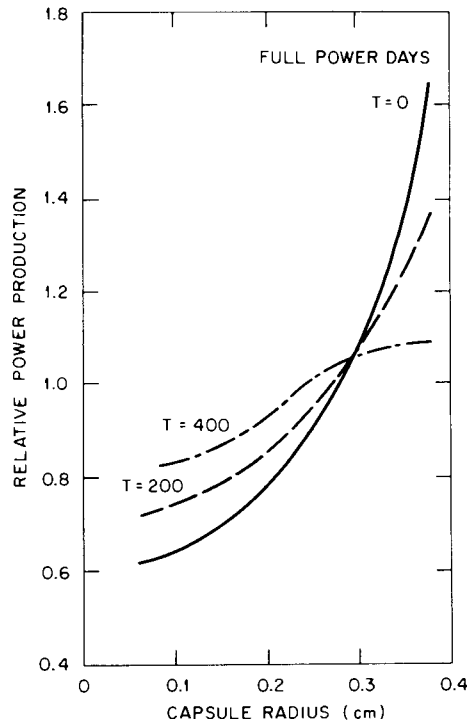


Fig. 12. Calculated radial power distribution as a function of burnup in capsule GB-9 (1 cm = 0.394 in.).

ORNL-DWG 77-16260

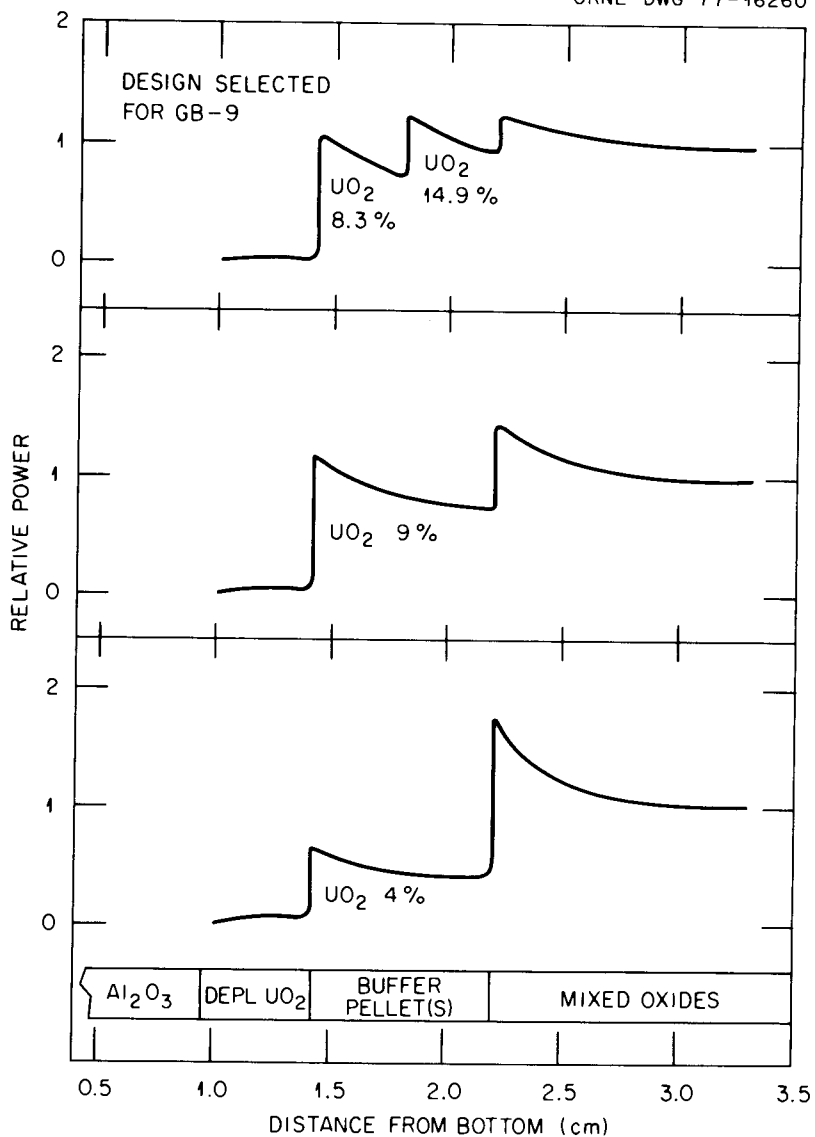


Fig. 13. Calculated axial power distributions in capsule GB-9 for three different UO<sub>2</sub>-buffer-pellet enrichment designs (1 cm = 0.394 in.).

#### 4.2 Predicted Temperature Distributions

The calculated R-θ power distribution at BOL was used as input to calculations of the R-θ temperature distribution. In the temperature calculations, the power level (but not the power distribution) was adjusted to produce a peak cladding-OD temperature of 685°C, which was the full-power operating condition specified for the experiment. The

calculated linear power of the fuel rod at BOL that corresponds to the peak cladding-OD temperature of 685°C is 48.6 kW/m (14.8 kW/ft). The predicted temperature pattern in the fuel for this BOL condition is shown in Fig. 14.

Thermal analysis of the GB-9 capsule also included calculations at ORNL of the R-Z temperature distribution for the case of an assumed uniform power distribution in the fuel. These calculations were made to evaluate the overall capsule design, whereas the R- $\theta$  temperature calculations were concentrated on only the fueled portion of the capsule. The final capsule design was such that, for the uniform power case (ignoring the effect of circumferential variation), a fuel-rod linear power of approximately 53 kW/m (16.1 kW/ft) was required to produce a uniform cladding-OD temperature of 685°C. The predicted cladding-OD temperature profile for the upper portion of the fuel rod under these assumed conditions is shown in Fig. 15. The predicted radial temperature profile across the capsule components at the peak-power axial position is given in Fig. 16 for the same assumed conditions. The HEATING program<sup>21</sup> was employed for these calculations.

The temperature hump at the top of the fuel rod in Fig. 15 was produced by the double-coil portion of the electrical heater. In the actual capsule, this hump was expected to be somewhat less pronounced, since NaK convection in this area will tend to smooth out the temperature distribution. Although NaK convection was not included in these calculations, it was considered in the overall capsule design. The NaK gaps, centering spacers, and baffle above the fuel rod were all designed with the intent of allowing some NaK circulation, but not the development of significant thermal convection loops.

#### 4.3 Thermocouple-to-Cladding-Hot-Side Temperature Corrections

In order to operate the GB-9 fuel rod at a controlled peak cladding-OD temperature, relationships between the readings of the thermocouples monitoring fuel-region cladding temperatures and the maximum temperature of the cladding OD had to be developed. The R- $\theta$  temperature distribution calculations made by GAC were used to develop these relationships.

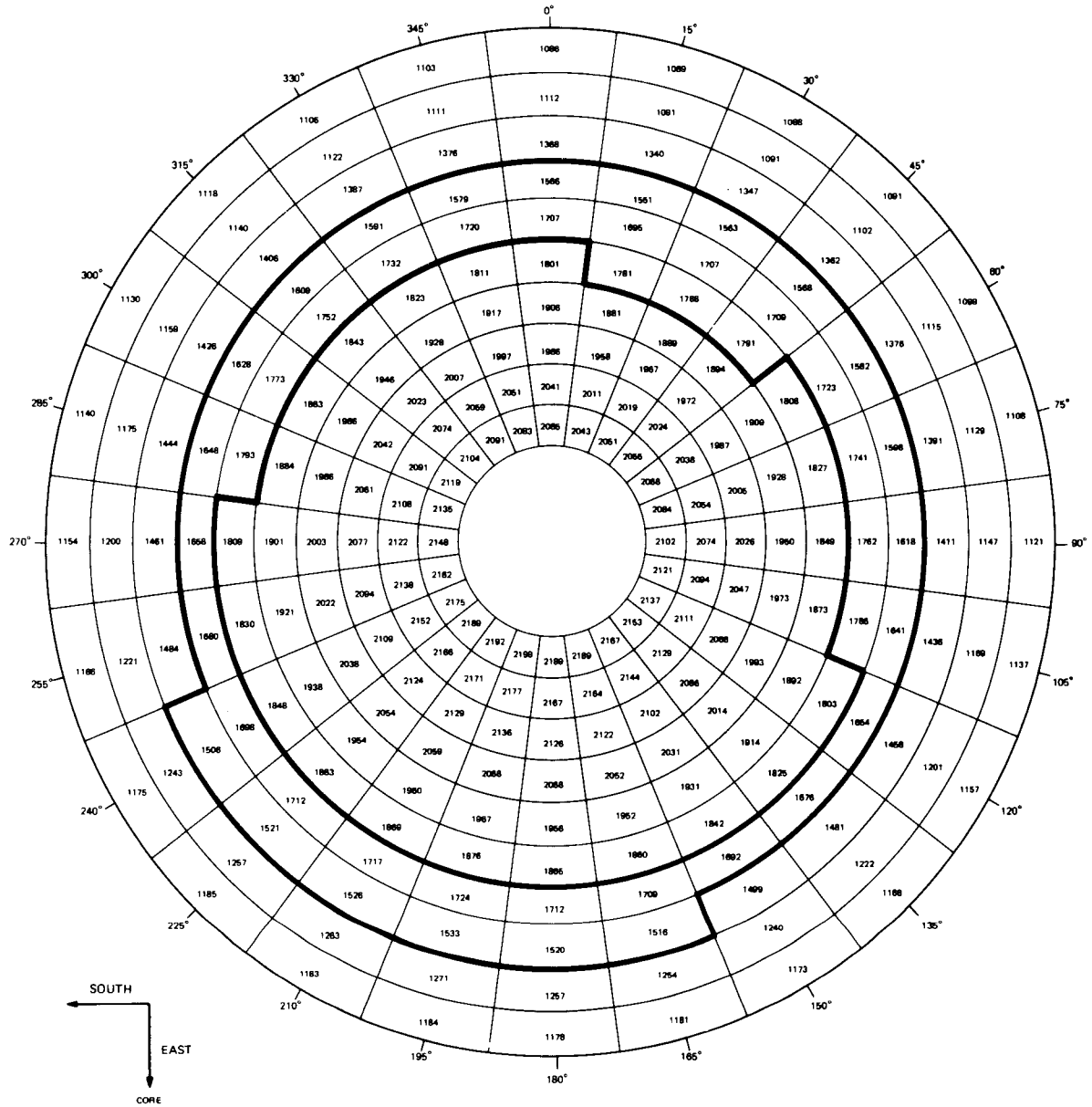


Fig. 14. Calculated temperatures ( $^{\circ}\text{C}$ ) in the GB-9 fuel at the maximum power elevation, showing boundaries of regions of columnar ( $>1800^{\circ}\text{C}$ ), equiaxed, and as-fabricated ( $<1500^{\circ}\text{C}$ ) grains.

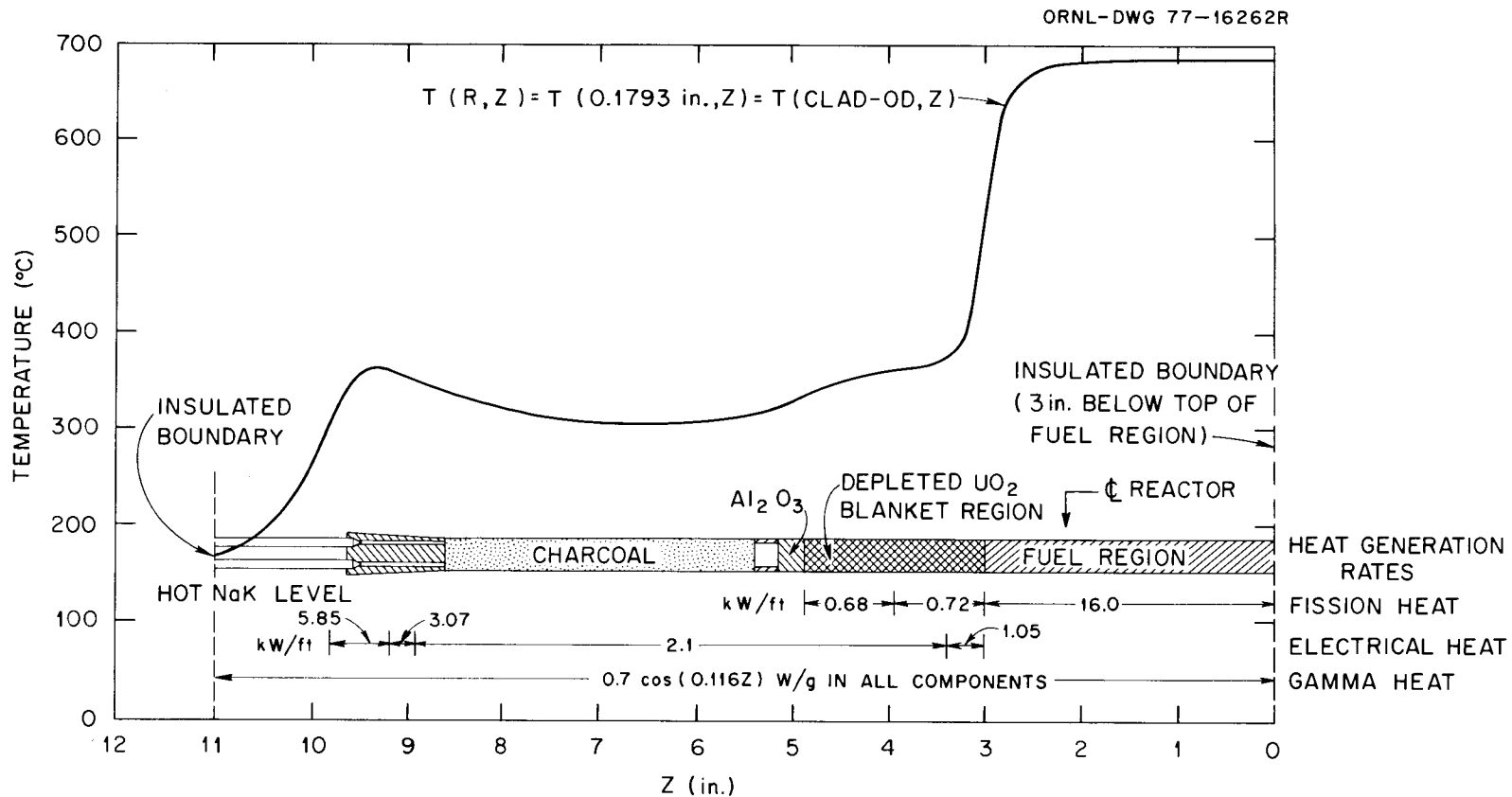


Fig. 15. Calculated axial temperature profile along cladding OD in capsule GB-9 for the case of an assumed uniform power distribution in the fuel region of 16.1 kW/ft (1 in. = 2.54 cm; 1 ft = 0.3048 m).

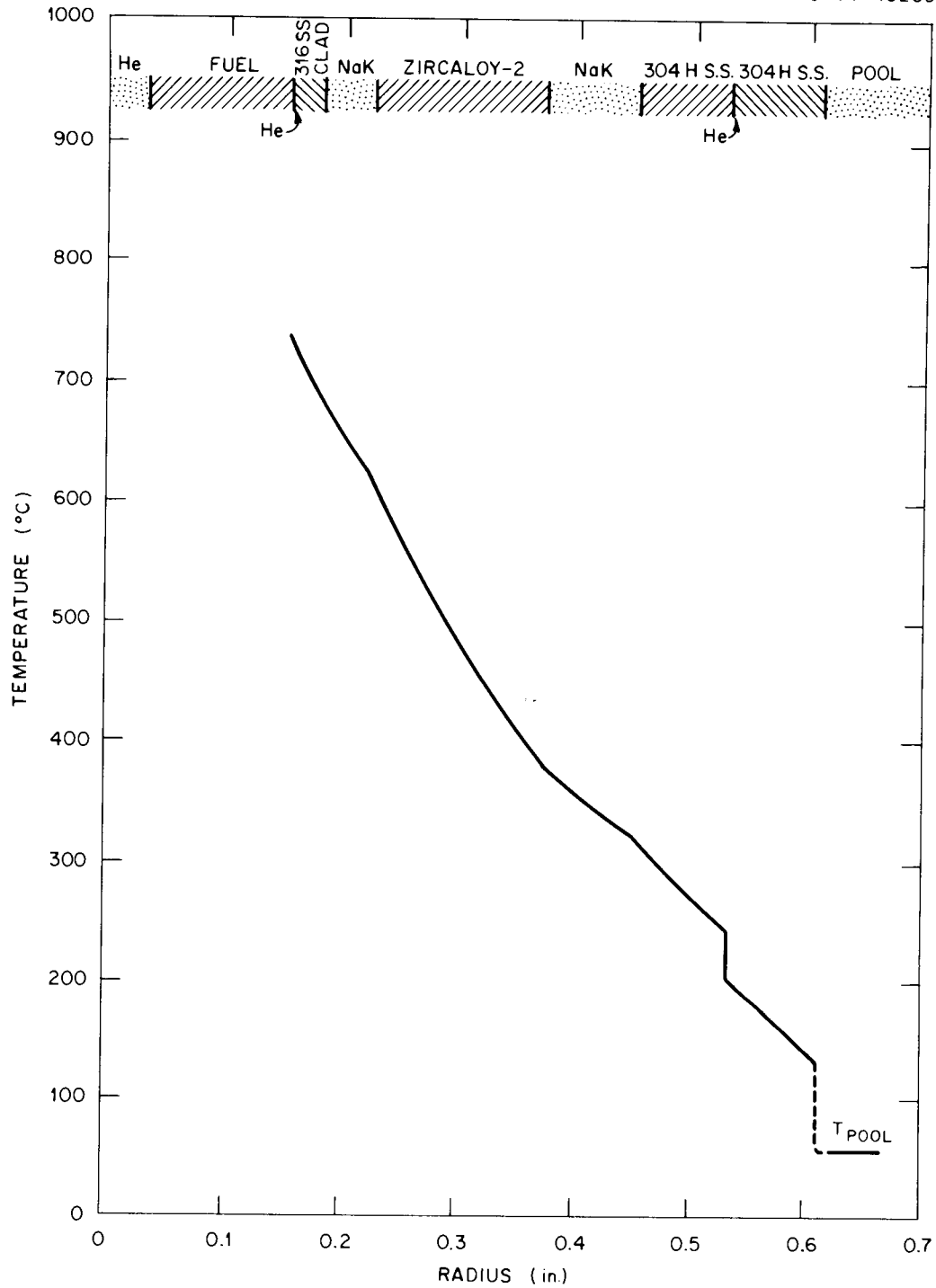


Fig. 16. Calculated radial temperature profile at a point 3 in. below top of fuel (lower insulated boundary) in capsule GB-9 for the case of an assumed uniform power distribution in the fuel region of 16.1 kW/ft (1 in. = 2.54 cm; 1 ft = 0.3048 m).

The BOL temperature corrections for each of the five thermocouples monitoring the fuel region of the rod were calculated, and a sensitivity analysis was performed to estimate the probable error in the corrections.<sup>20</sup> The radial positions of the five thermocouples were assumed to be the same, since all were located at the ID of the Zircaloy-2 sleeve. With the  $\theta$  positions of the thermocouples known, temperature corrections from the points of measurement to the maximum cladding-OD temperature could be taken from the R- $\theta$  temperature distribution calculated for the full-power [48.6 kW/m (14.8 kW/ft)] BOL condition. Listed in Table 2 are the full-power BOL temperature corrections for the five GB-9 fuel-region thermocouples.

The sensitivity of the temperature corrections to a number of uncertainties in the input data is shown in Fig. 17. At full power, it is seen that the parameters to which the corrections are most sensitive are the thermocouple radial location, NaK thermal conductivity, and NaK inner-annulus width. Based on the radial temperature distribution shown in Fig. 16, a change in the thermocouple radial location of 0.00254 cm (0.001 in.) produces a change in the temperature correction of approximately 2°C. Since the radial location of the thermocouple junction may differ as much as 0.0254 cm (0.010 in.) from where we think it is, this alone introduces an uncertainty of up to 20°C in the corrections. Based on the computed sensitivities and our experience to date, we estimate the probable error in the BOL temperature corrections to be about  $\pm 25^\circ\text{C}$ . This estimate does not take into account the effects on the power and temperature distributions of fuel burnup or large changes in the thickness of the inner NaK annulus that would occur if the fuel rod developed a significant bow during the irradiation. A bow of only 0.117 cm (0.046 in.) could eliminate the inner NaK annulus on one side at the point of maximum bow and double the annulus width on the opposite side. Calculation of the R- $\theta$  power and temperature distribution behavior as a function of burnup would be very useful, both for application to the thermocouple corrections and to aid in interpretation of fission-gas release behavior, since release was found to be extremely sensitive to fuel temperature level. However, these calculations were not made, mainly because of the extensive effort required and also

Table 2. Approximate full-power thermocouple-to-cladding-hot-side temperature corrections for the thermocouples monitoring the fuel-region cladding outer surface temperature in capsule GB-9

Thermocouple No.	Axial position, distance from bottom of fuel region <sup>a</sup> (in.)	$\theta$ , angular position <sup>b</sup> (degrees)	Temperature correction <sup>c</sup> (°C)		
			Radial component	Circumferential component	Total
401	1.14	60	105	38	143
402	3.56	120	118	16	134
403	6.06	180	121	1	122
412	7.93	270	116	14	130
413	9.45	210	116	0	116

<sup>a</sup>Bottom of fuel region is defined here as bottom of lower 8.3%-enriched UO<sub>2</sub> pellet (1 in. = 2.54 cm).

<sup>b</sup>When looking down on the capsule,  $\theta$  is the angle measured in a clockwise direction, with 0° being the farthest position from the reactor face.

<sup>c</sup>Based on a beginning-of-life R- $\theta$  fuel-rod power distribution equivalent to 48.6 kW/m (14.75 kW/ft) at each thermocouple axial position.

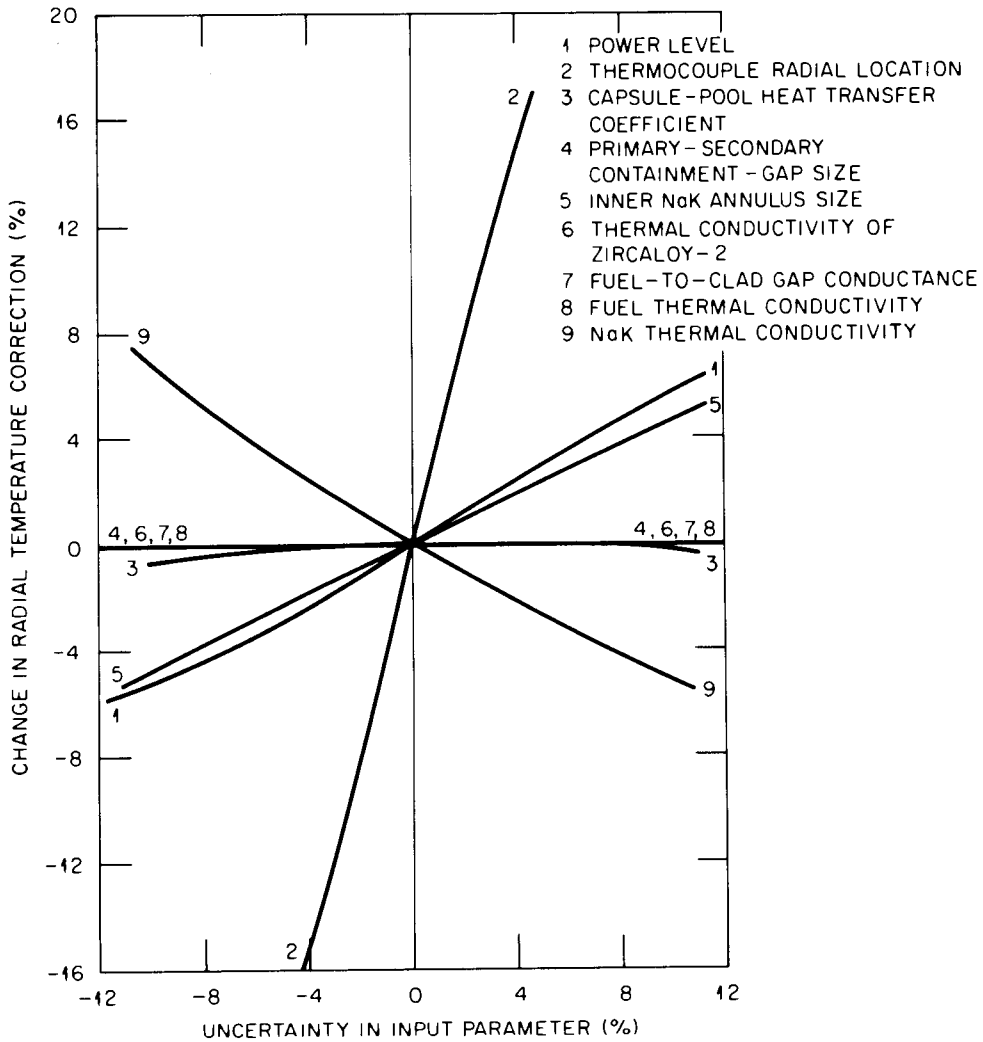


Fig. 17. Calculated sensitivity of fuel-region-thermocouple temperature corrections to uncertainties in input data.

because the changes to the thermocouple corrections with burnup were not expected to be large over most of the planned irradiation.

Since the temperature corrections of Table 2 assume full power at each thermocouple elevation, it was necessary to adjust the corrections, whenever they were used, to correspond to the local power along the rod. In making this adjustment, the assumption was made that the temperature drop from the cladding OD to the pool water outside the capsule is proportional to the level of fuel-rod linear power. This assumption is

a reasonably good one in this case, at least down to about 50% of full power. On this basis, the following equation was obtained for the local fuel-rod linear power at each thermocouple location:

$$\frac{P_i}{48.6 \text{ kW/m}} = \frac{[T_i + \frac{P_i}{48.6 \text{ kW/m}} (\text{FPC}_i)] - T_f}{685 - T_f} \quad (1)$$

or

$$\frac{P_i}{48.6 \text{ kW/m}} = \frac{T_i - 57}{628 - \text{FPC}_i}$$

where

$P_i$  = local fuel-rod linear power indicated by fuel-region thermocouple  $i$ , kW/m

$T_i$  = reading of fuel-region thermocouple  $i$ , °C

$\text{FPC}_i$  = full-power temperature correction for fuel-region thermocouple  $i$  (given in Table 2), °C

$T_f$  = pool water bulk fluid temperature (estimated to be 57°C), °C.

The indicated hot-side-cladding-OD temperature in °C at each thermocouple location,  $T$  (cladding OD, hot side,  $i$ ), is then given by the following equation:

$$T(\text{cladding OD, hot side, } i) = T_i + \frac{P_i}{48.6 \text{ kW/m}} (\text{FPC}_i) \quad (2)$$

#### 4.4 Predicted Fission-Gas Release Fractions

Only the krypton and xenon isotopes were expected to escape from the GB-9 fuel rod in significant quantities, since the other fission products (except perhaps for tritium) are either so refractory or reactive with the fuel-rod materials as to render them essentially fixed.<sup>20</sup>

Of course, one objective of the test was to verify that this expectation was true.

During steady-state operation of the capsule, the fractional release, or the ratio of release rate to birth rate (R/B), of the noble gases was expected to be controlled by diffusion of the gases upward from the fuel. Therefore, the noble gas release rates were expected to be strongly dependent on the half-lives of the isotopes.

Predicted fractional releases of the Kr and Xe isotopes from the upper blanket region of the rod (charcoal trap inlet) and from the top of the rod (charcoal trap outlet) for steady-state full-power operation of capsule GB-9 are plotted in Figs. 18 and 19. These predictions, taken from Ref. 20, are the results of calculations made at GAC at the time the GB-9 experiment was designed and do not reflect some later refinements that have been made to the release models.

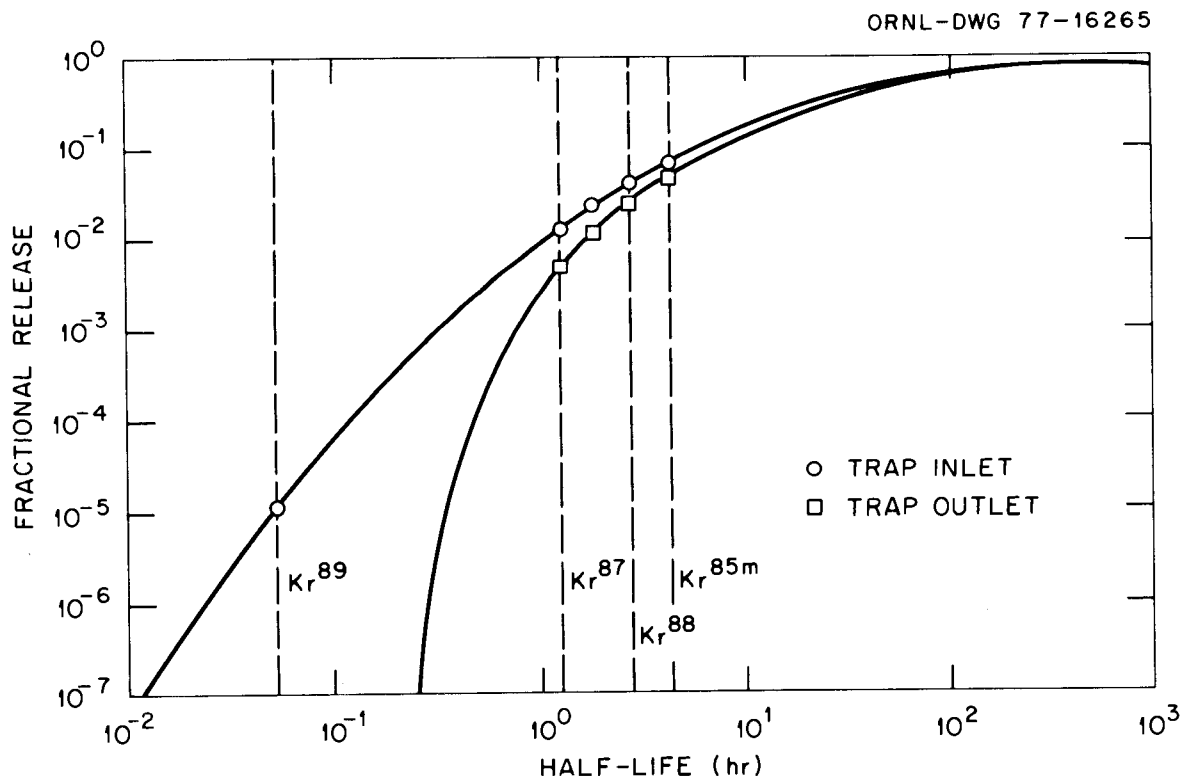


Fig. 18. Calculated fractional release of krypton isotopes in capsule GB-9.

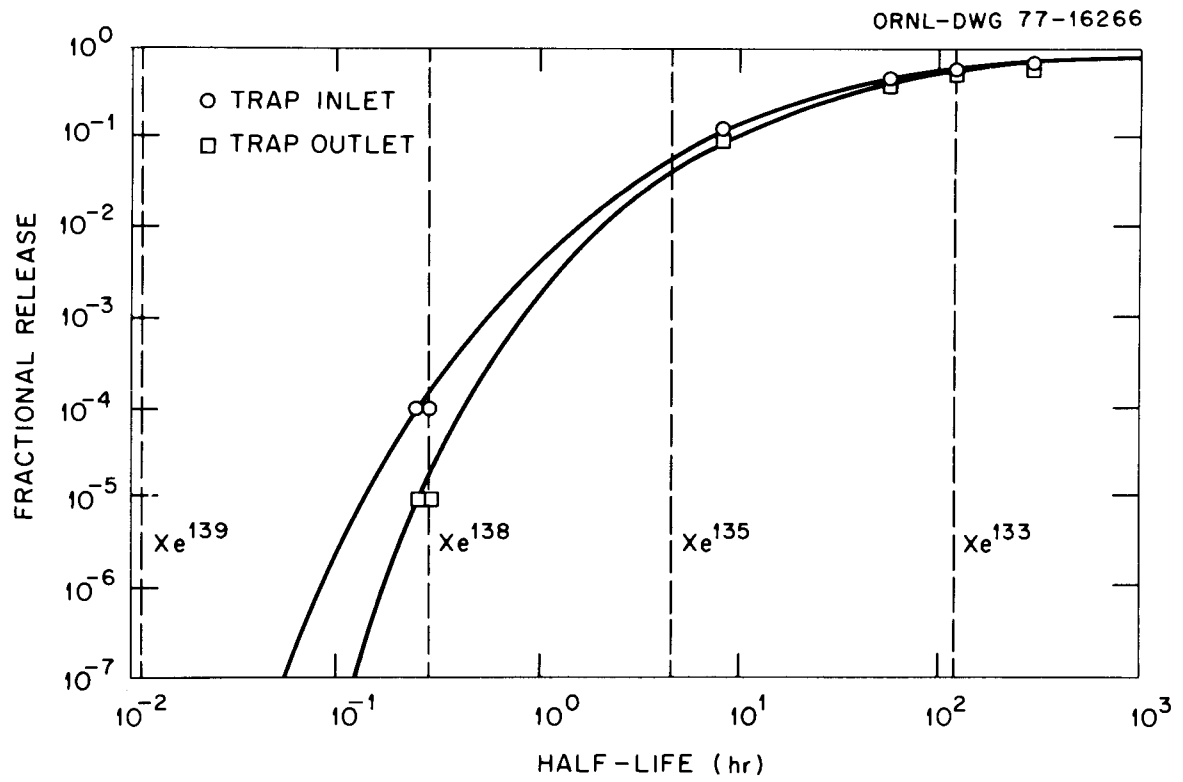


Fig. 19. Calculated fractional release of xenon isotopes in capsule GB-9.

## 5. GB-9 IRRADIATION CONDITIONS AND GENERAL OPERATING PROCEDURE

Capsule GB-9 was irradiated in the ORR poolside facility from Apr. 6, 1970, to Nov. 18, 1971. The fuel rod was operated at one nominal power level throughout its irradiation except for several short periods during which special tests were performed. The fuel rod operated at full power for 471 days under the nominal design conditions of 685°C peak cladding-OD temperature and 48.6 kW/m (14.8 kW/ft) peak power. Steady-state operating conditions and exposures reached in the GB-9 experiment are summarized in Table 3. The temperature conditions are typical of those designed for a GCFR rod. The absence of significant fast-neutron exposure (thermal-flux irradiation) and the low fuel burnup obtained compared to 100 MWd/kg heavy metal for the GCFR fuel are atypical. The estimated fuel burnup obtained of ~54 MWd/kg heavy metal [conservative estimate using Eq. (3); also see Sect. 13.2.2] was virtually equal to the original burnup goal for the test of 55 MWd/kg. However, the burnup goal had been extended to 75 MWd/kg during the course of the irradiation. The experiment was terminated before reaching the revised burnup goal because of a break that occurred in the capsule secondary

Table 3. Capsule GB-9 operating conditions and exposure

<u>Steady-state operating conditions</u>	
Fuel-rod operating power level, kW/m (kW/ft)	48.6 (14.8)
Cladding temperature, OD, °C	
Fuel region, peak	685
Charcoal trap	300
Cladding pressure, MPa gage (psig)	
External	6.7 (975)
Internal	6.9 (1000)
<u>Total exposure</u>	
Time at power, days	471
Estimated fuel burnup, MWd/kg heavy metal	~54 <sup>a</sup>
Fast-neutron exposure (E > 0.18 MeV), neutrons/cm <sup>2</sup>	~5 × 10 <sup>19</sup>

<sup>a</sup>Conservative estimate using Eq. (3). Also, see Sect. 13.2.2.

containment. A secondary gas line [0.32 cm OD, 0.051 cm wall (1/8 in. OD, 0.020 in. wall)], which exited from the bottom of the capsule secondary containment vessel, was broken while handling the capsule during a reactor shutdown, and the capsule operation could not be continued because of the loss of secondary containment. The fuel rod was still intact, however, and most of the test objectives had already been realized.

It should also be noted that the fuel-rod internal pressure was maintained 0.17 MPa (25 psi) higher than the pressure of 6.7 MPa gage (975 psig) external to the rod, the reverse of that in the GCFR. This was done to facilitate leak-checking of the cladding during operation and to minimize NaK ingress into the rod had a leak occurred.

In operating the capsule, small position adjustments were made as required to maintain the indicated peak cladding-OD temperature within  $\pm 15^\circ\text{C}$  of the design value of  $685^\circ\text{C}$ . The peak cladding-OD temperature was taken to be the highest indication obtained when the readings of the five fuel-region thermocouples were corrected to cladding-OD hot-side temperatures. Local fuel-rod linear power and cladding temperature at each thermocouple elevation at any given time were determined in accordance with Eqs. (1) and (2), Sect. 4.3. The full-power thermocouple corrections shown in Table 2, Sect. 4.3, were used in conjunction with Eqs. (1) and (2) throughout the irradiation. No adjustment of the full-power corrections was made to take into account fuel burnup. Fuel burnup at any given time during the irradiation was estimated using the following equation:

$$\text{Bu} = 0.1134 \tau \quad (3)$$

where

Bu = fuel burnup, MWd/kg heavy metal

$\tau$  = irradiation time accumulated at full power, days.

Equation (3) gives a reasonably close but conservative estimate of fuel burnup level. If fuel burnup levels were calculated on the basis of the BOL thermal analyses [i.e., based on assuming a constant fuel-rod power of 48.6 kW/m (14.8 kW/ft)], the calculated values would be approximately

18% higher. Suspecting that the latter basis might lead to burnup estimates somewhat too high, we elected to use the more conservative equation instead. Uncertainties in operating power, cladding temperature, fuel burnup, and other parameters are discussed in Sect. 13 for both the GB-9 and GB-10 experiments.

Sweep-gas flow was maintained, normally across the top of the fuel-rod charcoal trap, at all times the fuel rod was at power. Bottle samples of the effluent sweep gas were taken periodically and analyzed by gamma-ray spectrometry to determine isotopic fission-gas release rates. The sweep flow rate, normally 150 to 250 cm<sup>3</sup> STP/min during nonsampling periods to conserve helium, was increased to approximately 1300 cm<sup>3</sup> STP/min ( $\sim 19$  cm<sup>3</sup>/min at the sweep pressure of 6.9 MPa) prior to sampling. At the sampling flow rate of 1300 cm<sup>3</sup> STP/min, the sweep-gas travel time from the fuel rod to the sampling point was  $\sim 47$  sec, thereby making possible analysis for short-lived fission gases.

In taking gas samples under the steady-state operating conditions, the effluent sweep gas was normally sampled first with the sweep flowing across the top of the trap. The inlet flow was then switched to the bottom of the trap, and 1 to 2 hr later the blanket region effluent was sampled. After sampling was completed, the inlet flow was transferred back to the top of the trap. Subsequent samples were taken only after sufficient time had been allowed (normally at least 24 hr of steady-state operation) for the trap activity to return to equilibrium.

Although the capsule was operated under the steady-state design conditions most of the time, special tests were also performed to determine fission-gas release dependence on charcoal trap temperature, fuel-region power and temperature, and sweep pressure. Measurements were also made to obtain information on fission-gas release during pressure cycling, fission-product decay heating in the charcoal trap, and iodine deposition in the charcoal trap. Neutron radiography of the capsule was performed before and after the irradiation and at two intermediate points during the irradiation.

## 6. RESULTS FROM IRRADIATION TESTING OF CAPSULE GB-9

Experimental results obtained from the GB-9 irradiation are given in the following subsections. It should be emphasized that the values of fuel-rod linear power, fuel-region cladding temperature, and fuel burnup that are used in presenting the experimental data were estimated in accordance with the methods outlined in Sect. 5, using Eqs. (1), (2), and (3), respectively. Uncertainties in these and other parameters and in the experimental results are discussed in Sect. 13 for both the GB-9 and GB-10 experiments.

### 6.1 Description of Initial Startup

The GB-9 capsule was installed in the irradiation facility during an end-of-cycle reactor shutdown the week of Feb. 1, 1970. The capsule was operated at low power [ $\sim 6$  kW/m (1.8 kW/ft)] until the next end-of-cycle reactor shutdown the week of Mar. 29, 1970. During this time, the gas systems and instrumentation were checked out and the indicated moisture level in the sweep gas was reduced. Full power [ $\sim 48.6$  kW/m (14.8 kW/ft)] was reached on Apr. 10, 1970.

After the capsule was installed during the Feb. 1-9, 1970, shutdown, a helium purge of the sweep system was established to rid the system of any air and moisture that may have entered during installation. Although care was taken to minimize moisture contamination during construction and installation, it was virtually impossible to install the system completely free of moisture. The moisture content of the sweep gas was monitored by two aluminum oxide hygrometer probes, one located in the sweep supply line and the other downstream of the capsule (see AmE locations in Fig. 10). These probes were not expected to provide exact determination of moisture content, since their advertised accuracy for determining dew/frost point was  $\pm 2.5^\circ\text{C}$  over most of their range from  $+20$  to  $-110^\circ\text{C}$ . However, they were especially useful for monitoring changes in moisture levels during initial purging and operation of the system.

The inlet moisture probe indicated a moisture level of 1 ppm or less soon after the initial purging was started; however, the moisture level indicated by the outlet probe was much higher than expected. After 5 days of purging at a helium flow rate of 30 to 40 cm<sup>3</sup> STP/min, the outlet probe indicated about 250 ppm. The sweep effluent moisture-level indication remained high, with a slow rate of decrease, until the fuel-rod charcoal trap and blanket region were heated using the capsule heaters. After a week with the trap at 250°C, the effluent moisture level stabilized at about 60 ppm. Varying the sweep flow or raising the trap temperature from 250 to 300°C had little effect on the indicated moisture level. By this time, a calibration error or some other problem with the outlet probe was suspected, and it was decided to insert the capsule to power. When the capsule was initially brought up in power, the effluent moisture-level indication decreased slowly from 60 to about 40 ppm. Several months later, the indicated level was about 35 ppm. At this point, a check was made to determine if the long electrical lead being used with the outlet probe was responsible for the high reading. The same readout instrument was used for both probes, but the lead between the readout instrument and the outlet probe was about 21 m (70 ft) compared to about 1.8 m (6 ft) for the inlet probe. A reading was taken at a lead connection about 6 m (20 ft) from the outlet probe. The outlet probe then indicated less than 1 ppm compared with a reading of 35 ppm at the 21-m distance, indicating that the instrument lead was responsible, at least in part, for the high indications. After consultations with the manufacturer of the probes, a new instrument lead was installed that eliminated this problem.

Beginning on Apr. 4, 1970, the capsule was brought up to power in three steps, 40%, 70%, and 100% of full power [48.6 kW/m (14.8 kW/ft)], with sweep effluent samples taken after at least 24 hr of steady-state operation at each power level. Operation was found to be quite satisfactory, and the temperature patterns agreed reasonably well with predictions. After first reaching full power on Apr. 10, 1970, the fuel rod was operated at full power for the remainder of the irradiation except for several short periods during which special tests were performed.

## 6.2 Effluent Sweep Line Activity

The continuous radiation monitors on the effluent sweep line (see RE locations in Fig. 10) provided a sensitive indication of changes in operating conditions. Figure 20 shows the response of the ionization chamber on the high-pressure section of the effluent sweep line during a period in which the sweep-pressure-control system was functioning improperly and cycling the sweep pressure over a  $\pm 1.4$ -kPa ( $\pm 0.2$ -psi) range. The cycling started during unattended operation and lasted 28 hr before the situation was detected and corrected. The sweep flow was across the top of the trap during this time.

The activity release was much more sensitive to pressure changes with the sweep flowing across the top of the trap than through the trap. The reason for this behavior was that a relatively large volume of gas [ $\sim 68$  cm<sup>3</sup> ( $\sim 4.1$  in.<sup>3</sup>)] was trapped in the lower inlet sweep line [which extended about 21 m (70 ft) back to a valve box] when the sweep was directed across the top of the trap. This trapped gas expanded and contracted during pressure fluctuations and created gas flow in the charcoal trap.

The response of the same ionization chamber during a typical sampling period with the capsule operating under steady-state design conditions is shown in Fig. 21. At this time, the capsule had been at full power a total of 82 days. As the sweep flow rate was increased from 245 to 1295 cm<sup>3</sup> STP/min for sampling, the monitor reading decreased from a steady reading of 158 to 32 mR/hr. After the reading remained level for about 2 hr, two gas samples were taken with the sweep flowing across the top of the trap. The gas samples were frequently taken in pairs — one sample to be counted as a gas and the other sample bottle evacuated after a suitable delay time and counted for the plated-out daughter products of short-lived fission gases.

After the top-trap samples were taken, the range of the readout instrument was increased and the inlet sweep flow was switched to the bottom of the trap. The ionization chamber responded by going from the steady reading of 32 mR/hr, through a peak of 8600 mR/hr as the activity in the trap (and in the lower inlet sweep line) was swept out, and back

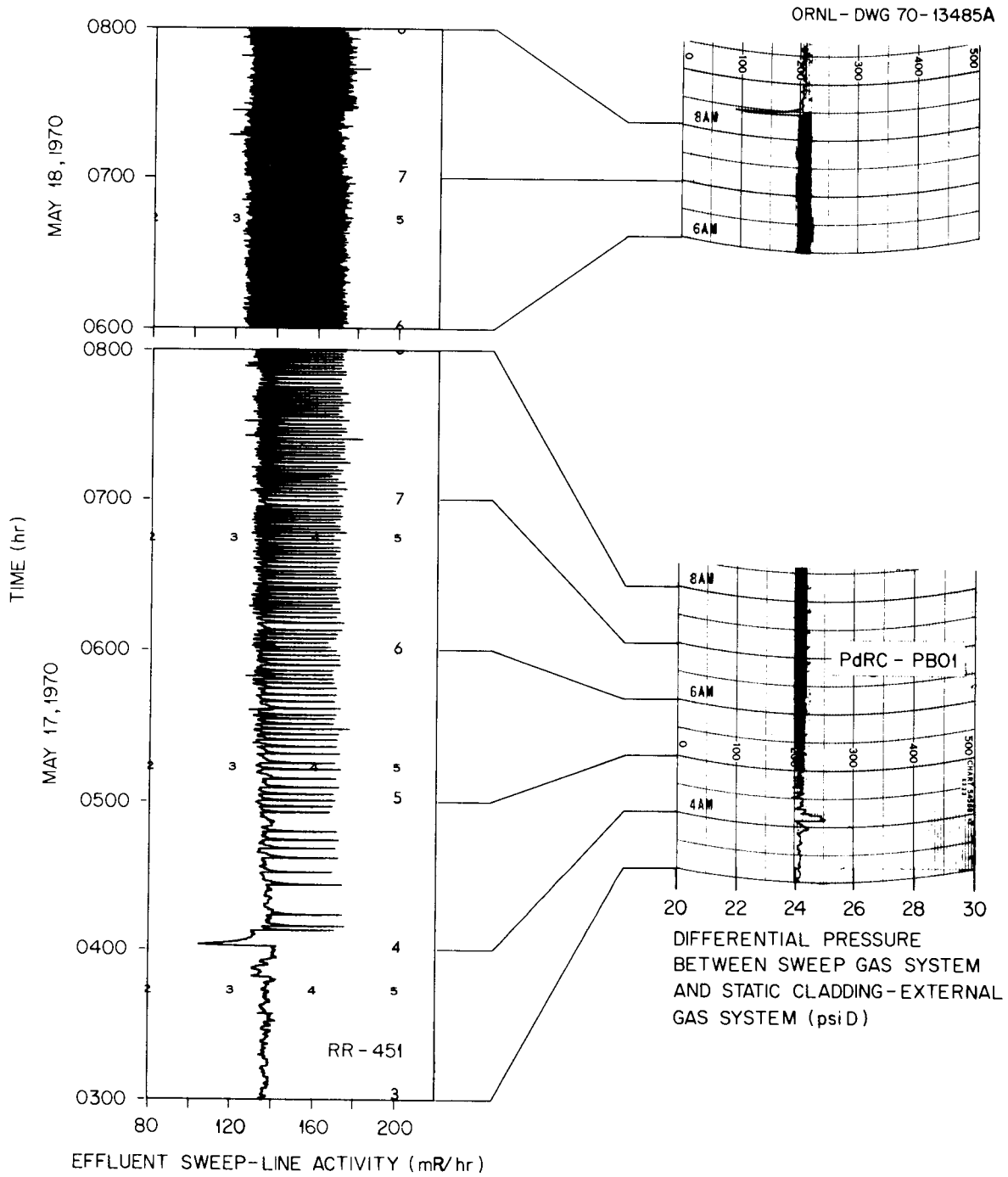


Fig. 20. Effluent sweep line activity during inadvertent cycling of the capsule GB-9 pressure-control valve on May 17-18, 1970 (1 psi = 6895 Pa).

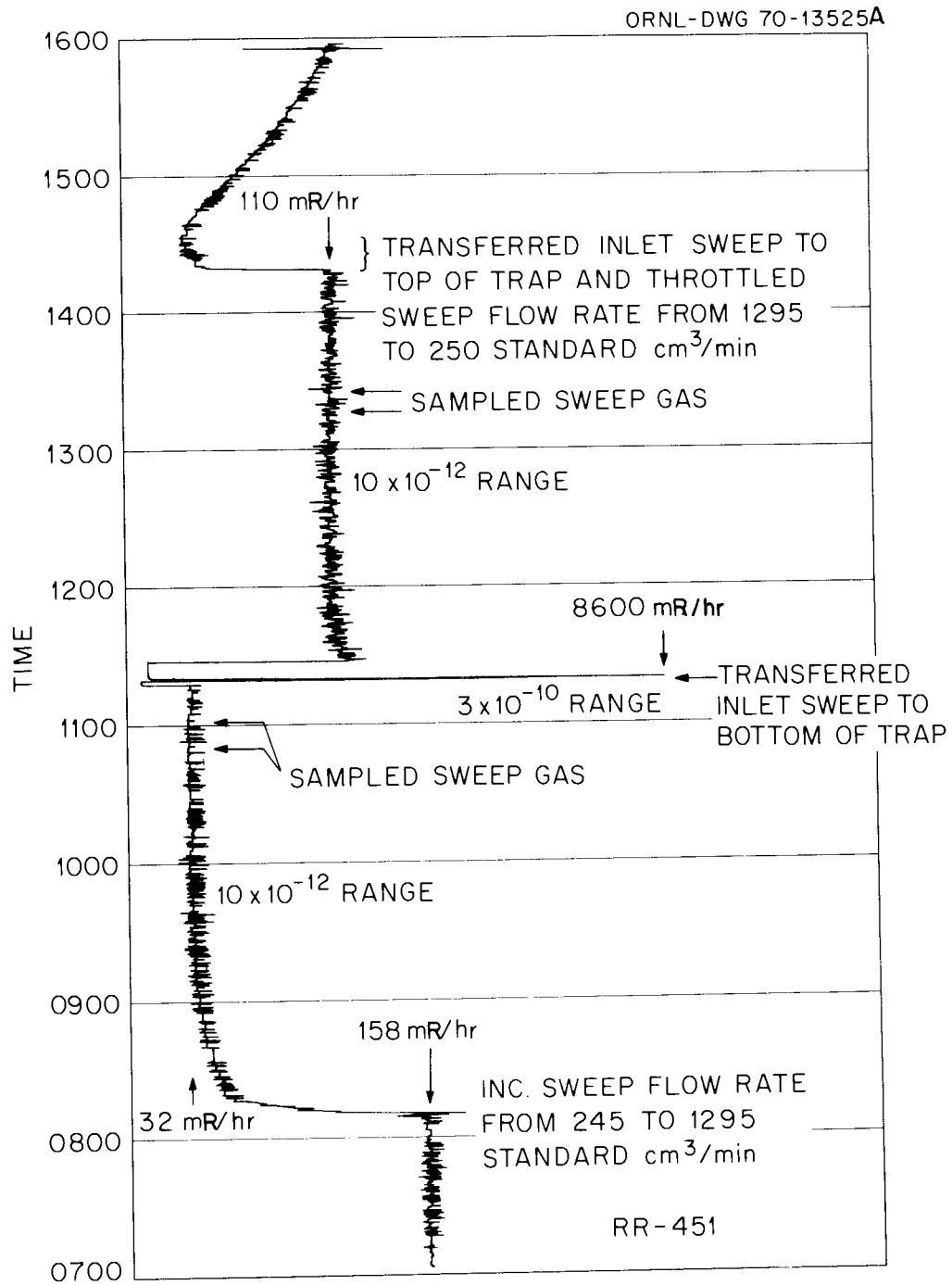


Fig. 21. Effluent sweep line activity while sampling capsule GB-9 sweep gas on July 9, 1970 ( $1 \text{ cm}^3 = 0.061 \text{ in.}^3$ ).

to a steady level of 110 mR/hr. After the reading was steady for about 1 1/2 hr, two samples of the blanket-region effluent were taken. With sampling completed, the inlet sweep was transferred back to the top of the trap, and the sweep flow rate was throttled from 1295 to 250 cm<sup>3</sup> STP/min.

The general behavior of the activity release from the fuel rod from startup in April 1970 to Jan. 22, 1971 (fuel burnup of ~25 MWd/kg heavy metal) is shown in Fig. 22. Plotted on a common time scale are readings of two of the five thermocouples opposite the fuel region of the rod and data points representing the effluent sweep line activity during periods of steady-state operation with the sweep flow across the top of the trap. The sweep line activity data points are readings of the ionization chamber on the high-pressure section of effluent sweep line normalized to a common sweep flow rate of 250 cm<sup>3</sup> STP/min. Also denoted in Fig. 22 are reactor shutdowns, capsule position adjustments, sweep-gas sampling periods, and special-test periods.

The thermocouple readings plotted in Fig. 22 are from TE-402, the second thermocouple up from the bottom of the fuel column, and TE-413, the uppermost of the five fuel-region thermocouples (see Table 2 for TE locations). Of the five thermocouples, TE-402 and occasionally TE-403 (the next highest thermocouple above TE-402) indicated the location of the peak cladding temperature of the rod. As described in Sect. 5, the peak cladding-OD temperature was estimated and maintained at  $685 \pm 15^\circ\text{C}$  by applying calculated temperature corrections to the five thermocouple readings.

As can be seen in Fig. 22, the release rate of activity from the fuel rod was quite sensitive to operating temperatures. The changes in fuel-rod power and fission-product production rates that accompanied fuel burnup and the occasional small adjustments in capsule position relative to the reactor (change in neutron flux) cannot alone account for the large changes in activity release rates observed.

The reactor shutdowns are also important in interpreting the activity release-rate data. Although the variation in fuel-rod total power during a given fuel loading was small, there was an upward shift and flattening out of the temperature profile over the fueled portion of the rod

CAPSULE OPERATING UNDER THE STEADY-STATE CONDITIONS LISTED IN TABLE 3.  
SWEEP FLOW ACROSS TOP OF TRAP.

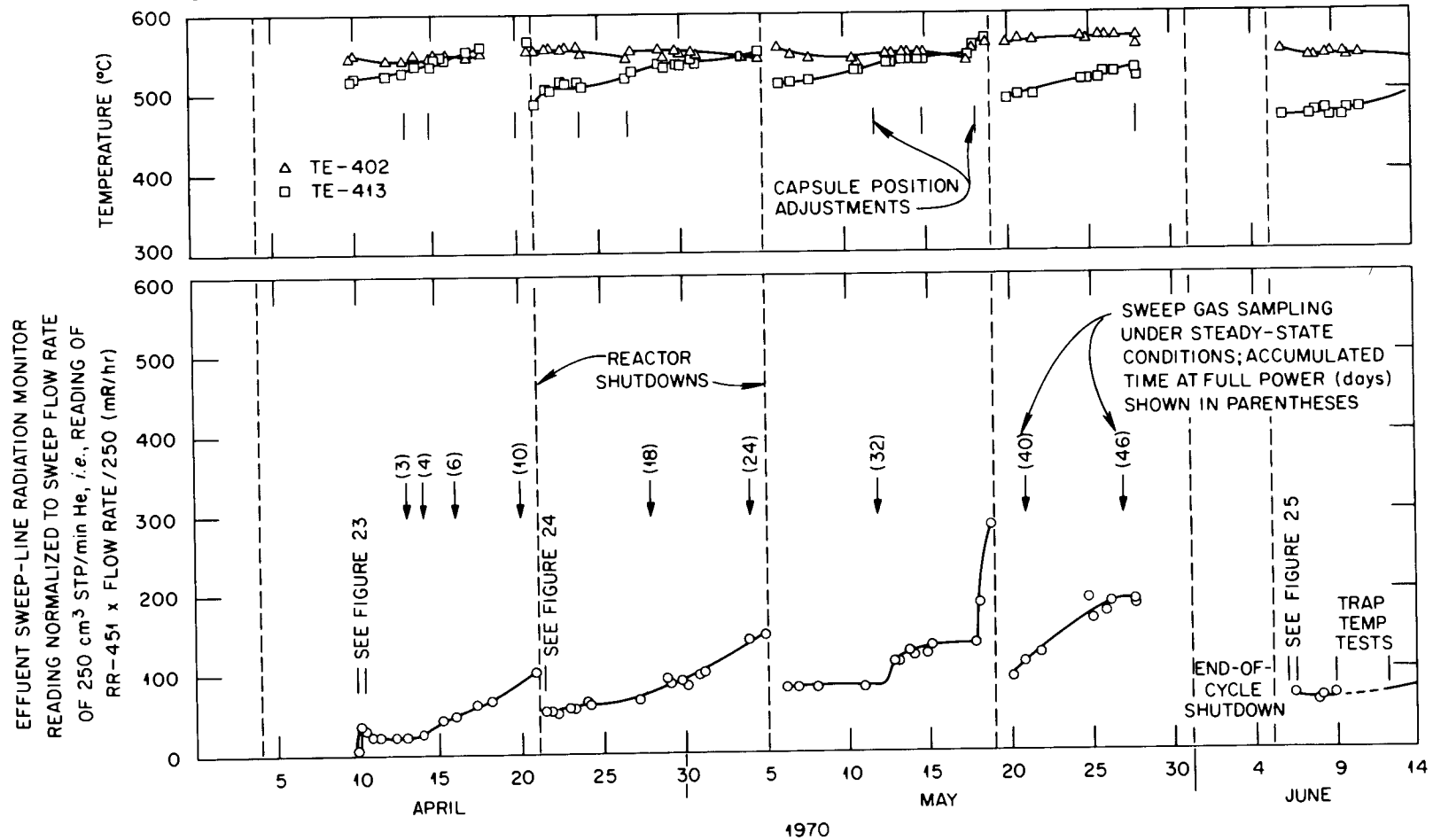


Fig. 22. Activity release from capsule GB-9 during steady-state operation.

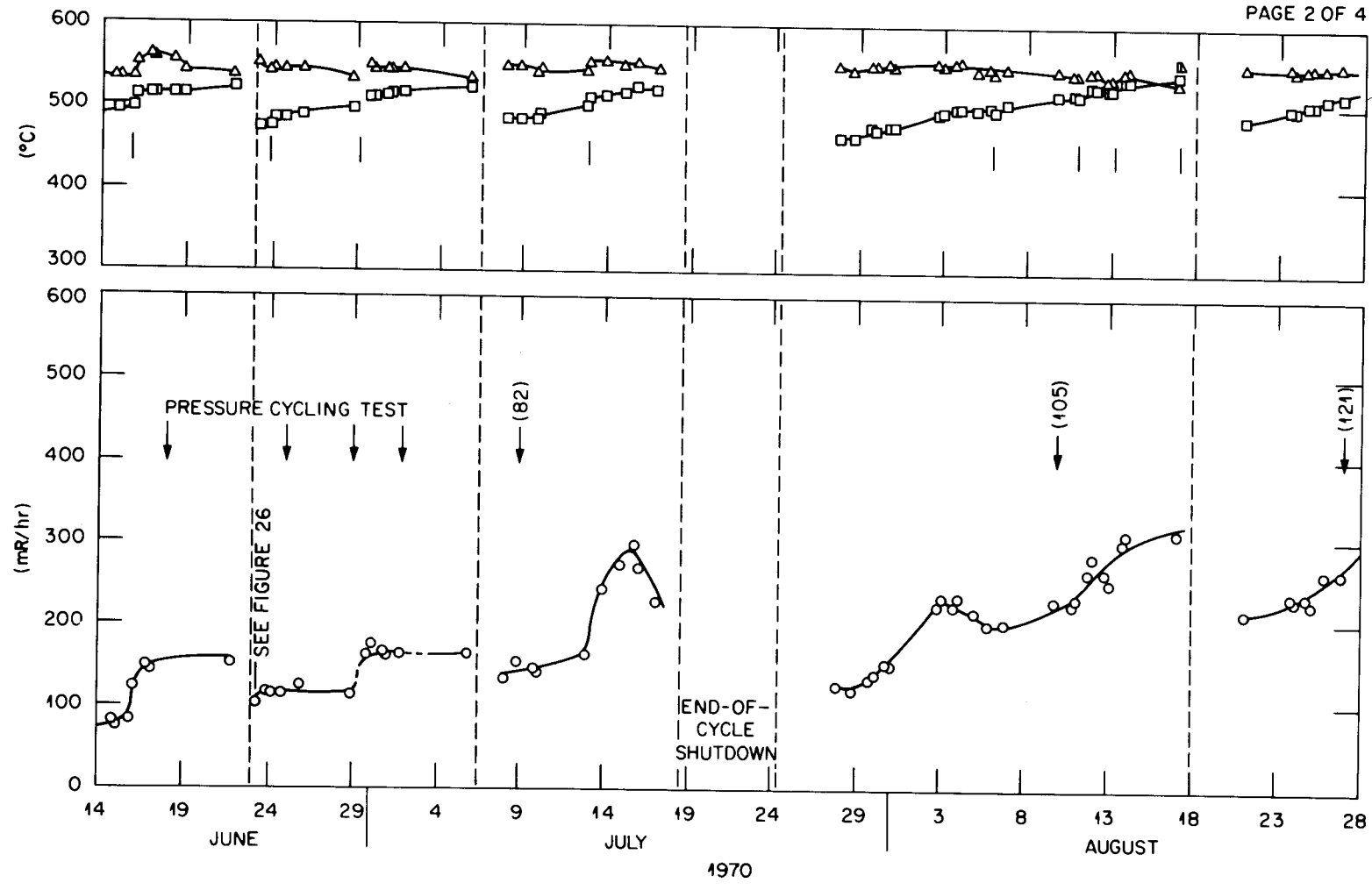


Fig. 22 (continued)

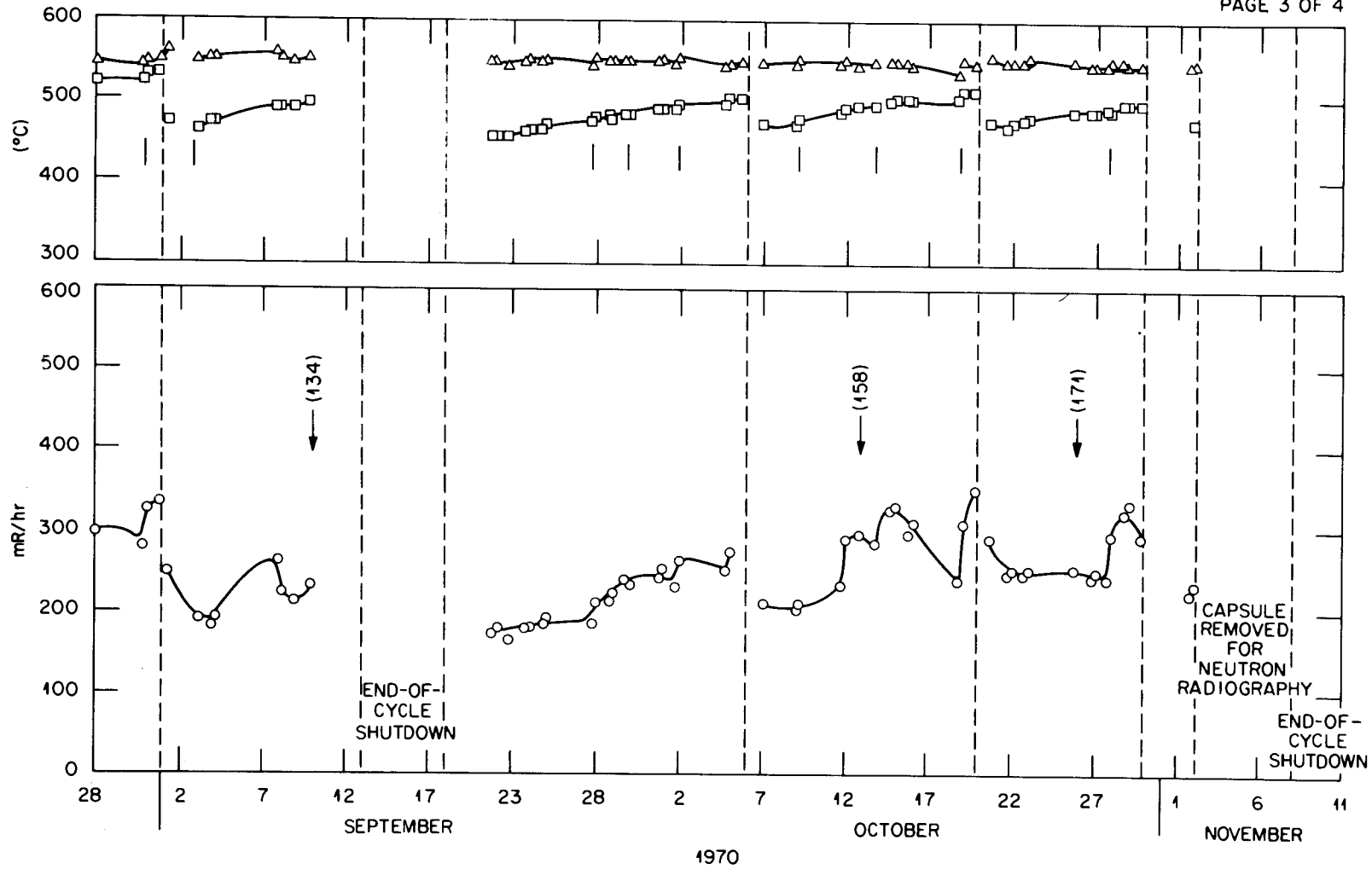


Fig. 22 (continued)

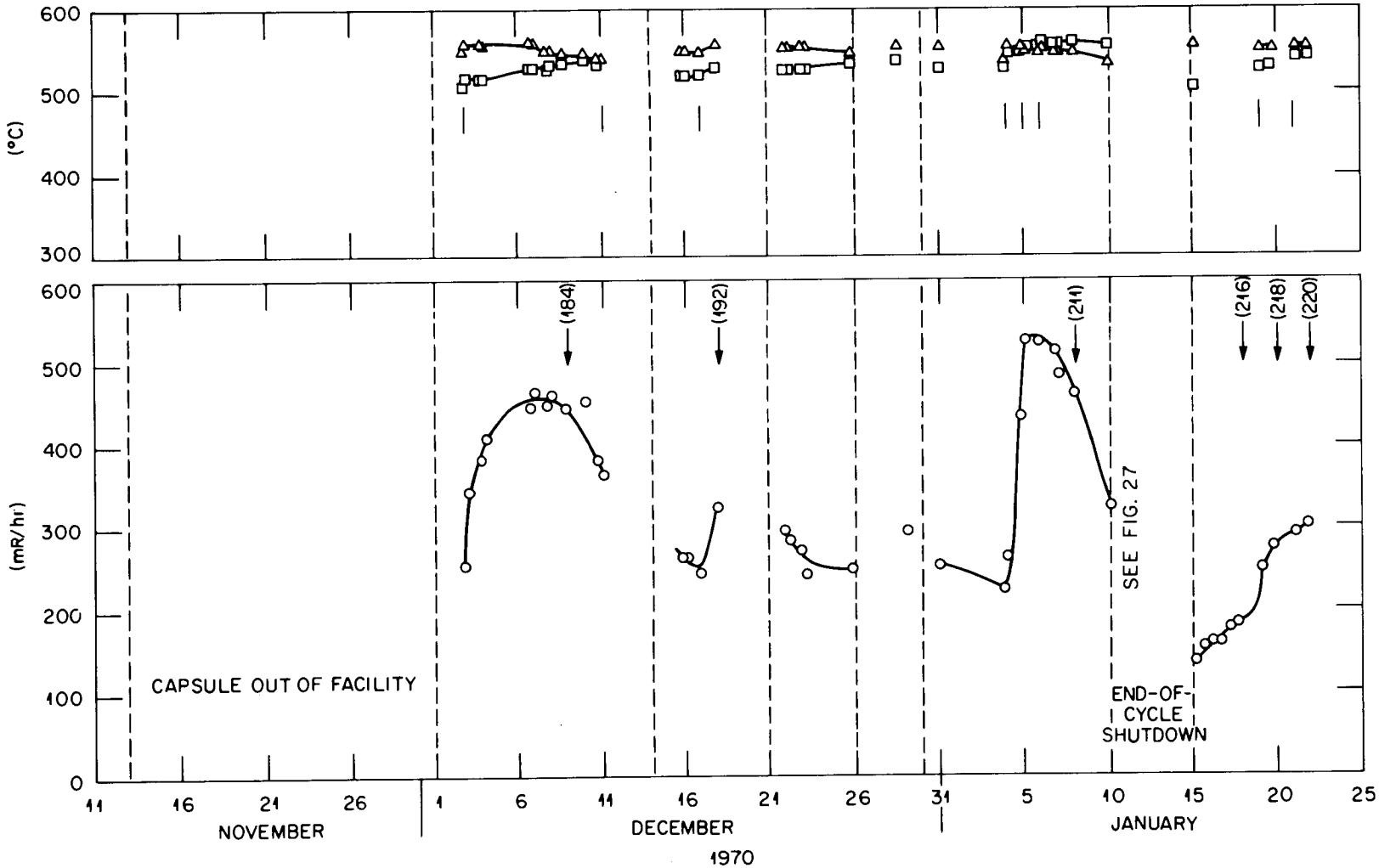


Fig. 22 (continued)

associated with the gradual withdrawal of the reactor control rods. As indicated by TE-413, cladding temperatures near the top end of the fuel column increased by as much as 50°C during a core life. A moderate decrease in cladding temperature near the bottom end of the fuel column was indicated by the lowermost thermocouple (not shown in Fig. 22) and to a lesser extent by TE-402.

The buildup of the activity release rate from the fuel rod following the initial insertion of the capsule from 70 to 100% of full power on Apr. 10, 1970, is shown in Fig. 23. The buildup following several subsequent reactor shutdown periods is shown in Figs. 24 to 27. The periods covered in Figs. 23 to 27 are also denoted in Fig. 22, so that the release-rate behavior following the initial buildup can be seen in each case. Figure 27 also shows the typical behavior of the effluent sweep line activity during a reactor shutdown. Upon shutdown, there was an inflow of clean gas into the rod; at the same time, gaseous activity was swept out of the sweep line, leaving only deposited activity, which gradually decayed.

As indicated by Figs. 23 to 27, there was a rapid initial buildup of the effluent sweep line activity, or activity release rate from the rod, upon startup following a reactor shutdown and/or capsule retraction period. This was followed by the more gradual changes in release rate shown in Fig. 22. The initial buildup took about 8-10 hr after a shutdown period of 1 day or longer.

### 6.3 Steady-State Fission-Gas Release vs Irradiation Time

The steady-state fission-gas release data obtained during the first 220 days of full-power operation to a fuel burnup of ~25 MWd/kg heavy metal are shown for the two sweep flow cases in Figs. 28 and 29. The data points represent the measured release rates of the various isotopes detected in the sweep-gas samples divided by their respective calculated total birth rates in the fuel rod at the time of sampling (R/B). All of these samples were taken with the capsule operating under the nominal steady-state operating conditions listed in Table 3 and in the manner indicated in the preceding section (Fig. 21).

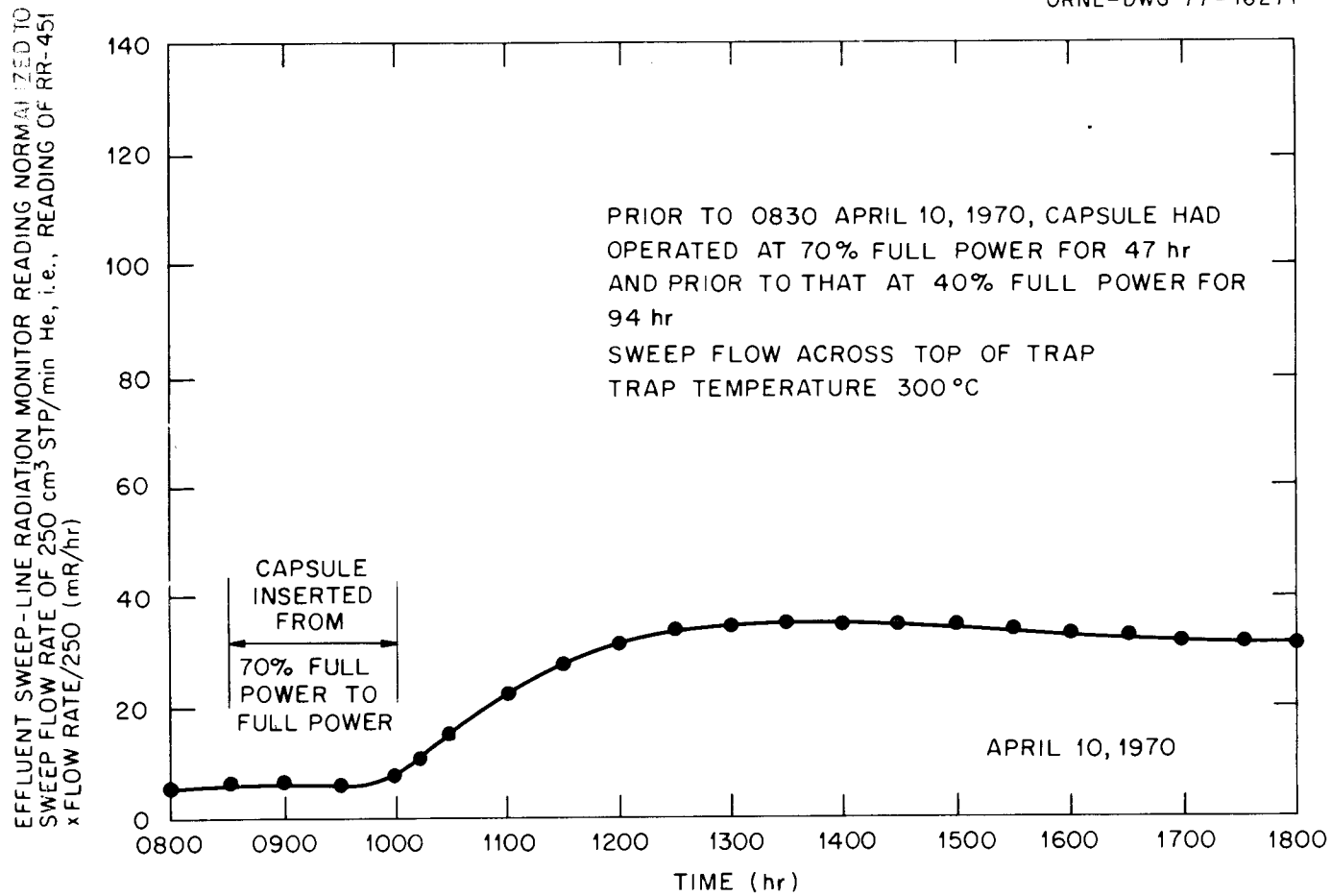


Fig. 23. Buildup of activity release from capsule GB-9 following initial insertion of capsule to full power.

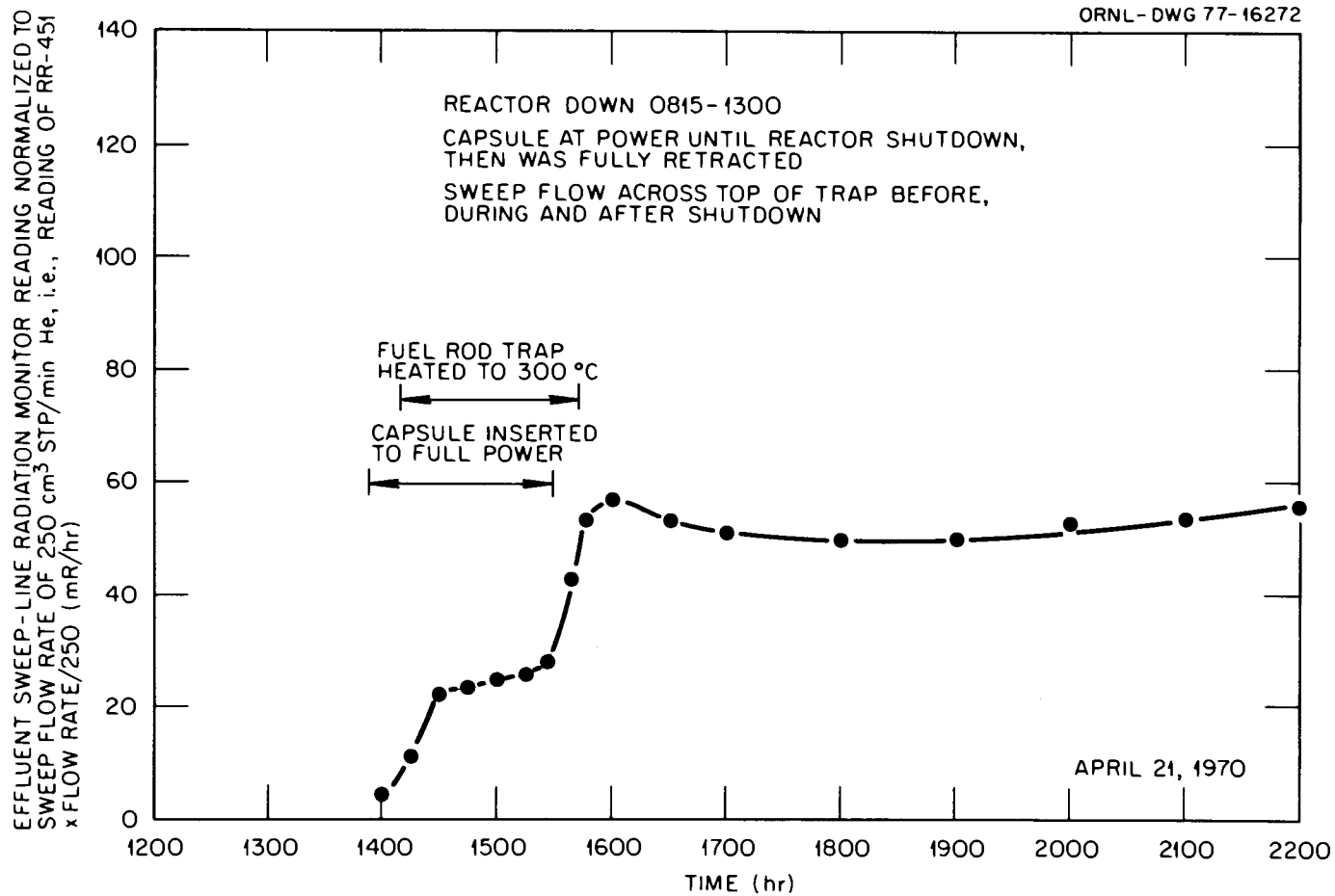


Fig. 24. Buildup of activity release from capsule GB-9 following first reactor refueling shutdown.

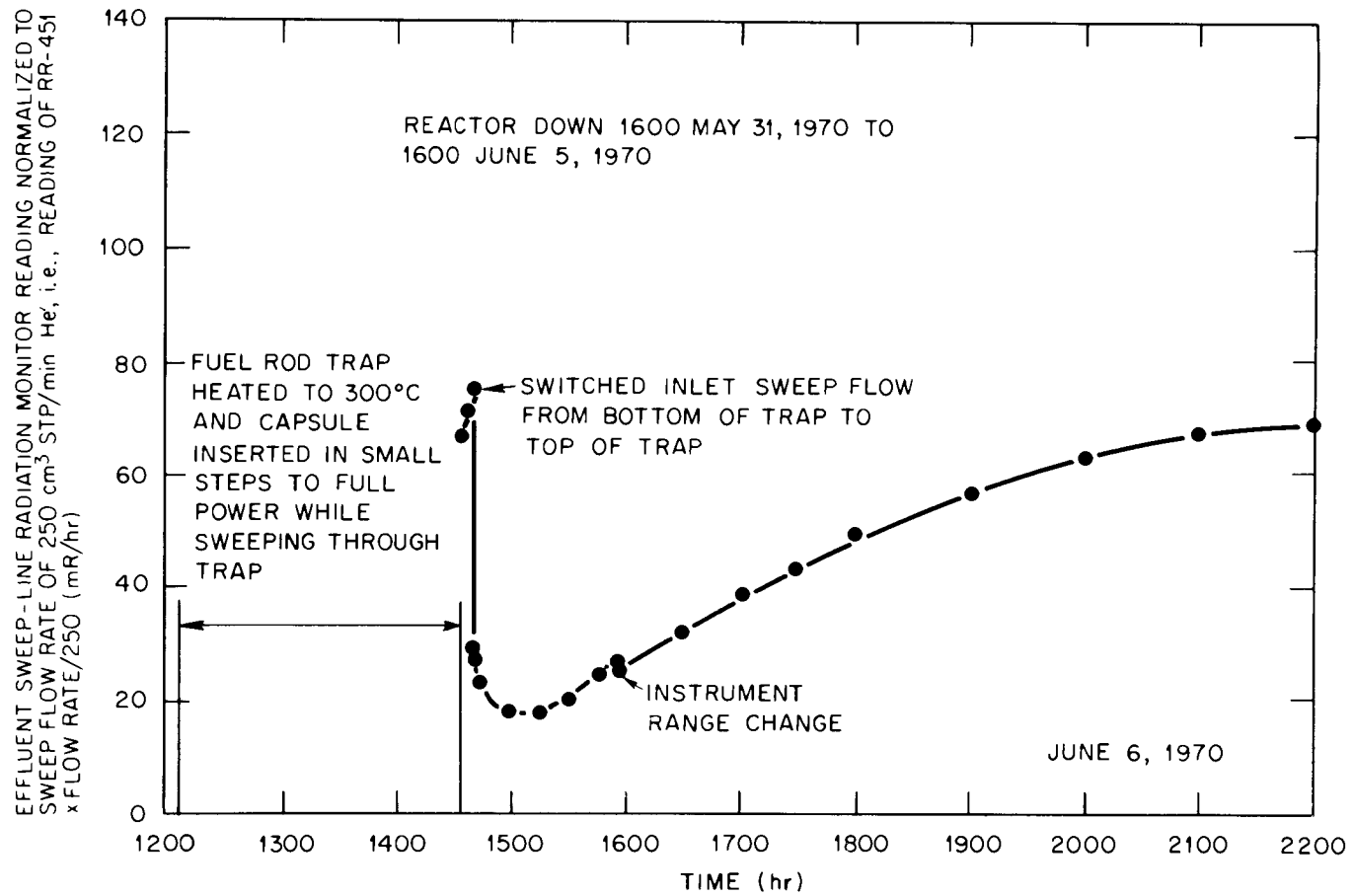


Fig. 25. Buildup of activity release from capsule GB-9 following first end-of-cycle reactor shutdown.

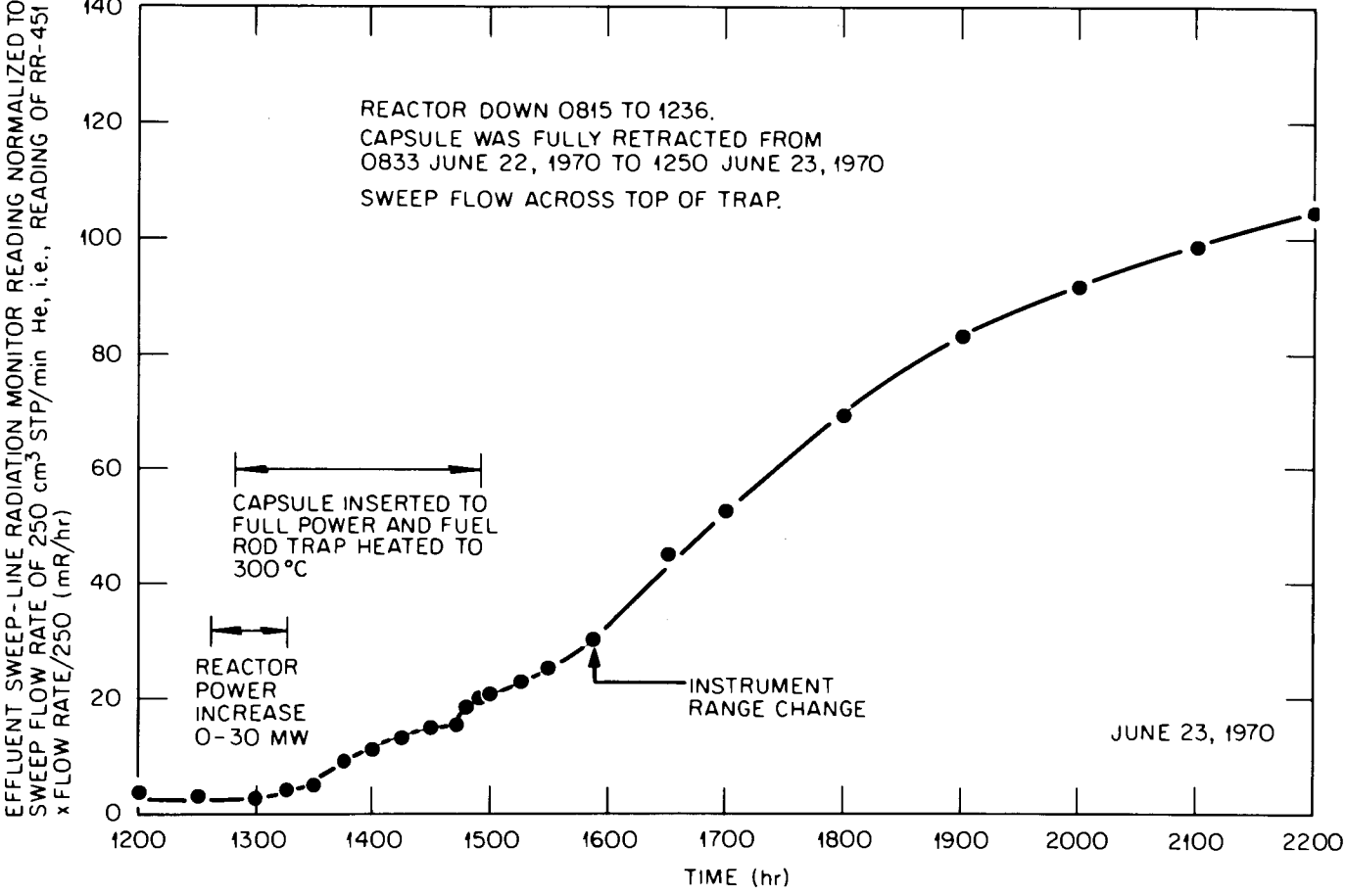


Fig. 26. Buildup of activity release from capsule GB-9 following reactor refueling shutdown on June 23, 1970.

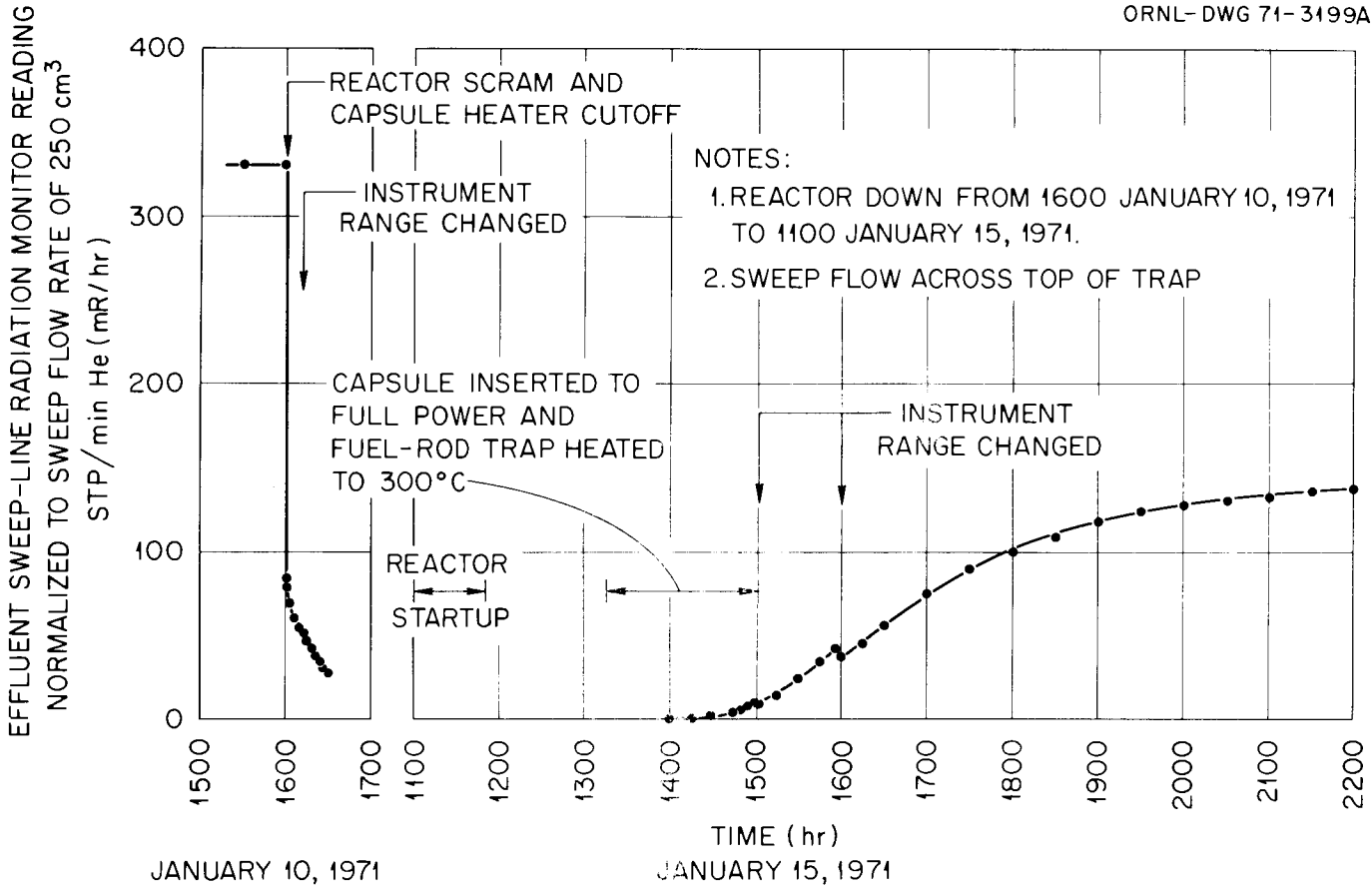


Fig. 27. Capsule GB-9 sweep line activity following reactor shutdown on January 10, 1971, and startup on January 15, 1971.

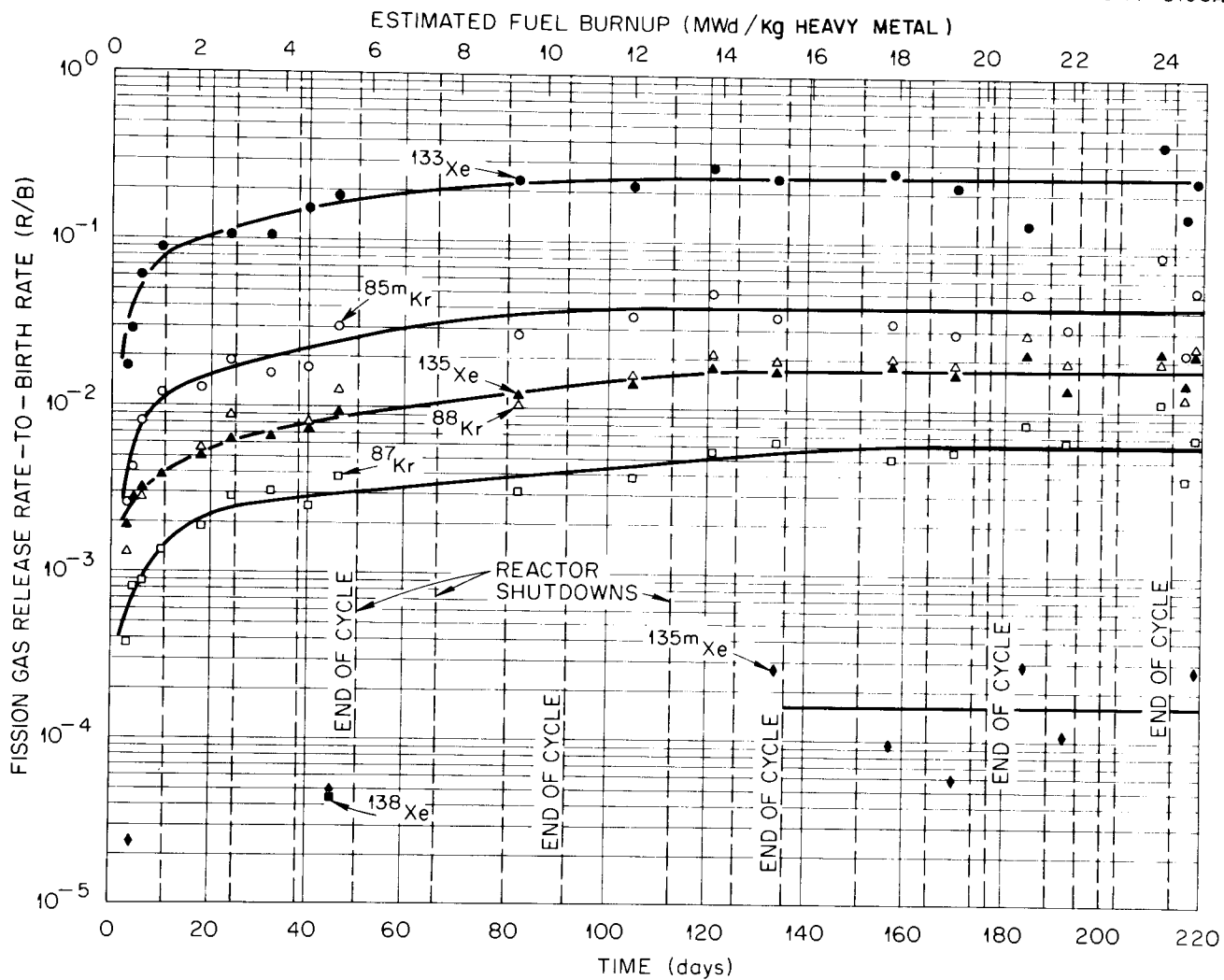


Fig. 28. Steady-state fission-gas release from capsule GB-9 vs time at full power for case of sweep flow across top of trap.

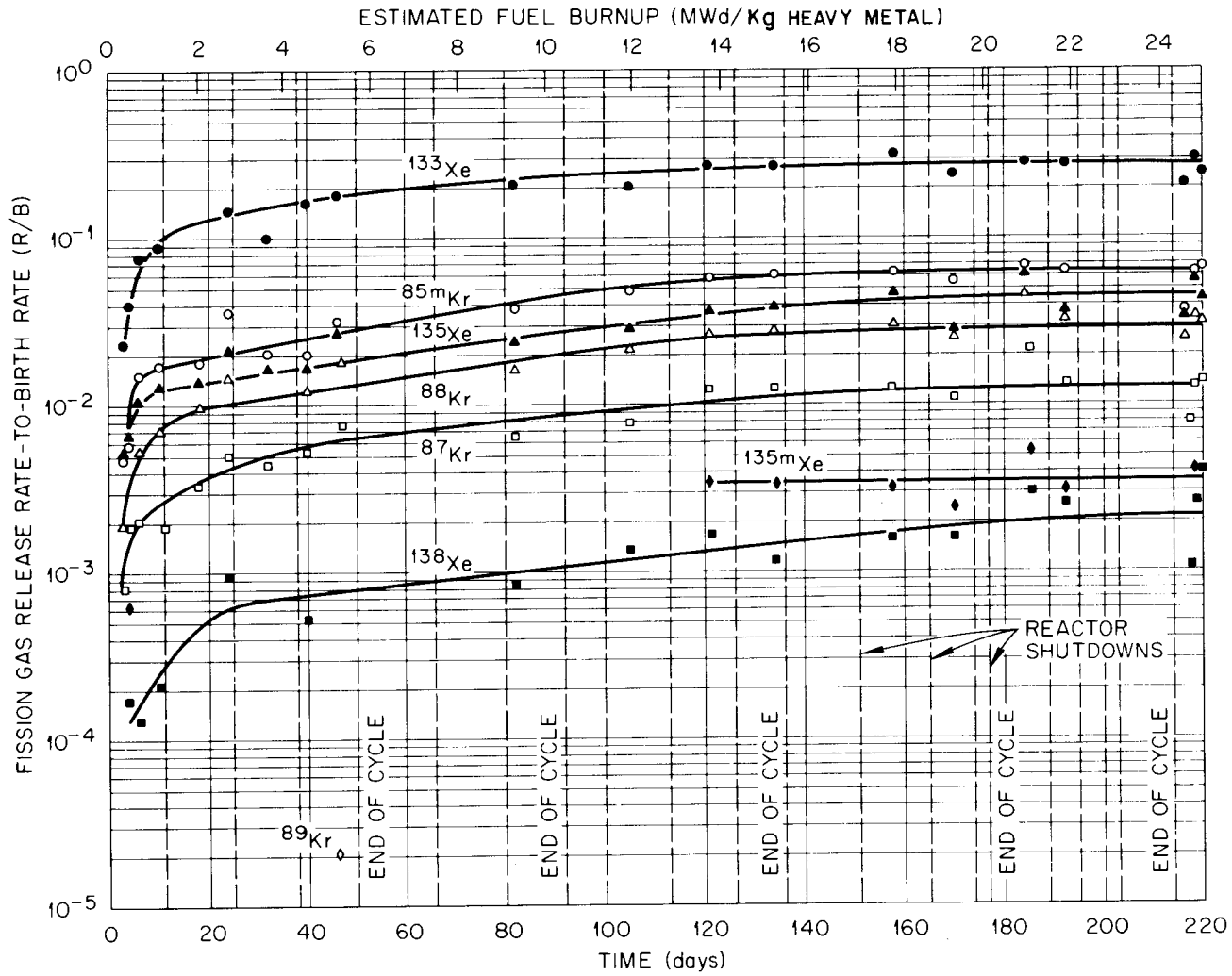


Fig. 29. Steady-state fission-gas release from capsule GB-9 vs time at full power for case of sweep flow through trap.

In reducing the release data to fractional release (or R/B) values, the birth rate B of each isotope was assumed to be at its equilibrium value corresponding to the fuel-rod total power at the time of sampling. The fuel-rod total power at the time of each gas sampling was routinely calculated on the basis of the temperatures indicated by the thermocouples opposite the fueled region of the rod. For the samples represented in Figs. 28 and 29, the calculated values of fuel-rod total power ranged from a low of 11.9 kW for the samples taken after 82 days at full power to a high of 12.5 kW for the samples taken after 46 days at power. Estimated fission-product birth rates corresponding to a fuel-rod total power of 12.15 kW are listed below for the various noble gas isotopes detected in the samples:

Isotope	Birth rate (atoms/sec)
$^{85m}\text{Kr}$	$3.34 \times 10^{12}$
$^{88}\text{Kr}$	$8.21 \times 10^{12}$
$^{87}\text{Kr}$	$5.90 \times 10^{12}$
$^{89}\text{Kr}$	$9.52 \times 10^{12}$
$^{133}\text{Xe}$	$2.85 \times 10^{13}$
$^{135}\text{Xe}$	$2.89 \times 10^{13}$
$^{138}\text{Xe}$	$1.71 \times 10^{13}$
$^{135m}\text{Xe}$	$9.69 \times 10^{12}$

As may be seen in Figs. 28 and 29, the steady-state fractional release values increased rapidly at first and then showed a steady slow increase to  $\sim 10$  Mwd/kg heavy metal burnup, where they began leveling off. After leveling off, the steady-state fractional release values remained approximately constant for the remainder of the irradiation to 54 Mwd/kg heavy metal burnup.

It should be noted that the curves drawn through the data points of Figs. 28 and 29 do not necessarily reflect the behavior of the fission-gas release during the periods between data points. The curves are intended to show only the overall trend in fission-gas release with time indicated by the gas-sample results.

All the release data shown in Figs. 28 and 29, with the exception of those at 4 and 46 days at power, were obtained by counting the samples with the ORR poolside-facility gamma-ray spectrometer which has a 7.62 cm by 7.62 cm (3 in. by 3 in.) NaI detector and a 512-channel analyzer. The samples were normally counted at 10 keV per channel. Some samples were counted at 5 and 2.5 keV per channel in an attempt to obtain better resolution, especially for  $^{89}\text{Rb}$ . However, a satisfactory count of  $^{89}\text{Rb}$  (from which the release of 3.2-min  $^{89}\text{Kr}$  could be determined) could not be obtained with the NaI detector because of interference from other activity.

The samples taken after 4 and 46 days at power were submitted to personnel of the ORNL Analytical Chemistry Division for counting with a 6-cm<sup>3</sup> planar Ge(Li) detector and 400-channel analyzer. Those results were in reasonably good agreement with the NaI detector results for the longer-lived fission gases and gave  $^{89}\text{Kr}$  R/B values for the case of sweep flow through the trap of  $\sim 9.4 \times 10^{-6}$  and  $2.0 \times 10^{-5}$  after 4 and 46 days at full power, respectively. For the case of sweep flow across the top of the trap, the  $^{89}\text{Kr}$  fractional release, or R/B, was too low to determine after 4 days at power and  $< 5.0 \times 10^{-6}$  after 46 days at power.

The effectiveness of the fuel-rod charcoal trap in reducing the steady-state release rates of the various isotopes is perhaps better shown by the release-rate ratios given in Table 4. These data show the effectiveness of the charcoal trap to be a function of the half-life of the isotope, as expected, and the values are reasonably close to those predicted. The better-than-predicted trap performance for the holdup of  $^{135}\text{Xe}$  was probably due to burnup of the  $^{135}\text{Xe}$  in the high thermal-neutron flux in the trap, which in effect reduced its half-life.

#### 6.4 Fission-Gas Release During Slow Pressure Cycling

The results of several slow pressure cycling tests conducted in June and July 1970 (burnup level of about 7.5 MWd/kg) are summarized in Fig. 30. Each of these tests was conducted with the sweep flow across the top of the trap at all times. Several days were allowed before the start of each test for fission products to reach steady-state levels.

Table 4. Effectiveness of fuel-rod trap in reducing the steady-state fission-gas release from capsule GB-9

Time at full power (days)	Ratio of fission-gas release rate with sweep flow across top of trap to that with sweep flow through trap							
	4.4-hr $^{85}\text{mKr}$	2.8-hr $^{88}\text{Kr}$	1.3-hr $^{87}\text{Kr}$	3.2-min $^{89}\text{Kr}$	5.27-day $^{133}\text{Xe}$	9.13-hr $^{135}\text{Xe}$	17.0-min $^{138}\text{Xe}$	15.3-min $^{135}\text{mXe}$
3	0.54	0.71	0.47		0.79	0.38		
4	0.74	0.72	0.43		0.71	0.41	0.036	0.038
6	0.53	0.53	0.44		0.81	0.30		
10	0.69		0.74		0.99	0.30		
18	0.68	0.58	0.52			0.37		
24	0.52	0.61	0.58		0.73	0.30		
32	0.76		0.68		1.0	0.41		
40	0.85	0.65	0.48		0.97	0.44		
46	0.95	0.72	0.51		1.0	0.35	0.040	
82	0.74	0.65	0.48		1.1	0.50		
105	0.75	0.73	0.49		1.1	0.49		
121	0.73	0.79	0.45		1.0	0.46		
134	0.59	0.70	0.51		0.89	0.43		0.082
158	0.54	0.61	0.41		0.85	0.41		0.030
171	0.53	0.66	0.51		0.91	0.59		0.025
184	0.75	0.64	0.39		0.46	0.34		0.054
192	0.49	0.60	0.48			0.37		0.034
216	0.59	0.49	0.50		0.69	0.39		
218	0.86	0.70	0.53		0.80	0.38		0.065
Average	0.68	0.65	0.51		0.87	0.40	0.038	0.047
Predicted (Ref. 20)	0.71	0.60	0.38	$10^{-4}$	0.98	0.81	0.10	0.10

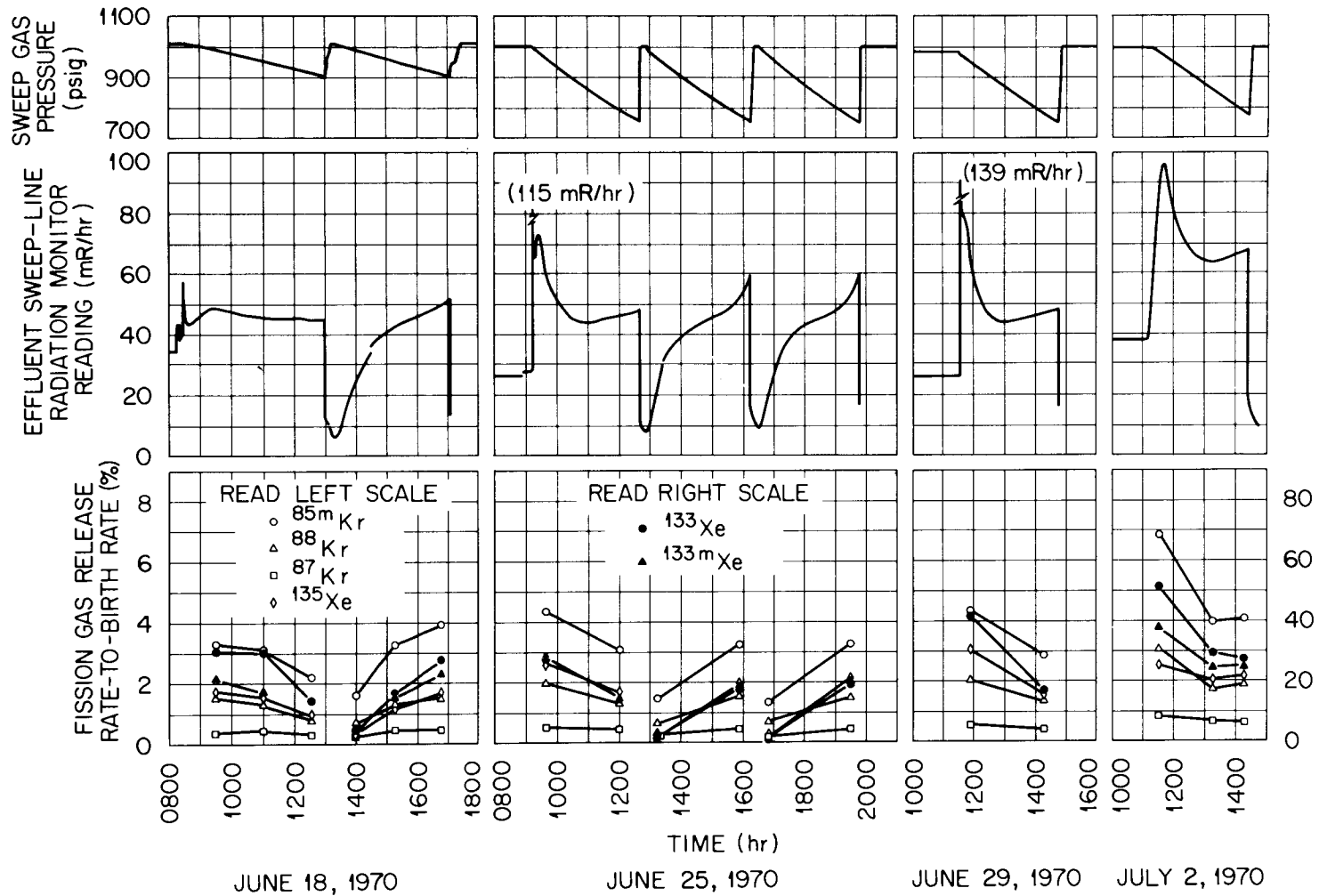


Fig. 30. Activity release from capsule GB-9 during slow pressure cycling tests conducted on June 18, 25, and 29 and July 2, 1970 (1 psi = 6895 Pa).

During each of the depressurizations, the volumetric flow rate (actual  $\text{cm}^3/\text{min}$ ) of sweep gas past the radiation monitor (on the high-pressure section of the effluent line) was approximately constant at  $19 \text{ cm}^3/\text{min}$ . This was a consequence of the manner in which the depressurizations were conducted (approximately exponential decay of pressure at pressure decay half-lives of 23.4 and 8.5 hr for the two different depressurization rates, respectively). The response of the radiation monitor can therefore be interpreted, without flow-rate corrections, as changes in the gross gamma activity release rate from the fuel rod, provided deposited activity on the sweep line was small compared with the gaseous activity.

During the first few depressurizations, it was difficult to start the pressure decay smoothly. The activity spikes at the start of the tests on June 18, 25, and 29 were caused by small pressure fluctuations.

The R/B results obtained during the pressure-cycle tests appear to be consistent with the on-line radiation monitor readings, with the exception of the third set of R/B results on June 18. This set of R/B results appears to be low compared with the radiation monitor readings.

The  $^{138}\text{Cs}$  activity found in the samples taken on June 18 was too low to count except for the first sample set. In each of the depressurizations at the higher-pressure decay rate,  $^{138}\text{Xe}$  release (determined from counting  $^{138}\text{Cs}$ ) was low early in the depressurization but increased to an appreciably higher level (R/B of  $\sim 1.5 \times 10^{-4}$ ) by the latter half of the depressurization.

The activity peaking that occurred early in the first cycle of each test is believed to have been caused primarily by displacement of the concentrated gaseous activity in the trap at the start of depressurization by a mixture of the gas expanding from the lower inlet sweep line [ $\sim 68 \text{ cm}^3$  ( $\sim 4.1 \text{ in.}^3$ )] and from the fuel-rod free volume below the trap [ $\sim 2.4 \text{ cm}^3$  ( $\sim 0.15 \text{ in.}^3$ )].

The steady increase in line activity that followed the activity peaks in the case of the latter tests at the higher pressure-decay rate may have been caused by increased release of the shorter-lived fission gases ( $^{135\text{m}}\text{Xe}$  and  $^{138}\text{Xe}$ ) from the rod during the latter part of the depressurizations and buildup of  $^{138}\text{Cs}$  deposition activity.

Soon after the start of the pressurization half of each pressure cycle, the radiation monitor reading dropped quickly to a level between 10 and 20 mR/hr as a result of the inflow of clean gas into the fuel rod. The subsequent decay of the radiation monitor reading indicated that this level of activity was deposition activity on the line at that particular time. Under the conditions of the test, the deposition activity was believed to be primarily  $^{88}\text{Rb}$  and  $^{138}\text{Cs}$ .

In general, the release behavior during these slow pressure cycling tests, with the sweep flowing across the top of the trap, agreed with expectations once the flow conditions within the fuel rod were evaluated. However, there is still some question as to what caused the line activity to increase so sharply near the end of the last two of the three consecutive depressurizations on June 25, 1970. Had one of these last two depressurizations been continued to a lower pressure level, a satisfactory explanation may have become obvious. One possibility is that the activity that was pushed back into the lower inlet sweep line during the repressurization part of the cycle began reappearing and contributing to the activity release of the subsequent depressurization.

#### 6.5 Correlation of Effluent Sweep Line Activity Data and Sweep-Gas Sample Data

A limited number of dose-rate calculations were made in an attempt to correlate the radiation monitor data and the sweep-gas sample data and to determine what the radiation monitors on the effluent sweep line were seeing under the various capsule operating conditions. In these calculations, the gas sample release-rate data were used to estimate dose rates at the radiation monitor for comparison with its actual response. Such calculations were made with the gas sample results obtained during the slow pressure cycling tests (Fig. 30). The calculated dose rates, normalized to the radiation monitor reading at the time of the first sample set, are shown by the starred points in Fig. 31. The gas sample data were found to be consistent with the radiation monitor data except for the third set of R/B results. Since no error could be found in the R/B calculations for that sample, an error in sampling or counting was suspected.

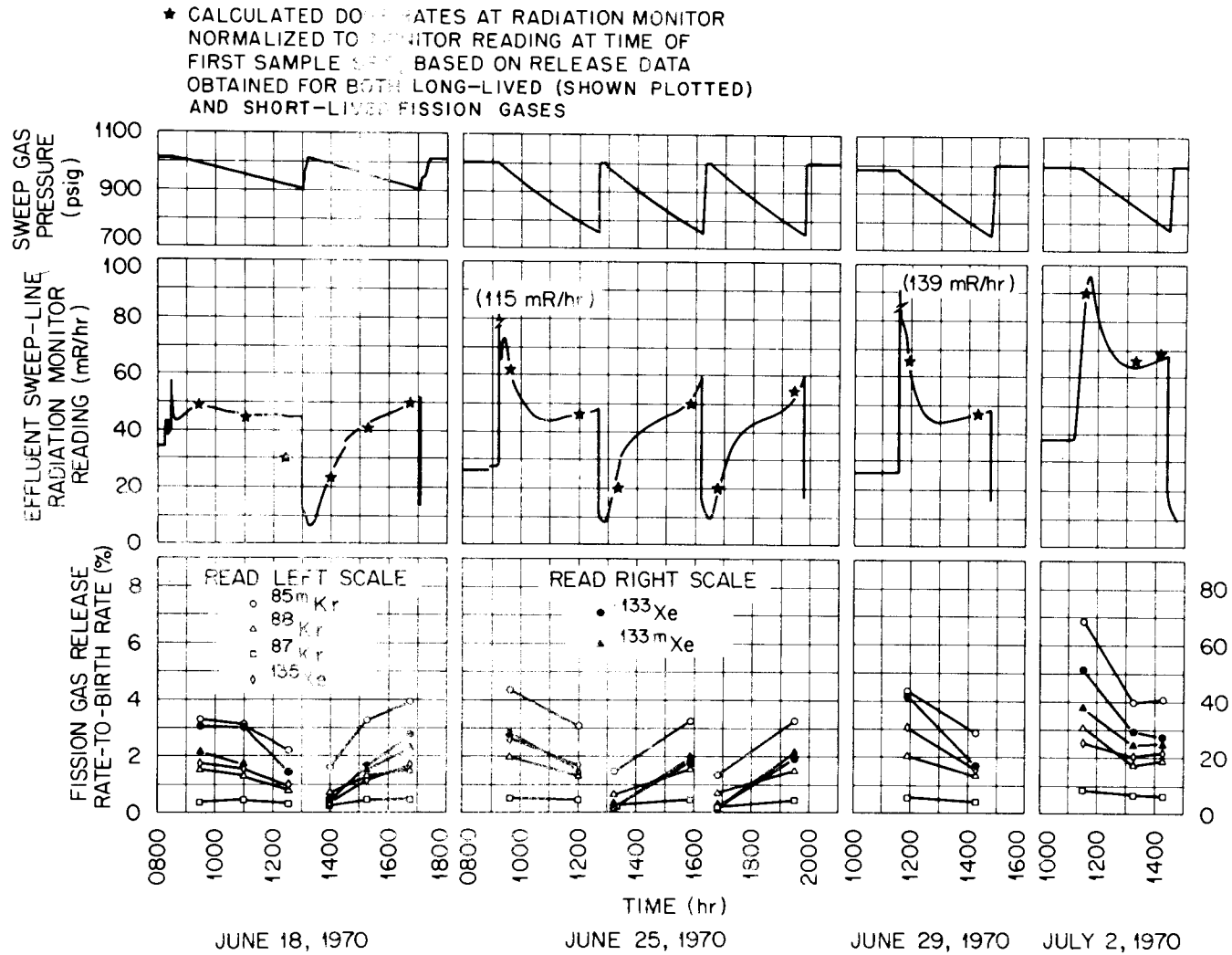


Fig. 31. Activity release from capsule GB-9 during slow pressure cycling tests conducted on June 18, 25, and 29 and July 2, 1970 (1 psi = 6895 Pa).

Similar dose-rate calculations made for the case of sweep flow across the top of the trap under the normal steady-state operating conditions have indicated the isotopic contributions to the total radiation monitor readings under these conditions to be roughly as follows:  $^{88}\text{Kr}$ ,  $\sim 58\%$ ;  $^{88}\text{Rb}$  deposition,  $\sim 13\%$ ;  $^{87}\text{Kr}$ ,  $\sim 8\%$ ;  $^{135}\text{Xe}$ ,  $\sim 8\%$ ;  $^{85\text{m}}\text{Kr}$ ,  $\sim 4\%$ ; and lesser percentages for  $^{135\text{m}}\text{Xe}$ ,  $^{138}\text{Cs}$  deposition,  $^{133}\text{Xe}$ , and  $^{133\text{m}}\text{Xe}$ . In the case of sweep flow through the trap, the release of short-lived fission gases was much higher, and calculations indicated that  $^{138}\text{Cs}$  deposition alone accounted for about one-third of the total monitor reading.

As can be seen in Figs. 28 and 29, there is significant scatter in the gas sample R/B data obtained as a function of time at the normal steady-state operating conditions. For comparison with Fig. 28, values (from Fig. 22) of effluent sweep-line activity immediately preceding the steady-state gas-sampling periods are plotted in Fig. 32. These data show about the same scatter as the R/B results and indicate that most of the scatter in the R/B results is not associated with measurement error, but rather with relatively small variations in the normal operating conditions. To better understand the release behavior, special tests were conducted to measure the steady-state release as a function of the temperature level of the electrically heated charcoal trap and upper blanket region and as a function of fuel-region power (and temperature). The results of these special tests are summarized in the next two sections.

#### 6.6 Fission-Gas Release vs Charcoal Trap Temperature

Special tests were conducted to determine the effect of temperature level of the fuel-rod charcoal trap and upper blanket region on fission-gas release. During the week of June 8, 1970, sets of sweep-gas samples were taken at fuel-rod trap temperatures of 200, 250, and 300°C. However, the sample results were erratic — perhaps caused in part by a short waiting time of only 1 day of steady-state operation between each step increase in temperature. There also appeared to be errors in sampling and/or counting some of these samples. Several minor modifications had

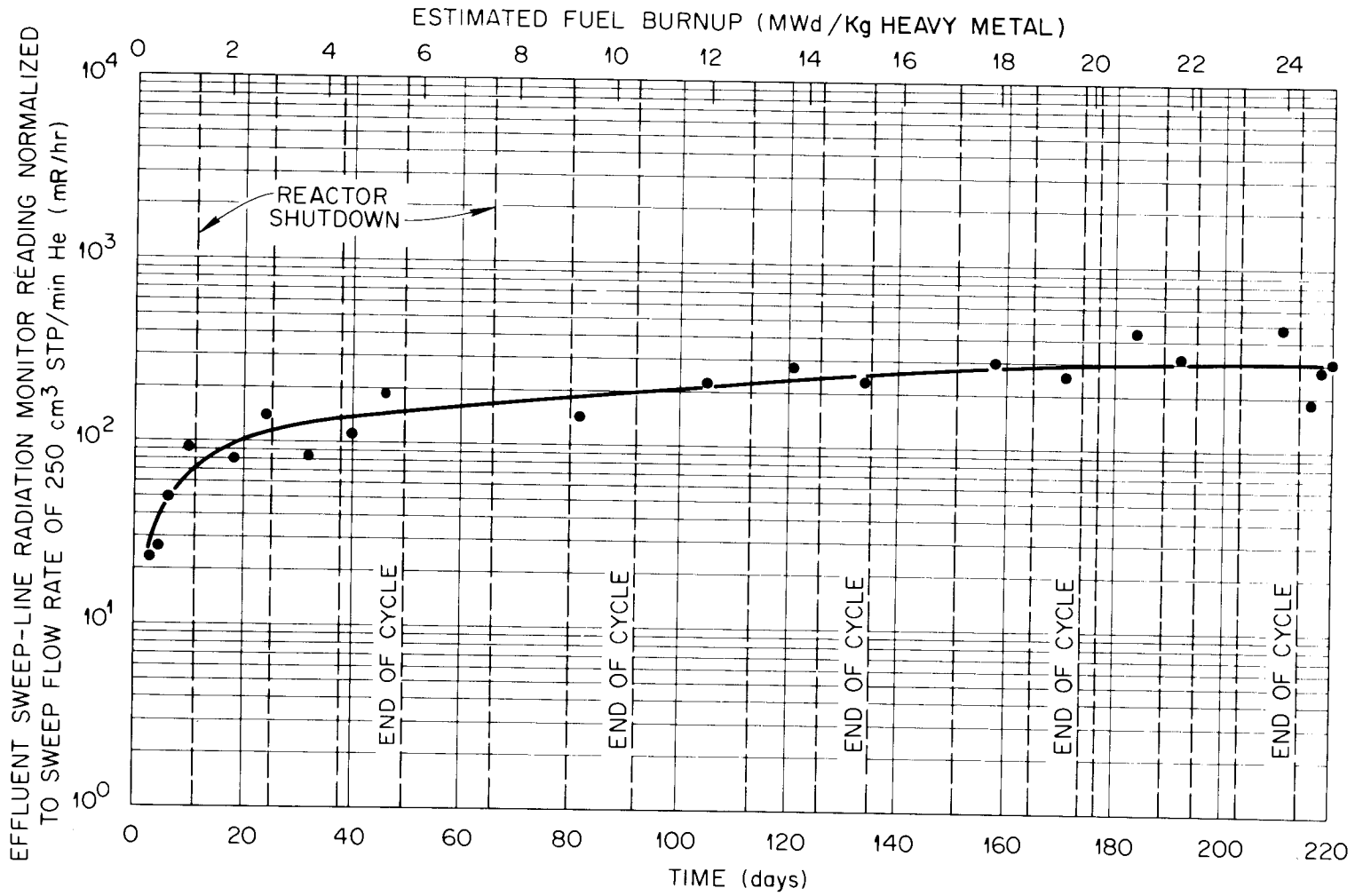


Fig. 32. Capsule GB-9 effluent sweep-line activity preceding steady-state gas-sampling periods.

been made to the sampling system immediately prior to the test, but this should not have caused a problem. A second trap temperature test was performed later in the irradiation in which more time was allowed to reach equilibrium at each temperature level.

The second trap temperature test was conducted the week of May 10, 1971, at a fuel burnup level of  $\sim 35$  MWd/kg heavy metal. In this test, steady-state fission-gas release rates were measured at charcoal trap temperatures of 200, 300, and 400°C while holding the fuel-region peak power constant at  $\sim 48.6$  kW/m (14.8 kW/ft). The estimated temperature profiles existing along the hot side of the rod (the side facing the reactor) during the test are shown in Fig. 33. The results of the gas-release measurements are shown in Fig. 34. The effluent sweep line activity levels indicated by the radiation monitors were reasonably consistent with the gas-sample results; in going from 200 to 400°C trap

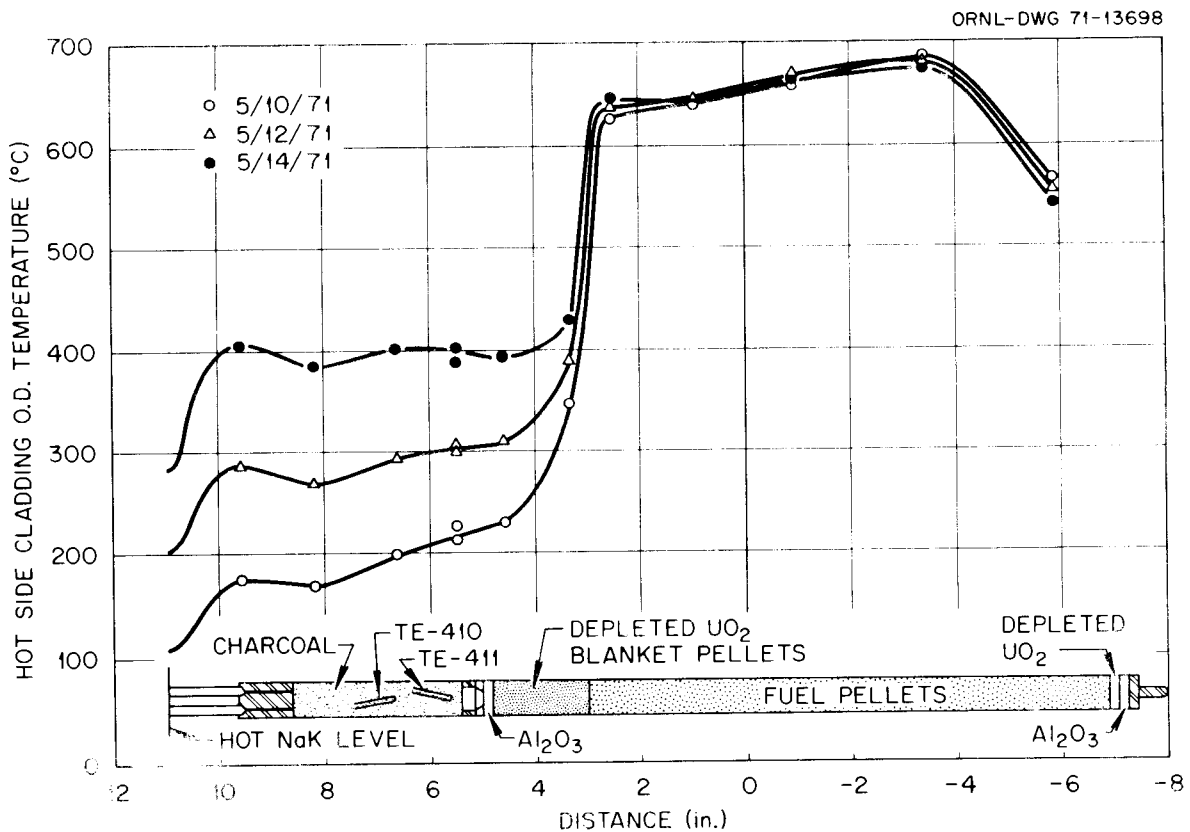


Fig. 33. Axial temperature profiles during capsule GB-9 release vs trap temperature test conducted May 10-14, 1971 (1 in. = 2.54 cm).

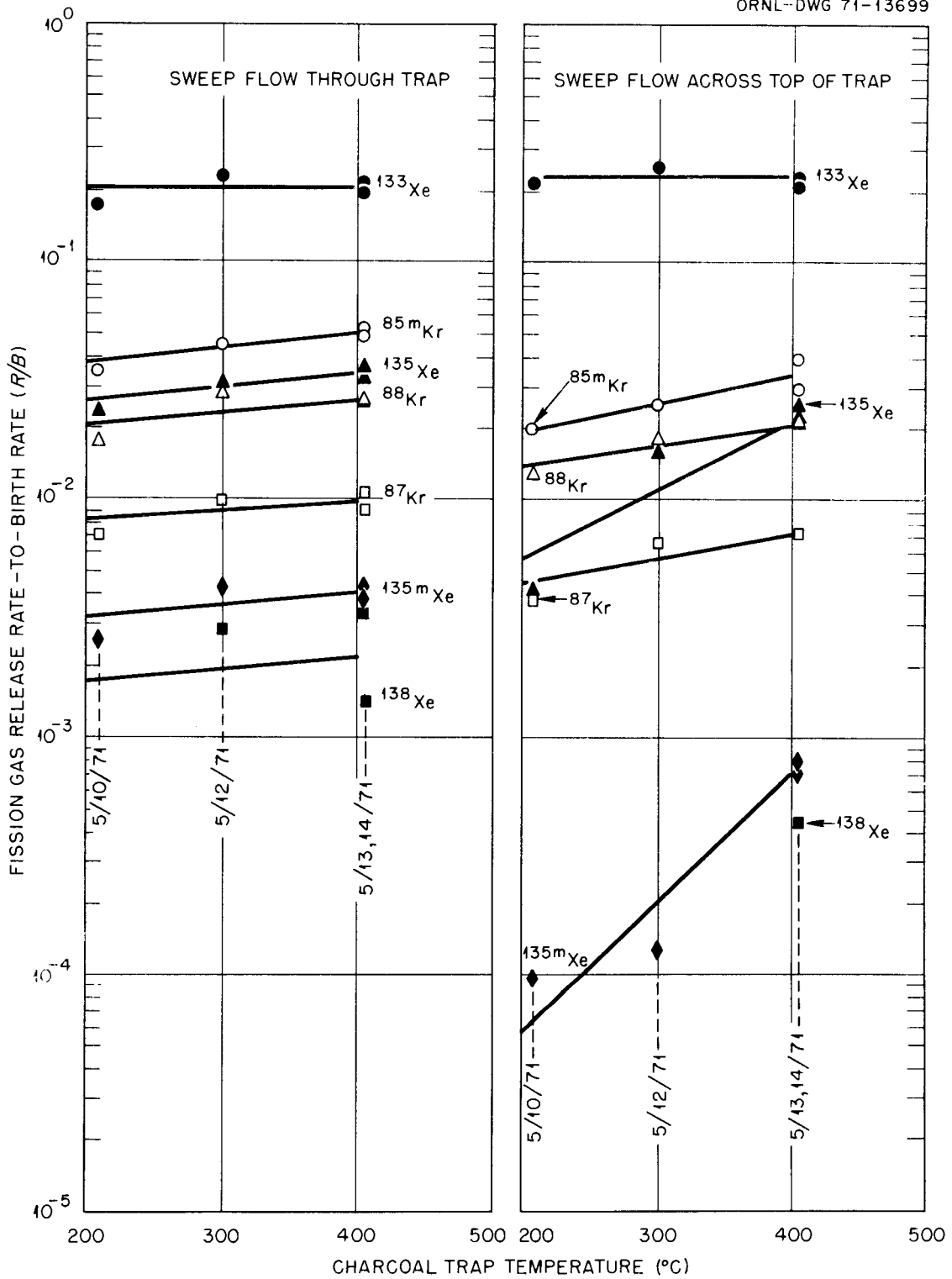


Fig. 34. Steady-state fission-gas release from capsule GB-9 during release vs trap temperature test conducted May 10-14, 1971.

temperature, the line activity increased by a factor of 2 for the case of sweep flow across the top of trap and by only 25% for the case of sweep flow through the trap.

### 6.7 Fission-Gas Release vs Fuel-Rod Power and Temperature

In both the GB-9 and GB-10 fuel-rod irradiations, the fuel-region power and resultant temperature could be varied over a wide range by adjusting the capsule's distance from the reactor core. There was no provision made for varying the fuel-region cladding temperature other than by varying the fuel-region power. Therefore, fuel-region power and cladding temperature are directly related to each other in these experiments.

Steady-state fission-gas release was measured as a function of fuel-rod power and temperature in special tests conducted May 19-25, 1971 (fuel burnup level of  $\sim 36$  MWd/kg heavy metal) and July 26-August 2, 1971 (burnup level of  $\sim 43$  MWd/kg heavy metal). These tests were conducted at peak cladding-OD temperatures ranging from 550 to 685°C [fuel-rod peak linear power levels ranging from 38.2 to 48.6 kW/m (11.6 to 14.8 kW/ft)] while holding the charcoal trap temperature constant at 300°C. The estimated temperature profiles existing along the hot side of the rod (the side facing the reactor) during the tests are shown in Figs. 35 and 36.

It is important to note the difference between the temperature patterns of the two tests. The temperature of the upper portion of the fuel region relative to the peak temperature was lower in the first test (Fig. 35) than in the second one (Fig. 36). The second test was conducted much closer to the end of a reactor core life than was the first test. There was an upward shift and flattening out of the temperature profile associated with the gradual withdrawal of the reactor control rods during the life of each core loading.

The gas-sample results and the indicated sweep line activity levels were consistent in these tests, and both showed an increase in fission-gas release of a factor of 10 in going from a peak cladding temperature of 550 to 685°C. The gas-sample R/B data from each test yielded smooth

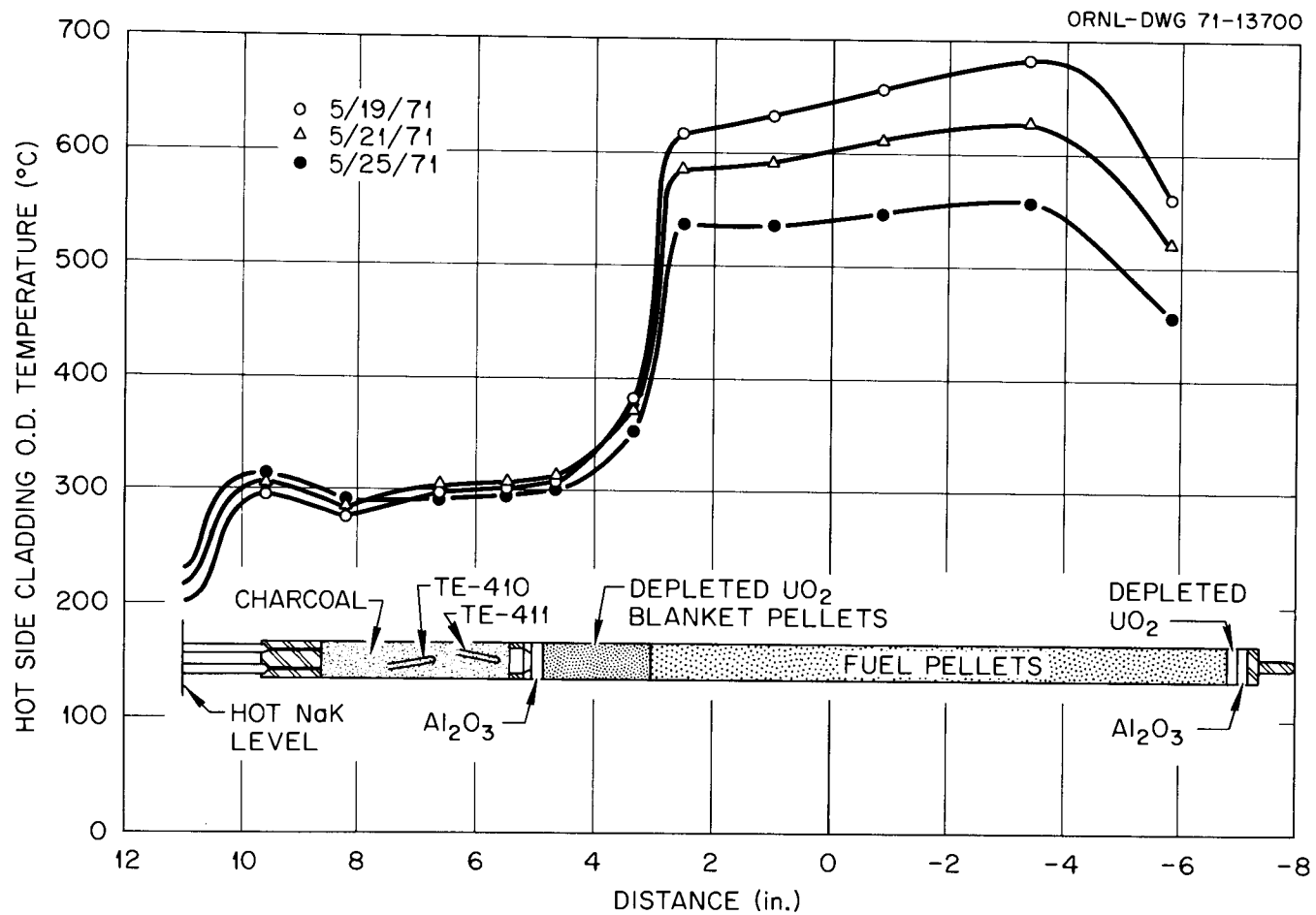


Fig. 35. Axial temperature profiles during capsule GB-9 release vs fuel-rod power-temperature test conducted May 19-25, 1971 (1 in. = 2.54 cm).

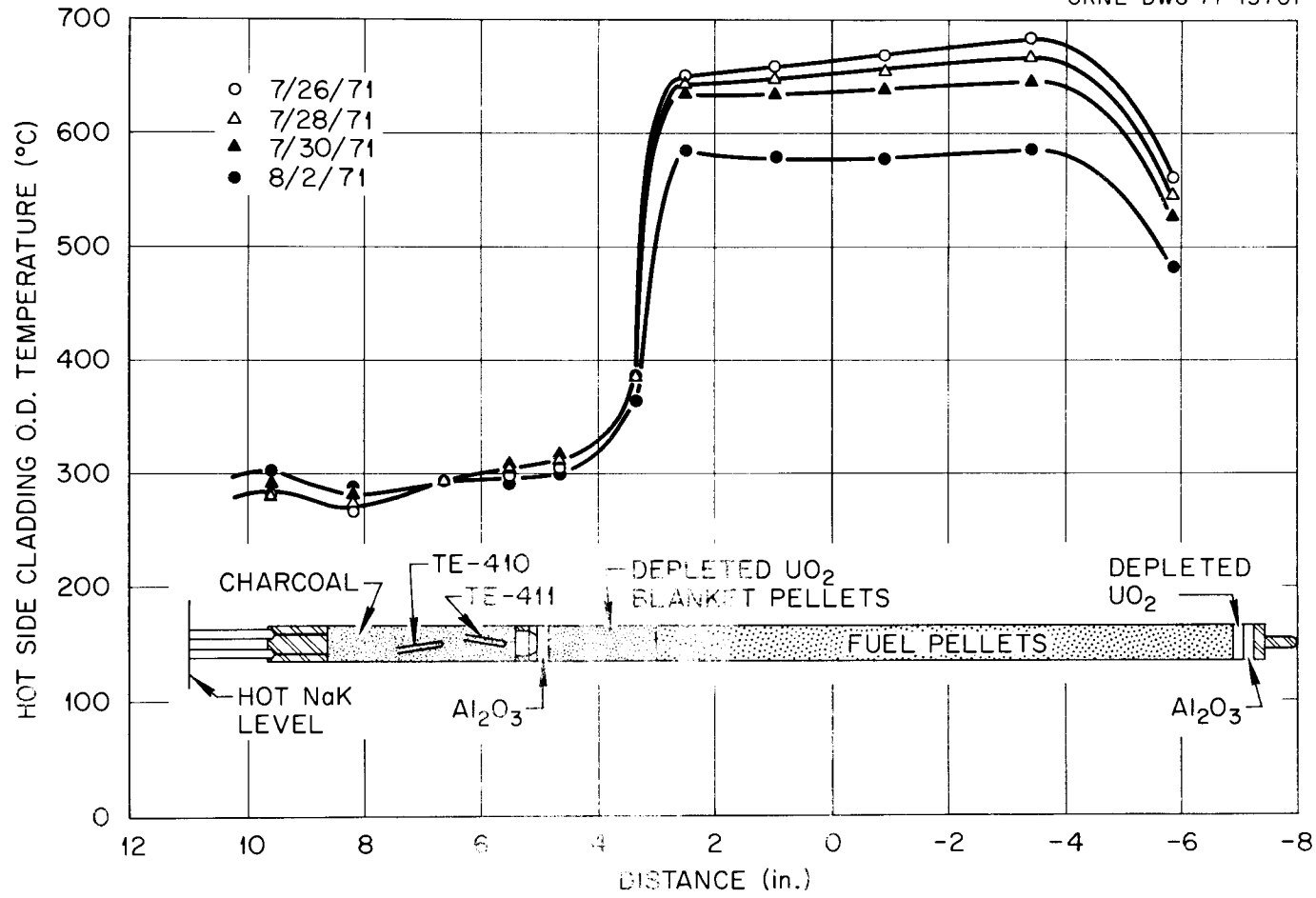


Fig. 36. Axial temperature profiles during capsule GB-9 release vs fuel-rod power-temperature test conducted July 26-August 2, 1971 (1 in. = 2.54 cm).

curves when plotted vs peak cladding temperature; however, attempts to correlate the combined data of the two tests with temperature indicated the release to be more dependent on the overall temperature profile than on the local peak cladding temperature. When the R/B data were plotted vs peak cladding temperature, the data points of the second tests were noticeably higher than those of the first test, and two curves were required to fit the combined test data for each isotope. Correlation with average cladding temperature yielded better results. The best fit, however, was obtained when the R/B data were plotted vs the cladding temperatures near the top of the fuel column. In Figs. 37 and 38, the R/B data for the two flow cases are shown plotted vs the estimated cladding temperature at a point 5.1 cm ( $\sim 2$  in.) below the top of the fuel column (the axial location of TE-412).

The results of these tests, together with the results of the trap temperature test, show the fission-gas release from the rod was much more sensitive to cladding temperature changes and temperature profile changes over the fuel region than to temperature changes of the charcoal trap and blanket region of the rod.

#### 6.8 Fission-Product Decay Heating in Charcoal Trap

Following several reactor shutdowns (at fuel burnup levels of 23, 28, and 32 MWd/kg heavy metal), the temperature decay indicated by thermocouples internal and external to the charcoal trap was monitored for a period of several hours in an attempt to detect fission-product decay heating in the trap. The electrical heaters used to maintain the trap at 300°C during normal operation were shut off immediately following reactor shutdown so that the only heat source would be decay heat. These tests indicated little or no residual fission-product heating in the trap following shutdown and suggested that volatile fission products, such as cesium, iodine, bromine, and tellurium, had not migrated to the trap in large quantities.

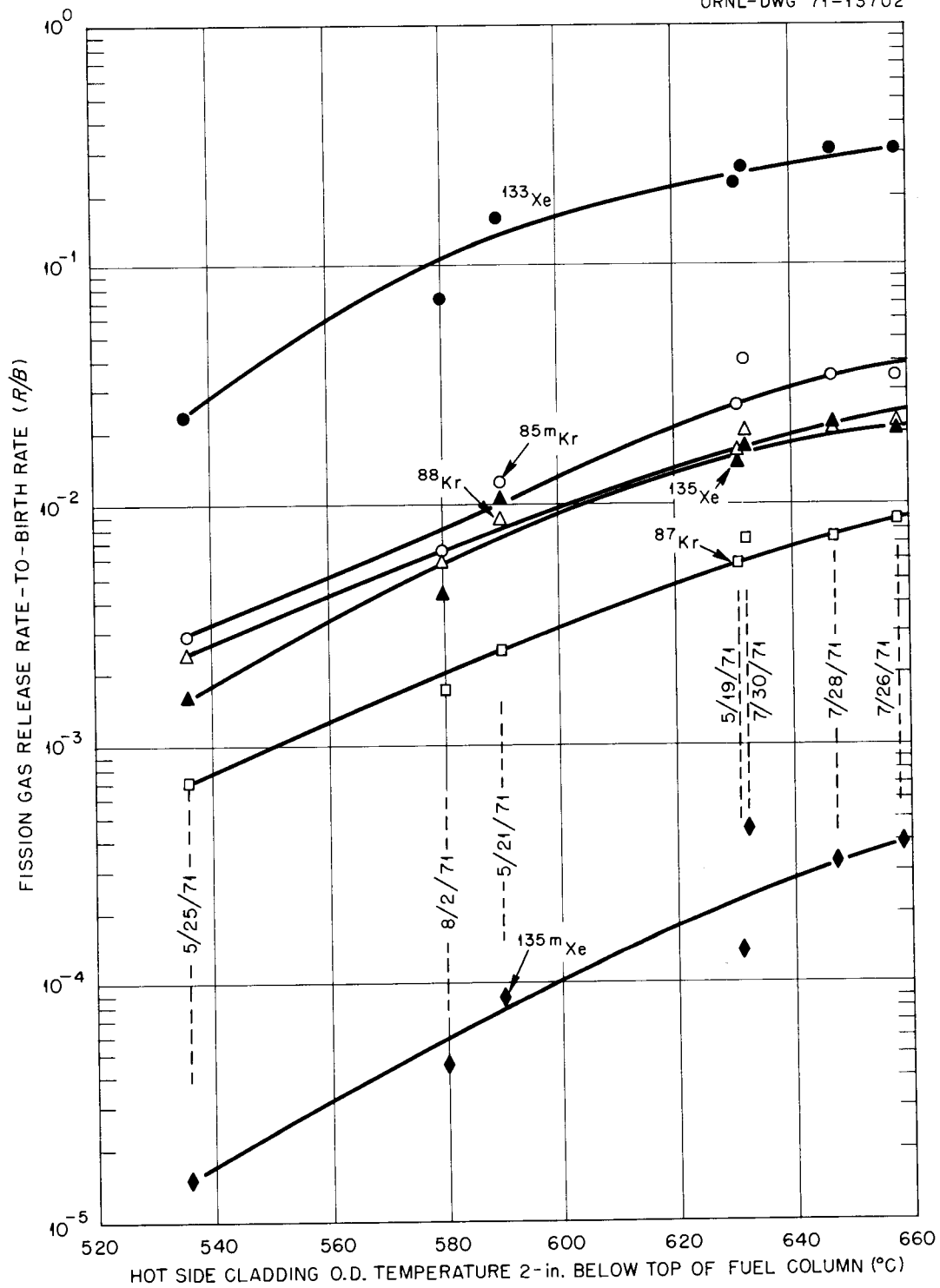


Fig. 37. Steady-state fission-gas release from ORR capsule GB-9 during release vs fuel-rod power-temperature tests conducted May 19-25 and July 26-August 2, 1971, for case of sweep flow across top of trap (1 in. = 2.54 cm).

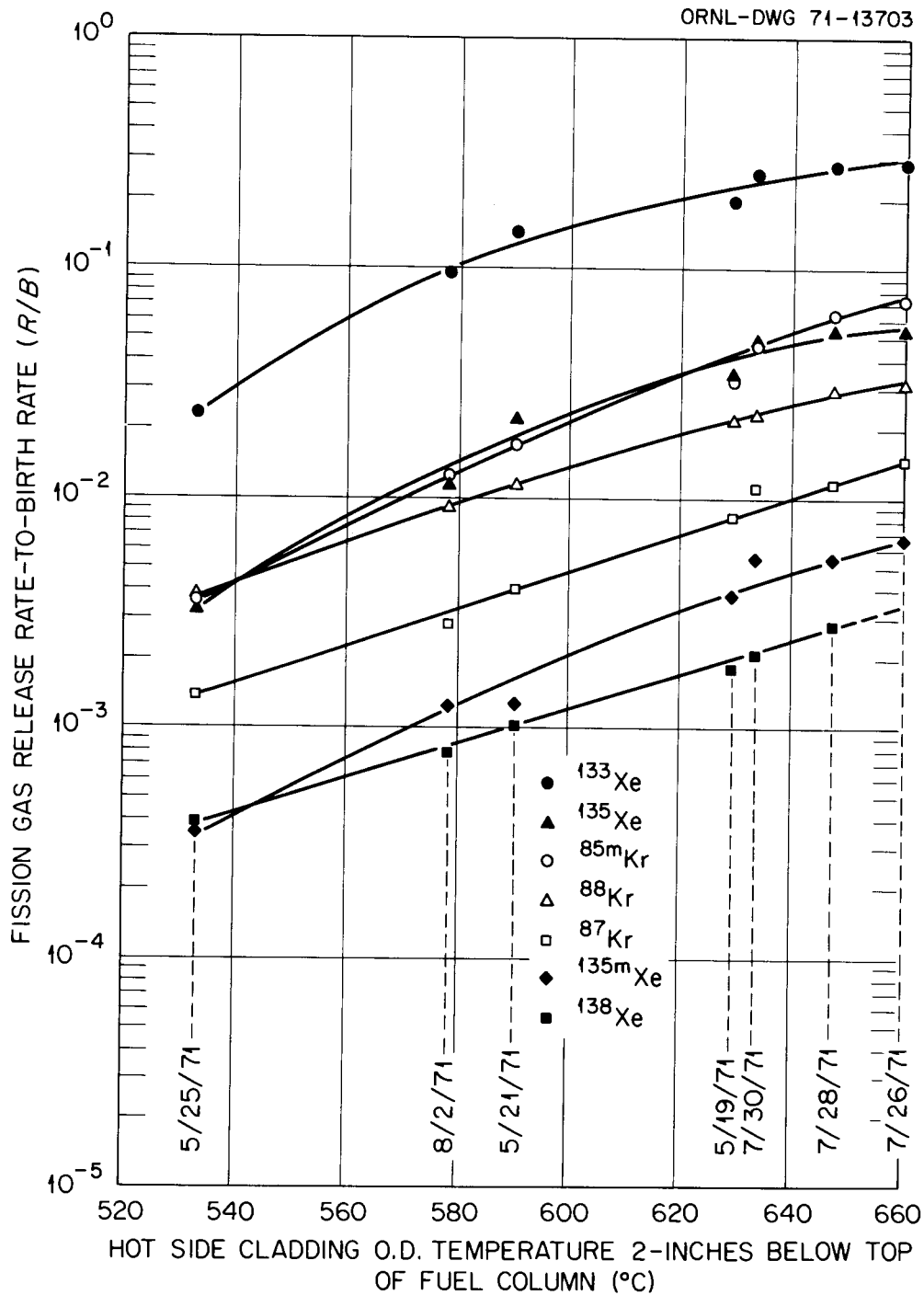


Fig. 38. Steady-state fission-gas release from capsule GB-9 during release vs fuel-rod power-temperature tests conducted May 19-25 and July 26-August 2, 1971, for case of sweep flow through trap (1 in. = 2.54 cm).

### 6.9 Iodine Deposition in Charcoal Trap

A series of gas samples were taken following a reactor shutdown when the fuel burnup level was  $\sim 24$  MWd/kg heavy metal in an attempt to determine the equilibrium deposition of  $^{133}\text{I}$  and  $^{135}\text{I}$  in the charcoal trap during the preceding period of steady-state operation. From the amount of  $^{133}\text{Xe}$  and  $^{135}\text{Xe}$  found in the samples, which were taken under carefully controlled pressure and flow conditions, the parent iodine deposition activities at the time of shutdown were deduced. Although there was considerable scatter in the data, the data indicated that there was no appreciable iodine deposition on the effluent sweep line and that the trap contained less than 1.5% of the total shutdown inventory of  $^{133}\text{I}$  of  $\sim 775$  Ci and less than 0.5% of the  $^{135}\text{I}$  inventory of  $\sim 650$  Ci. These values of iodine deposition represent upper limits; actual deposition may have been considerably less.

### 6.10 Fission-Gas Release vs Sweep Pressure

A special test to determine the steady-state fission-gas release as a function of sweep pressure was in progress at the 3.45 MPa gage (500 psig) sweep pressure level at the time the irradiation was terminated by a break in the capsule secondary containment. The release data obtained at 3.45 MPa showed no significant change in release rates of the longer-lived fission gases from their release rates at 6.9 MPa gage (1000 psig). There were some indications that the release of the short-lived fission gases (e.g., 3.2-min  $^{89}\text{Kr}$ ) was higher, but additional results at 3.45 MPa gage (500 psig) and lower sweep pressures would have been required to obtain meaningful results. The desired data at lower pressures were obtained in the subsequent GB-10 test.

### 6.11 Neutron Radiography

Neutron radiographs of the capsule were taken before and after the irradiation and at intermediate fuel burnup levels of 20 and 44 MWd/kg heavy metal. An examination of the radiographs showed no unexpected changes in the appearance of the fuel rod. There was no detectable

change in the fuel column length in any of the radiographs. The individual fuel pellets and most of the other fuel rod and capsule parts could be seen. The charcoal bed at the top of the fuel rod did not show up as well as components with higher neutron absorption cross sections. In the radiographs taken both at 20 MWd/kg and at 44 MWd/kg fuel burnup, it appeared that the top of the charcoal bed was about 1.5 cm (0.6 in.) below the top end plug of the rod. Some settling of the bed was expected because the charcoal as loaded in the rod was at a lower density than the normal charcoal bulk density in unrestricted geometry.

The radiographs taken at 44 MWd/kg fuel burnup showed the central hole of the fuel pellets much better than the earlier radiographs. The central hole was reasonably distinct, and several cracks in the fuel pellets were visible. The central hole had shifted about 0.033 cm (0.013 in.) from the geometric center of the pellets toward the hot side of the rod. Over most of the fuel column length, the central hole appeared to be close to its original size of 0.15 cm (0.060 in.) in diameter or slightly larger; however, the hole reduced to about half this size in the lowermost two or three mixed-oxide pellets. A slight enlargement of the central hole could be seen in the upper half of the top mixed-oxide pellet.

A postirradiation neutron radiograph indicated the final condition of the rod to be essentially the same as that shown by the radiographs taken at 44 MWd/kg fuel burnup.

## 7. GB-9 POSTIRRADIATION DISASSEMBLY AND EXAMINATION

Postirradiation disassembly and examination of capsule GB-9 were implemented as quickly as possible after the irradiation was terminated. This was necessary to permit gamma-ray analysis for the location of various fission products before their loss through radioactive decay. The principal short-lived fission-product activity of interest was  $^{131}\text{I}$ , which has an 8-day half-life.

The GB-9 secondary containment failed at a gas line which passed into the bottom of the capsule adjacent to a structural support member. This support piece was bent during capsule-handling operations and was pushed onto the gas line, causing the line to fail in the heat-affected zone where it was welded to the capsule.

Figure 39 shows a view of the bottom end of the capsule and two views of the broken gas line where it was joined to the capsule. The side of the gas line was bent inward by the support piece just below the point of failure. The bottom of the capsule was hemispherical, with the gas line welded into it. This weld is visible next to a cut which was made in the end of the capsule during postirradiation disassembly.

The GB-9 capsule was disassembled, and the fuel rod was recovered without difficulty. The gas lines entering the top of the fuel rod were sealed with an epoxy plug to prevent air from entering the fuel rod during handling and shipping to ANL where most of the postirradiation examination was performed.

The appearance of the fuel rod was excellent, as shown in Fig. 40. The top view of the figure shows the fuel rod before removal of the spiral heater which maintained the  $\text{UO}_2$  blanket and charcoal trap regions at the design temperature, and the lower view shows the fuel pin after removal of the heater. In both views the epoxy plug, capsule bulkhead, and instrumentation leads (cut off) are visible on the top of the fuel pin. Dimensional measurements on the fuel pin indicated less than 0.0025-cm (0.001-in.) diametral change.

The gross gamma activity profile of the fuel rod revealed that the components of the pin were in their normal positions. The only unusual feature of the gross scan was the presence of five activity peaks along

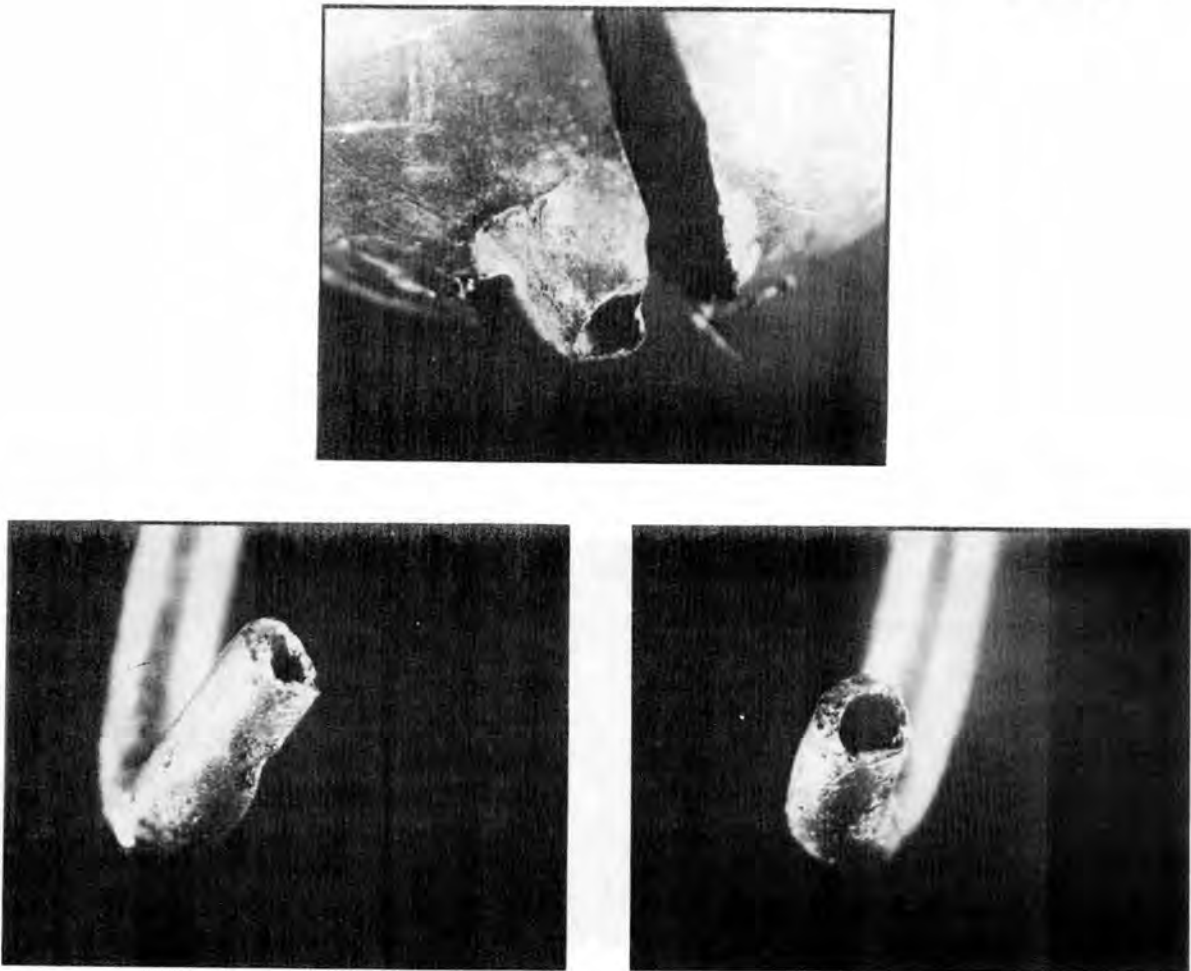


Fig. 39. Views of bottom of capsule GB-9 and broken gas line.

the fuel column portion of the rod. The source of these peaks could not be identified by spectral analysis of the gamma activity. The NaI crystal used for gamma scans performed in the High-Radiation-Level Examination Laboratory (HRLEL) at ORNL was not capable of resolving the  $^{131}\text{I}$  gamma activity from the background of other fission products and activated components of the stainless steel cladding. This result was expected and was the main reason for sending the fuel rod to ANL for detailed postirradiation examination using a more sensitive Ge(Li) crystal gamma-ray detection system. The results from gross gamma scanning of the GB-9 fuel rod at ORNL are shown in Fig. 41.

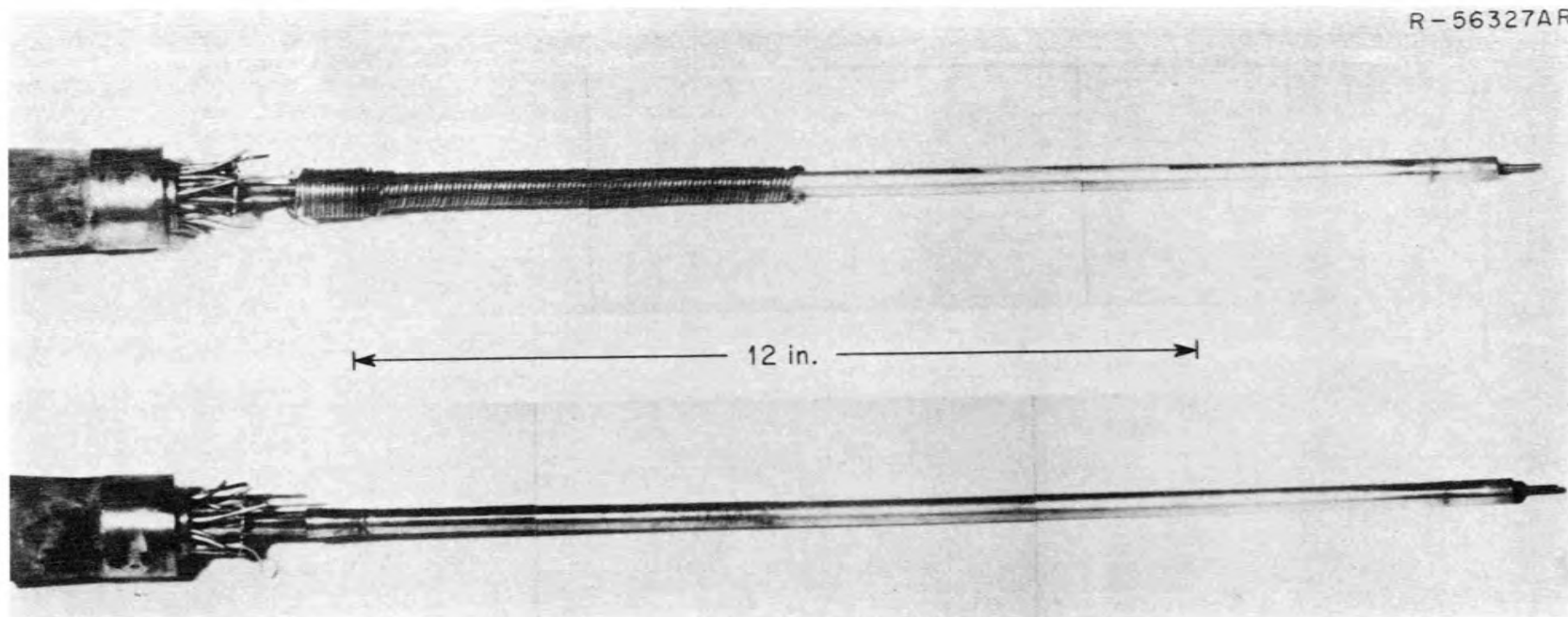


Fig. 40. Fuel rod from capsule GB-9 irradiated in the ORR  
(1 in. = 2.54 cm).

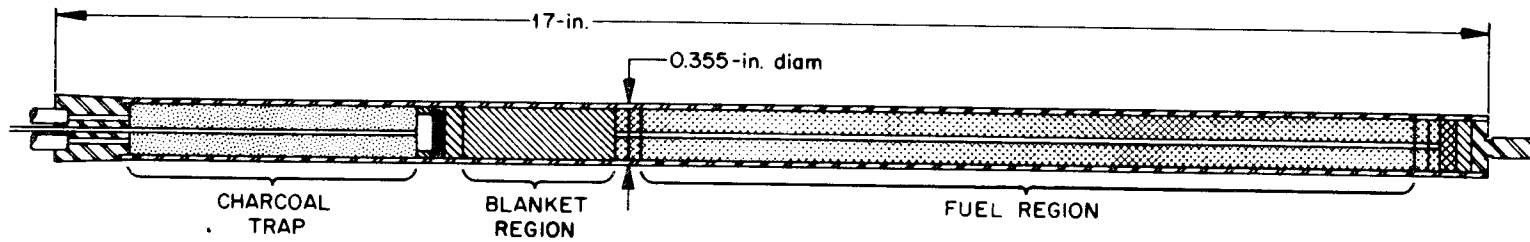
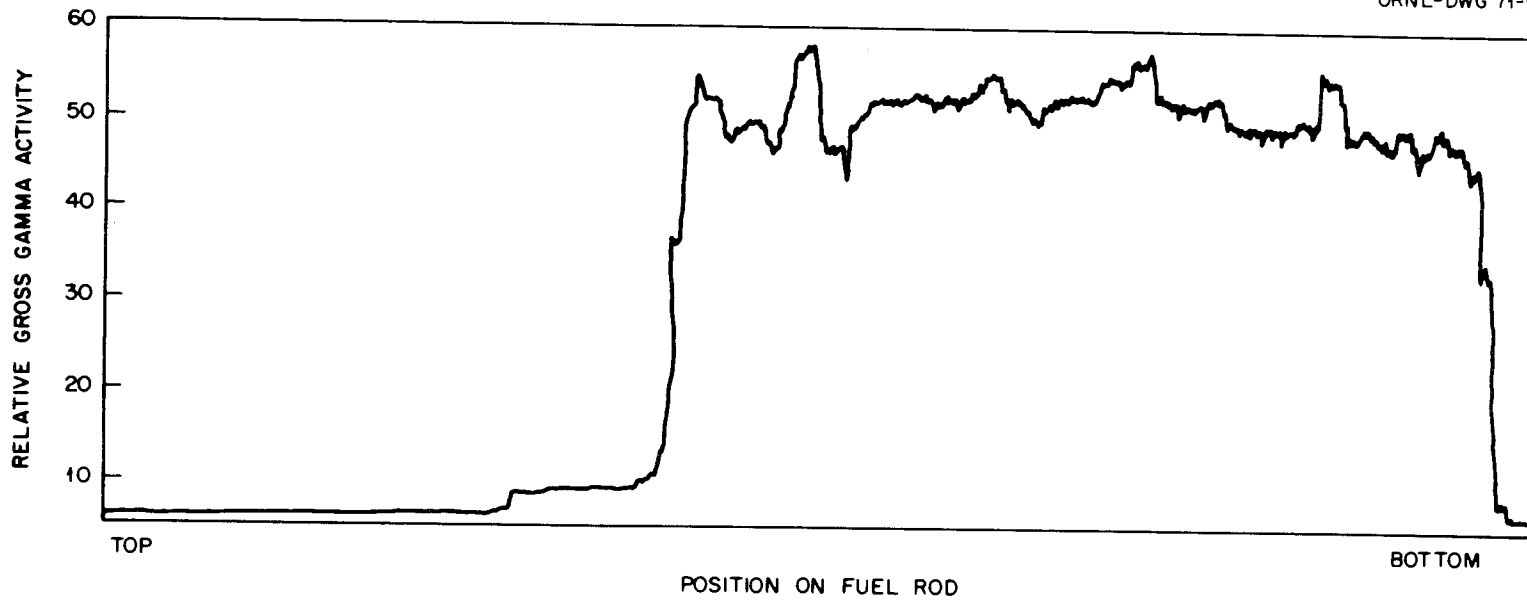


Fig. 41. Distribution of postirradiation gross gamma activity along GB-9 fuel rod (1 in. = 2.54 cm).

One sample of the GB-9 fuel rod was returned to ORNL from ANL for metallographic analysis. This sample was taken from the fuel rod 12 cm (4 3/4 in.) above the bottom of the fuel column, near the region of maximum heat generation. This sample was prepared and examined at ORNL for comparison with the earlier GCFR fuel rods examined here and to provide a comparison of the results obtained in an air-atmosphere hot cell (ORNL) with those obtained in an inert-atmosphere cell (ANL).

The only unusual microstructural feature noted in the metallographic examination of a transverse section from the GB-9 fuel rod was the presence of large amounts of metallic deposit at the fuel-cladding interface. After regrinding and repolishing the specimen, the metallic deposit was no longer present, indicating that the locations of these deposits are spotty and unpredictable.

The appearance of the transverse section after repolishing is shown in Fig. 42. An examination of this section revealed significant attack of the inner surface regions of the 0.062-cm-thick (0.0245-in.) type 316 stainless steel cladding. The attack varied in depth from about 0.0025 to 0.010 cm (0.001 to 0.004 in.). The attack of the cladding was intergranular, and in the regions of the most severe attack the grains were consumed and replaced by corrosion products (Fig. 43). The regions of the most severe attack occurred on the cooler side of the fuel rod. The cooler side was indicated by the movement of the central void in the fuel toward the hotter side of the fuel rod. Columnar grains began at the edge of the central void and continued to within  $\sim 0.115$  cm ( $\sim 0.045$  in.) of the outer surface of the fuel. Varying degrees of restructuring in the form of equiaxed grain growth and porosity redistribution occurred in a 0.115-cm (0.045-in.) band in the peripheral region of the fuel. A concentration of metallic fission products was noted about 0.065 cm (0.025 in.) from the outer surface of the fuel.

The results of the detailed postirradiation examination of the GB-9 fuel rod at ANL and GAC have been reported elsewhere.<sup>9,14,15</sup>

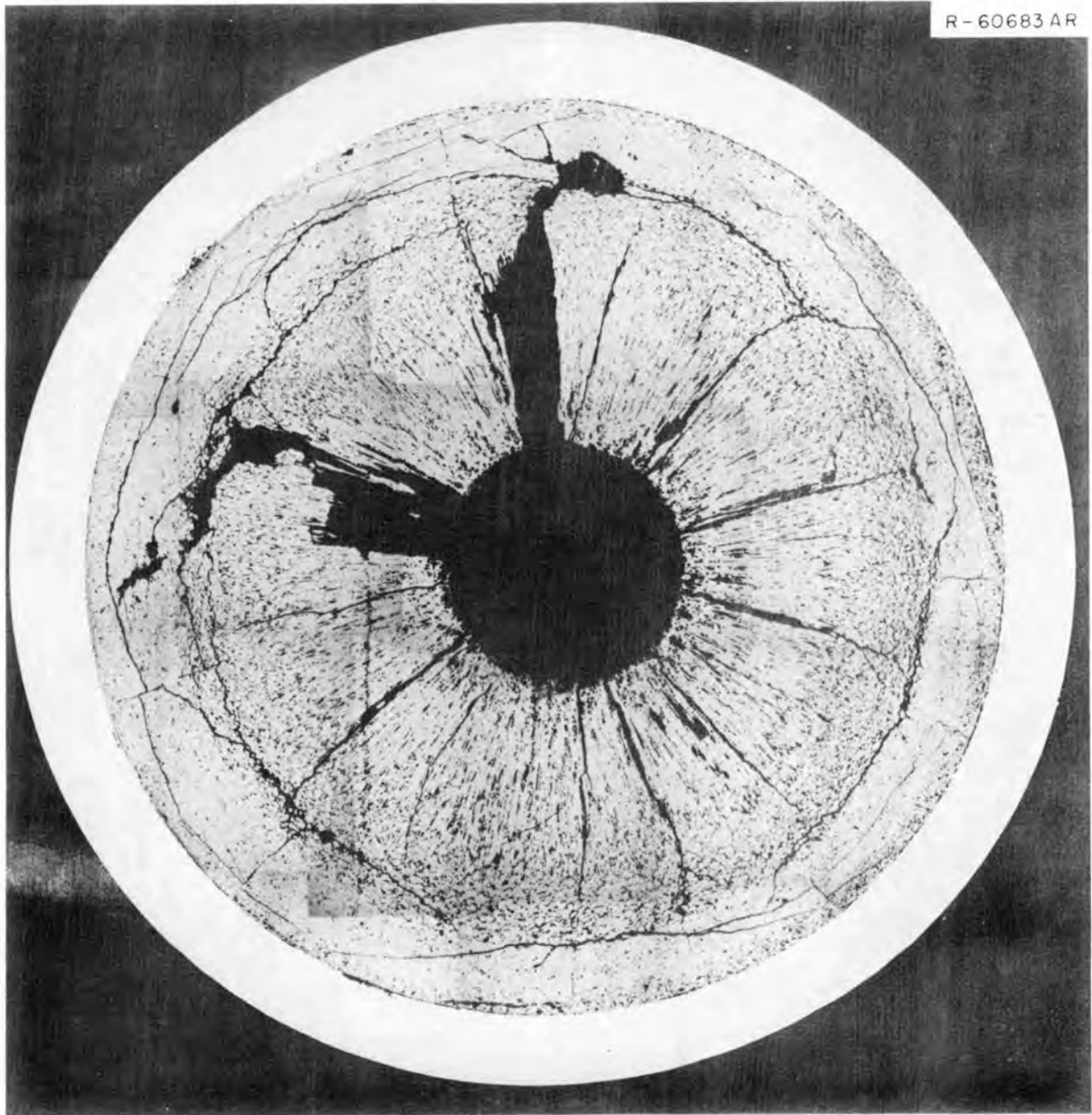


Fig. 42. Appearance of the transverse section from GB-9 fuel rod. As polished. (1 in. = 2.54 cm.)

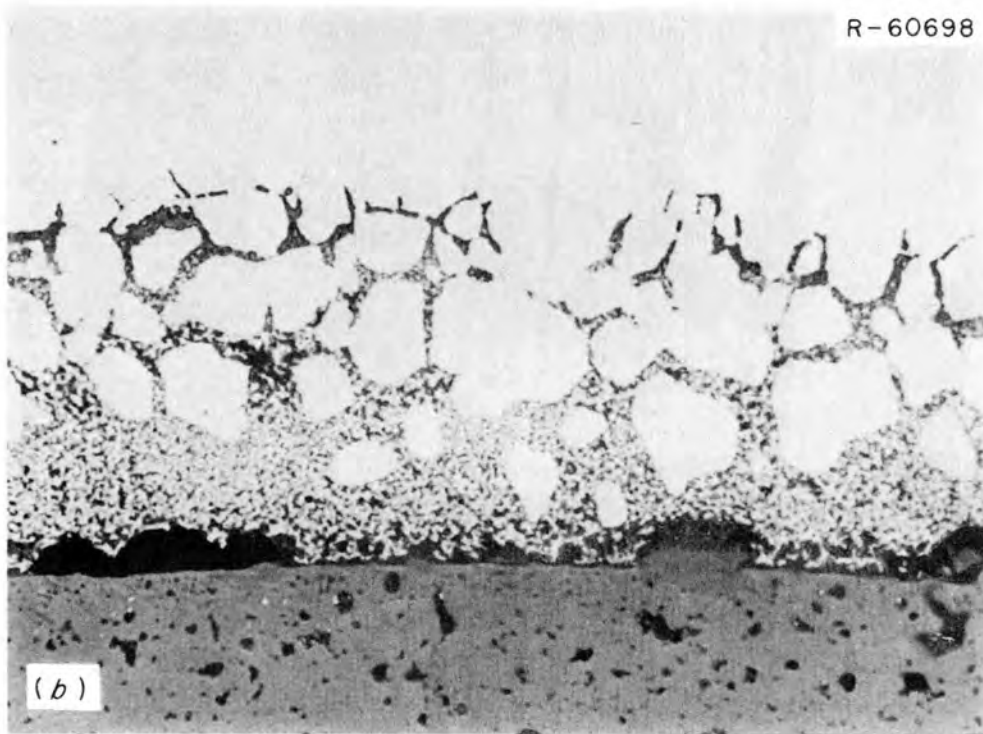
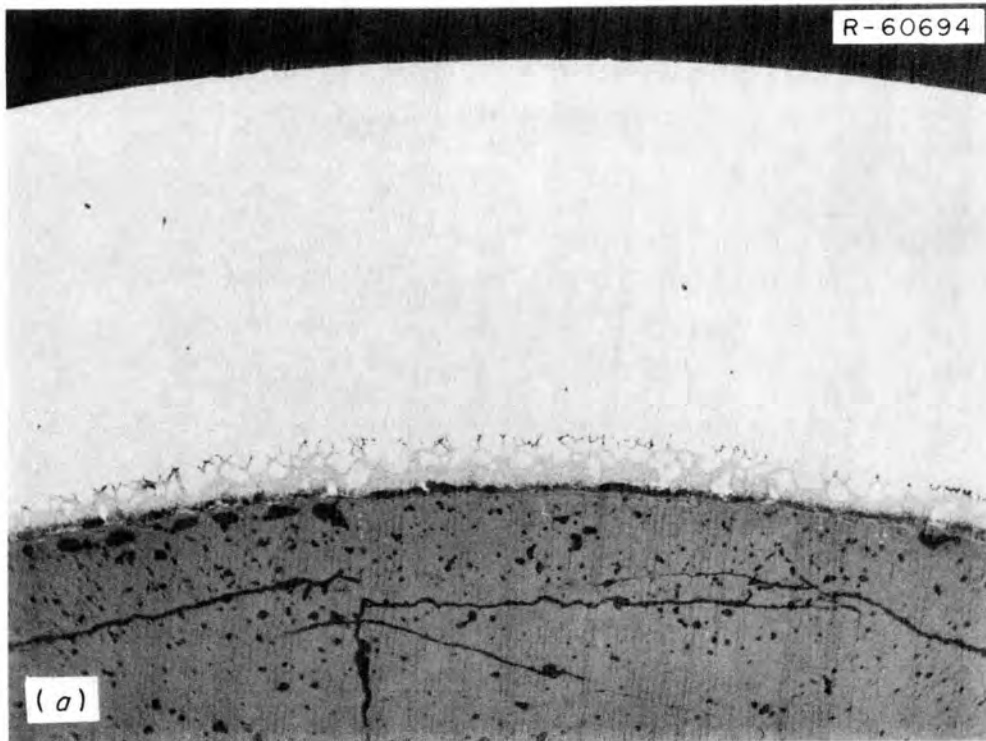


Fig. 43. Appearance of typical fuel-cladding interfaces from mixed-oxide fuel rod GB-9. As polished. (a) 100 $\times$ ; (b) 500 $\times$ .

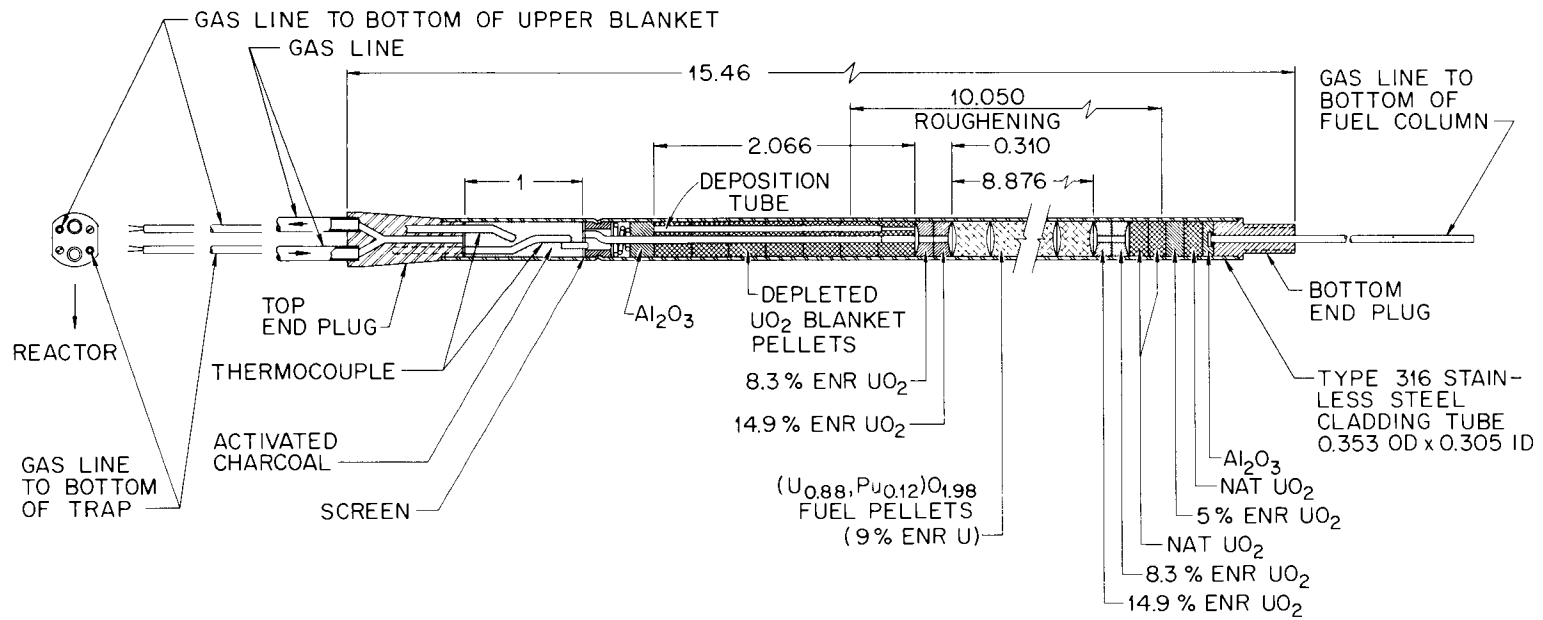
## 8. GB-10 EXPERIMENT DESCRIPTION

The GB-10 experiment was the second irradiation test of a GCFR vented-and-pressure-equalized fuel rod at ORNL. Capsule GB-9, being the first of a kind, yielded a large amount of information on the fission-product release and fuel behavior to be expected from the GCFR vented rod under normal operating conditions. The GB-10 capsule, with additional sweep lines, permitted experiments of greater depth involving both normal and off-normal conditions. Included for the first time was the capability for measuring fission gases released directly from the mixed-oxide fuel during irradiation. Thus, the GB-10 measurements were a continuation of the measurements started with capsule GB-9. The main objectives of GB-10 were to obtain detailed information on the release, transport, and trapping of gaseous and volatile fission products, to observe the general performance of the rod, and to look for any behavior that could be a potential problem for the GCFR.<sup>22</sup>

### 8.1 Fuel Rod

The GB-10 fuel rod (Fig. 44) was a shortened prototype of the GCFR rod with a 23-cm-long (9-in.) region of solgel-derived (U,Pu)O<sub>2</sub> test pellets, a 5.1-cm-long (2-in.) upper blanket region of depleted UO<sub>2</sub> pellets, and a 2.5-cm-long (1-in.) charcoal trap. Two partially enriched UO<sub>2</sub> half-pellets were included at each end of the mixed-oxide column to suppress power peaking at the ends of the test fuel, which is the same design as was used for the GB-9 rod. At the bottom end of the rod, there are two natural UO<sub>2</sub> blanket pellets, a 5%-enriched UO<sub>2</sub> pellet, another natural UO<sub>2</sub> pellet, and an alumina insulator pellet, all between the end of the active fuel region and the bottom end plug. The purpose of this design was to raise the temperature of the natural UO<sub>2</sub> lower blanket pellets and to create temperature gradients (in the vicinity of the 5%-enriched UO<sub>2</sub> pellet) that would discourage possible transport of volatile fission products to the relatively cold bottom end of the rod. The cladding is 20% cold-worked type 316 stainless steel.

The GB-10 rod was similar to the GB-9 rod, but there were other differences in addition to the different bottom end designs. The GB-10 rod



ALL DIMENSIONS IN INCHES

Fig. 44. Gas-cooled fast breeder reactor fuel rod specimen in ORR capsule GB-10 (1 in. = 2.54 cm).

had a roughened outer surface and contained solid instead of hollow (U,Pu)O<sub>2</sub> fuel pellets. The fuel column smear density was 84% of theoretical compared with 85% in the GB-9 rod. The fuel stack height was slightly less than that in the GB-9 rod, the upper blanket region of depleted UO<sub>2</sub> pellets was one pellet longer, and the charcoal trap was 2.5 cm long (1 in.) instead of 8.1 cm (3.2 in.). The charcoal trap was shortened to 2.5 cm in GB-10 to provide the same potential fission-product loading as the rod trap in the reference GCFR rod; that is, the trap contained the same ratio of charcoal mass to power generated within the rod as the reference design.

Five sweep-gas lines were built into the GB-10 rod. Four entered through brazed joints in the top end plug. Two of these lines terminated inside the top end plug, which had passages connecting the two lines to the top of the charcoal trap. A third line terminated at the bottom of the trap, and the fourth line terminated near the bottom of the upper blanket region. The fifth line entered through the bottom end plug and was welded to its top side. Thermocouples were located in the charcoal trap at two axial positions.

A summary of as-built data for the GB-10 fuel rod is given in Appendix A. Initial oxygen-to-metal ratios (O/M) were 1.98 in the (U,Pu)O<sub>2</sub> pellets, 2.004 in the UO<sub>2</sub> half-pellets, and 2.002 in the depleted UO<sub>2</sub> blanket pellets.

## 8.2 Capsule

A cross section of capsule GB-10 showing the fuel rod inside the capsule is shown in Fig. 45. The design of the capsule was essentially the same as that of capsule GB-9 (see Sect. 3.2). The main design changes from GB-9 were associated with the shorter charcoal trap and electrically heated upper portion of the capsule. Also, the secondary containment gas line which passed into the bottom of the GB-9 capsule was rerouted through the capsule bulkhead of GB-10, and the support piece at the bottom of the capsule was made thicker, thus eliminating the problems that caused early termination of GB-9. The GB-10 fuel-region thermal design is the same as that of GB-9. However, two thermocouples were

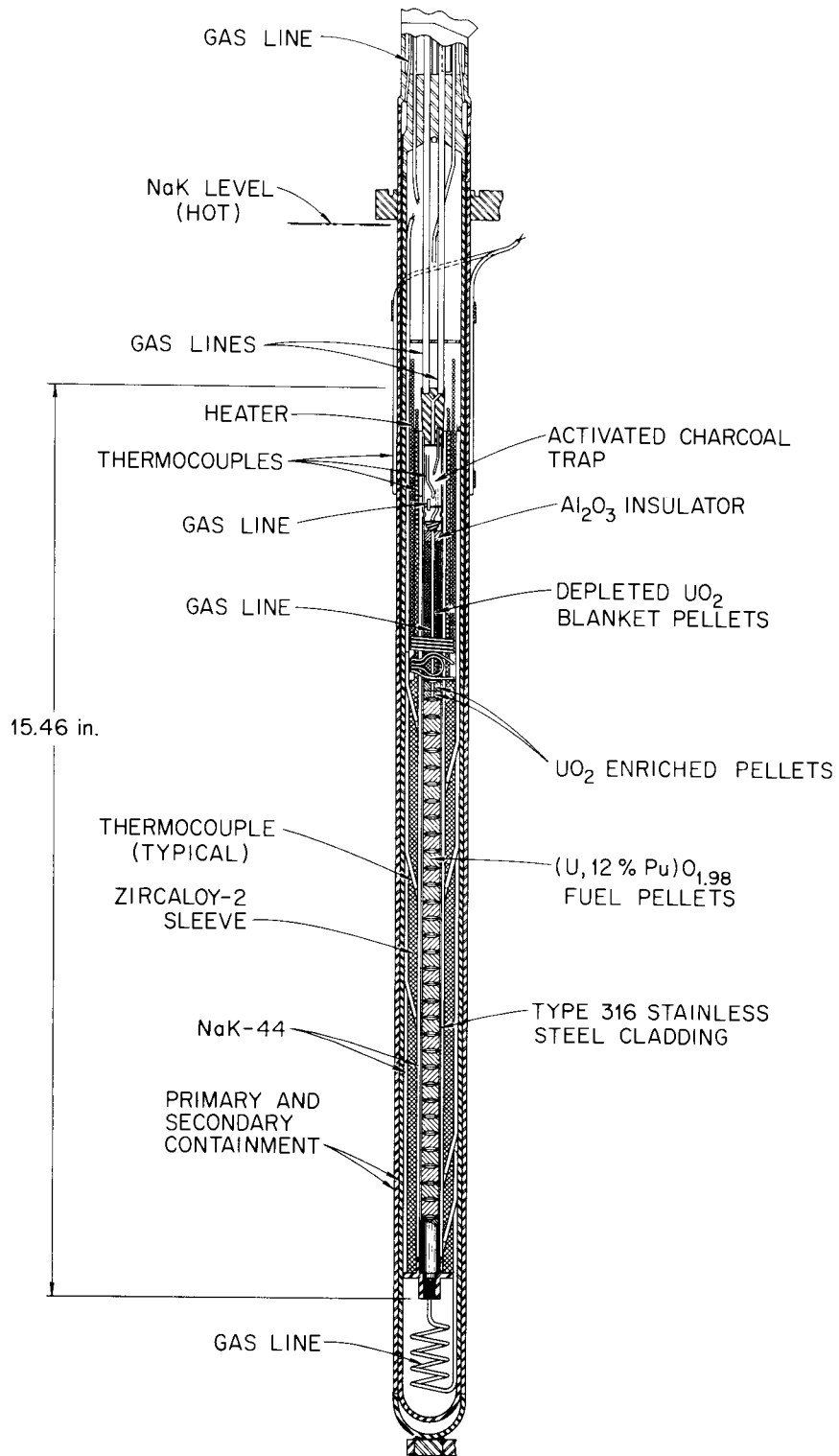


Fig. 45. GCFR-ORR capsule GB-10 (1 in. = 2.54 cm).

located at one elevation in the peak-power region (one on the cold side of the fuel rod and one on the hot side) to obtain indications of the angular temperature variation, whereas the GB-9 capsule did not have any two fuel-region thermocouples at the same elevation. As in the GB-9 capsule, the GB-10 fuel-region thermocouples were staked into place where they entered the outer surface of the Zircaloy-2 sleeve after their junctions were carefully positioned at the inside diameter of the Zircaloy-2 sleeve using a mandrel temporarily inserted into the sleeve. The volume inside the primary containment of the capsule was filled with NaK to a level above the fuel rod, as shown in Fig. 45. Centering spacers, one at the bottom of the rod and one at the upper blanket region, were intended to keep the fuel rod centered within the Zircaloy-2 sleeve.

The GB-10 capsule was equipped with eleven 0.16-cm-diam (1/16-in.) Chromel-Alumel thermocouples located at various axial positions along the length of the capsule to monitor cladding temperatures, in addition to the two thermocouples inside the fuel-rod trap. Two more thermocouples were strapped to the outer surface of the capsule to indicate the temperature of the pool water at the elevation of the fuel-rod trap.

A photograph of the GB-10 assembly taken before the primary and secondary containment vessels were installed is shown in Fig. 46. Close-up views of the lower and upper ends of the assembly are shown in Figs. 47 and 48. The 0.16-cm-diam (1/16-in.) sweep line to the bottom of the rod (Fig. 47) was coiled to accommodate thermal expansion and contraction of the fuel rod of  $\sim 0.25$  cm (0.10 in.) maximum travel at the lower end. The top end of the rod was held in a fixed position by two 0.32-cm-diam (1/8-in.) sweep lines, as can be seen in Fig. 45. A photograph of the finished capsule in an ORR poolside facility mock-up is shown in Fig. 49.

### 8.3 Gas Systems

The GB-10 arrangement of sweep lines and valves (Fig. 50) permitted flow across the top of the fuel rod, which was the normal sweep flow mode, or flow through the three main regions of the rod (trap, blanket, and fuel), either individually or in combination. As shown in Fig. 50,

ORNL PHOTO 79570A

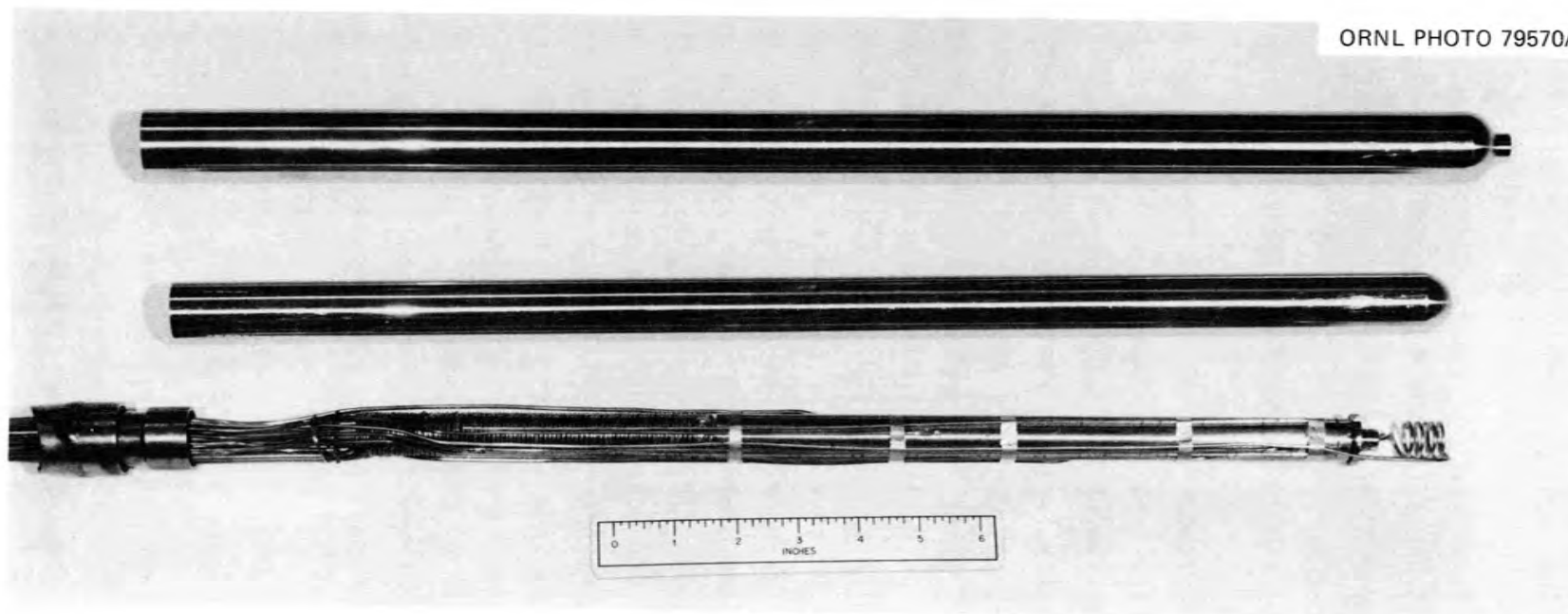


Fig. 46. Capsule GB-10 fuel-rod assembly (1 in. = 2.54 cm).



Fig. 47. Lower end of capsule GB-10 fuel-rod assembly (1 in. = 2.54 cm).

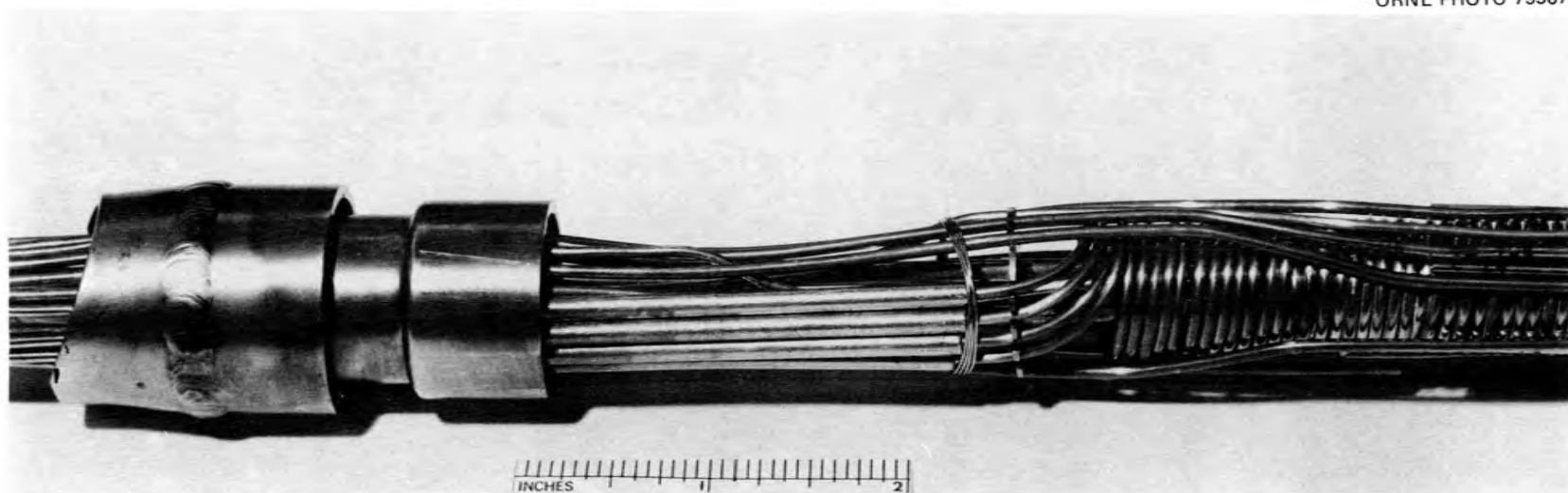


Fig. 48. Upper end of capsule GB-10 fuel-rod assembly (1 in. = 2.54 cm).

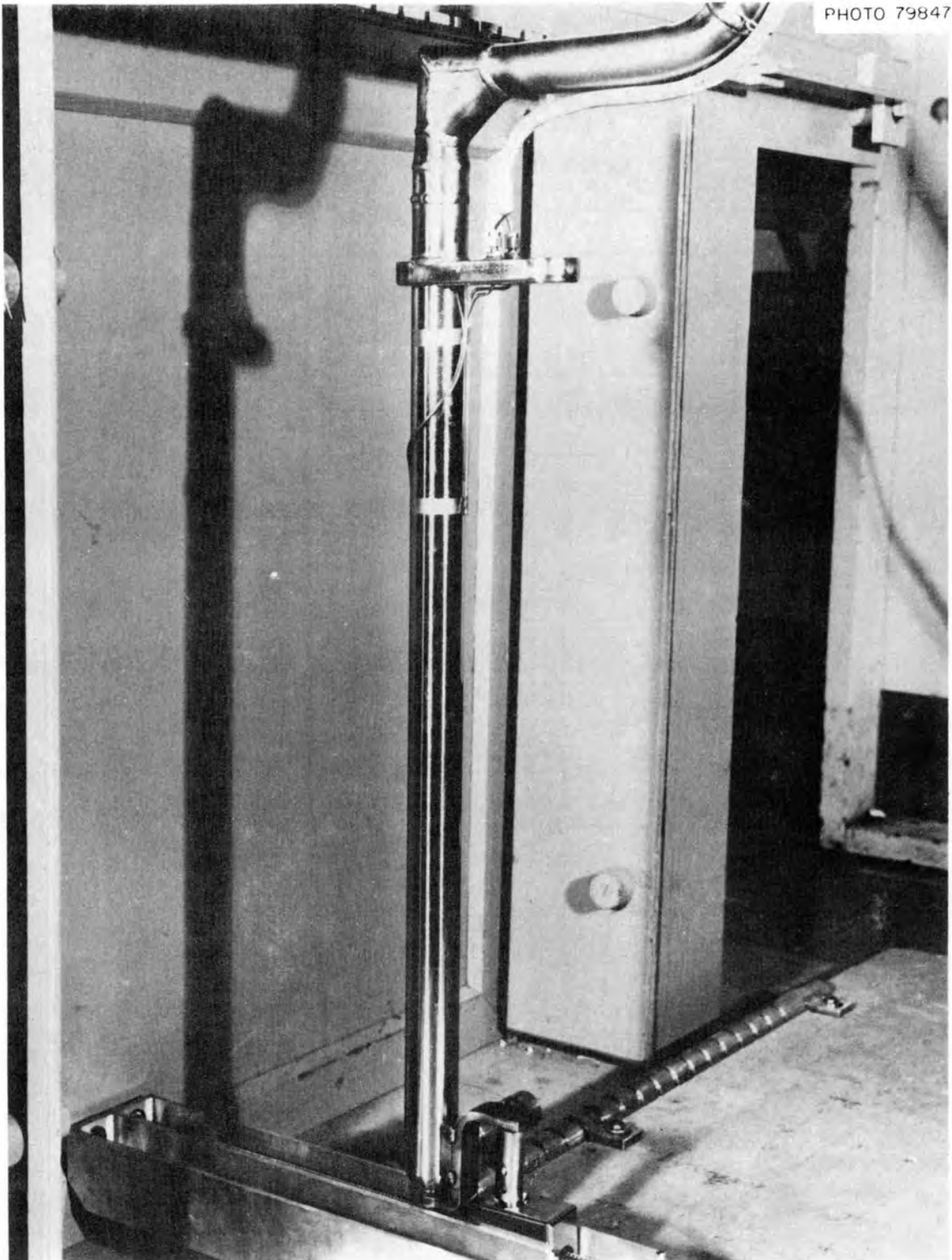


Fig. 49. Completed capsule GB-10 in ORR poolside facility mock-up.

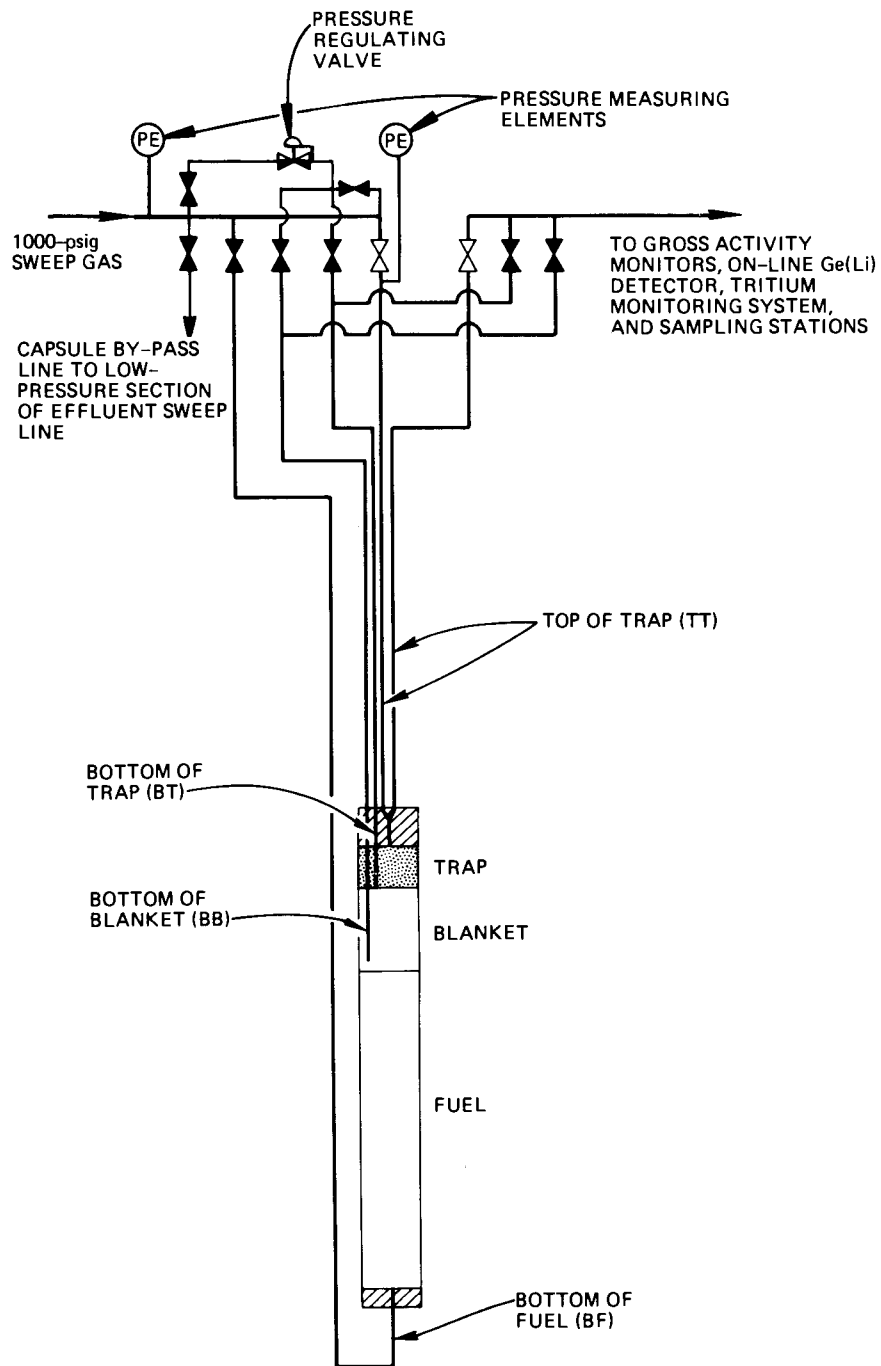


Fig. 50. Schematic of GCFR-ORR capsule GB-10 showing sweep gas lines (1 psi = 6895 Pa).

we designated the sweep lines as follows: BF = line to bottom of fuel, TT = lines to top of charcoal trap, BT = line to bottom of trap, and BB = line to bottom of upper blanket. Specific sweep flow modes are designated by two letters indicating the entrance point followed by two more letters indicating the exit point from the fuel rod. Thus, when the sweep flow was directed across the top of the rod, the flow mode was TT-TT, and when the sweep flow was directed into the bottom and out of the top of the rod, the flow mode was BF-TT. The latter flow mode (BF-TT) simulated a leak in the cladding of a GCFR fuel rod.

Two of the lines shown in Fig. 50, the one with the pressure-regulating valve and the capsule bypass line, were added to the system late in the irradiation to aid in making fission-gas release measurements at very low flow rates through the fuel region of the rod.

Most of the existing sweep and cladding external gas systems and associated equipment used for capsule GB-9 were reused for capsule GB-10. Additional valves and two sweep lines, one connected to the line to the bottom of the upper blanket region and one connected to the line to the bottom of the rod, were added to the sweep system for GB-10.

The GB-10 sweep and cladding external gas systems are shown in Fig. 51. As in the GB-9 system, sweep flow (150 to 1300 cm<sup>3</sup> STP/min) was regulated by adjusting the downstream flow resistance with a needle valve. Flow restrictors were employed immediately upstream of the needle valve to limit the flow rate out of the system to a maximum value. An automatic pressure differential control valve adjusted the inlet sweep flow and maintained the sweep pressure  $170 \pm 0.7$  kPa ( $25 \pm 0.1$  psi) above the pressure in the normally static cladding external gas system. High-purity analyzed helium was used as the sweep gas and was passed through room-temperature molecular sieve traps and then through 600°C titanium sponge traps before going to the capsule.

The two moisture probes (one in the sweep supply line downstream of the cleanup traps and the other downstream of the capsule) used for capsule GB-9 were replaced with new ones of the same type for capsule GB-10.

During the course of the GB-9 test and the first half of the GB-10 test, the stem and seat of the automatic pressure differential control

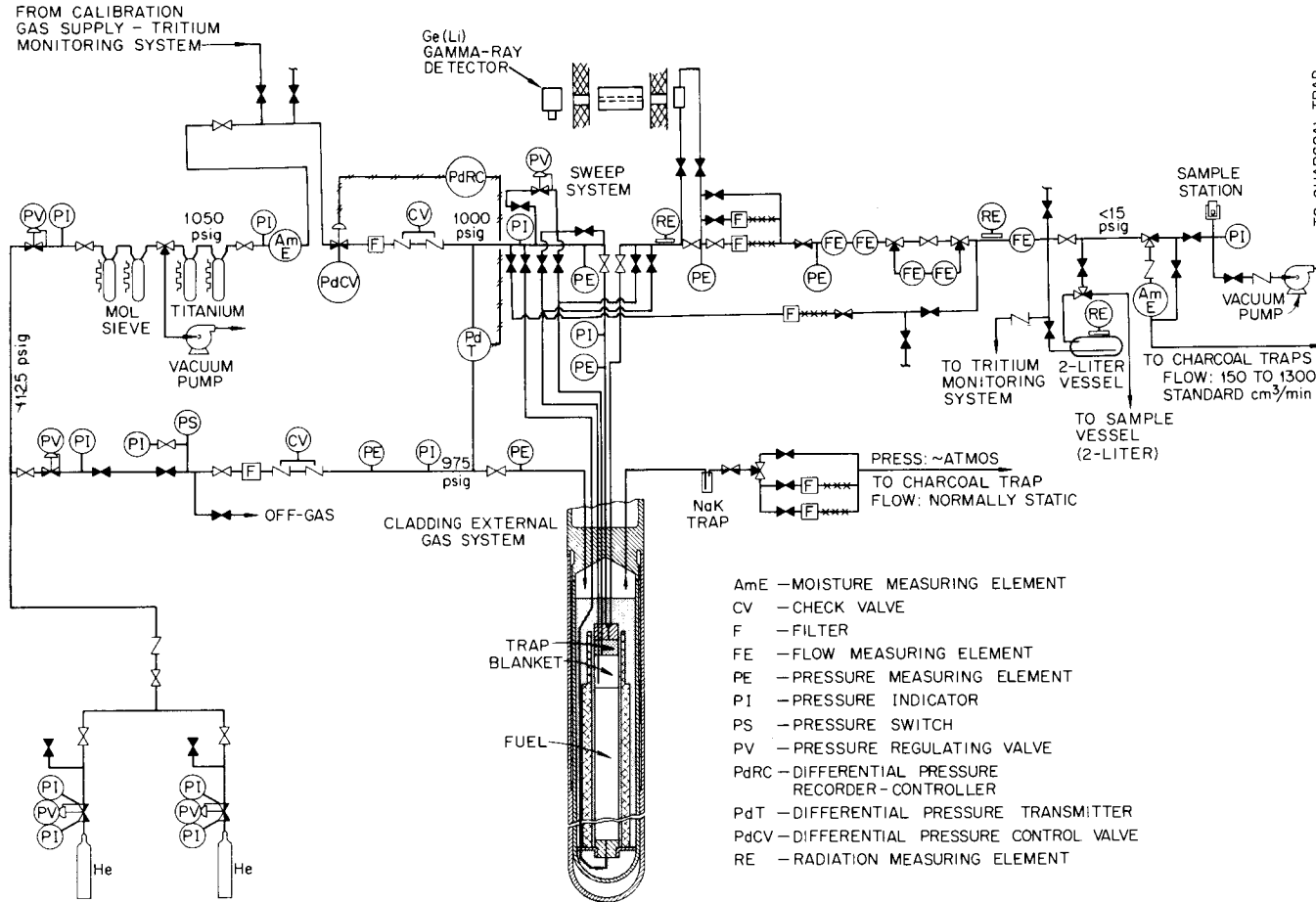


Fig. 51. GCFR-ORR capsule GB-10 sweep and cladding-external gas systems (1 psi = 6895 Pa).

valve in the inlet sweep line showed a tendency to gall in the dry helium and had to be replaced occasionally with a new stem and seat. A new stem and seat lasted anywhere from a few weeks to more than 6 months. This problem became a nuisance, and instead of getting better with time, it got worse. After trying different metallic seat materials without success, including cast iron, the problem was finally solved by using a modified seat with a small graphite liner pressed into it which served as the contact surface for the metallic stem.

At the start of the GB-10 irradiation, fission-gas release was monitored by the two on-line ionization chambers and by taking gas samples periodically and analyzing the samples by gamma-ray spectrometry, as was done in the capsule GB-9 experiment. The on-line ionization chambers, one located on the high-pressure section of the effluent sweep line and the other on the low-pressure section, continuously monitored the gross activity of the sweep line and provided a sensitive indication of the steadiness of fission-gas release from the rod. During the course of the GB-10 irradiation, three additional fission-product monitoring systems were designed and installed. An on-line Ge(Li) gamma-ray detector system (see Fig. 51) was added to the high-pressure section of the effluent sweep system to permit easier and more detailed fission-gas release measurements. The other two systems, both added to the low-pressure section of the effluent sweep system, were a system for taking a large gas sample for determination of stable krypton and xenon release rates and a tritium-monitoring system.

The GB-10 on-line gamma-ray spectrometer system consisted of a 0.635-cm-ID (0.250-in.) source section in the effluent sweep line, five 30.5-cm-long (12-in.) stainless-steel-lined lead collimators ranging from 0.16 cm ID (1/16 in.) to 3.2 cm ID (1 1/4 in.) to cover the wide activity range associated with the various GB-10 flow modes, a Ge(Li) detector (8.6% efficiency for  $^{60}\text{Co}$ ) with associated dewar and power supply, preamplifier located at the detector, main amplifier located at the analyzer, and a Nuclear Data 50/50 data-acquisition system (PDP-15 computer interfaced with a 4096 channel analyzer). The separation distance between the source section and the detector (centerline-to-centerline) was 59.7 cm (23 1/2 in.). Prior to installation, the detector system was calibrated

with each of the collimators in place using an exact mock-up of the actual experimental setup and calibrated radionuclide sources.

A schematic of the sampling system for taking large samples for determining the release of stable noble gases is shown in Fig. 52. In taking these samples, we directed the effluent sweep flow through the shielded 2-liter vessel inside the shielded valve box for an appropriate length of time (approximately 10 volume changes) and then trapped a sample of the gas in the vessel. The sample was allowed to decay for 6 weeks and then about half of it (0.1-liter STP of gas) was drawn off into a clean 2-liter sample vessel outside the valve box. The sample of stable noble gases was then removed and prepared for analysis by mass spectrometry. Special techniques were required to concentrate the krypton and xenon isotopes to measurable levels.

ORNL-DWG 75-11234

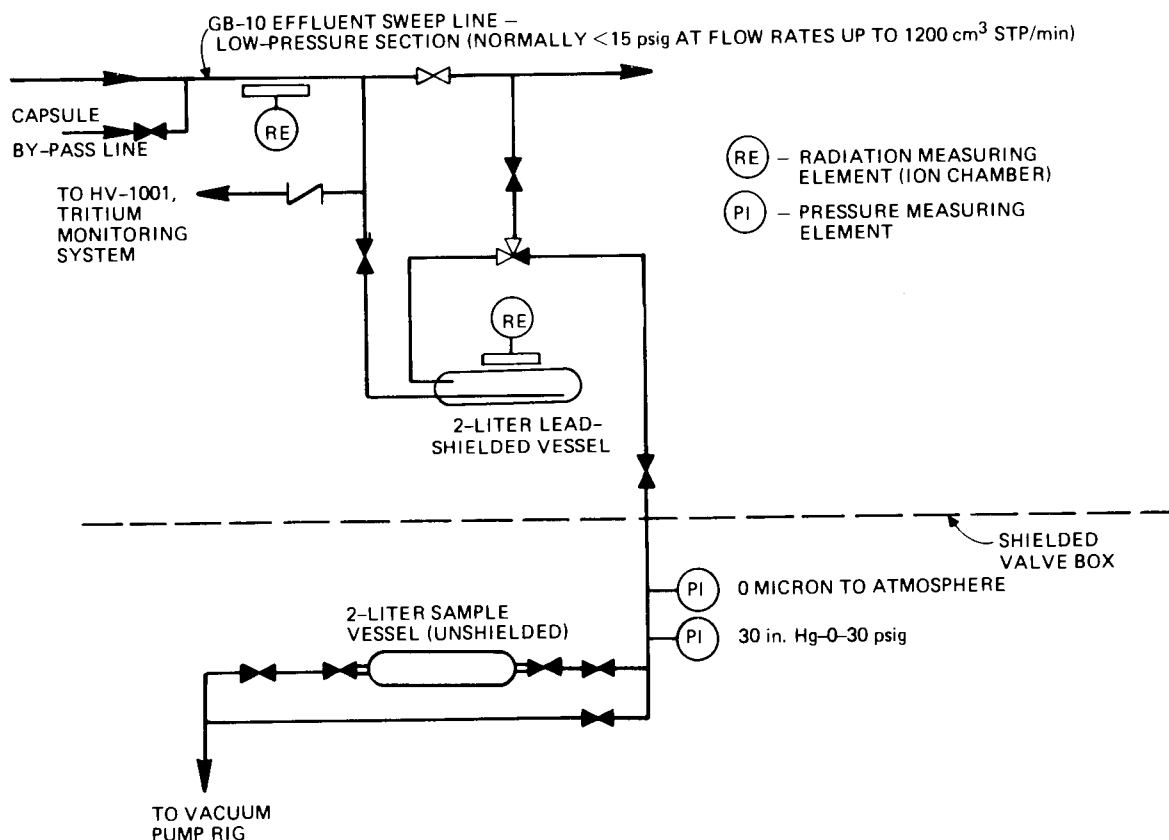
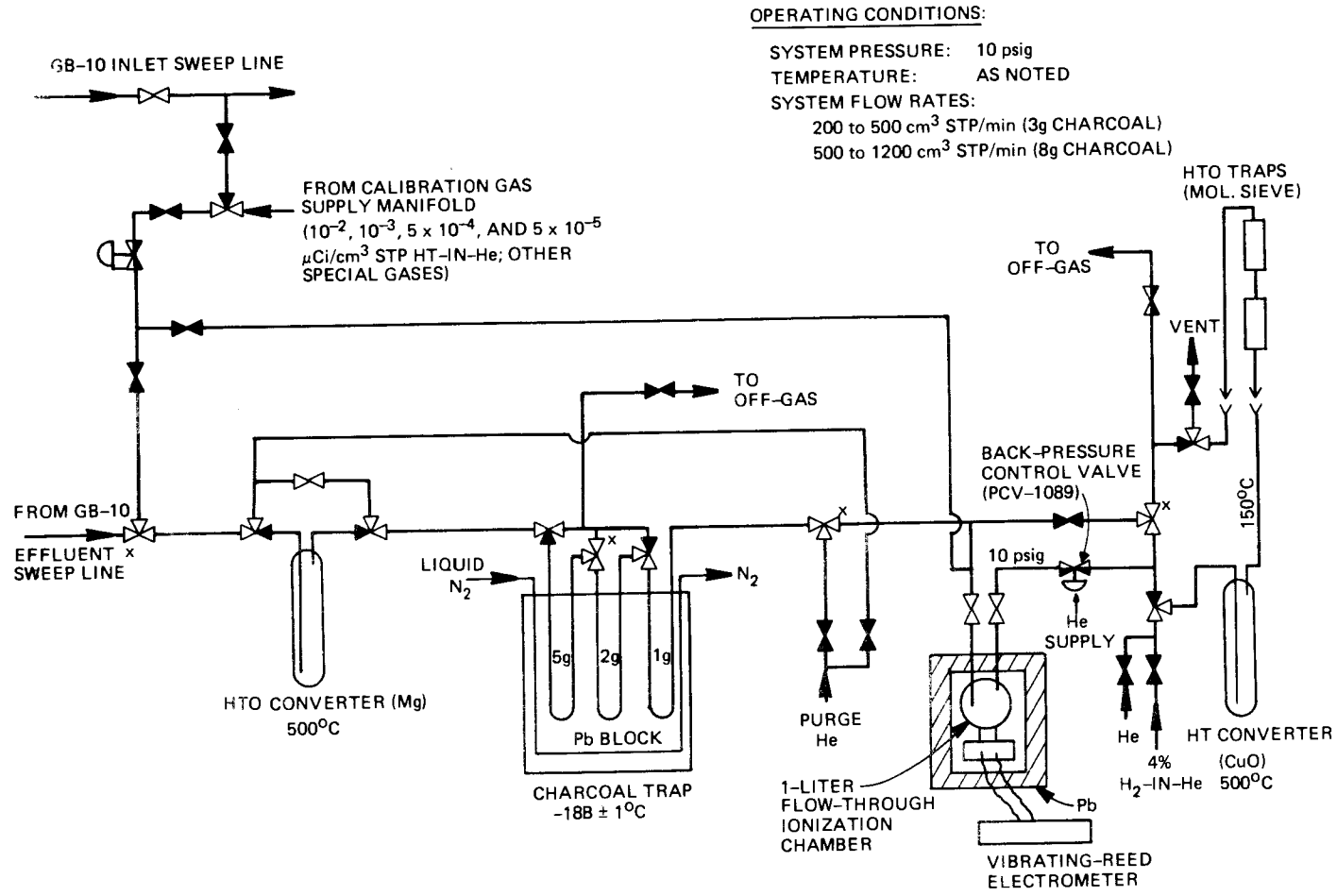


Fig. 52. Schematic of capsule GB-10 sampling system for stable noble gas release determination (1 psi = 6895 Pa).

The GB-10 tritium-monitoring system (Fig. 53) was designed to measure the tritium (T) concentration in the effluent sweep gas under various capsule operating conditions and sweep flow modes. In addition, provision was made for introducing HT-in-He calibration gases (at several different tritium concentrations) either directly to the tritium-monitoring system for calibration checks or to the GB-10 inlet sweep system for tritium transport experiments. The same gas supply manifold could be used to introduce other premixed gases to the inlet sweep system. The objectives of the tritium-monitoring experiments were to quantitatively determine tritium production from fission, release, cladding permeation, and the molecular species of released tritium (HT and/or HTO).

The main components of the tritium-monitoring system were a HTO-to-HT converter (Mg at 500°C), a liquid-nitrogen-cooled charcoal trap assembly (charcoal at -188°C), a calibrated flow-through ionization chamber and vibrating-reed electrometer, a HT-to-HTO converter (CuO at 500°C), and a removable HTO trap assembly (molecular sieve). Sweep gas from the capsule was passed through the charcoal trap, which was designed to delay all radioactive gases but tritium for long periods relative to the time required for the measurements. The tritium content in the gas stream leaving the charcoal trap was then determined by observing the response of the calibrated ion chamber and by batchwise collection and analysis of tritium using the removable HTO traps and beta liquid scintillation counting methods. The batchwise sampling method was used as needed to verify and/or supplement the ion chamber data. The HTO-to-HT converter upstream of the charcoal trap was designed to provide measurement of total tritium when it was valved in and only gaseous tritium when it was valved out, since the charcoal was expected to trap the moisture form. The charcoal trap was performance-tested and the ion chamber was calibrated prior to installation in the system. The other main components were simulated in laboratory-scale experiments to verify their design.



**OPERATING CONDITIONS:**  
 SYSTEM PRESSURE: 10 psig  
 TEMPERATURE: AS NOTED  
 SYSTEM FLOW RATES:  
 200 to 500 cm<sup>3</sup> STP/min (3g CHARCOAL)  
 500 to 1200 cm<sup>3</sup> STP/min (8g CHARCOAL)

Fig. 53. Schematic of capsule GB-10 tritium-monitoring system  
 (1 psi = 6895 Pa).

## 9. GB-10 DESIGN ANALYSES

Detailed design analyses of the fuel and cladding behavior, the power and temperature distributions in the capsule, and the fission-product behavior were made for capsule GB-10 and reported in the planning document for the experiment.<sup>22</sup> These analyses were a cooperative effort of GAC and ORNL and were performed in much the same way as the design analyses for the GB-9 experiment (see Sect. 4). Since the fuel, cladding, and operating conditions for GB-10 were similar to GB-9, much of the analyses for capsule GB-9 also apply to capsule GB-10. ORNL's main contributions to the design analyses for GB-10 consisted of detailed neutronic and thermal analyses of the capsule, gas systems flow and pressure drop analyses, shielding analyses, and hazards evaluation. Analyses performed by GAC included the detailed design of the fuel rod, analyses of the fuel and cladding behavior, and analyses of fission-product release and transport.

As was done for the GB-9 capsule, only the design information needed for presentation, interpretation, and discussion of the experimental results will be described in the present report. This information, consisting of predicted power distributions, predicted temperature distributions, thermocouple-to-cladding-hot-side temperature corrections, and predicted fission-product release, is given in the subsections below.

### 9.1 Predicted Power Distributions

The thermal design of the GB-10 capsule and the fissile-atom loading per unit length of fuel rod was essentially the same as that of the GB-9 capsule. Since the same irradiation facility position was used for GB-10, the only changes in input data required for the power-distribution calculations were the slightly different beginning-of-life (BOL) fuel geometry (solid pellets vs hollow pellets in GB-9) and an updated ORR core configuration (arrangement of fuel elements and experiments). Thus, the results of a  $R-\theta$  power-distribution calculation made at ORNL for GB-10 at BOL were similar to those made at GAC for GB-9 at BOL.

The techniques used in the  $R-\theta$  power-distribution calculations for GB-10 were described in detail in Ref. 22, and only the results will be

given here. The calculations were made for the BOL condition (solid pellets) and were based on the simplified reactor core and capsule configuration shown in Fig. 54. Capsule dimensions are listed in Table 5. The calculated BOL power-density distribution in the GB-10 fuel pellets is shown plotted in Fig. 55 as a function of  $\theta$  for six increments of R used in the calculations. The power density is in units of BTU/hr-in.<sup>3</sup> (which was a convenient unit for subsequent temperature-distribution calculations) and is normalized to a fuel-rod linear power of 52.5 kW/m (16 kW/ft).

ORNL-DWG 77-16279

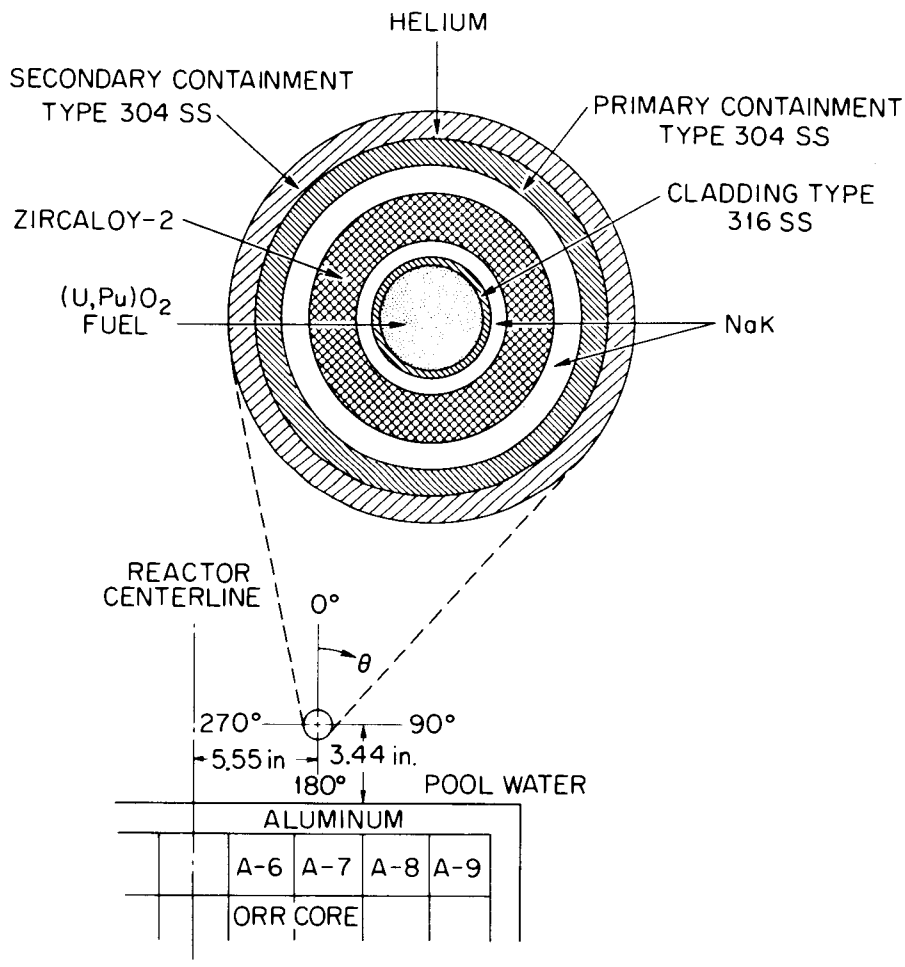


Fig. 54. Reactor and capsule configuration used in capsule GB-10 power-distribution calculations (1 in. = 2.54 cm).

Table 5. Capsule GB-10 dimensions at operating temperature for a cross section through the fueled portion of capsule

Material	Outer diameter at operating temperature (in.) <sup>a</sup>
Fuel	0.308
Cladding	0.357
Inner NaK	0.447
Zircaloy-2	0.742
Outer NaK	0.905
Inner type 304 stainless steel	1.061
Helium	1.062
Outer type 304 stainless steel	1.222

<sup>a</sup>1 in. = 2.54 cm.

ORNL-DWG 77-16280

○ CALCULATED POWER-DENSITY VALUES PLOTTED AT THE MIDPOINTS OF THE 15°θ INCREMENTS FOR WHICH THEY APPLY

ΔR<sub>1</sub>-ΔR<sub>6</sub> RADIAL INCREMENTS USED IN THE CALCULATIONS

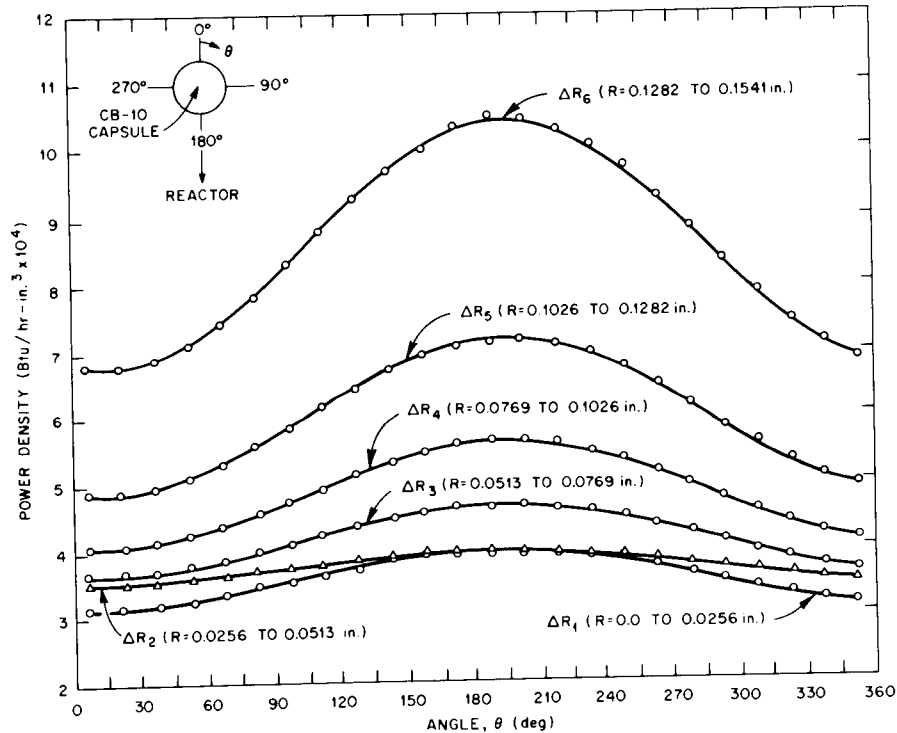


Fig. 55. Calculated angular power-density distributions in the capsule GB-10 fuel pellets normalized to a linear heat rate of 52.5 kW/m (16 kW/ft). (1 in. = 2.54 cm; 1 Btu/hr-in.<sup>3</sup> = 0.01788 W/cm<sup>3</sup>.)

The analysis of power peaking at the ends of the GB-9 fuel column (see Fig. 13, Sect. 4.1) applies equally as well for GB-10, since the same design was selected for the GB-10 rod.

## 9.2 Predicted Temperature Distributions

The calculated R- $\theta$  power distribution at BOL was used as input to calculations of the R- $\theta$  temperature distribution at BOL. For the temperature calculations, the calculated power-density curves of Fig. 55 were taken to be symmetrical about  $\theta = 195^\circ$  and are represented in the range between  $\theta = 15^\circ$  and  $195^\circ$  by the following equations:

$$Q(\theta')|_{\Delta R_1} = 3.16 \times 10^4 \left[ 1.137 - 0.00262 \left[ \frac{\pi}{180^\circ} \right] \theta' - 0.137 \cos \theta' \right],$$

$$Q(\theta')|_{\Delta R_2} = 3.51 \times 10^4 \left[ 1.090 - 0.0157 \left[ \frac{\pi}{180^\circ} \right] \theta' - 0.090 \cos \theta' \right],$$

$$Q(\theta')|_{\Delta R_3} = 3.65 \times 10^4 \left[ 1.130 + 0.00786 \left[ \frac{\pi}{180^\circ} \right] \theta' - 0.130 \cos \theta' \right],$$

$$Q(\theta')|_{\Delta R_4} = 4.10 \times 10^4 \left[ 1.178 + 0.00786 \left[ \frac{\pi}{180^\circ} \right] \theta' - 0.178 \cos \theta' \right],$$

$$Q(\theta')|_{\Delta R_5} = 4.90 \times 10^4 \left[ 1.228 + 0.00524 \left[ \frac{\pi}{180^\circ} \right] \theta' - 0.228 \cos \theta' \right],$$

and

$$Q(\theta')|_{\Delta R_6} = 6.78 \times 10^4 \left[ 1.239 + 0.02228 \left[ \frac{\pi}{180^\circ} \right] \theta' - 0.239 \cos \theta' \right],$$

where

$$\theta' = \theta - 15^\circ, \text{ degrees,}$$

$\Delta R_1 \rightarrow \Delta R_6$  = radial increments as defined in Fig. 55,

$Q(\theta')|_{\Delta R_i}$  = power density within  $\Delta R_i$  as a function of  $\theta'$ , Btu/hr-in.<sup>3</sup>.

The above equations fit the curves of Fig. 55 well, and when each is integrated from  $\theta' = 0^\circ$  to  $180^\circ$ , the sum of the integrals multiplied by 2 is equivalent to a linear heat rate of 52.7 kW/m (16.07 kW/ft). Other input data used in the temperature distribution calculations are listed in Table 6.

The HEATING3 program<sup>23</sup> was used to make the R- $\theta$  temperature-distribution calculations. Calculations were made for two fuel-rod linear heat ratings: 52.7 kW/m (16.07 kW/ft) and 48.4 kW/m (14.75 kW/ft). The 48.4 kW/m (14.75 kW/ft) heat rate was represented by multiplying each of the six equations given above by 0.918. The 48.4 kW/m case produced a peak cladding-OD temperature of 685°C, which was the full-power operating condition specified for the experiment. The calculated BOL angular temperature distributions at radii corresponding to the cladding outer surface and the radial position of the thermocouples monitoring the fuel-region cladding temperatures (near the Zircaloy-2 sleeve ID) are shown in Fig. 56 for the 48.4 kW/m (14.75 kW/ft) linear power case. Calculated BOL radial temperature distributions for the same linear power are shown in Fig. 57.

The HEATING3 program<sup>23</sup> was also used to make R-Z temperature-distribution calculations for the purpose of evaluating the overall capsule thermal design. The assumption of angular symmetry in these calculations permitted representation of the whole capsule in reasonable detail. Figure 58 shows the axial temperature profiles predicted for GB-10 for radii corresponding to the cladding ID and cladding OD. Also shown in the figure are the heat-generation rates used in the calculation. The total heat-generation rates in the fuel regions (fission plus gamma heating) were represented by Z-dependent analytical expressions in the calculation. These expressions, which are plotted in Fig. 58, represent a rough estimate of the power variation along the rod based on the axial shape of the unperturbed neutron flux in the facility (Fig. 7), the various pellet enrichments, and the power-peaking effects at the ends of the fuel column (Fig. 13, Sect. 4.1, which also applies for the GB-10 rod).

The predicted cladding temperature profile in Fig. 58 reasonably simulates that of a GCFR rod except for the lower end (below the fuel

Table 6. Input for R- $\theta$  temperature distribution calculations for capsule CB-10<sup>a</sup>

Dimensions at operating temperature for a cross section through fuel region	
Fuel pellet, OD, in. . . . .	0.308
Fuel-to-cladding radial helium gap (in lieu of using a thermal contact resistance), in. . . . .	0.0005
Type 316 stainless steel cladding thickness, in. . . . .	0.024
Cladding OD, in. . . . .	0.357
Inner NaK annulus thickness, in. . . . .	0.045
Zircaloy-2 thickness, in. . . . .	0.147
Outer NaK annulus thickness, in. . . . .	0.082
Primary containment (304 SS) thickness, in. . . . .	0.078
Helium gap between primary and secondary containments, in. . . . .	0.0005
Secondary containment (304 SS) thickness, in. . . . .	0.080
Capsule OD, in. . . . .	1.222
Heat-generation rates	
Fuel region . . . . .	See text
Other than fuel region (gamma heating), W/g of material . . . . .	1.3
ORR pool water temperature, °C . . . . .	57.0
Capsule-to-pool-water effective heat transfer coefficient (in lieu of representing subcooled pool boiling condition), Btu/hr-in. <sup>2</sup> -°C . . . . .	17.0
Thermal conductivity data <sup>b</sup>	

Material	Thermal conductivity (Btu/hr-in.-°C)								
	37.8°C	93°C	204°C	316°C	400°C	427°C	500°C	538°C	600°C
(U,Pu)O <sub>2</sub>					0.301		0.260		0.233
Helium	0.0138	0.0153	0.0180	0.0207		0.0234		0.0261	
316 SS	1.31	1.36	1.48	1.58		1.68		1.81	
NaK-44	2.21	2.24	2.31	2.36		2.42		2.45	
Zircaloy-2	0.995	1.05	1.14	1.25		1.42		1.62	
304 SS	1.22	1.30	1.47	1.63		1.80		1.97	
	649°C	700°C	760°C	800°C	871°C	900°C	982°C	1000°C	1093°C
(U,Pu)O <sub>2</sub>		0.213		0.198		0.187		0.178	
Helium	0.0290		0.0315		0.0344		0.0371		0.0398
316 SS	1.95		2.09		2.24		2.39		2.55
NaK-44	2.45		2.39		2.29		2.15		2.00
Zircaloy-2	1.80		1.86						
304 SS	2.13		2.30						
	1200°C	1204°C	1316°C	1400°C	1427°C	1538°C	1600°C	1649°C	1800°C
(U,Pu)O <sub>2</sub>	0.164			0.154			0.147		0.141
Helium		0.0426	0.0453		0.0480	0.0507		0.0536	
316 SS		2.72	2.88						
	2000°C	2200°C	2204°C	2400°C	2600°C	2760°C	2800°C	3000°C	3316°C
(U,Pu)O <sub>2</sub>	0.137	0.133		0.130	0.127		0.125	0.123	
Helium			0.0671			0.0807			0.0944

<sup>a</sup>Conversion factors: 1 in. = 2.54 cm; 1 Btu/hr-in.<sup>2</sup>-°C = 0.0454 W/cm<sup>2</sup>-°C; 1 Btu/hr-in.-°C = 0.115 W/cm-°C.

<sup>b</sup>The HEATING3 program performs linear interpolation to obtain the thermal conductivity at a particular temperature within the input range.

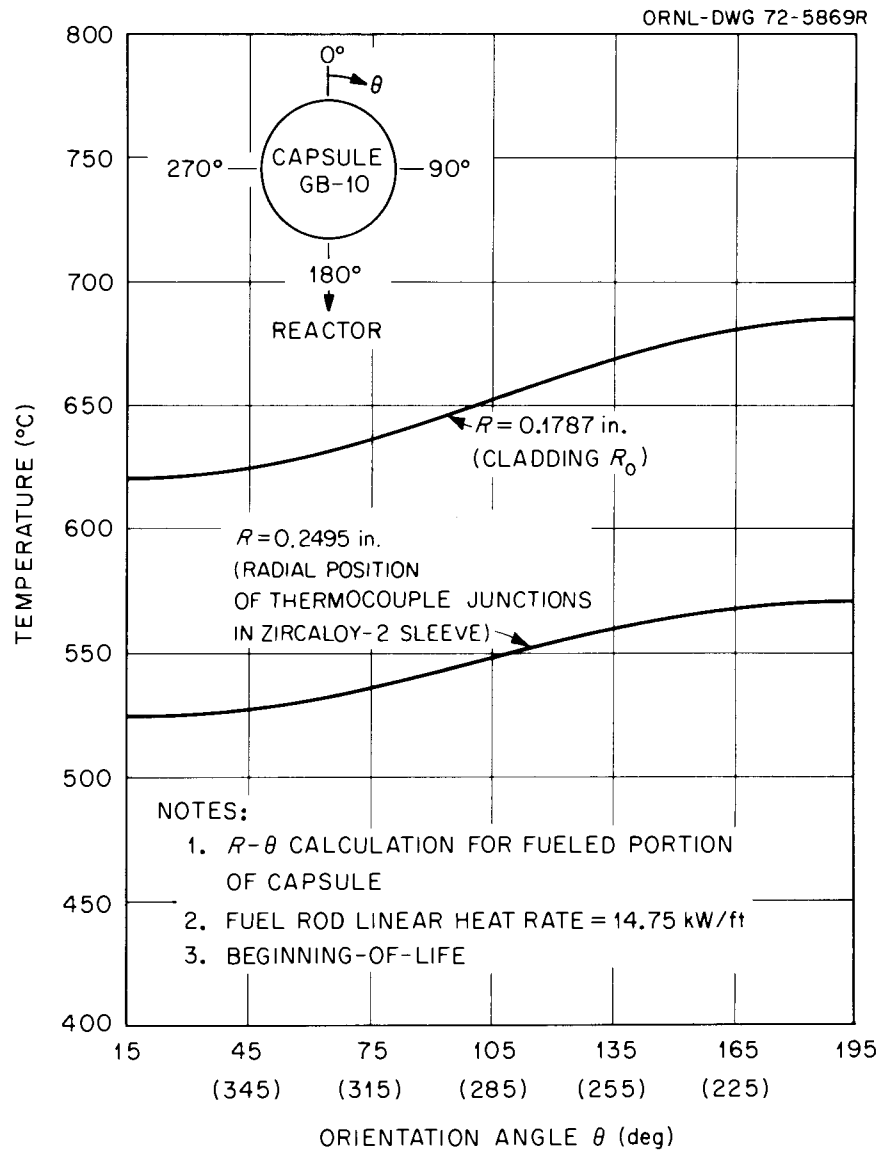


Fig. 56. Calculated angular temperature distributions for capsule GB-10 (1 in. = 2.54 cm; 1 ft = 0.3048 m).

region). The downward flow of hot coolant gas in the GCFR will keep the lower blanket and bottom end of the GCFR rod at a higher temperature (200 to 300°C higher) than that of the upper blanket region. The 5%-enriched  $UO_2$  pellet was included at the lower end of the GB-10 rod in an attempt to minimize the effect of the cold lower end on fission-product transport within the rod. Temperature peaking within the 5%-enriched  $UO_2$  pellet should discourage volatile fission-product transport downward past this

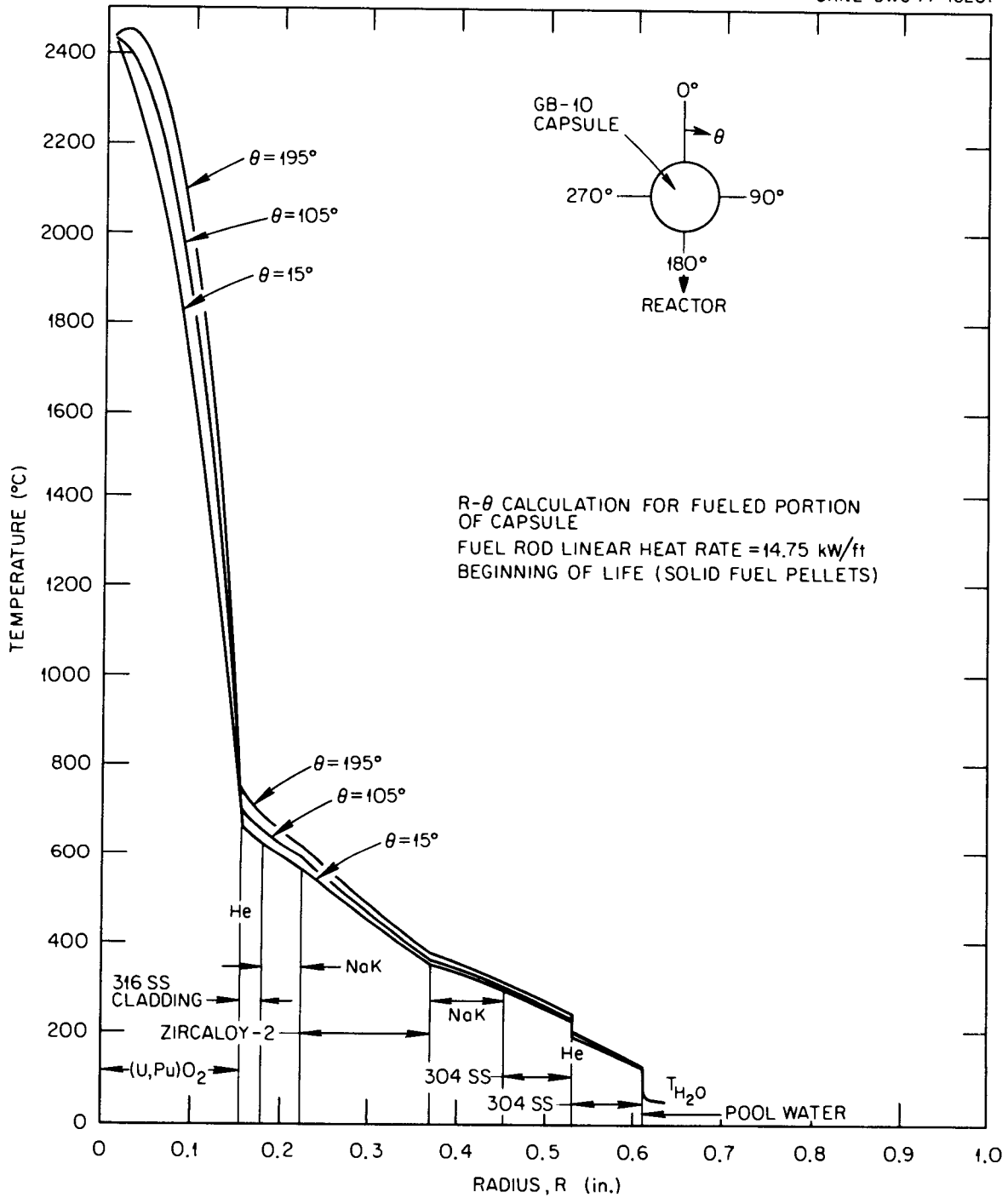


Fig. 57. Calculated radial temperature distributions for capsule GB-10 (1 in. = 2.54 cm; 1 ft = 0.3048 m).

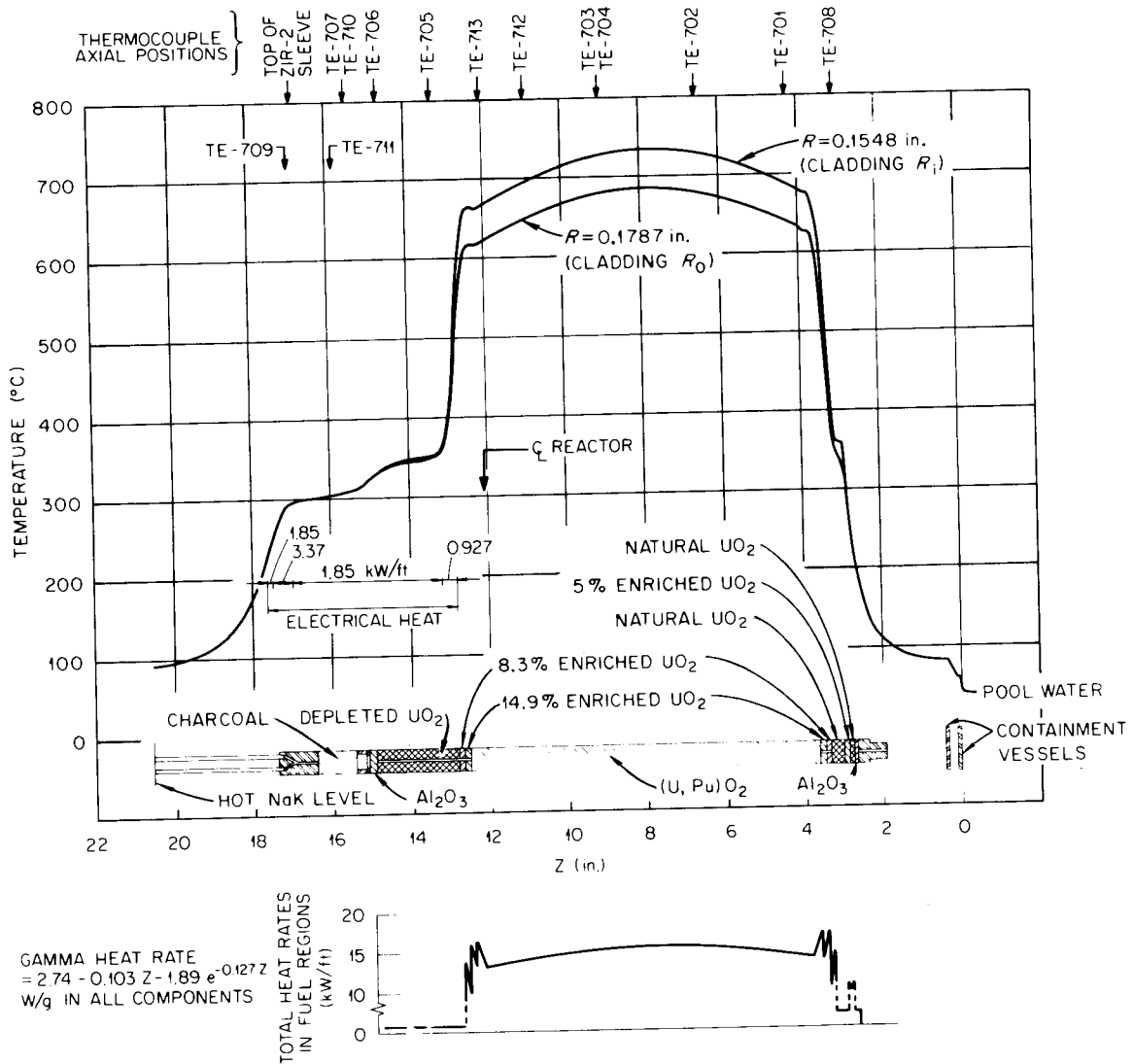


Fig. 58. Calculated axial temperature distributions for capsule GB-10 (1 in. = 2.54 cm; 1 ft = 0.3048 m).

point in the rod. Postirradiation gamma scans of the GB-9 fuel rod, which had an unheated lower blanket of one depleted  $UO_2$  pellet, indicated plate-out of the volatile fission products  $^{134}Cs$ ,  $^{137}Cs$ , and  $^{131}I$  at both fuel-blanket interfaces, with very little transport beyond these points. The plateout peaks at the lower fuel-blanket interface were larger than the peaks at the top interface (this can be seen in Fig. 1 of Ref. 9), and this was the main reason for changing the lower end design for GB-10.

### 9.3 Comparison of GB-9 and GB-10 Predicted Power Levels

The GB-10 capsule design was such that, for the uniform-angular-power case (Fig. 58), a fuel-rod linear power of approximately 51 kW/m (15.5 kW/ft) was required to produce a uniform cladding-OD peak temperature of 685°C. The GB-9 fuel-rod linear power required to produce the uniform cladding-OD temperature of 685°C in a similar R-Z temperature calculation (Fig. 15) was approximately 53 kW/m (16.1 kW/ft). The difference in these calculated linear power values is only about 4% and is due to slight differences in the capsule dimensions and the values for gamma heating used in the calculations. The gamma heating values were revised upward for GB-10 from the peak value of 0.7 W/g used in the GB-9 R-Z temperature calculation (Fig. 15) to a peak value of 1.25 W/g used in the GB-10 temperature calculations. Although the difference in gamma heating rates used was large, the effect on the calculations was small because the principal source of heat in both capsules was fission heat. For all practical purposes, then, the full-power operating conditions of the GB-9 and GB-10 fuel rods were the same: 48.4 kW/m (14.75 kW/ft) fuel-rod linear power to produce a peak cladding-OD temperature of 685°C based on the R- $\theta$  temperature calculations at BOL and 51 kW/m (15.5 kW/ft) for the assumed uniform-angular-power case. The latter case is of interest at high fuel-burnup levels, since preferential depletion of fuel on the high-neutron-flux side of the rod results in an actual trend toward the uniform-angular-power case with time.

### 9.4 Thermocouple-to-Cladding-Hot-Side Temperature Corrections

As was done in the GB-9 experiment, the calculated GB-10 temperature distributions were used as a basis for controlling the peak cladding-OD temperature at the desired level during the irradiation. The R- $\theta$  temperature-distribution calculations were used to develop BOL temperature corrections for each of the six thermocouples monitoring the GB-10 fuel-region cladding temperatures. With the  $\theta$  positions of the thermocouples known, full-power temperature corrections from the points of measurement to the maximum cladding-OD temperature (685°C) could be taken directly

from the calculated R- $\theta$  temperature distributions of Fig. 56. The radial positions of the six fuel-region thermocouples were taken to be the same, since their junction ends were positioned at the ID of the Zircaloy-2 sleeve, using a close-fitting mandrel inserted into the sleeve for this purpose. The full-power BOL temperature corrections thus obtained for the six GB-10 fuel-region thermocouples are listed in Table 7.

The sensitivity of the temperature corrections to uncertainties in the input data, such as the radial location of the thermocouple junction, thermal conductivities, etc., was estimated for the GB-9 capsule (see Sect. 4.3), which had the same design, and applies equally as well for GB-10. As in that analysis, the probable error in the BOL temperature corrections for GB-10 is estimated to be  $\pm 25^\circ\text{C}$ , most of which is due to the uncertainty in the exact radial locations of the thermocouple junctions in the fairly steep temperature gradient. Not taken into account in the probable error estimate is the possibility of fuel-rod bowing, which would change the dimensions of the inner NaK gap.

Since the temperature corrections of Table 7 assume full power at each thermocouple elevation, it was necessary to adjust the corrections, whenever they were used, to correspond to the local power along the rod. By assuming that the temperature drop from the cladding OD to the pool water outside the capsule is proportional to the fuel-rod linear power at each thermocouple elevation (a reasonably good assumption for the GB-10 capsule, at least down to about 50% of full power), the following equation is obtained for the local fuel-rod linear power as a function of the thermocouple reading and its full-power temperature correction:

$$\frac{P_i}{48.6 \text{ kW/m}} = \frac{[T_i + (P_i/48.6 \text{ kW/m}) (\text{FPC}_i)] - T_f}{685 - T_f}$$

or

$$\frac{P_i}{48.6 \text{ kW/m}} = \frac{T_i - 40}{645 - \text{FPC}_i}, \quad (4)$$

Table 7. Approximate full-power thermocouple-to-cladding-hot-side temperature corrections for the thermocouples monitoring the temperature of the fuel-region cladding outer surface in capsule GB-10

Thermocouple No.	Axial position, distance from bottom of fuel region <sup>a</sup> (in.)	$\theta$ , angular position <sup>b</sup> (degrees)	Temperature correction <sup>c</sup> (°C)		
			Radial component	Circumferential component	Total
701	0.97	60	99	54	153
702	3.28	120	107	24	131
703	5.74	180	114	1	115
704	5.74	0	96	63	159
712	7.65	270	107	24	131
713	8.74	210	114	1	115

<sup>a</sup>Bottom of fuel region is defined here as bottom of lower 8.3%-enriched UO<sub>2</sub> pellet. (1 in. = 2.54 cm.)

<sup>b</sup>When looking down on the capsule,  $\theta$  is the angle measured in a clockwise direction, with 0° being the farthest position from the reactor face.

<sup>c</sup>Based on the calculated beginning-of-life R- $\theta$  power and temperature distributions with normalization to 48.4 kW/m (14.75 kW/ft) linear power at each thermocouple axial position.

where

$P_i$  = local fuel-rod linear power indicated by fuel-region thermocouple  $i$ , kW/m,

$T_i$  = reading of fuel-region thermocouple  $i$ , °C,

$FPC_i$  = full-power temperature correction for fuel-region thermocouple  $i$  (Table 7), °C,

$T_f$  = pool-water bulk fluid temperature (estimated to be 40°C), °C.

Previously, a pool-water temperature of 57°C was used in the GB-9 and GB-10 design calculations. The value was revised early in the operation of capsule GB-10 when the two thermocouples strapped to the capsule OD indicated the lower value. The difference of 17°C has very little significance in the calculations.

The indicated hot-side cladding-OD temperature in °C at each thermocouple location,  $T$  (cladding OD, hot side,  $i$ ), is then given by the following equation:

$$T(\text{cladding OD, hot side, } i) = T_i + \frac{P_i}{48.6 \text{ kW/m}} (FPC_i) . \quad (5)$$

In general, the full-power temperature corrections should be adjusted with increasing fuel burnup, since the power distribution across the rod will tend to flatten as fuel is preferentially depleted on the high-neutron-flux side of the rod. We had planned to make some calculations of the  $R-\theta$  power- and temperature-distribution behavior to be expected as a function of fuel burnup in the GB-10 rod. However, this has not been done because the funding available for the experiment did not permit the rather large effort that would be required. These calculations would also aid in the interpretation of fission-gas release behavior.

### 9.5 Predicted Fission-Gas Release Fractions

Release fractions for capsule GB-10 were computed by GAC at the time the experiment was designed. These calculations<sup>22</sup> were based on diffusional release models in which the release fractions were separated into

two parts: (1) the release from the solid oxide matrix and (2) the release by gas-phase diffusion through the major regions of the rod [i.e., the fuel, upper blanket, charcoal trap, and top end plug (or fuel-rod exit)].

In the calculations, release from the solid oxide matrix was assumed to proceed according to a diffusion process. Release parameters used in the diffusion model were derived by Findley et al.<sup>24</sup> The predicted release fractions of gaseous and volatile fission-products from the oxide-fuel matrix for full-power operation of GB-10 are given in Table 8.

During normal steady-state operation of GB-10 under sweep flow mode TT-TT (see Fig. 50 and associated text in Sect. 8.3 for flow mode definitions), gases must diffuse upward to the top end plug of the rod before entering the sweep stream. Under this condition, the volatile fission products were expected to plate out rapidly in the cooler regions of the fuel and at the fuel-blanket interfaces, as was found to be the case in capsule GB-9. When the sweep was directed through the fuel region, volatile fission products may have been transported farther from the fuel region by the sweep itself. Under the BF-TT flow mode, the charcoal trap was expected to remove volatile fission products. Even when the flow was directed through the fuel rod and the trap was bypassed (BF-BT or BF-BB flow mode), any volatile fission products remaining in the gas were expected to plate out rapidly on the effluent sweep line, perhaps within a short distance of the fuel rod. Thus, during active sweeping of the fuel, the activity in the sweep gas a short distance from the capsule was expected to consist almost entirely of that from krypton and xenon gases. Plating out on the lines would be the daughter products of the noble gases.

The release of six of the krypton and xenon gases from the main regions of the GB-10 rod for the case of normal steady-state full-power operation was computed by GAC based on two different assumptions regarding the fuel region.<sup>22</sup> These predicted release fractions are given in Table 9, where the release fractions from each region were obtained by multiplying the release fractions from the oxide matrix by the gas-phase release-suppression factors. In the first calculation, the actual fuel

Table 8. Calculated gaseous and volatile fission-product release fractions from oxide-fuel matrix of irradiation capsule GB-10

Isotope	Half-life	R/B (%)	Isotope	Half-life	R/B (%)
<sup>81</sup> Br	Stable	100.0	<sup>127</sup> I	Stable	97.3
<sup>83</sup> Br	2.3 hr	24.9	<sup>129</sup> I	Stable	97.3
<sup>84</sup> Br	31.8 min	13.3	<sup>131</sup> I	8.05 day	68.8
<sup>85</sup> Br	3.00 min	4.33	<sup>132</sup> I	2.33 hr	24.4
<sup>87</sup> Br	55.0 sec	2.42	<sup>133</sup> I	20.9 hr	47.4
<sup>88</sup> Br	15.5 sec	1.30	<sup>134</sup> I	54.0 min	16.5
<sup>89</sup> Br	4.5 sec	0.701	<sup>135</sup> I	6.75 hr	35.2
<sup>83m</sup> Kr	1.87 hr	22.9	<sup>136</sup> I	1.43 min	3.00
<sup>83</sup> Kr	Stable	100.0	<sup>137</sup> I	24.0 sec	1.60
<sup>84</sup> Kr	Stable	100.0	<sup>138</sup> I	6.00 sec	0.807
<sup>85m</sup> Kr	4.40 hr	31.7	<sup>139</sup> I	2.00 sec	0.465
<sup>85</sup> Kr	10.3 year	100.0	<sup>131m</sup> Xe	12.0 day	72.1
<sup>86</sup> Kr	Stable	100.0	<sup>131</sup> Xe	Stable	97.3
<sup>87</sup> Kr	1.30 hr	19.7	<sup>132</sup> Xe	Stable	97.3
<sup>88</sup> Kr	2.80 hr	26.80	<sup>133m</sup> Xe	2.30 day	57.4
<sup>89</sup> Kr	3.20 min	4.47	<sup>133</sup> Xe	5.27 day	65.2
<sup>90</sup> Kr	33.0 sec	1.88	<sup>134</sup> Xe	Stable	97.3
<sup>91</sup> Kr	10.0 sec	1.04	<sup>135m</sup> Xe	15.3 min	9.36
<sup>92</sup> Kr	3.0 sec	0.573	<sup>135</sup> Xe	5.76 hr <sup>a</sup>	33.0
<sup>93</sup> Kr	2.0 sec	0.468	<sup>136</sup> Xe	Stable	97.3
<sup>94</sup> Kr	1.0 sec	0.331	<sup>137</sup> Xe	3.90 min	4.89
<sup>131</sup> Sn	3.40 min	4.77	<sup>138</sup> Xe	17.0 min	9.83
<sup>131</sup> Sb	23.1 min	11.3	<sup>139</sup> Xe	41.0 sec	2.09
<sup>125m</sup> Te	58.0 day	83.3	<sup>140</sup> Xe	16.0 sec	1.31
<sup>125</sup> Te	Stable	97.3	<sup>141</sup> Xe	2.00 sec	0.465
<sup>126</sup> Te	Stable	97.3	<sup>133</sup> Cs	Stable	97.3
<sup>127m</sup> Te	105.0 day	87.1	<sup>134</sup> Cs	2.20 year	96.7
<sup>127</sup> Te	9.35 hr	38.7	<sup>135</sup> Cs	Stable	97.3
<sup>128</sup> Te	Stable	97.3	<sup>136</sup> Cs	13.0 day	72.7
<sup>129m</sup> Te	33.0 day	79.5	<sup>137</sup> Cs	30.0 year	97.3
<sup>129</sup> Te	1.23 hr	18.9	<sup>138</sup> Cs	32.2 min	13.2
<sup>130</sup> Te	Stable	97.3	<sup>139</sup> Cs	9.50 min	7.47
<sup>131m</sup> Te	1.21 day	50.9	<sup>140</sup> Cs	1.10 min	2.64
<sup>131</sup> Te	24.8 min	11.7	<sup>141</sup> Cs	1.00 sec	0.340
<sup>132</sup> Te	3.21 day	60.6	<sup>142</sup> Cs	1.00 min	2.11
<sup>133m</sup> Te	53.0 min	16.4	<sup>143</sup> Cs	1.00 sec <sup>*</sup>	0.330
<sup>133</sup> Te	2.00 min	3.53	<sup>144</sup> Cs	1.00 sec	0.330
<sup>134</sup> Te	44.0 min	15.1			

<sup>a</sup>Actual half-life is 9.13 hr; an effective half-life is used here to account for burnup of <sup>135</sup>Xe in the high thermal neutron flux.

Table 9. Release fractions predicted for oxide-fuel matrix and gas-phase regions in irradiation capsule GB-10

Isotope	Half-life	Release fraction from oxide-fuel matrix (%)	Gas-phase release-suppression factors				Release fractions, R/B (%)			
			To top of fuel	To top of blanket	To top of trap	To fuel-rod exit	From fuel region	From blanket region	From trap	From fuel-rod exit
<u>Actual-fuel-length assumption</u>										
<sup>85m</sup> Kr	4.40 hr	32	0.189	0.102	0.0822	0.0794	6.1	3.3	2.6	2.5
<sup>87</sup> Kr	1.30 hr	20	0.0958	0.0216	0.0120	0.0107	1.9	0.43	0.24	0.21
<sup>88</sup> Kr	2.80 hr	27	0.146	0.0606	0.0442	0.0419	3.9	1.6	1.2	1.1
<sup>133</sup> Xe	5.0 day	65	0.786	0.766	0.758	0.757	51.1	49.8	49.3	49.3
<sup>135</sup> Xe	9.13 hr	33	0.201	0.114	0.0937	0.0908	6.6	3.8	3.1	3.0
<sup>138</sup> Xe	17.0 min (5.76 hr) <sup>a</sup>	9.8	0.0396	0.000715	0.000132	0.0000741	0.39	0.0070	0.0013	0.00073
<u>Shortened-fuel-length assumption</u>										
<sup>85m</sup> Kr	4.40 hr	32	0.678	0.449	0.363	0.351	21.7	14.4	11.6	11.2
<sup>87</sup> Kr	1.30 hr	20	0.578	0.159	0.0890	0.0794	11.6	3.18	1.78	1.59
<sup>88</sup> Kr	2.80 hr	27	0.643	0.329	0.240	0.228	17.4	8.88	6.48	6.16
<sup>133</sup> Xe	5.0 day	65	0.988	0.953	0.943	0.942	64.2	61.9	61.3	61.2
<sup>135</sup> Xe	9.13 hr	33	0.685	0.477	0.394	0.382	22.6	15.7	13.0	12.6
<sup>138</sup> Xe	17.0 min (5.76 hr) <sup>a</sup>	9.8	0.411	0.00896	0.00167	0.000947	4.03	0.0878	0.0164	0.00928

<sup>a</sup>An effective half-life of <sup>135</sup>Xe of 5.76 hr was used in the calculations to account for burnup of the <sup>135</sup>Xe in the high thermal neutron flux as well as loss by decay.

length was used, and thermal convection in the fuel region was ignored. In the second calculation, it was assumed that thermal convection did occur and that this condition could be simulated by a shortened fuel region, which effectively reduced the resistance in the fuel region to a low value. Thus, the predicted release fractions of Table 9 may be interpreted as predicted ranges of release fractions for the various isotopes.

While the fission-product release and transport models are still being refined, the original calculations for the GB-9 and GB-10 experiments served both as a starting point for model development for the GCFR and as a means of providing the information needed for experiment design, especially for design of the sweep system and associated equipment.

## 10. GB-10 IRRADIATION CONDITIONS AND GENERAL OPERATING PROCEDURE

Capsule GB-10 was irradiated in much the same manner as its predecessor, capsule GB-9, except that GB-10 was operated at three successive power levels instead of one: 39.4, 44.3, and 48.6 kW/m (12, 13.5, and 14.8 kW/ft) fuel-rod nominal peak-power levels at nominal peak cladding-OD temperatures of 565, 630, and 685°C, respectively. Capsule GB-9 was operated at the one nominal peak-power level of 48.6 kW/m (685°C nominal peak cladding-OD temperature). This plan for the GB-10 irradiation was designed to best meet the needs of both the GCFR and LMFBR fuel-development programs. The GB-10 capsule had the unique capability of providing basic fission-gas release data for the oxide fuel, which could be applied to either GCFR or LMFBR fuel rods. Primary LMFBR interest was at the reduced power levels.

The irradiation of capsule GB-10 in the ORR poolside facility was started in August 1972 and successfully completed on Aug. 1, 1976. Steady-state operating conditions and exposures reached in the GB-10 experiment are summarized in Table 10. The fuel rod was operated first at the nominal power level of 39.4 kW/m (12 kW/ft) for 295 days, then at 44.3 kW/m (13.5 kW/ft) for 498 days, and finally at 48.6 kW/m (14.8 kW/ft) for 179 days, for a total of 972 days at power. The two power increases occurred on Sept. 12, 1973, and Nov. 6, 1975. The nominal peak cladding temperatures corresponding to the three power levels of operation are 565, 630, and 685°C, respectively. Power level and temperature are directly related, since the capsule was not designed for temperature control independent of power, except for the electrically heated upper portion of the rod, which was controlled to give a 300°C charcoal trap temperature. Pressures were maintained at 6.9 MPa gage (1000 psig) inside the rod and 975 psig external to the rod. The fuel burnup goal of 100 MWd/kg heavy metal was reached. The original burnup goal was 75 MWd/kg but was revised to 100 MWd/kg to permit additional experimental measurements. These operating conditions and exposure are reasonably close to those expected for a GCFR fuel rod, except for the absence of significant fast-neutron exposure.

Table 10. GCFR capsule GB-10 operating conditions

<u>Steady-state operation conditions</u>			
Fuel-rod operation power levels, <sup>a</sup> kW/m (kW/ft)	39.4 (12.0)	44.3 (13.5)	48.6 (14.8)
Cladding temperatures, <sup>a</sup> OD, °C			
Fuel region, peak	565	630	685
Charcoal trap	300	300	300
Cladding pressure, MPa gage (psig)			
External	6.7 (975)	6.7 (975)	6.7 (975)
Internal	6.9 (1000)	6.9 (1000)	6.9 (1000)
<u>Total exposure</u>			
Time at power, days			972
Fuel burnup, <sup>a</sup> MWd/kg heavy metal			~100
Fast-neutron exposure (E > 0.18 MeV), neu- trons/cm <sup>2</sup>			~1 × 10 <sup>20</sup>

<sup>a</sup>Nominal values.

In operating the capsule, small position adjustments were made as required to maintain the indicated peak cladding-OD temperature within  $\pm 15^\circ\text{C}$  of the desired value at each power level of operation. As in operating the GB-9 capsule, the peak cladding-OD temperature was taken to be the highest indication obtained when the readings of the six fuel-region thermocouples were corrected to cladding-OD-hot-side temperatures. Local fuel-rod linear power and cladding temperature at each thermocouple elevation at any given time were determined in accordance with Eqs. (4) and (5), Sect. 9.4. The full-power thermocouple corrections listed in Table 7, Sect. 9.4 were used in conjunction with Eqs. (4) and (5) throughout the irradiation. No adjustment of the full-power corrections of Table 7 was made to take into account the effect of fuel burnup. Fuel burnup at any given time during the irradiation was estimated using the

following equation:

$$Bu = 0.09186\tau_1 + 0.1037\tau_2 + 0.1134\tau_3 \quad (6)$$

where:

Bu = fuel burnup, MWd/kg heavy metal,

$\tau_1, \tau_2, \tau_3$  = irradiation time accumulated at each of the three successive power levels of operation [39.4, 44.3, and 48.6 kW/m (12, 13.5, and 14.8 kW/ft)], respectively, days.

Equation (6), which is consistent with Eq. (3) used for estimating GB-9 fuel burnup, gives a reasonably close but perhaps conservative estimate of fuel burnup level. If fuel burnup levels were estimated for GB-10 on the basis of the BOL thermal analyses (i.e., based on assuming constant power operation at each of the three successive nominal power levels of 39.4, 44.3, and 48.6 kW/m), the calculated values would be approximately 18% higher. Suspecting the latter basis might lead to burnup estimates that were too high, we elected to use the more conservative burnup equation instead.

The uncertainties introduced and problems associated with using the GB-10 BOL temperature corrections throughout the irradiation were greater than was the case for GB-9, because GB-10 was irradiated to a much higher burnup level. Also, the fuel-rod power was raised to the full-power level only after operation at the two reduced-power levels to a fuel burnup of  $\sim 78.7$  MWd/kg heavy metal. At this point, burnup effects on the temperature corrections were already significant. A more detailed discussion of the uncertainties in the operating power, cladding temperature, fuel burnup, and other parameters is given in Sect. 13 for both the GB-9 and GB-10 experiments. The procedures described above for estimating nominal power levels and cladding temperatures were used during the irradiation, but they should not be regarded as our best estimates of actual conditions (see Sect. 11.2).

The flow of sweep gas was maintained, normally across the top of the rod (TT-TT flow mode), whenever the GB-10 capsule was at power. Fission

gases were therefore free to diffuse out of the fuel rod, as in the case of the GCFR rod. The irradiation was interrupted occasionally for short periods for reactor refueling shutdowns ( $\sim 4-6$  hr once every 10 to 14 days) and reactor end-of-cycle shutdowns (5 to 6 days every 2 months). Other interruptions of a few weeks occurred for the installation of new equipment and maintenance work.

At the start of the GB-10 irradiation, fission-gas release was monitored by taking gas samples periodically and analyzing the sample by gamma-ray spectrometry. In addition, the effluent sweep line activity was monitored continuously by two ionization chambers, as was done in the GB-9 irradiation. During the course of the irradiation, the GB-10 measurements and goals were expanded and three new systems were installed to increase capability for the study of fission-product release and transport: (1) an on-line Ge(Li) gamma-ray detector system for easier and more detailed fission-gas release measurements, (2) a sampling system for determination of stable noble gas release rates using mass spectrometry, and (3) a tritium-monitoring system (see Sect. 8.3 for a description of these systems). The design, installation, and debugging of these three systems required considerable effort and expenditure of limited GB-10 funding. The on-line Ge(Li) detector system was placed in operation in March 1974 (fuel burnup level of  $\sim 41$  MWd/kg heavy metal); the system for determination of stable noble gas release rates was placed in operation in July 1974 (fuel burnup level of  $\sim 48$  MWd/kg); and the tritium-monitoring system was placed in operation in June 1975 (fuel burnup of  $\sim 69$  MWd/kg).

In making fission-gas release measurements under steady-state operating conditions, the normal sampling order, or on-line analyses order, was to start at the top of the rod (TT-TT sweep flow mode — see Fig. 50 and associated text in Sect. 8.3 for flow mode definitions) and work downward so that the inventory of fission products below the sweeping point in each case was not unnecessarily disturbed. Following each change in sweep flow mode, a period of 1-2 hr was allowed for the activity release rate to level out before taking the sample or starting the on-line analysis. After completion, the flow mode was switched back to the TT-TT flow mode. Subsequent steady-state measurements were made only after allowing at least 24 hr for the rod activity to return to equilibrium.

In addition to measurements of the steady-state fission-gas release as a function of fuel burnup and power level, measurements of the internal gas-flow conductance of the fuel rod were obtained each time the sweep was directed through the fuel region. The latter data are important in ensuring adequate pressure equalization of the GCFR rod. Special tests were also performed to determine fission-gas release dependence on pressure level and to obtain information on fission-gas release behavior during shutdowns and startups, on fission-product decay heating in the charcoal trap, and on volatile fission-product deposition in the system. Neutron radiography of the capsule was performed before, during, and near the end of the irradiation.

Funding for the GB-10 experiment became a critical problem two times during the irradiation. Although this affected our ability to realize the full potential of the experiment, most of the original goals for the experiment were reached, and a good portion of the expanded work, including a number of significant tritium-monitoring experiments, were completed. The first funding problem occurred the second 6 months of operation (latter half of FY 1973) and was caused by higher-than-anticipated costs of constructing and installing the capsule. The second problem period occurred between Oct. 1, 1975, and late February 1976 and was caused by underfunding of the complex measurements being attempted. During both periods, the capsule had to be operated on a minimum-effort basis until additional funding was obtained. During the latter period, significant development work in progress had to be terminated, including a relatively simple modification being made to the stable noble gas sampling system. Instruments and equipment for accurate measurement of  $H_2$  and  $H_2/H_2O$  levels in the GB-10 sweep gas upstream and downstream of the capsule and for eventual injection and control of these impurity levels were being evaluated and calibrated in the laboratory. This work, as well as some of the routine GB-10 measurements, had to be terminated. Funding for additional tritium-monitoring experiments (also terminated on Oct. 1, 1976) was not obtained until the middle of June 1976.

## 11. RESULTS FROM IRRADIATION TESTING OF CAPSULE GB-10

Experimental results obtained from the GB-10 irradiation are given in the following subsections. The GB-10 measurements were a continuation of the measurements started with capsule GB-9 and include measurements which could not be obtained with GB-9, such as the internal gas-flow conductance of the fuel rod and fission-gas release from the oxide-fuel matrix. The results obtained from the two similar experiments are complementary and, taken together, provide substantial information on the behavior to be expected from the GCFR vented-and-pressure-equalized fuel rod.

It should be emphasized that the nominal values of fuel-rod linear power, fuel-region cladding temperature, and fuel burnup that are used in presenting the GB-10 experimental data were estimated in accordance with the methods outline in Sect. 10, using Eqs. (4), (5), and (6), respectively. What we consider to be better estimates of the thermal operating history of the GB-10 rod are given in Sect. 11.2 below. A detailed discussion of uncertainties in these and other parameters and in the experimental results is given in Sect. 13 for both the GB-9 and GB-10 experiments.

The measurements that were considered during the GB-10 irradiation include those listed in Table 11. Most of the measurements were completed; some were deferred to the next experiment (assuming there is another one similar to GB-10). Measurement and control of  $H_2$  and  $H_2/H_2O$  ratio in the sweep gas was found to be too complex and expensive to add to the GB-10 experiment, considering the funding and time limitations.

A few comments on the items listed in Table 11 will serve to indicate the scope of the GB-10 work and the results to be presented in the following sections. With respect to the first item listed, we believe that detailed evaluation of the thermal operating data to minimize uncertainties in the temperature and power history of the rod is especially important for interpreting and characterizing the other GB-10 measurements. The fuel-rod flow conductance measurements made as a function of time during the irradiation are also considered to be important; the data indicated development of a severe flow constriction during the latter part of the irradiation.

Table 11. GB-10 measurements

---

Thermal operating data
Fuel-rod internal gas-flow conductance
Fission-product release and transport
Radioactive gamma-emitting noble gases
Stable noble gases
Volatile fission products
Tritium
Simulated fuel-rod leak test (release spectrum as a function of flow rate)
Depressurization tests (deferred to GB-11)
Power cycling tests (deferred to GB-11)
Neutron radiography
Measurement and control of H <sub>2</sub> and H <sub>2</sub> /H <sub>2</sub> O ratio in sweep gas (deferred to GB-11)

---

Most of the planned measurements on fission-product release and transport were completed. Release of the radioactive noble gases was measured as a function of time, fuel-rod power level, and pressure level, and during shutdown and startups. We had measurement difficulties with the stable noble gases, and funding did not allow successful completion of that effort. Our measurements, during irradiation, pertaining to release and transport of volatile fission products, such as cesium, iodine, bromine, and tellurium, were limited to iodine deposition measurements, observations of decay heating in the fuel-rod trap, and observations of long-lived activity deposition at accessible points in the sweep system. Detailed distributions of a number of the volatile fission products, including <sup>131</sup>I, have been determined from extensive postirradiation gamma scanning.

A number of tritium-monitoring experiments were conducted to obtain information on tritium release and transport behavior; both the normal GB-10 high-purity helium sweep containing <5 ppm hydrogen and specially prepared 10,000-ppm-H<sub>2</sub>-in-helium gas were used in the experiments. The tritium experiments represented a relatively large effort, and the results

of this work will be reported in detail in a separate report.<sup>25</sup> Only general statements of the findings will be included here.

The simulated fuel-rod leak test was not much different from our routine release analysis. This test was designed to acquire the release data over a wide range of flow rates, or simulated leak rates, at one given point during the irradiation.

The depressurization tests were of lower priority than some of the other tests and were deferred to the next experiment. Release behavior during several slow pressure-cycling tests was observed in the GB-9 experiment (see Sect. 6.4).

Preparations were made to conduct power cycling tests near the end of the irradiation, but it was decided that they should not be done because of the risk of fuel-rod failure and possible loss of subsequent postirradiation data if NaK entered the rod. The GB-10 rod had shown a sharp decrease in internal gas-flow conductance at power by this time, and this partially plugged condition was believed to significantly increase the chance of a cladding failure. Plans for these tests were to cycle the fuel-rod power between 44.3 and 39.9, 35.4, 31.0, and 26.6 kW/m (13.5 and 8-12 kW/ft) in a series of tests, at a rate of power change of  $\sim 3\%/min$ , to obtain release data and determine the number of cycles to reach cyclic equilibrium release conditions in each test.

Neutron radiography of the capsule was successfully completed before irradiation, after operation at 39.4 kW/m (12 kW/ft), and after operation at 48.6 kW/m (14.8 kW/ft). The neutron radiography rig was not in service during the 44.3-kW/m (13.5-kW/ft) operating period. In addition, postirradiation neutron radiography was successfully performed on the fuel rod after it was removed from the capsule.

Substantial development work was done in the area of measurement and control of  $H_2$  and  $H_2/H_2O$  ratio in the sweep gas, which may be applied to the next experiment. The GCFR coolant is expected to contain much higher levels of  $H_2$  and  $H_2O$  than were in the GB-9 and GB-10 sweep gas, and the  $H_2/H_2O$  ratio, or oxygen potential, is expected to be an important parameter that could influence fuel-fission-product chemistry. Of particular interest is the effect of the  $H_2/H_2O$  ratio in the coolant on transport and reaction of volatile fission products. There is evidence that cesium reactions with

UO<sub>2</sub> and mixed-oxide fuel occur in fast breeder reactor fuel rods and that cesium has a tendency to migrate to the fuel-blanket interface areas where the cooler UO<sub>2</sub> pellets act as a sink for cesium. Formation of cesium-urania compounds may occur, depending on oxygen availability, and cause swelling of the pellets. Studies of fission-product migration and reaction in GCFR fuel rods are under way at GAC<sup>26</sup> and an out-of-pile testing program is being conducted at ANL.<sup>27</sup>

### 11.1 Description of Initial Startup

We had planned to start the GB-10 irradiation on Aug. 8, 1972, after the sweep system had been purged free of moisture and the capsule and gas system instrumentation had been checked out. However, an increase of the indicated moisture level in the effluent helium was detected when the system was depressurized prior to the Aug. 8 reactor refueling shutdown. It was found that the indicated moisture level increased from ~3 to ~30-200 ppm when the system was depressurized from 6.9 to ~0.138 MPa gage (1000 to ~20 psig), with the increase starting abruptly after the sweep system pressure reached ~1.38 to 2.07 MPa gage (~200 to 300 psig). This behavior was similar to that which would be expected if moisture were present in a side leg of the main line. Thus, we decided to postpone the startup until the moisture indication could be reduced or the behavior satisfactorily explained.

As in the case of the capsule GB-9 experiment, the moisture content of the sweep gas was monitored by two aluminum oxide hygrometers, one located in the sweep supply line and the other downstream of the capsule [see locations of moisture-measuring elements (AmE) in Fig. 51]. These probes were not expected to provide exact determination of moisture content, since their advertised accuracy for determining dew/frost point was  $\pm 2.5^\circ\text{C}$ , but we found them very useful for monitoring changes in moisture levels during the initial purging and subsequent operation of the sweep system.

Repeated depressurizations did not prove to be an effective method for removing the moisture. Therefore, during a reactor refueling shutdown

on Aug. 22, 1972, a valve was installed in the GB-10 effluent sweep line downstream of the gas-sampling station to permit evacuation of the sweep system. Three evacuations of the sweep system were conducted, with the effluent passing over the downstream moisture probe in each case. During the first evacuation, the moisture indication increased from a dew point of  $\sim -71$  to  $\sim -19^{\circ}\text{C}$ , which indicated that moisture was present somewhere in the system. After a second evacuation during which heat was applied to part of the system, the sweep system was pressurized to 6.9 MPa gage (1000 psig) and purged overnight under a constant pressure at a slow sweep flow rate; the next day the system was depressurized from 1000 psig to a vacuum. There was no increase of the indicated moisture level during the depressurization and only a small increase as the system was evacuated.

The capsule irradiation was started on Aug. 29, 1972, by slowly inserting the capsule first in  $25^{\circ}\text{C}$  steps, then in  $50^{\circ}\text{C}$  steps, and finally in  $100^{\circ}\text{C}$  steps until a fuel-rod power of 39.4 kW/m (12 kW/ft) was reached ( $565^{\circ}\text{C}$  peak cladding outer surface temperature). The sweep was passed through the fuel region during the startup. There was only a slight increase (from  $\sim 0.9$  to 1.2 ppm) in the indicated moisture level of the effluent helium during heatup of the fuel. The indicated moisture levels at the start of the irradiation were  $\sim 0.035$  ppm upstream of the capsule [at 6.9-MPa gage (1000-psig) pressure] and  $\sim 0.90$  ppm downstream of the capsule [at 0.072 MPa gage ( $\sim 10.5$  psig)]. We observed no significant changes in the indicated moisture levels throughout the irradiation. We did observe that the indications increased very slowly whenever the system was left static for a few days at the time, but we did not know if this was a true indication of moisture slowly coming off the stainless steel walls and/or diffusing into the system from the outside, or if it was only a characteristic of the moisture probes. Since we were not sure, we always purged the system until the indications were close to their normal values before resuming operation at power. It should also be mentioned that the moisture probe calibrations were not checked during the irradiation because this would have required breaking into the system; instead, we decided to replace them if their indications became suspect (which they did not) and to rely upon them only to indicate a large change in moisture content, should this occur for some reason.

The effluent sweep line activity indicated by the on-line ionization chamber on the high-pressure section of the effluent line increased to 800 mR/hr during the initial capsule startup. The sweep-gas flow mode was with the gas flowing into the bottom of the fuel rod and out of the top at a flow rate of  $\sim 1000 \text{ cm}^3 \text{ STP/min}$ . The indicated line activity responded to each temperature increase and became increasingly sensitive to temperature as the fuel-rod power of 39.4 kW/m (12 kW/ft) was approached. Following each temperature increase, the line activity increased and leveled off in a smooth manner. Soon after reaching 39.4 kW/m, the sweep flow was valved across the top of the fuel rod, which was the normal flow mode during nonsampling periods. Under this sweep flow mode the steady-state line activity was  $\sim 20 \text{ mR/hr}$  at a sweep flow rate of  $\sim 200 \text{ cm}^3 \text{ STP/min}$ .

The startup of capsule GB-10 went smoothly and we began isotopic fission-gas release-rate measurements under the planned sweep flow modes on Aug. 31, 1972, after the fuel rod had operated at 39.4 kW/m (12 kW/ft) for  $\sim 40 \text{ hr}$ . Operation was found to be quite satisfactory, and the temperature patterns agreed reasonably well with predictions. Details of the thermal operating history of the rod are discussed in the following section. Observations of the internal gas-flow conductance of the fuel rod during the initial startup are included in Sect. 11.3, where flow conductance data for the entire irradiation are presented.

### 11.2 Thermal Operating History

An evaluation of the GB-10 thermal operating data was made to estimate the histories of the GB-10 fuel-rod power, cladding temperature, and fuel burnup for the irradiation. This evaluation, which is described in more detail in Appendix B, was needed to point out some of the problems involved in determining the GB-10 fuel-rod temperature and power and to resolve some of the uncertainties known to be present in the "nominal values" of temperature and power listed in Table 10.

As described in Sect. 10, heat transfer calculations were utilized to estimate cladding temperatures and power levels from the readings of the six fuel-region thermocouples. This approach was complicated by the fact

that the capsule was in a fairly steep neutron-flux gradient, so that detailed R- $\theta$  power- and temperature-distribution calculations were needed. These calculations were made only for the BOL condition; thus, the expected flattening of the angular power and temperature distributions with preferential burnup of fuel on the hot side of the rod were not calculated in detail. As a result, the operating criteria for GB-10 included using the BOL heat transfer analysis throughout the irradiation and conservatively controlling the fuel-rod temperature and power level on the basis of the thermocouple indicating the highest power.

Another uncertainty, which became progressively worse during the irradiation, was disagreement in the readings of the two fuel-region thermocouples that were located at the same elevation at the expected peak-power location, one on the hot side of the rod, TE-703, and one on the cold side, TE-704 (see Table 7 for axial and angular positions of the fuel-region thermocouples). As shown in Fig. 45, a total of six fuel-region thermocouples were located at the ID of the Zircaloy-2 sleeve that surrounded the fuel rod. They were staked into place where they entered the outer surface of the sleeve. The fuel rod was centered within the Zircaloy-2 sleeve at two points: at the bottom end of the rod and at a point about one-third of the way up the upper blanket region. Assuming that there was no bowing of the rod and that the thermocouples stayed in place with their junctions all at a calculated radial position of 0.634 cm (0.2495 in.), each fuel-region thermocouple junction was about 1.8 mm (0.071 in.) away from the cladding.

Figure 59 shows a plot of the difference in the readings of thermocouples TE-703 and TE-704 during the irradiation, along with the predicted difference based on the BOL thermal calculations and the predicted difference based on what is labeled burnup-dependent thermal approximations. The burnup-dependent approximations, described in Appendix B, were made for lack of the detailed R- $\theta$  calculations. In these calculations, it was assumed that the relative BOL angular power and temperature distributions changed at a linear rate with fuel burnup until they became uniform with respect to angle  $\theta$  at a burnup of 100 MWd/kg heavy metal. TE-704 on the cold side of the rod indicated the highest power and was the controlling thermocouple throughout the irradiation.

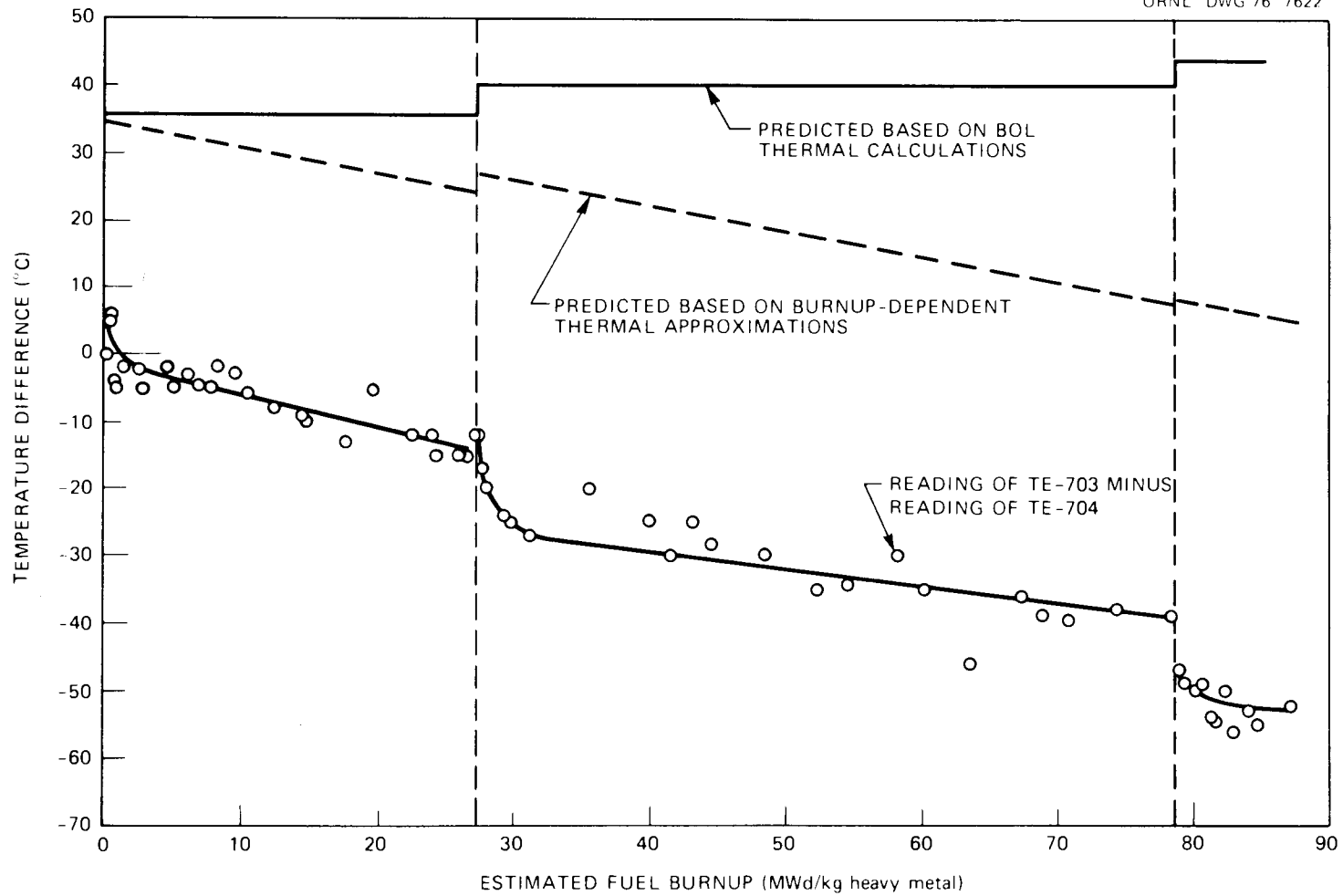


Fig. 59. Difference between readings of GB-10 thermocouples TE-703 (hot side) and TE-704 (cold side at same elevation as TE-703) as a function of estimated fuel burnup.

The initial temperature difference was within the expected uncertainty of  $\pm 25^{\circ}\text{C}$  in each thermocouple reading. The long-term trend of the temperature differences show reasonably good agreement with the burnup-dependent prediction, but the trend following each step increase in power was not predicted. Neutron radiography near the end of the irradiation showed that TE-704 on the cold side was closer to the rod than was TE-703, by at least 0.38 mm (0.015 in.), and the rod appeared to be slightly bowed toward the cold side. Also, the "as-built" orientation of the Zircaloy-2 sleeve assembly (and the thermocouples located in the Zircaloy-2 sleeve) was observed in the radiographs to be shifted about  $20^{\circ}$  counterclockwise from the specified orientation on the construction drawings (Table 7); but, based on the temperature distributions of Fig. 56, this would cause a change in the readings of TE-703 and TE-704 of only  $\sim 5^{\circ}\text{C}$  and would reduce the predicted difference in their readings by only  $\sim 10^{\circ}\text{C}$ . The maximum change in the readings of the other fuel-region thermocouples caused by the  $20^{\circ}$  shift in orientation would be  $\sim 10^{\circ}\text{C}$  for thermocouple TE-702.

It seems reasonable to assume that the rod may have been bowed in the hot condition and that some of the temperature differences shown in Fig. 59 may have been caused by fuel-rod bowing. In this case, it would also be reasonable to average the temperature and power indications of these two thermocouples.

By using the average indications of TE-703 and TE-704 and applying the burnup-dependent approximations to the GB-10 operating data, we came up with what we believe at this time to be the most probable peak cladding-OD temperature history and peak-power history for the GB-10 rod (see Fig. 60). Instead of operating at constant power at each of the nominal power levels, the power level decreased slowly between each step increase. Peak values for the irradiation are estimated to be 43.8 kW/m (13.3 kW/ft) power and  $600^{\circ}\text{C}$  cladding-OD temperature. Fuel burnup, shown by the scale at the top of the figure, was calculated on the basis of the fission-rate history that corresponds to the peak-power history. Thus, our best estimate of fuel burnup for the irradiation is 112 MWd/kg heavy metal. A curve of fuel burnup at the peak-power axial position vs irradiation time based on this evaluation of GB-10 operating data is given in Fig. 61.

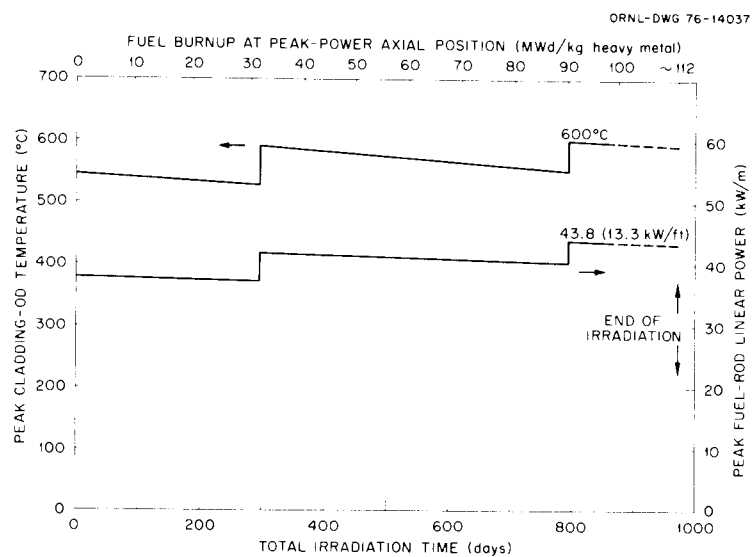


Fig. 60. Peak power, cladding temperature, and fuel burnup of GB-10 fuel rod as a function of irradiation time based on an evaluation of GB-10 thermal operating data (1 ft = 0.3048 m).

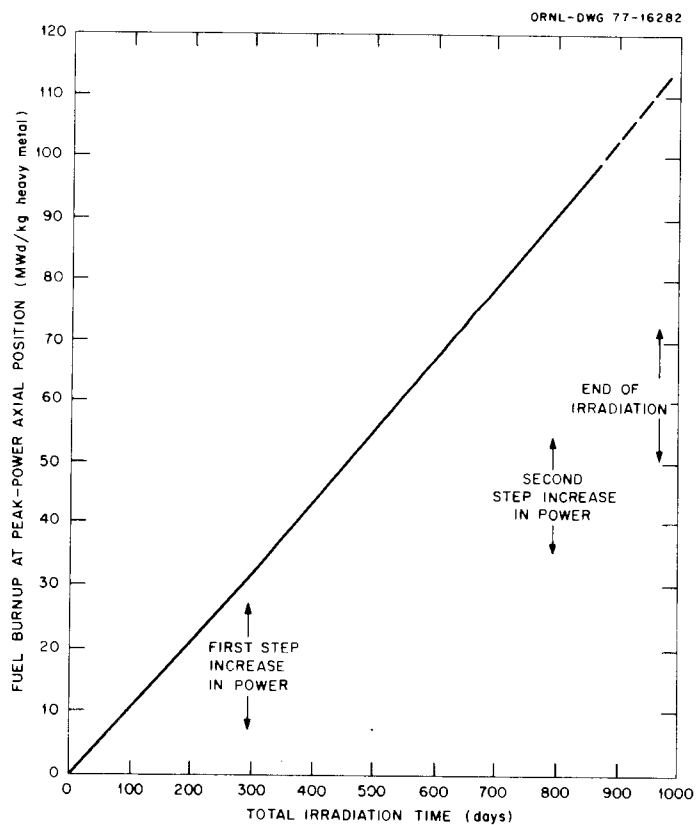


Fig. 61. GB-10 fuel burnup as a function of irradiation time based on an evaluation of GB-10 thermal operating data.

For the sake of convenience, the nominal values of power, cladding temperature, and fuel burnup will be used in presenting the remaining GB-10 results. However, we believe that for detailed interpretation of the results, especially the fission-gas release data, Fig. 60 should be kept in mind, at least until a better evaluation of the thermal operating data is made.

### 11.3 Fuel-Rod Internal Gas-Flow Conductance vs Irradiation Time

Flow conductance measurements were routinely obtained whenever the inlet sweep flow was changed from the normally used TT inlet line to the BT, BB, or BF inlet line (see Fig. 50 and associated text in Sect. 8.3 for definitions of sweep line and flow mode). The two pressure elements (0- to 1500-psig pressure transducers) shown in Fig. 50 provided a measurement of the pressure drop ( $\Delta P$ ) across the inlet line being used and the portion of the fuel rod being swept. Because of their locations, the two elements measured essentially the same pressure when the TT inlet line was being used; thus, a check of their agreement was obtained under the normal TT-TT flow condition. From the  $\Delta P$  and flow-rate measurements, flow conductance could be estimated.

A pressure element (0- to 1500-psig pressure transducer) was installed in the effluent sweep line downstream of the on-line Ge(Li) detector system loop (see Fig. 51) in November 1973 (after 320 days at power). This pressure element permitted flow conductance measurements while the TT inlet line was being used, such as for the TT-BT and TT-BB flow modes. Prior to installation of the downstream pressure element, rough indications of TT-TT, TT-BT, and TT-BB flow conductances were obtained from the flow data itself, since full flow through the downstream capillary flow restrictor was a function of the pressure upstream of the restrictor.

It should be noted that the  $\Delta P$  measurements always included the pressure drop in the  $\sim 21$  m ( $\sim 70$  ft) of inlet line being used. The  $\Delta P$  measurement included the pressure drop in the  $\sim 21$  m ( $\sim 70$  ft) of effluent line only when the downstream pressure element was used (i.e., when the TT inlet line was used to measure TT-TT, TT-BT, or TT-BB flow conductance).

All of the sweep lines in the high-pressure section of the system were 0.686 mm (0.027 in.) ID except for the TT inlet line. The TT inlet line was 2.16 mm (0.085 in.) ID. Pressure-drop calculations indicated that ~21 m (~70 ft) of 0.686-mm-ID (0.027-in.) sweep line accounted for about 27.6 to 34.5 kPa (4 to 5 psi) of the measured  $\Delta P$  for the conditions of 6.9 MPa gage (1000 psig) pressure and 1000 cm<sup>3</sup> STP/min flow rate. Thus,  $\Delta P$  measurements that were much greater than 34.5 kPa (5 psi) indicated fuel-rod resistance to flow and/or possible plugging of the lines. It should also be mentioned that the pressure instrumentation was not designed specifically for the  $\Delta P$  measurements and the accuracy of the  $\Delta P$  determinations was limited to no better than  $\pm 34.5$  kPa ( $\pm 5$  psi).

The flow conductance measurements were normally made at the same time the routine (once per week or 2 weeks) steady-state fission-gas release measurements were made under the various sweep flow modes. During the latter part of the irradiation, the fuel-rod flow conductance decreased sharply, and several special tests were performed to better characterize the constriction.

The pertinent information obtained from the flow conductance measurements may be classified into the following areas: (1) flow conductance of the sweep lines and the charcoal trap region of the rod, (2) partial plugging of the BB line, and (3) flow conductance of the fuel and blanket regions of the rod. The information obtained in each area is presented in the following subsections.

#### 11.3.1 Flow conductance of sweep lines and charcoal trap

During the first few weeks of GB-10 operation, the flow conductances of the various sweep flow modes were high and close to expected values. [The flow conductance of the BF-TT flow mode was somewhat lower than expected during the initial startup, but increased to a reasonably high value soon after 34.9 kW/m (12 kW/ft) fuel-rod power was reached, as described in Sect. 11.3.3.] Operation under the various flow modes showed that early in the irradiation the upper blanket and charcoal trap sections of the rod offered negligible resistance to flow and that the pressure drops through the sweep lines were close to calculated values.

After the first 2 months at power, the BB line started to show a tendency to plug up, as described in Sect. 11.3.2.

Throughout the irradiation, the TT-TT and TT-BT (and BT-TT) flow conductances remained high and unchanged. There was no evidence of any tendency for plugging in the charcoal trap, TT lines, or BT line. The same was true in the case of the GB-9 fuel rod which had only the BT and TT sweep lines.

### 11.3.2 Partial plugging of BB line

The BB sweep line (see Fig. 50) started showing a tendency to plug up after about 2 months at power. By the end of the first year of operation, the BB line was partially plugged, and we discontinued its use on a routine basis.

It should be noted that the BB line, which terminated 0.79 mm (1/32 in.) into the top of the lowermost depleted UO<sub>2</sub> upper blanket pellet, as indicated in Fig. 44, was included in the GB-10 rod to permit measurements of the fission products released directly from the fuel matrix (BF-BB flow mode) and those released by diffusion from the fuel column (TT-BB flow mode). The BB, BT, and BF lines were all included for experimental purposes and are not present in a GCFR fuel rod (see Fig. 1).

We first observed a serious constriction that threatened continued use of the BB line on Nov. 29, 1972, after the fuel rod had operated at power for 74 days. Prior to this time, the flow conductance of the BB line had decreased sharply by a factor of  $\sim 10$  from values the first 2 months of irradiation, but flow capability was still more than adequate for making the planned fission-gas release measurements.

While taking gas samples for fission-gas release analyses on Nov. 29, 1972, an instability in the sweep-gas flow rate occurred while operating in the BF-BB flow mode. A flow constriction gradually developed as was evidenced by a gradual decrease in flow rate and effluent line activity. [The two pressure elements shown in Fig. 50 indicated the constriction was in the BB line and not the fuel column, since they were indicating only 34 to 69 kPa (5 to 10 psi)  $\Delta P$  at a flow rate of  $\sim 1050 \text{ cm}^3$  STP/min; the downstream pressure element had not been installed at this

time.] Twice during the 2 or 3 hr of BF-BB operation the constriction disappeared, as was evidenced by a sudden return of the flow rate and effluent line activity to near their original levels, but the constriction gradually redeveloped in each case. Each time the constriction disappeared it allowed the gas from the rod to pass through the lines at a somewhat faster rate than normal.

Following the sampling period on Nov. 29, 1972, the sweep flow was returned to the TT-TT flow mode, which was the normal mode of operation during nonsampling periods. At this time, we observed that the effluent line activity indicated by the on-line ionization chamber on the high-pressure section of the system (see RE locations in Fig. 51) did not decay back to its normally low level in 2 to 3 hr as expected. Instead of indicating the presence of only short-lived deposited activity on the line, the radiation monitor indicated longer-lived activity at a level more than a factor of 10 above normal, which decayed away over a period of about 3 weeks in a manner similar to that which might be expected if iodine isotopes had been transported through the  $\sim 21$  m ( $\sim 70$  ft) of 0.686-mm-ID (0.027-in.) line to the monitor. These observations suggested that iodine, or whatever the longer-lived activity consisted of, could be transported through the small-diameter sweep lines in significant quantities if the rate of gas flow through the fuel column and BB line was fast enough. The condition where the BF-BB constriction suddenly disappeared, allowing gas leaving the rod to pass through the effluent line at a faster rate than normal, did not occur again and no additional efforts were made to observe BF-BB fission-product transport and line deposition at sweep flow rates higher than the normal  $1200 \text{ cm}^3 \text{ STP/min}$ .

During the next few months of operation, a similar constriction developed each time the BF-BB flow mode was used, but there was no recurrence of the line becoming temporarily unconstricted while under the BF-BB flow condition or of the high level of deposition of longer-lived activity on the line at the radiation monitor in the valve box. When the sweep flow mode was changed to BF-BB, the flow rate typically dropped off gradually about 25% in 2 hr. On at least one occasion, a similar behavior was observed using the TT-BB flow mode, but in general the constriction did not tend to develop under the TT-BB flow mode as rapidly as under the

BF-BB flow mode. At that time, there was no evidence of significant loss of flow conductance under any of the other sweep flow modes, and the BB line constriction was not considered to be too much of a problem. In fact, after one week of operation under the TT-TT sweep flow mode prior to a sampling period, the BB line constriction would be relieved enough to permit nearly full flow of  $\sim 1200 \text{ cm}^3 \text{ STP/min}$ , and the constriction tended to redevelop to a point of reducing the normal full flow to less than  $1000 \text{ cm}^3 \text{ STP/min}$  only when the BF-BB flow mode was used. The normal full-flow condition was with the needle valve used for flow regulation, located immediately downstream of the flow restrictors (see Fig. 51), in its fully opened position; the normally used flow restrictor then limited the flow rate to  $\sim 1200 \text{ cm}^3 \text{ STP/min}$  when the pressure upstream of the flow restrictor was the full operating pressure of 6.9 MPa gage (1000 psig). A lower flow rate, then, would indicate a lower pressure than normal upstream of the flow restrictor and hence a constriction elsewhere in the flow path.

The tendency of the BB line constriction to disappear during TT-TT flow mode operation suggests the possibility that radioactive decay or chemical reactions may have caused a change in the constrictive material with time. Another possibility is that the gas flow actually pressed pellet material against or into the end of the BB line and caused the observed behavior in some way.

By the end of the first year of irradiation, the BB line constriction had become somewhat worse; it did not tend to be relieved as much during periods of nonuse, and it was decided to discontinue its use on a routine basis. The TT-BB flow mode was later used four times while operating at the 44.3 kW/m (13.5 kW/ft) fuel-rod nominal power level, and the BB-TT flow mode was used twice while operating at the 48.4 kW/m (14.8 kW/ft) power level. Flow conductance did not change significantly from that observed prior to discontinuing the routine use of the BB line. With a pressure differential of 1.72 MPa (250 psi) across the TT-BB or BB-TT flow-path constriction, a flow rate of  $\sim 1000 \text{ cm}^3 \text{ STP/min}$  could be obtained. Both the TT-BB and the BF-BB flow modes were used several times during shutdown periods to check flow conductances under the cold condition. The TT-BB flow conductance did not show much dependence on power level,

nor was there much difference between at-power and shutdown measurements, unlike the BF-TT flow conductance behavior described in Sect. 11.3.3.

Postirradiation neutron radiography of the fuel rod after it was removed from the capsule indicated that a small amount of material may be present in the open end of the BB line. This area of the rod is to be examined in detail at ANL when the rod is sectioned.

### 11.3.3 Flow conductance of fuel and blanket regions

The fuel-rod flow conductance information presented in this section shows a trend toward loss of internal gas-flow conductance (fuel-rod plugging) at power at high fuel burnup for the particular high-purity-helium sweep and the fuel-fission-product environment of the GB-10 test. The data indicate that more work is needed in this area to ensure that plugging does not occur under GCFR and LMFBR conditions or to establish that the extent of the loss of flow conductance will be within tolerable limits. Long-lived and stable fission gases must be able to migrate to the vent ports in GCFRs<sup>2</sup> and to gas plenums in LMFBRs to prevent excessive pressure buildup in the fuel region. In GCFRs, gas should be able to flow in and out of the fuel region to maintain the desired small pressure differential across the cladding, which ensures that coolant will flow into the rod in the case of cladding leakage and carry the fission gases to cleanup traps in the pressure-equalization system, thereby minimizing leakage of fission gases into the reactor coolant.

The BF-TT sweep flow mode, which simulated the condition of a leaking GCFR fuel rod, was used in obtaining most of the fuel-rod flow conductance data given in this section. The BF-TT flow conductance measurement gave the overall flow conductance of the BF line and the entire fuel rod. Thus, a sharp decline observed in the BF-TT flow conductance at power was caused by increased resistance to flow within the fuel rod and/or possible plugging of the BF line to the bottom of the rod. We believe the trends in the BF-TT flow conductance data and the behavior of the constriction with respect to temperature level and shutdowns strongly indicate that the constriction was in the fuel rod rather than in the BF line, although

the latter possibility cannot be absolutely ruled out. Also, we could see no evidence of a problem in the BF line from examination of neutron radiographs taken of the capsule at the end of the irradiation. The BF line appeared to be open and in good condition from where it could be seen between the Zircaloy-2 sleeve OD and the stainless steel primary containment tube ID in the upper portion of the capsule to where it terminated at the top of the bottom end plug of the rod. For these reasons, it will be assumed in the following discussions that the BF line was unstricted and that the BF-TT flow conductance measurements may be interpreted and referred to as flow conductances for the fuel rod (and unstricted BF line), or as indications of the flow conductance of the fuel and blanket regions of the rod since the charcoal trap and TT effluent line showed negligible flow resistance throughout the irradiation.

During the initial startup of the capsule on Aug. 29, 1972, the internal gas-flow conductance of the fuel rod was monitored while operating in the BF-TT sweep flow mode. We observed the following behavior of the pressure differential ( $\Delta P$ ) across the fuel rod and BF line while flowing 6.9-MPa gage (1000-psig) helium via the BF-TT flow mode at a flow rate of  $\sim 1000 \text{ cm}^3 \text{ STP/min}$ . The initial  $\Delta P$  at startup was  $\sim 0.45 \text{ MPa}$  ( $\sim 65 \text{ psi}$ ), somewhat higher than was expected for the initial cold condition. The  $\Delta P$  remained constant during the early part of the capsule heatup and then behaved as follows: (1) it decreased from  $\sim 0.45$  to  $\sim 0.17 \text{ MPa}$  ( $\sim 65$  to  $\sim 25 \text{ psi}$ ) as a fuel-rod power of  $\sim 29.5 \text{ kW/m}$  ( $\sim 9 \text{ kW/ft}$ ) was approached and remained constant at  $\sim 0.17 \text{ MPa}$  during a 1-hr hold at  $\sim 29.5 \text{ kW/m}$ ; (2) it fluctuated between  $\sim 0.17$  and  $\sim 0.48 \text{ MPa}$  ( $\sim 25$  and  $\sim 70 \text{ psi}$ ) for a period of 30 min while the fuel-rod power was increased from  $\sim 29.5$  to  $39.4 \text{ kW/m}$  ( $\sim 9$  to  $12 \text{ kW/ft}$ ) and for another 30 min after reaching  $39.4 \text{ kW/m}$ ; and (3) it stabilized at  $\sim 0.17 \text{ MPa}$  ( $\sim 25 \text{ psi}$ ). Similar measurements during the first few weeks of irradiation showed a gradual decrease in the  $\Delta P$  to  $\sim 69 \text{ kPa}$  ( $\sim 10 \text{ psi}$ ).

Measurements of fuel-rod internal gas-flow conductance made under steady-state operating conditions are presented in Fig. 62, where the measured flow rate and  $\Delta P$  data were reduced to expected flow rates at a

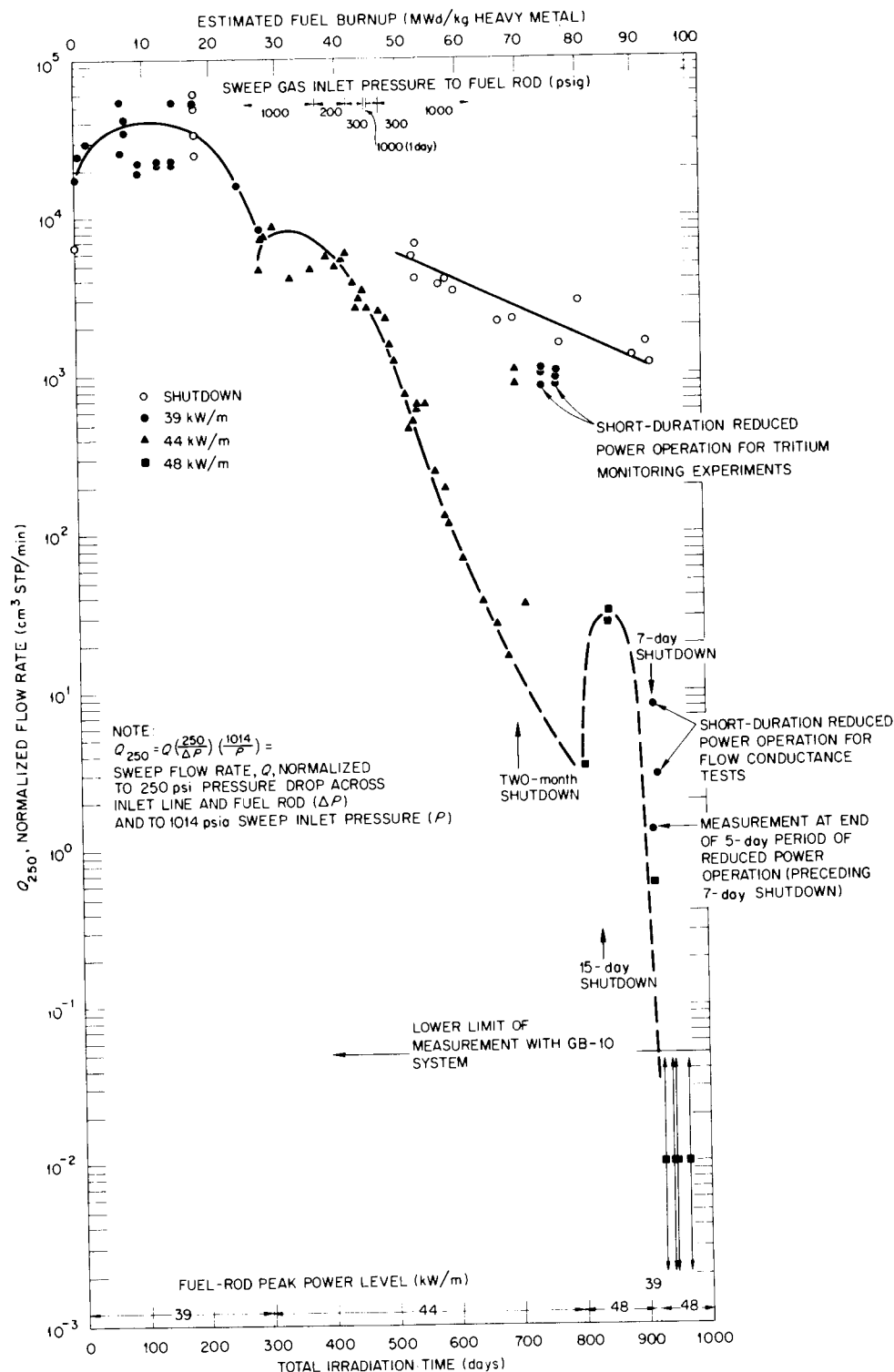


Fig. 62. GB-10 fuel-rod flow conductance vs irradiation time (1 m = 3.28 ft; 1 psi = 6895 Pa; 1 cm<sup>3</sup> = 0.061 in.<sup>3</sup>).

$\Delta P$  of 1.72 MPa (250 psi) and inlet pressure of 6.9 MPa gage (1000 psig),  $Q_{250}$ , and plotted vs irradiation time. The reason for normalization to 1.72 MPa  $\Delta P$  was that this was an arbitrary limit that was placed on the  $\Delta P$  for fear that higher  $\Delta P$ s might redistribute the hot fuel. The data shown in Fig. 62 represent all the fuel-rod flow conductance data obtained under steady-state operating conditions for the entire irradiation. The data include reduced-power and shutdown measurements and measurements made closely following long shutdown periods that reflected a temporary increase in conductance, but these measurements were not used in drawing in the curves which were intended to represent the trends during the three power levels of operation.

As mentioned previously, most of the fuel-rod flow conductance data was obtained using the BF-TT sweep flow mode. A few of the data points in Fig. 62 were BF-BT measurements, and some during the first year of irradiation were BF-BB measurements. The BF-TT and BF-BT measurements were equivalent, since the upper portion of the rod was unconstricted throughout the irradiation. The BF-BB measurements during the first year of irradiation were also essentially equivalent to the BF-TT measurements when the  $\Delta P$ s indicated by the two pressure elements shown in Fig. 50 were used in conjunction with the measured flow rates to calculate  $Q_{250}$  [in this case, the expected flow rate at 1.72 MPa (250 psi)  $\Delta P$  across the BF line and the portion of the fuel rod up to the end of the BB line]. After about the first year of irradiation, the BF-BB sweep mode was not used again while the fuel rod was at power.

The first two curves in Fig. 62 for the first two power levels of GB-10 operation show an almost exponential decline in the fuel-rod flow conductance after an initial period in which the flow conductance tended to increase and pass through a peak.

During the first half of the irradiation, the desired sweep flow rate of  $\sim 1200 \text{ cm}^3 \text{ STP/min}$  through the fuel rod could be achieved, but increasing  $\Delta P$ s were required. We normally preferred to make fission-gas release measurements at this flow rate, which reduced gas travel time from the fuel rod to the monitoring points to less than a minute. However, with higher burnup, the normalized flow rate,  $Q_{250}$ , declined to the point where

sweep gas could not flow through the rod while it was operating at power. The last curve of Fig. 62 for the final power level of GB-10 operation was extrapolated to this no-measurable-flow condition. It should also be noted that the curve for 48-kW/m (14.8-kW/ft) operation is shown as a broken curve, because the number of data points was too few to establish the shape of the curve with reasonable confidence.

The last four data points shown in Fig. 62 were plotted below the line indicating the lower limit of detection with the GB-10 system and represent no measurable flow. The lower limit of detection of  $Q_{250} \approx 5 \times 10^{-2} \text{ cm}^3 \text{ STP/min}$  was reached by setting up  $\sim 1.38 \text{ MPa}$  ( $\sim 200 \text{ psi}$ )  $\Delta P$  across the BF-TT constriction, closing off the system valves, and monitoring for pressure changes over 2 or 3 days. No flow could be measured in this way in the case of the last four data points in Fig. 62.

We found that a shutdown or a reduction in power level tended to open up the BF-TT flow passages, as shown by the shutdown and reduced-power data plotted in Fig. 62. This behavior indicated that the constriction was in the heated portion of the flow path. Upon return to power following a short shutdown, the fuel-rod flow conductance would return to about its previous level. Following a long shutdown of a week or more, we could detect some constriction relief upon return to power. For example, when the capsule was shut down for 2 months (after 700 days of irradiation) for installation of the tritium-monitoring system, we found on return to power that the flow conductance had increased by about 2 orders of magnitude; but 2 weeks later when we next attempted flow through the rod, the constriction had returned (see Fig. 62). The degree of constriction relief and the time to reestablish the preshutdown conductance appeared to be nearly proportional to the length of the shutdown, but there is insufficient data to be very confident about this observation. However, this behavior of the fuel-rod constriction was somewhat similar to the behavior of the BB line constriction (Sect. 11.3.2) and again may be an indication that radioactive decay or chemical reactions may have been causing a change in the constrictive material with time — in this case, during the shutdown period.

Special tests were conducted late in the irradiation in an attempt to further characterize the fuel-rod flow constriction, which by this

time appeared to be a complete flow blockage at power which was relieved upon shutdown or a large reduction in power. In one special test, fuel-rod flow conductance measurements were made as the fuel-rod power was decreased in a stepwise manner. The results of this test are summarized in Table 12. There was no measurable flow in a 1-hr check at the start of the test (100% power), which followed 6 days of continuous operation under steady-state conditions [TT-TT flow mode, 48.6 kW/m (14.8 kW/ft) fuel-rod power level]. There was detectable flow indicating some relief of the constriction when the fuel-rod power was reduced to 81% power, much larger flow indicating greater relief of the constriction at 64% power, and nearly maximum relief of the constriction by the time the power was reduced to 53%.

Table 12. Results of GB-10 fuel-rod flow conductance measurements showing relief of the BF-TT flow constriction upon stepwise power reduction on May 11, 1976<sup>a,b</sup>

Fuel-rod power level <sup>c</sup>		Q <sub>250</sub> , maximum BF-TT flow rate <sup>d</sup> (cm <sup>3</sup> STP/min)
kW/m	% of full power	
48.6	100	No measurable flow in 1-hr check
39.2	81	3.0
31.1	64	665
26.0	53	1020
21.0	43	1170
11.1	23	1200
≤2	≤4	1180

<sup>a</sup>1 m = 3.28 ft; 1 psi = 6895 Pa.

<sup>b</sup>As of May 11, 1976, the fuel rod had operated at power for 920 days to a fuel burnup of ~93.1 MWd/kg heavy metal.

<sup>c</sup>The stepwise power reduction followed 6 days of steady-state operation at 48.6 kW/m.

<sup>d</sup> $Q_{250} = Q \left( \frac{250}{\Delta P} \right) \left( \frac{1014}{P} \right)$  = sweep flow rate, Q, normalized to 250 psi pressure drop across inlet line and fuel rod ( $\Delta P$ ) and to 1014 psia sweep inlet pressure (P).

Three attempts were made to correlate relief of the fuel-rod constriction upon reactor scram with capsule temperatures. In each attempt, relief of the constriction was monitored by observing the rapid equalization of pressures upstream [ $\sim 6.9$  MPa gage (1000 psig)] and downstream [ $\sim 5.2$  MPa gage (759 psig)] of the BF-TT constriction. The pressure difference was set up beforehand. In the last two attempts, high-speed recording of capsule temperatures, pressures, and reactor power level was employed using a Honeywell Model 1858 CRT Visicorder. A test that was conducted on June 21, 1976, was successful in providing a simultaneous recording of all the signals. The signal leads from each of the sensing elements selected was disconnected from its normal recorder and connected directly to the Visicorder for the test; thus, there was essentially no delay in the recorded responses, except for the delay associated with each of the sensing elements, which in each case was estimated to be insignificant compared to the indicated rate of change in the signal during the test.

Figure 63 shows the simultaneous recording of the relief of the fuel-rod constriction upon reactor scram on June 21, 1976 (after 946 days of irradiation) and the capsule temperature decay indicated by thermocouples TE-704 and TE-708 (both located near the ID of the Zircaloy-2 sleeve surrounding the fuel rod). Prior to the reactor scram, there was no detectable flow across the constriction with a pressure of 6.9 MPa gage (1002 psig) set up in a static  $\sim 180\text{-cm}^3$  volume upstream of the constriction and a pressure of 5.2 MPa gage (759 psig) set up in a static  $\sim 155\text{-cm}^3$  volume downstream of the constriction. Upon reactor scram, the reactor power signal decreased to a low level in 0.15 sec, capsule temperatures began to decrease about 1/4 sec later, and the start of pressure equalization across the constriction could be detected about 2 sec after that. Within 2 min the temperatures were less than  $100^\circ\text{C}$ , and the pressures had equalized to approximately 6.0 MPa gage (875 psig).

The experimental results given in this section may be summarized by stating that the fuel-rod internal gas-flow conductance decreased to or below the lower limit of detection of  $Q_{250} \approx 5 \times 10^{-2} \text{ cm}^3 \text{ STP/min}$  by the end of the irradiation, but there was no evidence that the constriction would not be relieved significantly by a shutdown or a large power

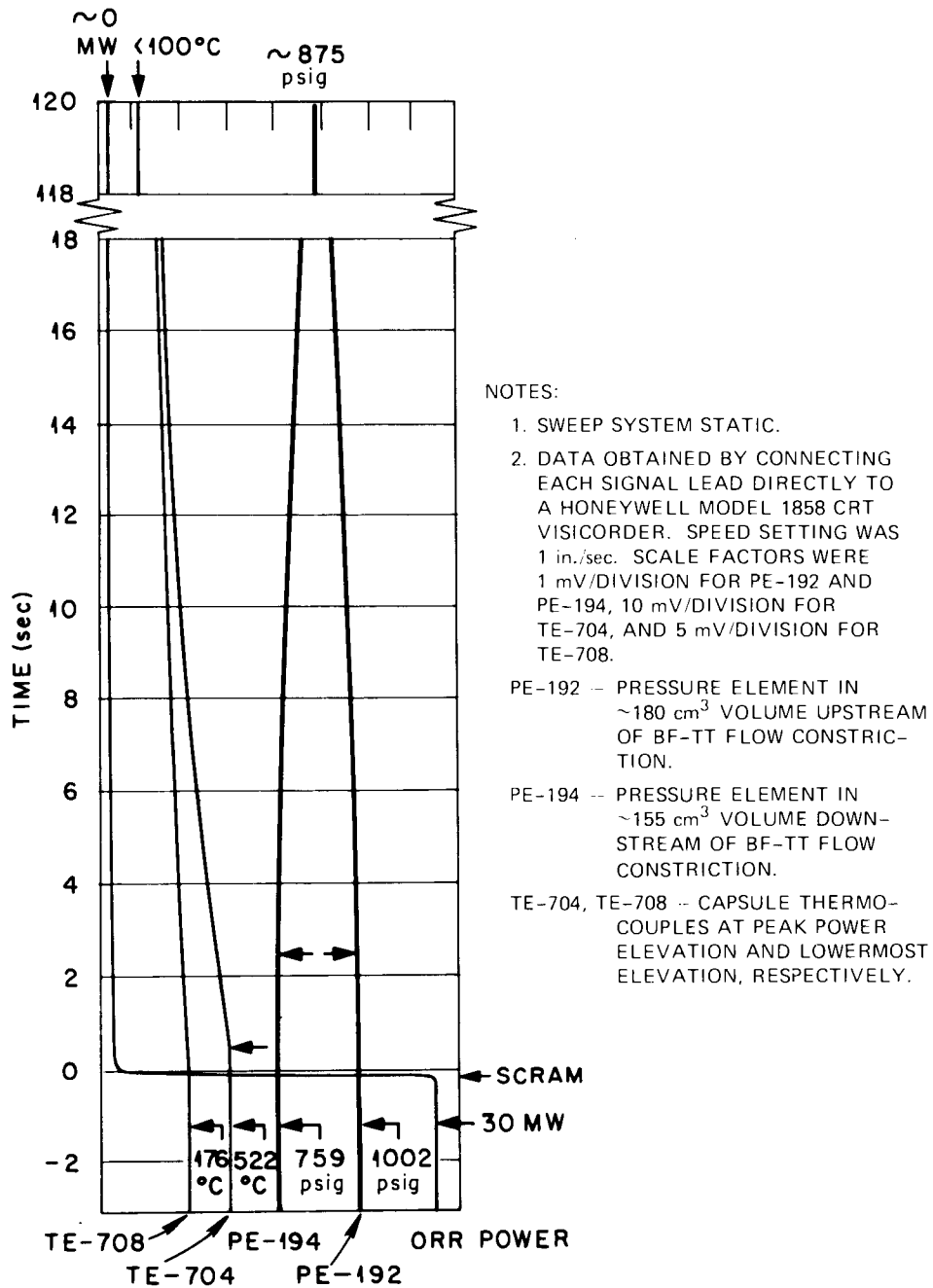


Fig. 63. Results of fast-speed recording of reactor power, GB-10 temperatures, and sweep pressures, showing relief of the BF-TT flow constriction upon reactor scram on June 21, 1976 (1 psi = 6895 Pa; 1 in. = 2.54 cm).

reduction. We believe the constriction was in the fuel and/or fuel-blanket interface regions of the rod.

The generation rate of stable and long-lived fission gases in a full-length GCFR fuel rod, assuming 50 kW/rod and total yield per fission for these fission gases of 0.3, is about  $10^{-3}$  cm<sup>3</sup> STP/min. Thus, only a constriction that would limit the flow rate out of the GCFR rod to less than this value could cause a pressure buildup within the rod.

Although the fission-gas generation rate in a GCFR rod is much lower than the lower limit of internal gas-flow detection in GB-10 of  $Q_{250} \approx 5 \times 10^{-2}$  cm<sup>3</sup> STP/min, the GB-10 data did show a loss of flow conductance to below the detectable level. Whether or not this result has significance for a fast breeder reactor (GCFR or LMFBR) is unclear at this time. The extent to which the GB-10 conditions were characteristic of fast breeder reactor conditions is of paramount importance and requires detailed analysis and possibly further experimentation. An important feature of the behavior of the GB-10 constriction was that it was relieved upon shutdowns and power reductions. Thus, normal shutdowns and power changes in a fast breeder reactor may be sufficient to produce adequate internal gas flow even if constrictions developed that limited internal gas flow during operation. It is also possible, and even likely, that the flow rates and pressures differentials [up to 1.72 MPa (250 psi)] applied to the GB-10 rod may have contributed to the development of its flow constriction.

The loss of internal gas-flow conductance in GB-10 is of interest, and an understanding of the nature and cause of the constriction formation is needed. Investigation of the constriction is a priority item of the GB-10 postirradiation examination at ANL. As results from postirradiation examination of the GB-10 rod become available, its flow constriction formation should become better understood.

Important parameters in the formation and transport of many chemical species in a fast breeder reactor fuel rod are thought to include fuel- and blanket-region oxygen potentials, temperature, and hydrogen partial pressure. Control of the H<sub>2</sub> level and H<sub>2</sub>/H<sub>2</sub>O ratio in the sweep gas of a future experiment may be a possible means of controlling the fuel-fission-product chemistry to an extent that would reduce the potential for flow

constriction formation, assuming that certain chemical reactions are found to be the cause of the GB-10 constriction. Additional design alternatives [such as adjustment of the oxygen-to-metal (O/M) ratio in the mixed-oxide fuel and/or blanket pellets and changes in configuration or smear density of blanket pellets adjacent to the fuel, including the use of central holes and/or grooves to provide flow passages and volume to accommodate deposited material] are discussed in Ref. 26. These alternatives may be evaluated as flow constriction formation becomes better understood and impact design as needed or desired.

#### 11.4 Steady-State Fission-Gas Release vs Irradiation Time and Operating Pressure

Steady-state fission-gas release rates for the radioactive gamma-emitting gases were measured as a function of time under the planned sweep flow modes. All the measurements were made with the capsule operating under the nominal steady-state operating conditions listed in Table 10, except for a period of steady-state operation at reduced sweep pressures to determine the effect of operating pressure on release and gas-phase transport. The measurements were made in accordance with the general operating procedure described in Sect. 10. The order for a given set of measurements was to start at the top of the rod (TT-TT sweep flow mode — see Fig. 50 and associated test in Sect. 8.3 for flow mode definitions) and work downward so that the inventory of fission products below the sweeping point in each use was not unnecessarily disturbed.

As was done in the case of the GB-9 capsule, the release data from GB-10 were reduced to fractional release (or R/B) values, which is defined as the measured release rates of the various isotopes detected in the sweep gas divided by their respective calculated total birth rates in the fuel rod at the time of the measurement. In the calculations, the birth rate B was assumed to be at its equilibrium value corresponding to the fuel-rod total power at the time of measurement, but all the birth rate calculations were made on the basis of the initial-loading ratios of fissile atoms. Corrections were made for the decay of the fission

gases during their travel to the point of measurement; therefore, release rates  $R$  are release rates from the rod or from the portion of the rod being swept. Travel times for the various sweep flow modes ranged from about 40 to 55 sec at measurement conditions of 6.9 MPa gage (1000 psig) operating pressure and  $\sim 1200$  cm<sup>3</sup> STP/min sweep flow rate. Uncertainties in the R/B data are discussed in Sect. 13.

During the first year of operation, fission-gas release data were obtained under all the planned sweep flow modes. Routinely, sets of measurements were made under the TT-TT, TT-BT, TT-BB, and BF-BB flow modes; these R/B data are shown in Figs. 64 through 67, respectively. These data not only provide fission-gas release rates from the mixed-oxide fuel of an operating fast breeder fuel rod for the first time (BF-BB flow mode — Fig. 67), but also permit separation of the solid-state transport delay time and the gas-phase transport delay times through the main regions of the rod.

All the release data shown in Figs. 64 through 67 were obtained by taking gas samples, some of which were analyzed with a Ge(Li) detector ("primed" points) and others with a NaI detector ("unprimed" points). With this method of measurement, we obtained release data for isotopes with half-lives ranging from 3.18-min <sup>89</sup>Kr to 5.27-day <sup>133</sup>Xe.

The initial release rates from the oxide fuel (Fig. 67) were relatively high, but they decreased, turned around, and then continued a gradual increase with burnup during operation at 39.4 kW/m (12 kW/ft). This behavior is believed to be associated with changes in fuel temperature caused by fuel restructuring and by changes in the fuel-cladding gap and fuel thermal conductance. At any given time, release was extremely sensitive to temperature level.

After the fission-product gases were released from the solid oxide-fuel matrix, their transport and venting from the top of the rod were controlled during steady-state operation by their diffusion through the high-pressure helium. As expected, the same trends showed up in the releases from the fuel column (TT-BB, Fig. 66), from the upper blanket (TT-BT, Fig. 65), and from the top of the rod (TT-TT, Fig. 64) as were observed in the release from the oxide fuel (BF-BB, Fig. 67). The release rate of the long-half-life <sup>133</sup>Xe was about the same for all four flow modes, as expected, and

1. "PRIMED" DATA POINTS ARE RESULTS OF SAMPLES COUNTED WITH A 30-cm<sup>3</sup> Ge(Li) DETECTOR (4.4% EFFICIENCY FOR <sup>60</sup>Co) AND 4096-CHANNEL ANALYZER SYSTEM.
2. "UNPRIMED" DATA POINTS ARE RESULTS OF SAMPLES COUNTED WITH A 3x3-in. NaI DETECTOR AND 512-CHANNEL ANALYZER.

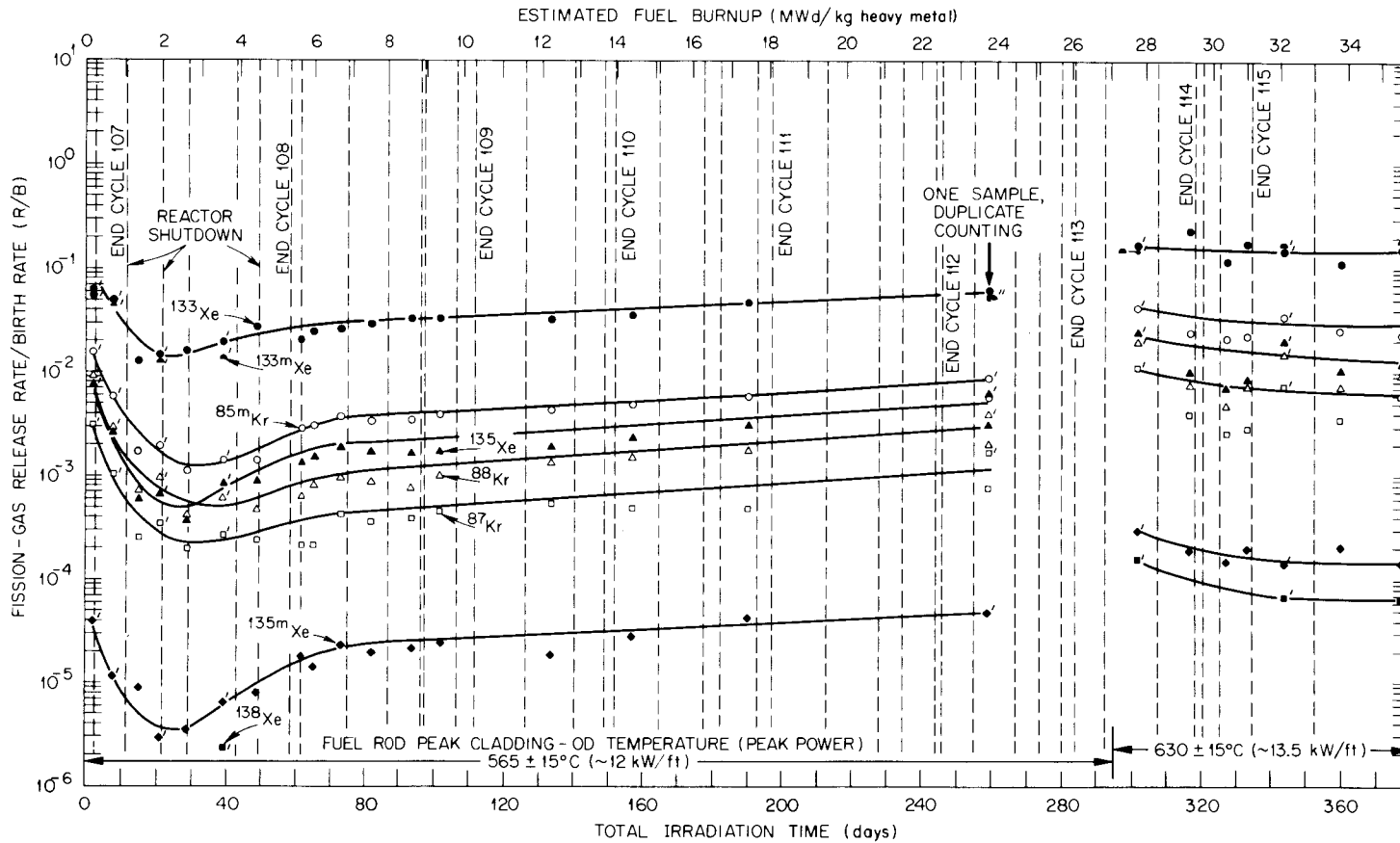


Fig. 64. Steady-state fission-gas release from GB-10 fuel rod vs time for case of sweep flow mode TT-TT (1 in. = 2.54 cm; 1 ft = 0.3048 m).

1. "PRIMED" DATA POINTS ARE RESULTS OF SAMPLES COUNTED WITH A 30 cm<sup>3</sup> Ge (Li) DETECTOR (4.4 % EFFICIENCY FOR <sup>60</sup>Co) AND 4096-CHANNEL ANALYZER SYSTEM.

2. "UNPRIMED" DATA POINTS ARE RESULTS OF SAMPLES COUNTED WITH A 3 in. x 3 in. NaI DETECTOR AND 512-CHANNEL ANALYZER.

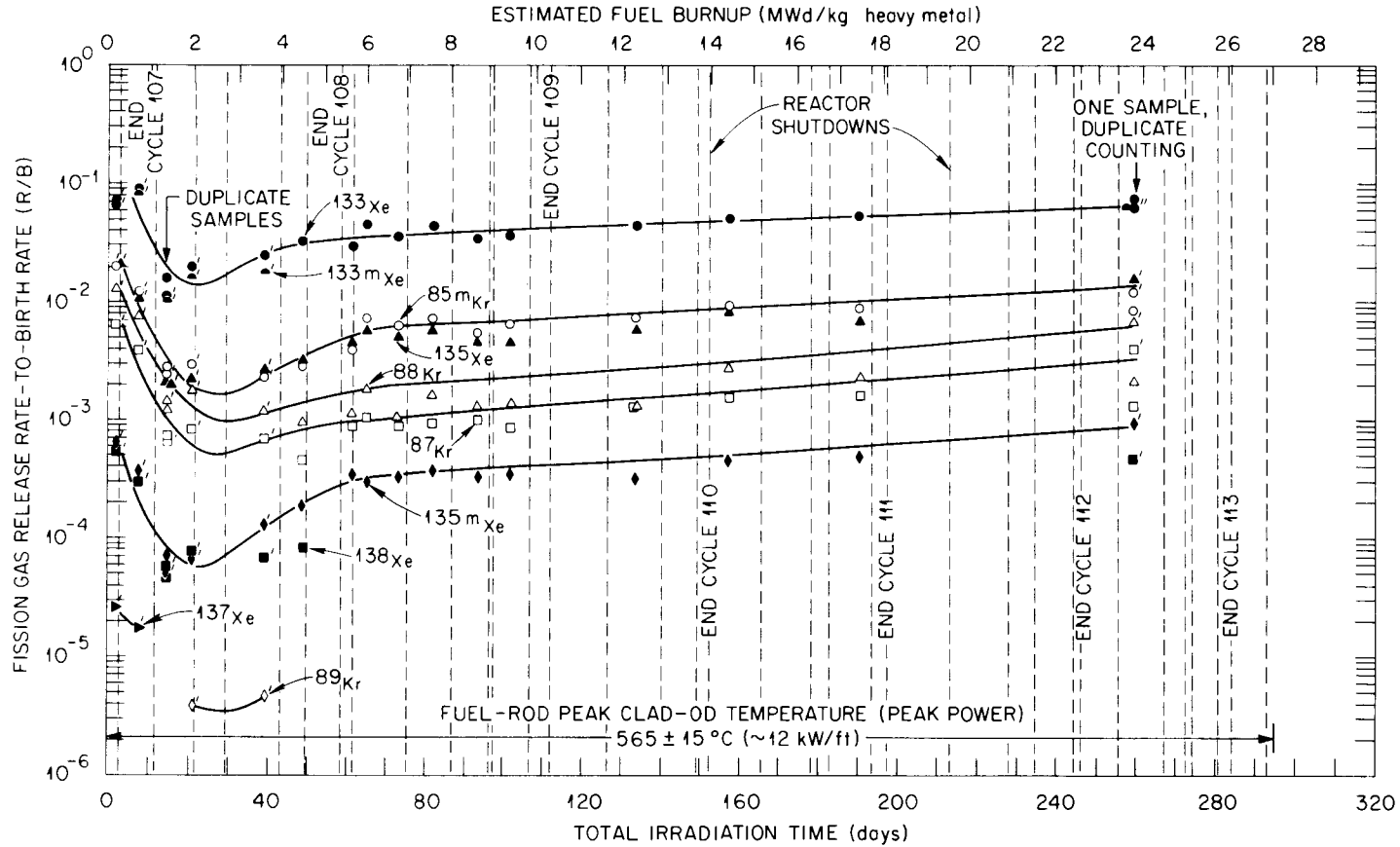


Fig. 65. Steady-state fission-gas release from GB-10 fuel rod vs time for case of sweep flow mode TT-BT (1 in. = 2.54 cm; 1 ft = 0.3048 m).

1. "PRIMED" DATA POINTS ARE RESULTS OF SAMPLES COUNTED WITH A 30 cm<sup>3</sup> Ge(Li) DETECTOR (4.4% EFFICIENCY FOR <sup>60</sup>Co) AND 4096-CHANNEL ANALYZER SYSTEM.
2. "UNPRIMED" DATA POINTS ARE RESULTS OF SAMPLES COUNTED WITH A 3 in. x 3 in. NaI DETECTOR AND 512-CHANNEL ANALYZER.

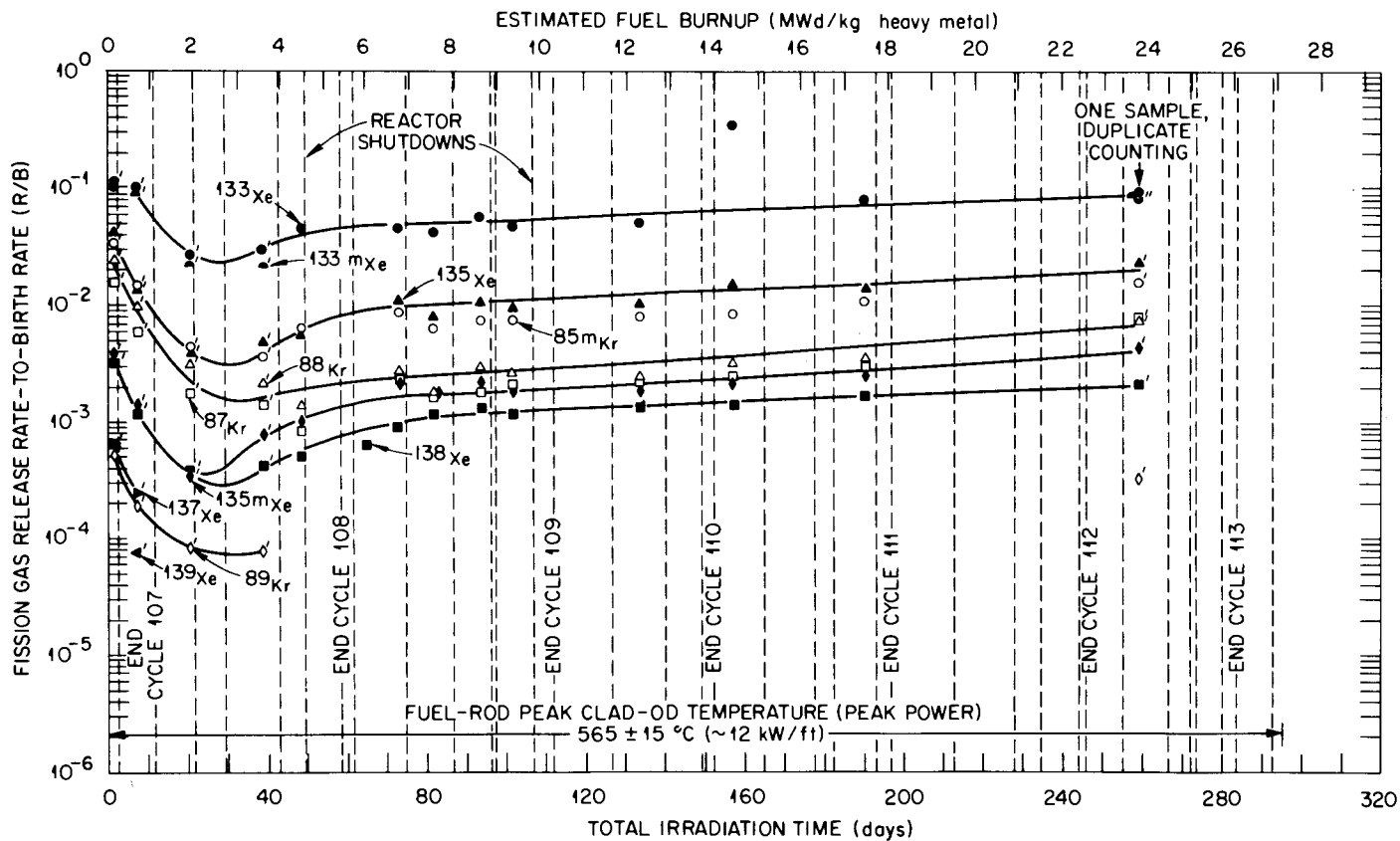


Fig. 66. Steady-state fission-gas release from GB-10 fuel rod vs time for case of sweep flow mode TT-BB (1 in. = 2.54 cm; 1 ft = 0.3048 m).

1. "PRIMED" DATA POINTS ARE RESULTS OF SAMPLES COUNTED WITH A 30-cm<sup>3</sup> Ge(Li) DETECTOR (4.4% EFFICIENCY FOR <sup>60</sup>Co) AND 4096-CHANNEL ANALYZER SYSTEM.
2. "UNPRIMED" DATA POINTS ARE RESULTS OF SAMPLES COUNTED WITH A 3 x 3-in. NaI DETECTOR AND 512-CHANNEL ANALYZER.

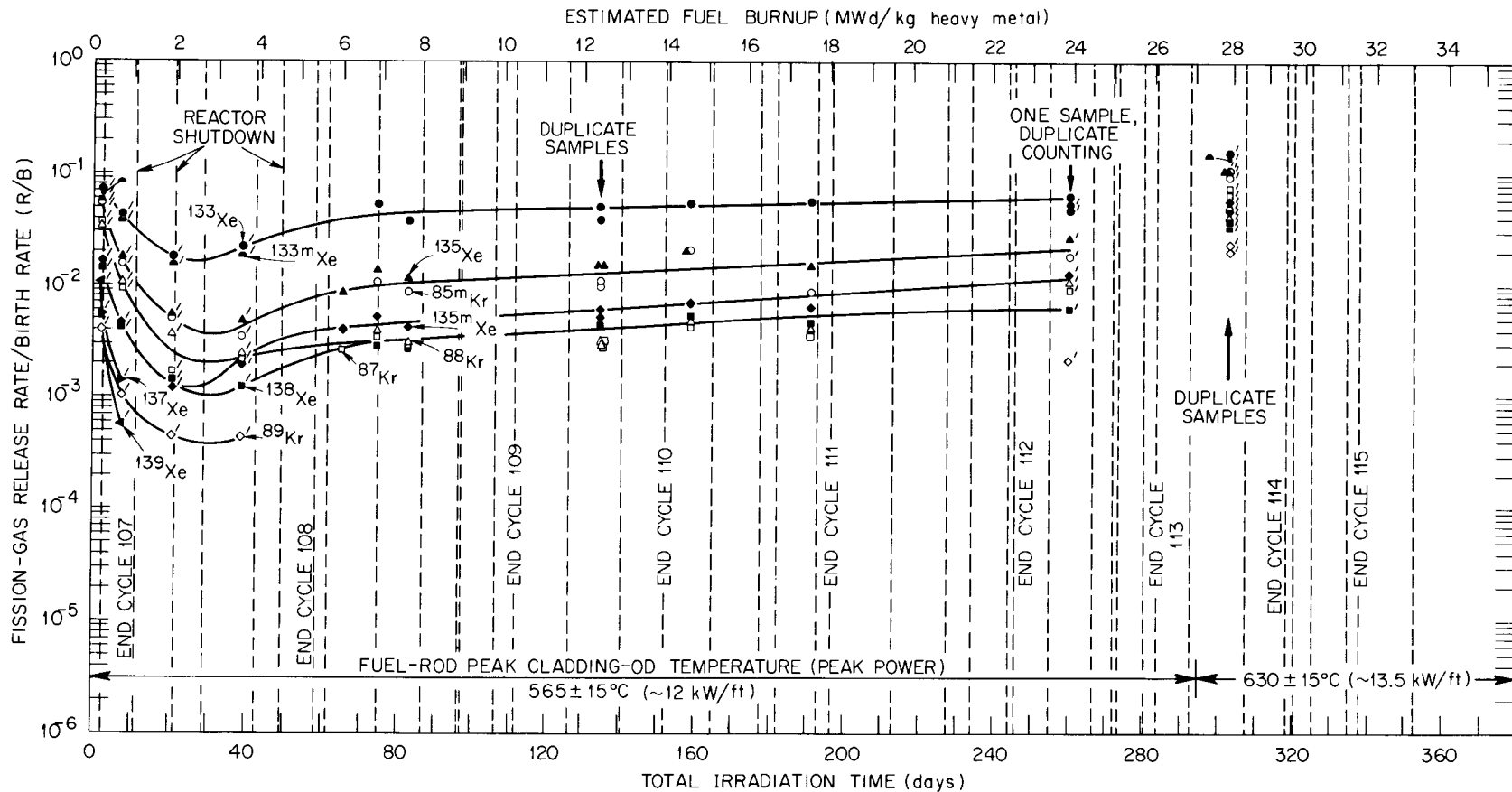


Fig. 67. Steady-state fission-gas release from GB-10 fuel rod vs time for case of sweep flow mode BF-BB (1 in. = 2.54 cm; 1 ft = 0.3048 m).

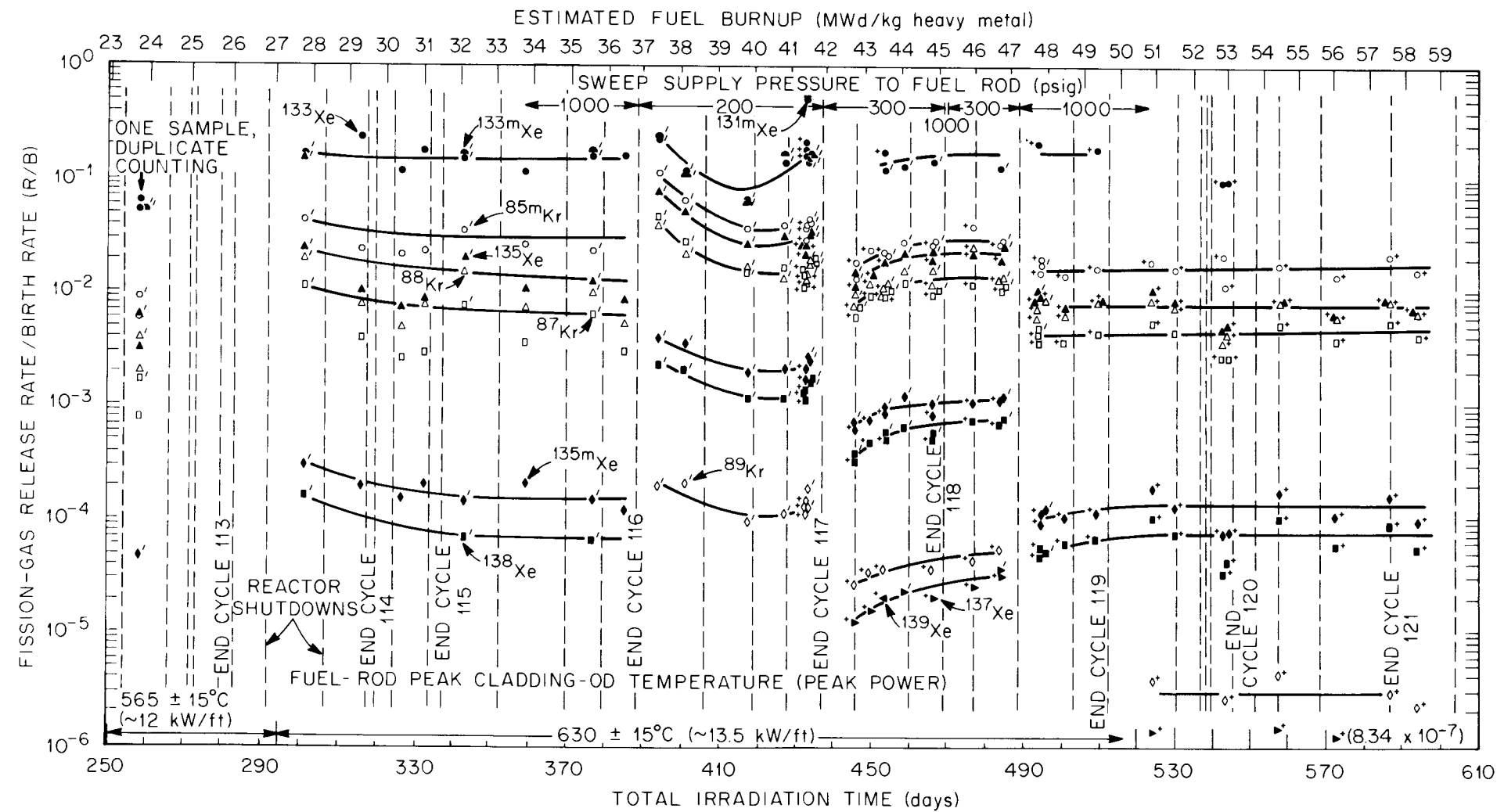
the spread, as a function of half-life, became greater the further the gases had to diffuse before reaching the sweep stream.

The early trends in the release data obtained from capsule GB-9 were reviewed and compared with the GB-10 release data. In the case of GB-9, the first set of gas samples were taken after 3 days at full power of  $\sim 48.6$  kW/m (14.8 kW/ft). Subsequent samples indicated a rise in fission-gas release rates, which continued until the release rates leveled off at  $\sim 10$  to 15 MWd/kg heavy metal burnup. The data from the effluent sweep line activity monitors, however, showed that at the beginning of the irradiation the initial activity release rate decreased by almost a factor of 2 the first 2 days at full power (see Fig. 22). The line activity then leveled off and started the long-term increasing trend. Thus, this transient period appears to be much longer and more pronounced at the lower power level of GB-10 [39.4 vs 48.6 kW/m (12 kW/ft vs 14.8 kW/ft)]. The difference in the initial condition of the fuel may have also been a big factor in the early release behavior ( $\sim 87\%$  dense solid pellets in GB-10 vs  $\sim 91\%$  dense hollow pellets in GB-9, with about the same fuel-column smear density as in GB-10).

A continuation of the venting (TT-TT flow mode) and fuel release data are shown in Figs. 68 and 69, respectively. At the burnup level of approximately 25 MWd/kg, we started using the BF-TT flow mode (Fig. 69) on a routine basis in place of the BF-BB flow mode, since a partial flow blockage of the BB line had developed. With respect to release of the fission gases, we saw no significant differences when using any of the three fuel sweep modes, BF-BB, BF-BT, or BF-TT.

During the fuel-rod power increase from 39.4 to 44.3 kW/m (12 to 13.5 kW/ft), the sweep flow was directed through the fuel rod under mode BF-TT. Two gas samples were taken under steady-state conditions prior to the power increase; one was taken soon after the power increase, and two were taken the following day. The results of these samples, together with the response of the ionization chamber on the high-pressure section of the effluent sweep line, described release behavior of the mixed-oxide fuel during the power-increase period fairly well. These release data and pertinent operating conditions during and following the

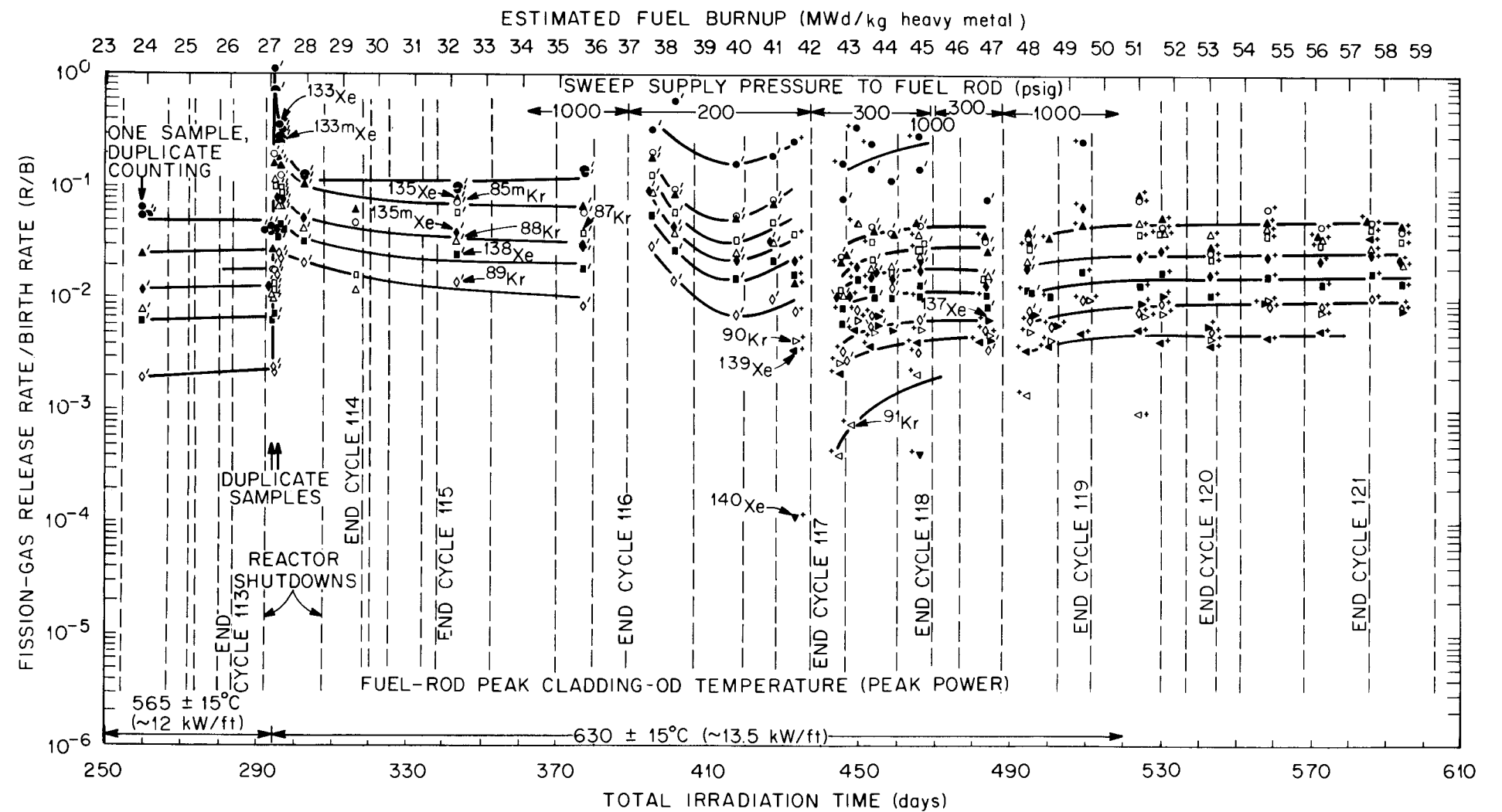
- 1 "PRIMED" DATA POINTS ARE RESULTS OF SAMPLES COUNTED WITH A 30 cm<sup>3</sup> Ge(Li) DETECTOR (4.4% EFFICIENCY FOR <sup>60</sup>Co) AND 4096-CHANNEL ANALYZER SYSTEM.
- 2 "UNPRIMED" DATA POINTS ARE RESULTS OF SAMPLES COUNTED WITH A 3 x 3-in. NaI DETECTOR AND 512-CHANNEL ANALYZER.
3. DATA POINTS IDENTIFIED WITH "PLUS" SIGN ARE RESULTS OF ON-LINE ANALYSES MADE WITH THE GB-10 ON-LINE SYSTEM Ge(Li) DETECTOR (8.6% EFFICIENCY FOR <sup>60</sup>Co) AND A 4096-CHANNEL ANALYZER SYSTEM.



FLOW MODES ARE DESIGNATED BY TWO LETTERS INDICATING THE ENTRANCE POINT FOLLOWED BY TWO MORE LETTERS INDICATING THE EXIT POINT FROM THE FUEL ROD. BF = BOTTOM OF FUEL, TT = TOP OF CHARCOAL TRAP, BT = BOTTOM OF CHARCOAL TRAP, BB = BOTTOM OF UPPER BLANKET.

Fig. 68. Steady-state fission-gas release from GB-10 fuel rod vs time for case of sweep flow mode TT-TT (1 in. = 2.54 cm; 1 ft = 0.3048 m; 1 psi = 6895 Pa).

1. "PRIMED" DATA POINTS ARE RESULTS OF SAMPLES COUNTED WITH A 30 cm<sup>3</sup> Ge(Li) DETECTOR (4.4% EFFICIENCY FOR <sup>60</sup>Co) AND 4096-CHANNEL ANALYZER SYSTEM.
2. "UNPRIMED" DATA POINTS ARE RESULTS OF SAMPLES COUNTED WITH A 3 x 3-in. NaI DETECTOR AND 512-CHANNEL ANALYZER.
3. DATA POINTS IDENTIFIED WITH "PLUS" SIGN ARE RESULTS OF ON-LINE ANALYSES MADE WITH THE GB-10 ON-LINE SYSTEM Ge(Li) DETECTOR (8.6% EFFICIENCY FOR <sup>60</sup>Co) AND A 4096-CHANNEL ANALYZER SYSTEM.



FLOW MODES ARE DESIGNATED BY TWO LETTERS INDICATING THE ENTRANCE POINT FOLLOWED BY TWO MORE LETTERS INDICATING THE EXIT POINT FROM THE FUEL ROD. BF = BOTTOM OF FUEL, TT = TOP OF CHARCOAL TRAP, BT = BOTTOM OF CHARCOAL TRAP, BB = BOTTOM OF UPPER BLANKET.

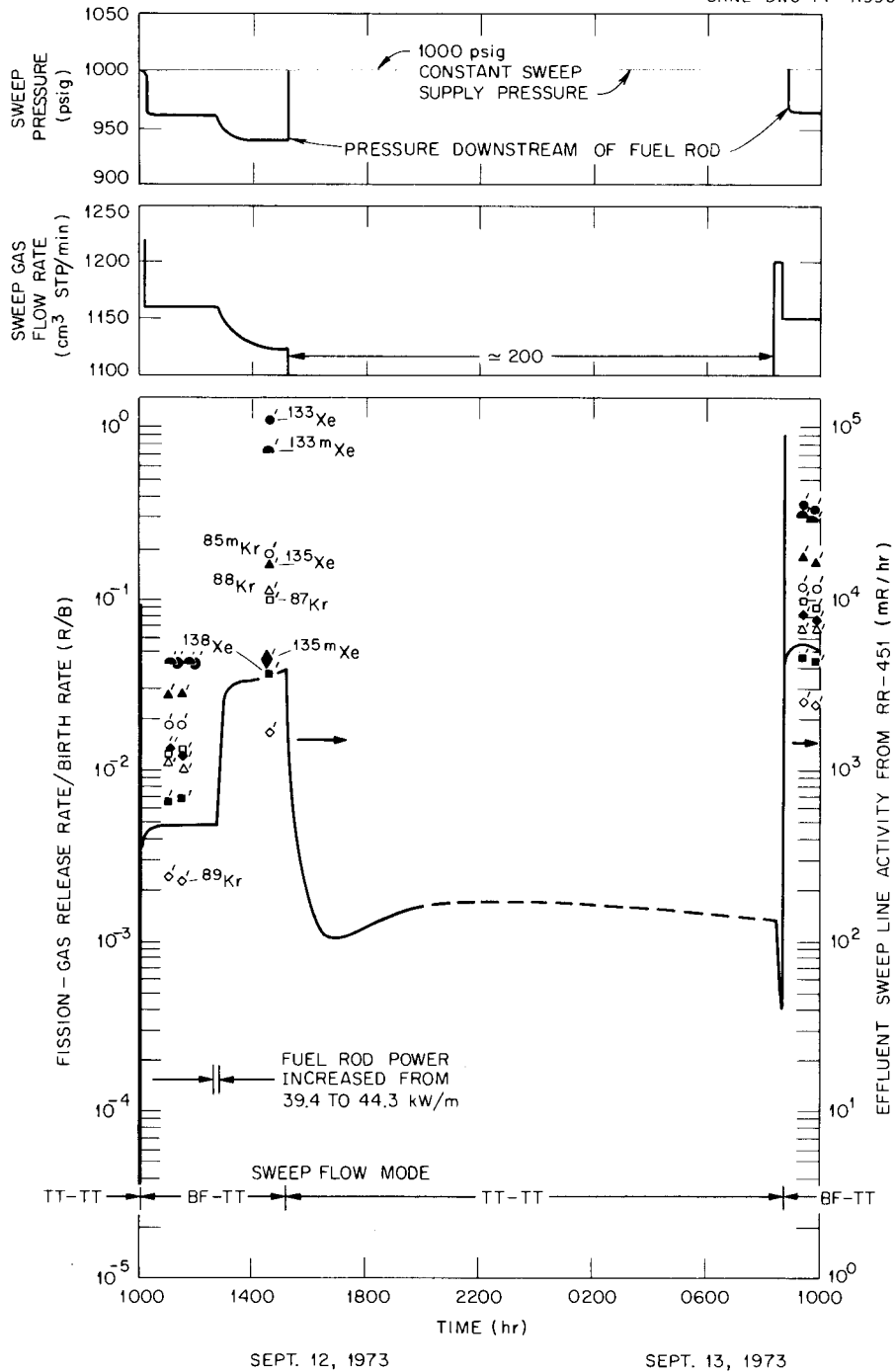
Fig. 69. Steady-state fission-gas release from GB-10 fuel rod vs time for case of sweep flow mode BF-TT (in. - 2.5 cm; 1 ft = 0.3048 m; 1 psi = 6895 Pa).

power increase are plotted in Fig. 70. The spikes in line activity upon changing the flow mode from TT-TT to BF-TT occurred as the inventory of fission gases that accumulated in the rod under the TT-TT flow mode was swept from the rod and passed by the ionization chamber on the effluent sweep line.

When the fuel-rod power was increased, very high release rates from the fuel were observed initially, as can be seen in Fig. 69 (the R/B data of Fig. 70 are also plotted in Fig. 69). Apparently, part of the higher fission-gas inventory in the mixed-oxide fuel at the lower temperature and power level was released when the temperature and power were increased, causing the temporary excessive release fractions.

After the release rates had stabilized following the power increase to 44.3 kW/m (13.5 kW/ft), we started operation at reduced sweep pressure to determine the effect of operating pressure on steady-state fission-gas release. The capsule was operated at a reduced sweep pressure of 1.38 MPa (200 psig) for 2 months (5.0 MWd/kg burnup) and then at 2.07 MPa (300 psig) for the same length of time. The effect of pressure on release from the fuel (Fig. 69) was greater than expected. Apparently, helium pressure affects release from the fuel, and after each large change in the pressure level, the establishment of a new equilibrium takes a long time. After returning to 6.9-MPa gage pressure (1000 psig), the release rates returned to a level consistent with those attained before the reduced-pressure operation.

The GB-10 on-line Ge(Li) detector system was placed in operation in March 1974, when the estimated fuel burnup was about 41 MWd/kg. Data points obtained with the on-line system are identified with a "plus" sign in Figs. 68 and 69. Using the on-line system eliminated sample handling and permitted measurement of isotopes with shorter half-lives than was possible by the gas-sampling method. From some spectra, we determined the release rates of 10-sec  $^{91}\text{Kr}$  and 16-sec  $^{140}\text{Xe}$  (see Fig. 69). The measurements were easier with the on-line system; gas samples containing less than 0.01 cm<sup>3</sup> STP of the BF-TT gas typically read 1 R/hr or more on contact.



"PRIMED" DATA POINTS ARE RESULTS OF SAMPLES COUNTED WITH A 30-cm<sup>3</sup> Ge(Li) DETECTOR (4.4% EFFICIENCY FOR <sup>60</sup>Co) AND 4096-CHANNEL ANALYZER SYSTEM.

Fig. 70. Activity release from capsule GB-10 during and following the fuel-rod power increase from 39.4 to 44.3 kW/m on Sept. 12, 1973 (1 in. = 2.54 cm; 1 ft = 0.3048 m; 1 psi = 6895 Pa).

The release rates for the TT-TT flow mode, or venting rates, during the reduced-pressure operation (Fig. 68) showed the same release patterns shown by the fuel release rates and also showed the effect of pressure on gas-phase transport, the effect being greater the shorter the half-life of the isotope. For example, the venting rates of 15.6-min  $^{135m}\text{Xe}$  and 17-min  $^{138}\text{Xe}$  were more than a factor of 10 higher at 1.38 MPa (200 psig) than at 6.9 MPa (1000 psig). These data clearly show how the high operating pressure suppresses steady-state venting of the fission gases. In fact, we had originally planned to go to a pressure of 0.69 MPa gage (100 psig) following the 1.38 MPa gage (200 psig) operation, but we decided instead to obtain the release data at the intermediate pressure of 2.07 MPa gage (300 psig) because of the high activity release at low pressures.

During the latter part of the irradiation, the routine release analyses were reduced to a minimum because of funding problems. The release information that was obtained consisted primarily of the effluent line activity levels indicated by the two on-line ionization chambers plus three sets of isotopic release analyses while operating at the final fuel-rod nominal power level of 48.6 kW/m (14.8 kW/ft). These data indicated an increase in release levels when the power was increased from 44.3 to 48.6 kW/m (13.5 to 14.8 kW/ft), but the release then gradually decreased back to a level about equal to that at 44.3 kW/m (13.5 kW/ft). Additional data indicated that the fuel-rod flow constriction retarded the release somewhat during the last few months of irradiation, but not to an extent where the steady-state release would be below the levels at 44.3 kW/m (13.5 kW/ft). Complete evaluation of these data were not possible because all GB-10 work was discontinued on Oct. 1, 1976.

### 11.5 Stable Noble Gas Release Measurements

We had difficulties in measuring the stable noble gases, and funding did not permit successful completion of this effort. While we believe the stable noble gas release data obtained is of little value, mention of the problems we encountered may be useful to someone attempting similar measurements.

The sampling system (Fig. 52) for taking large gas samples ( $\sim$ 1 liter STP) for the determination of release rates of stable noble gases using

mass spectrometry was placed in operation on July 1, 1974 (after ~500 days of irradiation). A total of five samples were taken at about 2-month intervals between samples; all were taken while the fuel rod was operated at the 44.3-kW/m (13.5-kW/ft) nominal power level. Preliminary release rate to birth rate (R/B) results for the samples are listed in Table 13. Some of the krypton results were close to the values expected — that is, greater than 30% fractional release — but the xenon results were all too low by almost a factor of 10.

Table 13. Preliminary results of GB-10 stable noble gas release measurements at 44.3 kW/m (13.5 kW/ft)

Date	Sweep flow mode	Ratio of fission-gas release rate to birth rate, %							
		<sup>83</sup> Kr	<sup>84</sup> Kr	<sup>85</sup> Kr	<sup>86</sup> Kr	<sup>131</sup> Xe	<sup>132</sup> Xe	<sup>134</sup> Xe	<sup>136</sup> Xe
7-1-74	TT-TT	8.34	11.0	8.89	10.3	1.56	1.67	1.38	2.52
10-1-74	BF-TT	33.2	51.3	61.3	42.4	3.07	3.52	3.39	6.11
11-21-74	BF-TT	23.2	23.8	21.8	21.8	4.14	4.52	4.81	8.64
1-28-75	TT-TT	14.2	15.0	14.0	14.6	0.99	1.06	1.01	1.91
3-25-75	TT-TT	24.6	25.9	23.4	25.0	2.94	3.23	3.00	5.53

After the R/B results were calculated for the first sample, we began examining the special techniques being used to analyze the samples. In preparing the samples for analysis by mass spectrometry, the sample gas was spiked with <sup>38</sup>Ar and then concentrated to bring the krypton and xenon isotopes up to measureable levels. Several steps in the sample transfer and preparation process were varied in an attempt to locate a problem, but, as seen in Table 13, these efforts did not significantly improve the results. Next, we examined the way we were taking the samples. Our method of sampling was as follows: After trapping a sample of the GB-10 effluent gas in the shielded 2-liter vessel inside the valve box and waiting 6 weeks for decay of the radioactive gases, we evacuated the lines and then slowly opened a valve to allow the gas to pass through about 3 m (10 ft) of 3.2-mm-OD (1/8-in.) line to an evacuated 2-liter sample vessel outside the valve box (see Fig. 52). When the pressure in the two vessels had

equalized, we closed the valves and removed the sample vessel. After discussing this sampling procedure with others, we believe we may have been fractionating the gas mixture by this method of sampling, tending to leave the heavier isotopes, especially the xenons, in the first vessel. (A similar situation existed in taking the much smaller gas samples for determining the release rates of radioactive noble gases using gamma-ray spectrometry, except in that case the gas was slowly withdrawn from the flowing sweep stream as opposed to withdrawal from a large static volume in the case of the stable gas samples. We saw no evidence of fractionation in the case of the radioactive samples, and we believe that significant fractionation of the gas mixture will not occur in the flowing sweep stream situation.)

After the results were obtained for the fifth stable gas sample, we decided to discontinue sampling until the sampling system could be modified. A modification of the system that would have permitted circulation and mixing of the gases in the two vessels before isolation and removal of the sample was nearly completed, but this work was terminated because of inadequate funding and could not be restarted in time to obtain measurements using the new sampling technique.

#### 11.6 Fission-Gas Release Behavior During Startup and Shutdown

There was no evidence of significant bursts of activity release from the initially solid-pellet fuel in GB-10 during startup and shutdown periods. When no bursts were observed from the annular-pellet fuel in GB-9, it was thought that perhaps activity pulses from the fuel might disperse and not be detected because of the limitations of the sweep line arrangement. In GB-10, however, we could sweep the fuel region directly while monitoring the effluent sweep line activity for activity bursts.

On two occasions early in the GB-10 irradiation (after 3 and 22 days at power), activity release from the rod was monitored during rapid cooloff (reactor scram) and heatup periods with the sweep passing through the fuel region. The release behavior was the same during both shutdowns. In each case, there was a small, short-duration spike of ~20 to 30% increase in the effluent sweep line activity upon shutdown followed by

rapid decay of the line activity to a background level. The amount of activity released during the spikes or bursts was insignificant (short duration) compared with the activity released during steady-state operation. During the startup periods, the indicated line activity responded to each temperature increase and leveled off in a smooth manner. The release behavior was similar to that during the initial capsule startup in that there were no obvious burst-type releases of activity upon heatup of the mixed-oxide fuel.

Although the specific tests described above were not repeated, it was obvious during the remainder of the irradiation that the bulk of the radioactive gas release was occurring during operation at power and not during startups and shutdowns. No attempts were made to measure the release of stable noble gases during startups and shutdowns.

### 11.7 Tritium-Monitoring Experiments

Several tritium-monitoring experiments were conducted to obtain information on tritium release and transport behavior; both the normal GB-10 high-purity helium sweep containing <5 ppm hydrogen and specially prepared 10,000-ppm-H<sub>2</sub>-in-helium gas were used in the experiments. They represented a relatively large effort and yielded a large amount of information on tritium transport behavior in the GB-10 system. The results will be reported in detail in a separate report now in preparation;<sup>25</sup> therefore, only general statements of some of the findings will be given here.

Funding for the GB-10 tritium-monitoring system (Fig. 53) was provided in late November 1974. By the middle of June 1975, the complex system had been designed, fabricated, performance-checked, and installed, and a trial run using clean helium had been conducted. A "zero baseline" reading was obtained on the ion chamber under helium flow before any tritium was introduced into the system. This reading, 0.45 mV, was about the same as that obtained in laboratory performance tests before installation at the reactor.

The next two tritium-monitoring system runs were system calibration checks using  $5 \times 10^{-5}$   $\mu\text{Ci}/\text{cm}^3$  STP HT-in-helium calibration gas. The results

were encouraging in that both the response of the calibrated ion chamber [about 54 mV at 70 kPa gage (10 psig) operating pressure] and the results for tritium samples collected in HTO traps indicated that the tritium concentration in the gas stream was reasonably close to the known concentration in the supply cylinder. Also, we were able to clean up the system in about 3 hr to an ion chamber reading within a factor of 2 of the "zero baseline" value (i.e., to a baseline reading below 1 mV).

Eight more tritium-monitoring system runs were completed before the tritium work had to be terminated on Oct. 1, 1975, because of inadequate funding. During this time, sufficiently high sweep flow rates (up to  $\sim 1000 \text{ cm}^3 \text{ STP/min}$ ) through the fuel region could be achieved by reducing the fuel-rod nominal power level from 44.3 to 39.4 kW/m (13.5 to 12 kW/ft) at the start of each experiment that involved flow through the fuel.

Two problems were encountered in the initial experiments. The first was the retention of tritium by the HTO converter when the normal GB-10 high-purity helium sweep ( $< 5 \text{ ppm H}_2$ ) was used as the carrier gas. This problem was eliminated by adding hydrogen to the helium carrier ( $> 2000 \text{ ppm H}_2$ ) upstream of the HTO converter (downstream of the capsule). The second problem was the presence of  $^{24}\text{Ne}$  in the sweep gas when the gas was passed through the fuel region. The  $^{24}\text{Ne}$  was not retained by the charcoal trap (breakthrough time  $< 1 \text{ min}$ ), and under certain system operating conditions the magnitude of the ion chamber response due to  $^{24}\text{Ne}$  precluded the direct measurement of tritium. Liquid scintillation beta measurement of the tritium retained on the molecular sieve was used to measure the HT in the carrier gas when the  $^{24}\text{Ne}$  interfered with the ion chamber measurement. The source of  $^{24}\text{Ne}$  was thought to be due to activation of impurities in the fuel region.

When the normal GB-10 high-purity helium was directed via the BF-TT flow mode,  $\sim 1\%$  of the predicted tritium production was detected (assuming a tritium yield per fission of  $1 \times 10^{-4}$ ). Directing the gas via the BF-BT flow mode (bypassing the fuel-rod trap) yielded a tritium release of about 10%.

When a standard gas mixture of tritium (HT) in high-purity helium was passed through the sweep system but bypassed the capsule, 100% recovery

of tritium was obtained. Less than 10% recovery was obtained when the standard gas was passed via the TT-TT flow mode, and less than 1% was recovered using the BT-TT flow mode. The data indicated that tritium in high-purity helium was retained in the areas exposed to fission-product plateout.

Approval for additional GB-10 tritium-monitoring experiments was received on June 18, 1976. The tritium-monitoring system, idle since October 1975, was readied and a calibration run made on June 29, 1976.

The principal objective of the additional tritium experiments was to observe the transport and release behavior of tritium in the presence of hydrogen (10,000 ppm H<sub>2</sub>), since the earlier tritium experiments without the addition of hydrogen showed that the fuel rod and the fission-product-coated lines acted as a sink for tritium. Time and funding did not permit desired moisture injections to maintain the desired oxygen potential in the gas. Instead, premixed and analyzed H<sub>2</sub>-in-He bottle gas (with and without tritium) was used. Time limitations permitted use of only one hydrogen concentration; 10,000 ppm was selected.

In general, the use of 10,000 ppm H<sub>2</sub> in the latter tritium experiments proved successful in transporting tritium through the capsule sweep lines and the fuel-rod trap. It was decided not to inject the hydrogen in the BF-TT mode, which would have allowed measurement of tritium inventory and release rate from the fuel, because of a small risk that the flow constriction might be affected. The flow constriction information was thought to be more important to the GCFR design than was the additional tritium information at this time. A final measurement of the BF-TT flow conductance at full power was made following the tritium experiments to determine if the 10,000 ppm of H<sub>2</sub> used in these experiments had affected the constriction by diffusing into the blanket and fuel. No change in the constriction could be detected.

#### 11.8 Fission-Product Decay Heating in Charcoal Trap

Throughout the GB-10 irradiation, we observed no significant fission-product decay heating in the rod charcoal trap. The fuel rod was operated under the BF-TT sweep flow mode numerous times for several

hours at a time and at each power level of operation, but little or no decay heating in the trap was detected. The BF-TT flow mode simulated the GCFR leaking-rod condition and was the GB-10 flow mode in which transport of volatile fission products to the rod trap and resultant decay heating were expected to be the greatest. Our observations of decay heating in the GB-9 and GB-10 rod traps and the other measurements related to volatile fission-product transport, both iodine-deposition measurements during irradiation and measurements of volatile fission-product distributions in postirradiation gamma scanning, indicate that the cooler upper blanket region in the rod is an effective barrier that prevents significant escape of volatile fission products beyond the upper blanket under normal conditions.

### 11.9 Iodine-Deposition Measurements

Iodine-deposition measurements were made after operation at the nominal fuel-rod power levels of 39.4 and 48.6 kW/m (12 and 14.8 kW/ft). The measurements consisted of measuring the release rates of  $^{135}\text{Xe}$  and  $^{133}\text{Xe}$  as a function of time after a reactor shutdown (or full retraction of the capsule) and then extrapolating the release data back to the time of shutdown in accordance with the half-lives of the parent isotopes  $^{135}\text{I}$  and  $^{133}\text{I}$ . The assumption is then made that the shutdown deposition activities (or decay rates) of  $^{135}\text{I}$  and  $^{133}\text{I}$  in the flow path are equal to the "extrapolated shutdown release rates" of their xenon daughters.

The measurements were made under carefully controlled flow conditions using several different flow modes in an attempt to determine the equilibrium deposition of  $^{135}\text{I}$  and  $^{133}\text{I}$  in the various regions of the fuel rod and in the effluent sweep line during the preceding period of normal steady-state operation under the TT-TT sweep flow mode.

The capsule was fully retracted on Apr. 17, 1973 [after 197 days of irradiation to a fuel burnup of  $\sim 18.1$  MWd/kg heavy metal at 39.4 kW/m (12 kW/ft)] for iodine-deposition measurements. Three sets of sweep-gas samples were taken, and in each case the sampling order was BF-TT, BF-BT, BF-BB, TT-BB, TT-BT, and TT-TT. All samples were taken with the charcoal trap and upper blanket regions of the rod electrically heated to a charcoal

temperature of 235°C, except for the TT-TT samples, which were taken with the heaters off. All the samples were counted using the NaI detector system (3 × 3 in. NaI detector and 512-channel analyzer).

The shutdown  $^{135}\text{Xe}$  and  $^{133}\text{Xe}$  release data for 39.4-kW/m (12-kW/ft) operation are shown in Figs. 71 and 72, respectively, where the release rates in atoms/sec are plotted as a function of time after shutdown. Also shown in these figures are the extrapolations (broken lines) of the xenon release data back to the time of shutdown. These "extrapolated shutdown release rates" were used to make estimates of the shutdown deposition of iodine in each flow path and in each main region of the system.

The xenon release data in Figs. 71 and 72 departed from the expected straight-line behavior and, instead, showed an initial buildup. We do not have a satisfactory explanation for the curvature of the xenon release data. The data indicated a need to follow the shutdown xenon release for a longer period of time than we were able to in this case.

The capsule was fully retracted on Mar. 15, 1976 (after 891 days of irradiation to a fuel burnup of  $\sim 89.9$  MWd/kg heavy metal) for the iodine-deposition measurements after operation at the 48.6-kW/m (14.8-kW/ft) nominal power level. The shutdown xenon release measurements were made in a similar manner and under the same temperature conditions as the measurements after the 39.4-kW/m (12-kW/ft) power level, but the GB-10 on-line Ge(Li) gamma-ray detector system was used instead of the gas-sampling method, and five sets of release data were obtained over a 3-day period instead of three sets over a 25-hr period. Another difference that might be significant was that sweep flow rates in the range 900–1200  $\text{cm}^3$  STP/min were used for the measurements after 39.4-kW/m (12-kW/ft) operation, whereas sweep flow rates in the range 300–550  $\text{cm}^3$  STP/min were used for the measurements after 48.6-kW/m (14.8-kW/ft) operation to increase the measurement capability of the on-line detector system in this application. Waiting times following each flow mode change were adjusted accordingly to allow time for the new gas to reach the point of measurement ( $\sim 15$  min vs  $\sim 5$  min). Also, live counting times of up to 10 min for all flow modes except TT-TT and up to 30 min for flow mode TT-TT were used with the on-line detector system as compared to gas-sample

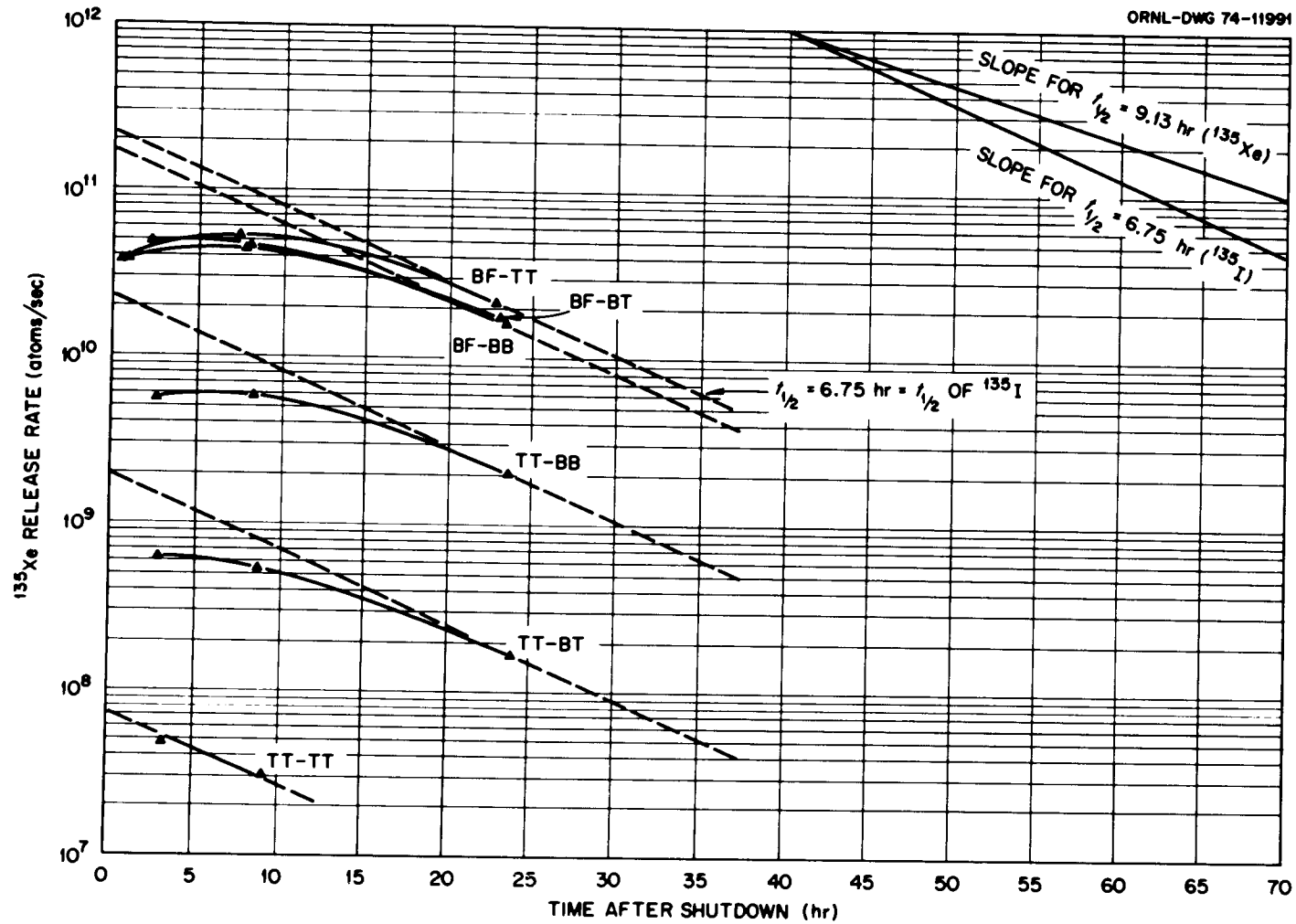


Fig. 71. Measured  $^{135}\text{Xe}$  release rates following full retraction of capsule GB-10 on Apr. 17, 1973, after 197 days at 39 kW/m (12 kW/ft) to a fuel burnup of  $\sim 18.1$  MWd/kg heavy metal.

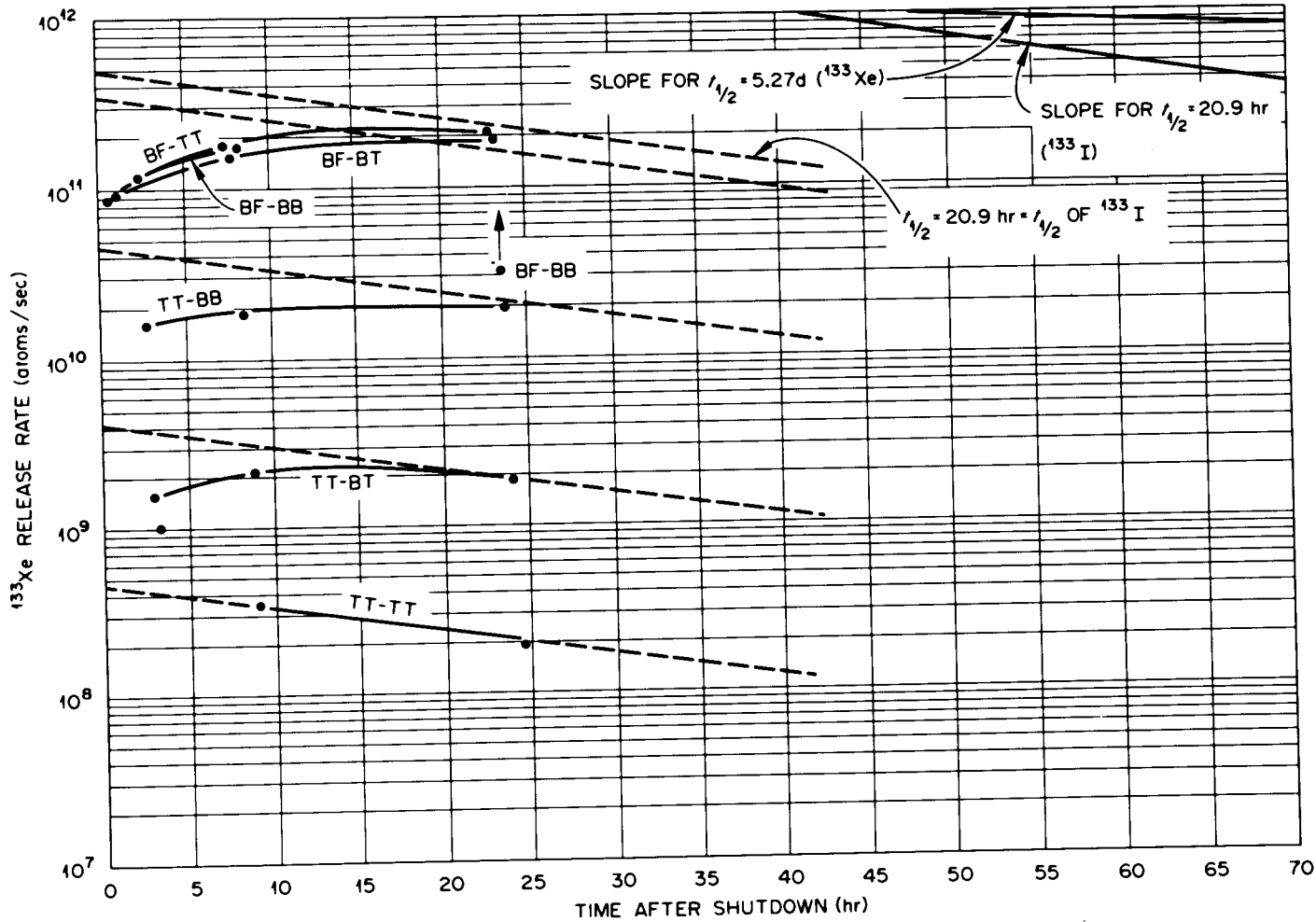


Fig. 72. Measured  $^{133}\text{Xe}$  release rates following full retraction of capsule GB-10 on Apr. 17, 1973, after 197 days at 39 kW/m (12 kW/ft) to a fuel burnup of  $\sim 18.1$  MWd/kg heavy metal.

withdrawal times for the measurements at 39.4 kW/m (12 kW/ft) that were within the range 20-50 sec. Thus, the gas-sample results were really closer to being instantaneous values. On the other hand, the on-line detector system results are inherently more consistent than the gas-sample results, and more detailed analyses are obtained with the on-line system.

The shutdown  $^{135}\text{Xe}$  and  $^{133}\text{Xe}$  release data for 48.6-kW/m (14.8-kW/ft) operation are shown in Figs. 73 and 74, respectively. The  $^{133}\text{Xe}$  release (Fig. 74) did not follow the expected straight-line relationship well at all over the first 2 days of shutdown. We do not have a satisfactory explanation for the release behavior indicated. Nevertheless, we made the extrapolations back to the time of shutdown, as shown by the broken lines in the figures, and used the "extrapolated shutdown release rates" to make rough estimates of the shutdown deposition of iodine in each flow path and in each main region of the system.

The iodine-deposition results for both power levels of operation are summarized in Table 14. It might be noted that if one assumes that no significant amount of iodine passed through the system undetected, then the data may also be interpreted in terms of fractional release values by summing the inventory fractions beyond each point of interest. For example, summing all the inventory fractions indicates less than about 1 1/2 and 2 1/2% release of  $^{135}\text{I}$  and  $^{133}\text{I}$ , respectively, from the fuel matrix during 39.4-kW/m (12-kW/ft) operation and about 10% and 35% release from the fuel matrix during 48.6-kW/m (14.8-kW/ft) operation. Because of the large uncertainties in the data, perhaps the most important aspect of the results is the indication that very little iodine was transported beyond the upper blanket region of the rod. The results in Table 14 indicate that during normal operation (TT-TT flow mode), the fuel-rod charcoal trap contained only about 0.012% of the total  $^{135}\text{I}$  inventory and 0.022% of the total  $^{133}\text{I}$  inventory at 39.4-kW/m (12-kW/ft) operation and about 1/4% of the  $^{135}\text{I}$  inventory and 1% of the  $^{133}\text{I}$  inventory at 48.6-kW/m (14.8-kW/ft) operation. These values are in agreement with the results of the GB-9 iodine deposition measurements (see Sect. 6.9).

Table 14. Summary of iodine-deposition results obtained for 39.4- and 48.6-kW/m operation of capsule GB-10

Region of GB-10 sweep system	Estimated iodine deposition at time of shutdown			
	$^{135}\text{I}$		$^{133}\text{I}$	
	Curies	Fraction of total inventory	Curies	Fraction of total inventory
<u>39.4 kW/m (12 kW/ft)</u>				
TT-TT lines	0.0020	$4.5 \times 10^{-6}$	0.0124	$2.4 \times 10^{-5}$
Fuel-rod charcoal trap	0.0541	$1.2 \times 10^{-4}$	0.114	$2.2 \times 10^{-4}$
Upper blanket	0.568	$1.3 \times 10^{-3}$	1.13	$2.1 \times 10^{-3}$
Fuel-region surfaces	5.33	$1.2 \times 10^{-2}$	11.8	$2.2 \times 10^{-2}$
<u>48.6 kW/m (14.8 kW/ft)</u>				
TT-TT lines				
Fuel-rod charcoal trap	1.20	$2.3 \times 10^{-3}$	~5.68	$\sim 9.1 \times 10^{-3}$
Upper blanket	3.58	$6.9 \times 10^{-3}$	~11.6	$\sim 1.9 \times 10^{-2}$
Fuel-region surfaces	45.2	$8.7 \times 10^{-2}$	~186	$\sim 3.0 \times 10^{-1}$

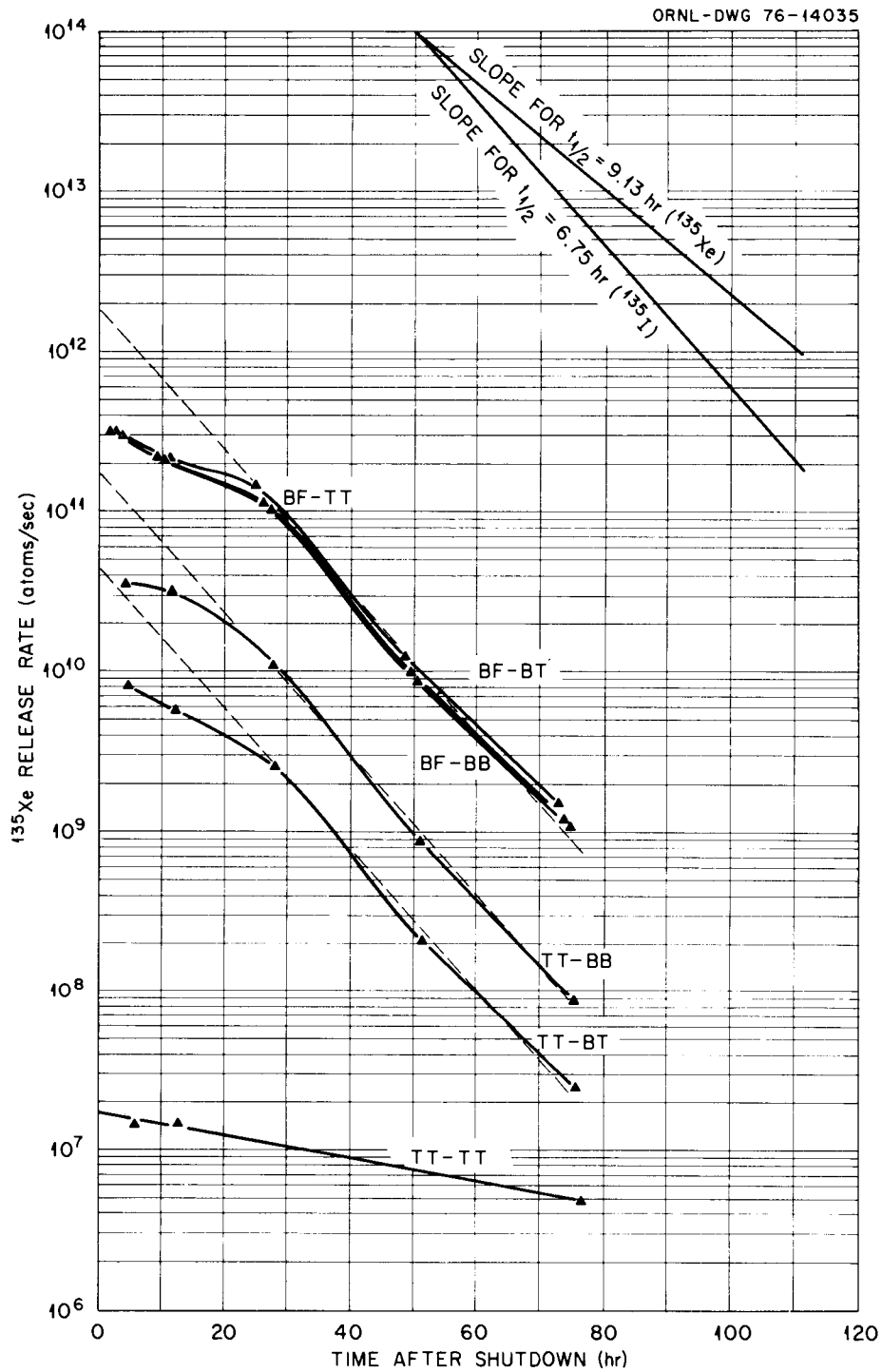


Fig. 73. Measured  $^{135}\text{Xe}$  release rates following full retraction of capsule GB-10 on Mar. 15, 1976, after 891 days at 39.4, 44.3, and 48.6 kW/m (12, 13.5, and 14.8 kW/ft) to a fuel burnup of  $\sim 89.9$  MWd/kg heavy metal.

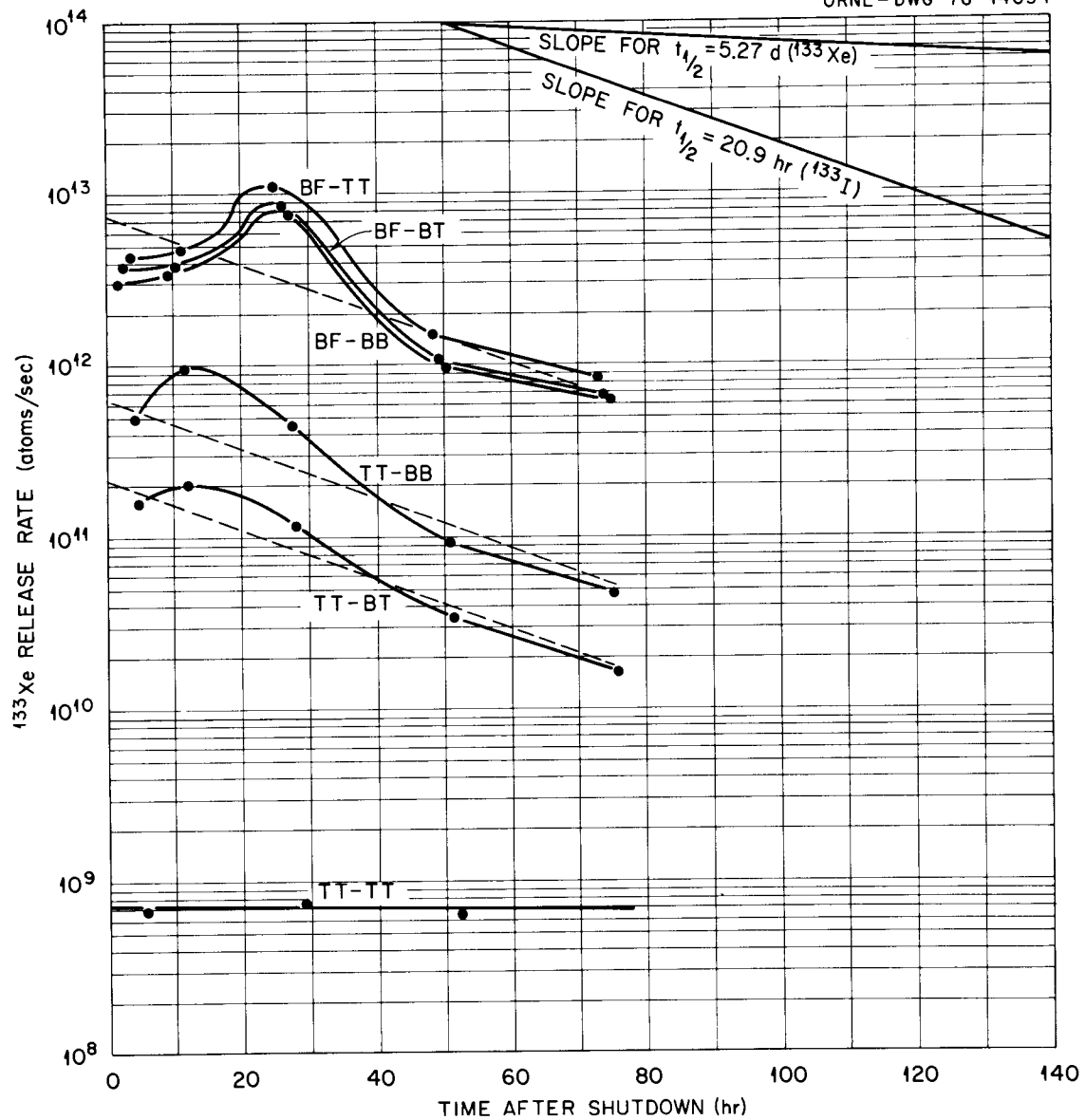


Fig. 74. Measured  $^{133}\text{Xe}$  release rates following full retraction of capsule GB-10 on Mar. 15, 1976, after 891 days at 39.4, 44.3, and 48.6 kW/m (12, 13.5, and 14.8 kW/ft) to a fuel burnup of  $\sim 89.9$  MWd/kg heavy metal.

#### 11.10 Deposition of Long-Lived Activity in Effluent Sweep System

Results of a typical radiation survey of the long-lived activity plated out on the GB-10 lines in the reactor pool are shown in Fig. 75. These surveys were made routinely at long reactor shutdown periods.

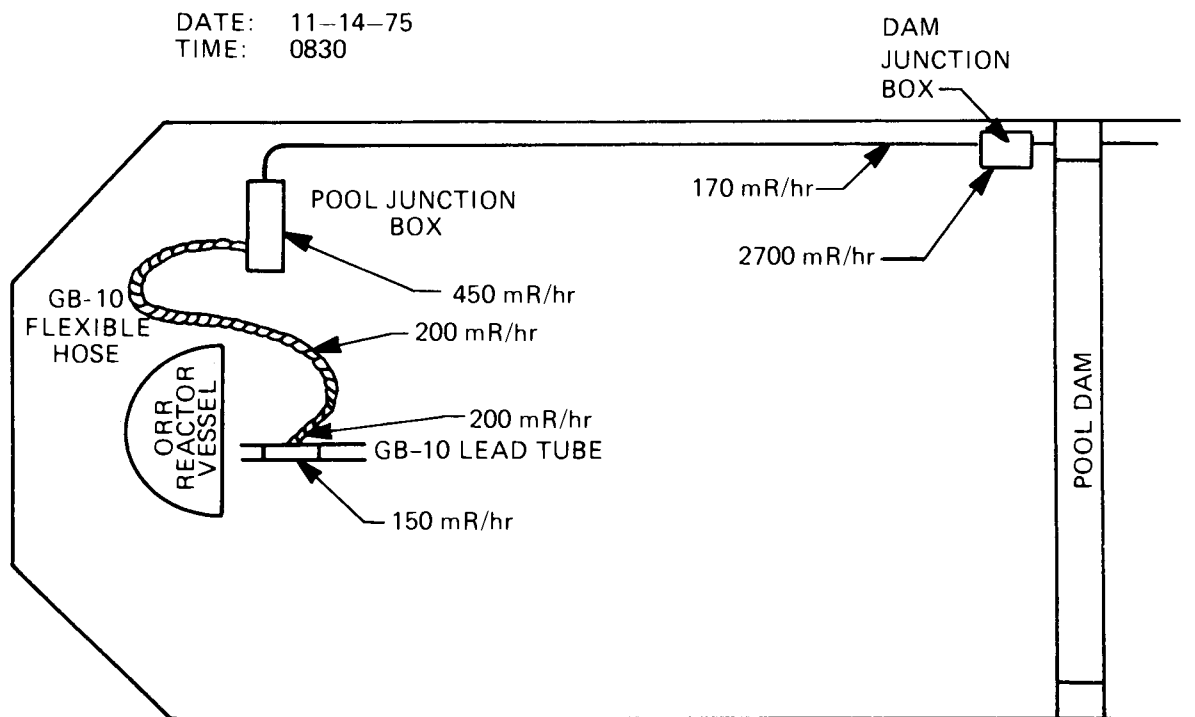


Fig. 75. Radiation survey of GB-10 lines in ORR pool.

Distances involved are  $\sim 9$  m ( $\sim 30$  ft) from the fuel rod to the pool junction box and another 5 to 6 m (15 to 20 ft) to the dam junction box. Radiation levels of deposition activity were typically 200 to 300 mR/hr on the lines, with higher levels of 500 to 700 mR/hr at mechanical couplings in the pool junction box and several R/hr at welded couplings in the dam junction box.

At one point during the irradiation, we analyzed a 13-cm (5-in.) segment of sweep line taken from the high-pressure section of the effluent sweep system which read 300 mR/hr and a needle valve from the downstream low-pressure section which read 7 mR/hr. The long-lived deposition activity found on these components is given in Table 15. The activities are very low when compared to inventories in the fuel rod.

Table 15. Long-lived activity deposition identified in GB-10 effluent sweep system

Isotope	Half-life	Activity at time of counting <sup>a</sup>			
		Needle valve HCV-110 <sup>b</sup>		Segment of sweep line <sup>c</sup>	
		dis/sec	μCi	dis/sec	μCi
<sup>131</sup> I	8.05 days	$2.4 \times 10^3$	0.064	$6.77 \times 10^4$	1.83
<sup>134</sup> Cs	2.1 years	$7.4 \times 10^2$	0.02	$2.3 \times 10^5$	6.3
<sup>137</sup> Cs	26.6 years	$1.4 \times 10^4$	0.37	$3.5 \times 10^6$	95.0
<sup>140</sup> Ba	12.8 days	$4.8 \times 10^3$	0.13	$8.1 \times 10^4$	2.2
<sup>140</sup> La	40.2 hr	$6.3 \times 10^3$	0.17	$9.3 \times 10^4$	2.5
<sup>141</sup> Ce	32 days	$7.4 \times 10^1$	0.002		

<sup>a</sup> Needle valve was counted on Nov. 7, 1973, and the line segment was counted on Nov. 8, 1973. The capsule had been shut down since Oct. 14, 1973.

<sup>b</sup> Needle valve HCV-110, used to regulate sweep flow rate, read ~7 mR/hr after removal from system.

<sup>c</sup> The line segment [0.32 cm OD × 0.069 cm ID (1/8 in. OD × 0.027 in. ID)] was ~12.7 cm (~5 in.) long, with a fitting on one end. It was removed from the high-pressure section of the effluent sweep line [downstream of the Ge(Li) detector system loop] and read ~300 mR/hr after removal.

### 11.11 Neutron Radiography

Neutron radiographs were taken of the GB-10 capsule before the start of irradiation, after operation at 39.4 kW/m (12 kW/ft), and after operation at 48.6 kW/m (14.8 kW/ft). Positive prints of neutron radiographs taken at a capsule orientation angle of 270° (see Fig. 54) are shown in Fig. 76 and indicate the condition of the capsule and fuel rod at each of these times during irradiation. Neutron radiography following operation at 44.3 kW/m (13.5 kW/ft) was not possible because the radiography rig was not in service at that time.

Neutron radiography after operation at 48.6 kW/m (14.8 kW/ft) included radiographs at capsule orientation angles of 270°, 255°, 245°, 235°, and 225° (see Fig. 54), as shown in Fig. 77. The angles were chosen to best show the position of thermocouples TE-703 and TE-704 relative to the fuel rod. Preirradiation radiographs had shown the Zircaloy-2 sleeve assembly to be rotated about 20° counterclockwise as viewed from the top from the

PHOTO 3463-74A

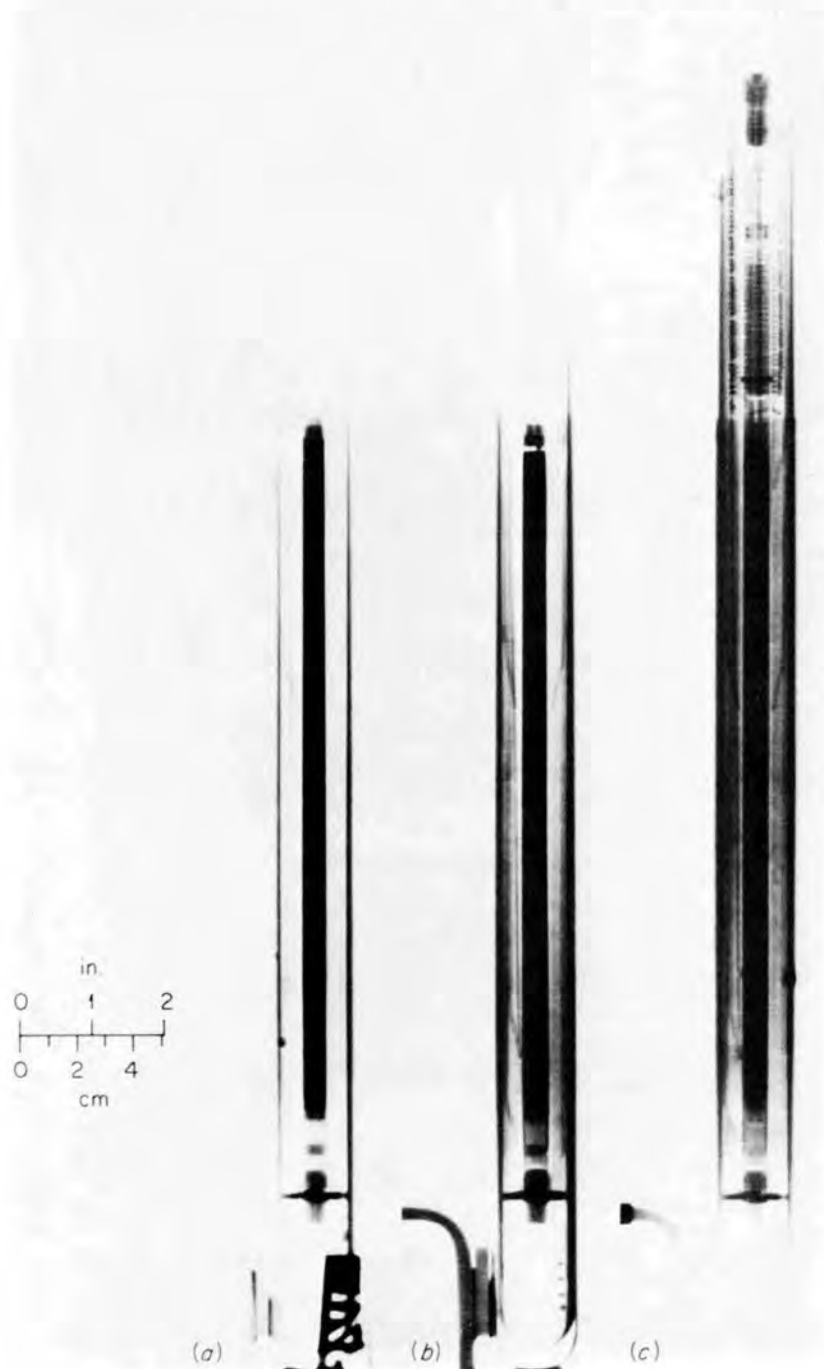


Fig. 76. Neutron radiographs of GCFR capsule GB-10 taken at a capsule orientation angle of  $270^\circ\text{C}$ : (a) preirradiation; (b) after 284 days at 39 kW/m (12 kW/ft) to  $\sim 26.1$  MWd/kg heavy metal burnup; (c) after 969 days at 39, 44, and 48 kW/m (12, 13.5, and 14.8 kW/ft) to  $\sim 100$  MW/kg burnup (2.7 days before end of irradiation).

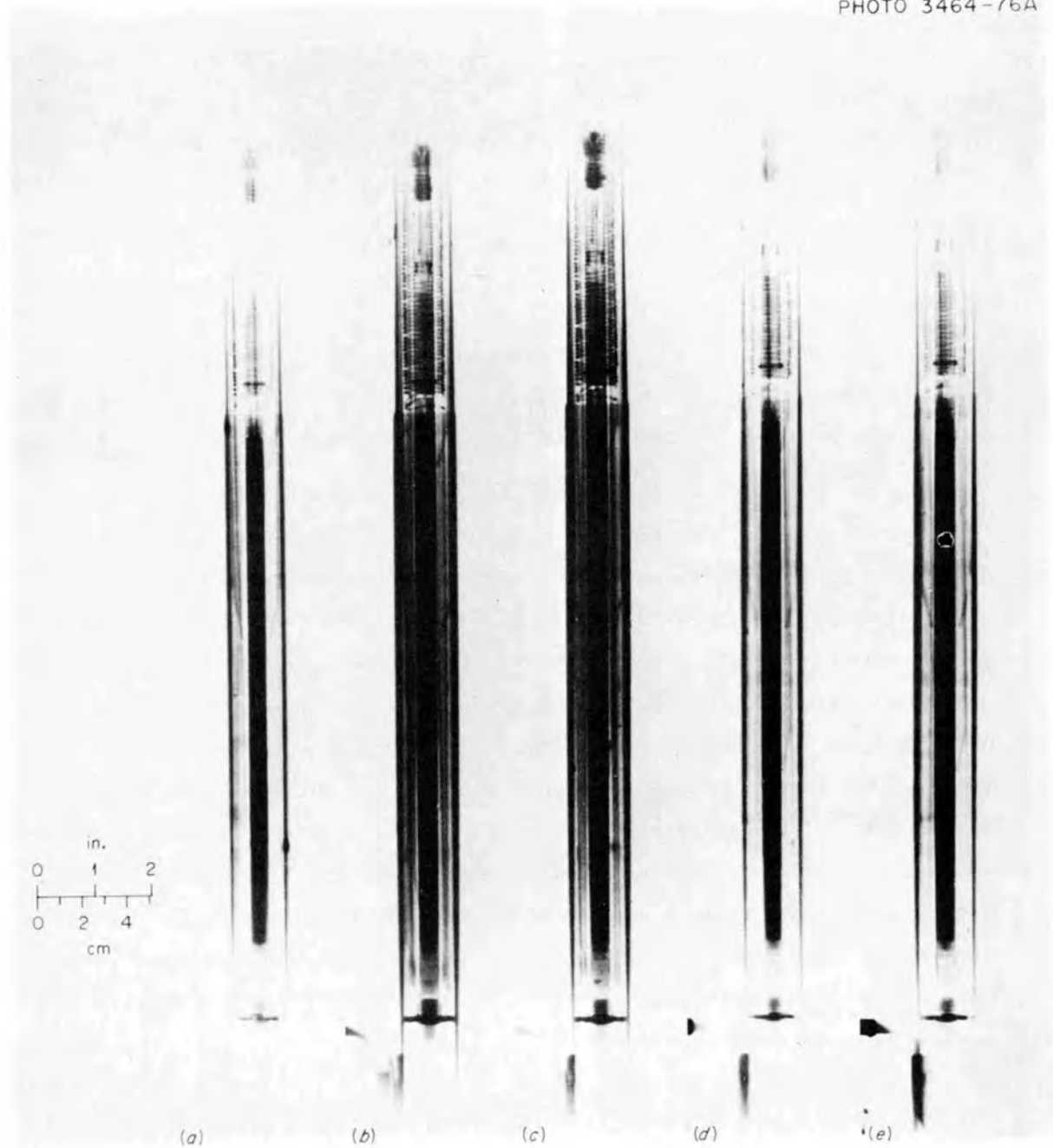


Fig. 77. Neutron radiographs of GCFR capsule GB-10 taken at 2.7 days before end of irradiation to show thermocouple positions. Capsule orientation angles are: (a)  $270^\circ$ ; (b)  $255^\circ$ ; (c)  $245^\circ$ ; (d)  $235^\circ$ ; (e)  $225^\circ$ .

orientation specified on the construction drawings; thus, a radiograph at a capsule orientation angle of approximately  $250^\circ$  (instead of  $270^\circ$ ) was expected to be perpendicular to the plane of TE-703 and TE-704. These radiographs indicated about the same Zircaloy-2 sleeve assembly orientation shift and showed that TE-704 on the cold side was closer to the rod than TE-703 on the hot side, by at least 0.38 mm (0.015 in.), and the rod appeared to be slightly bowed toward the cold side. This information was used in interpretation of the GB-10 thermal operating data (Sect. 11.2). Following the neutron radiography at 48.6 kW/m (14.8 kW/ft), which involved 8 days of capsule downtime, the capsule was reinstalled in the irradiation facility and operated at the nominal fuel-rod power level of 48.6 kW/m for 2.7 additional days to enhance the levels of  $^{131}\text{I}$  and other fission products for the postirradiation gamma scanning studies.

Examination of the neutron radiographs taken near the end of the 39.4-kW/m (12-kW/ft) operating period showed that the fuel column had settled about 0.4 cm (5/32 in.). Numerous cracks, especially in the longitudinal direction, could be seen in the fuel pellets, but no central hole could be detected in the initially solid pellets. A central hole of less than about 0.5 mm (0.020 in.) probably could not be detected. The as-fabricated central hole in the lower two enriched- $\text{UO}_2$  half-pellets [below the  $(\text{U,Pu})\text{O}_2$  column] had become slightly funnel shaped, with the smaller diameter of the funnel at the bottom. The central hole in the upper two enriched- $\text{UO}_2$  half-pellets could not be seen clearly because of instrumentation leads. The remainder of the fuel rod and capsule parts appeared to be normal, and no other changes from the preirradiation radiographs were detected.

The settling of the fuel column observed in GB-10 did not occur in the GB-9 test rod. However, the GB-9 rod contained annular fuel pellets having an initial density of 91%, and the rod was operated at the nominal power level of 48.6 kW/m (14.8 kW/ft) throughout its irradiation. The initial density of the solid fuel pellets in GB-10 was lower (87%), giving about the same initial fuel-column smear density as in GB-9 (84% of theoretical density in GB-10 vs 85% in GB-9). The test pellets in both rods had 0.015-cm (0.006-in.) dished ends.

The radiographs taken near the end of the irradiation indicated a number of areas of interest for postirradiation study, including fuel redistribution in the vicinity of the fuel column ends, changes in appearance of the enriched-UO<sub>2</sub> half-pellets next to the (U,Pu)O<sub>2</sub> column and the adjacent blanket pellets at both ends, and an inclusion in the fuel central hole about 2.5 cm (1 in.) from the bottom of the (U,Pu)O<sub>2</sub> column. The radiographs showed development of a central hole as expected. The hole diameter appeared to be about 0.76 to 1.0 mm (0.030 to 0.040 in.) near the bottom end of the column, about 1.3 mm (0.050 in.) about one-third of the way up the column, and about 1.5 mm (0.060 in.) over most of the upper half of the column; the change in hole diameter from one of these points to the next was very gradual. The hole was enlarged in the uppermost mixed-oxide pellet to about 1.9 to 2.0 mm (0.075 to 0.080 in.) maximum diameter. The fuel column length had increased, recovering about one-third to one-half of its original length loss [the radiographs after 39.4-kW/m (12-kW/ft) operation showed the fuel column had settled about 0.4 cm (5/32 in.)].

## 12. GB-10 POSTIRRADIATION DISASSEMBLY AND PRELIMINARY EXAMINATION

Postirradiation disassembly and examination were implemented as quickly as possible after the irradiation was terminated to permit gamma-ray scanning analyses for the location of various fission products before their loss by radioactive decay. Following termination of the irradiation on Aug. 1, 1976, the capsule was transferred to hot cells on Aug. 2, and disassembly was started. The rod was successfully recovered from the capsule and appeared to be in excellent condition. The rod was gamma scanned extensively with a Ge(Li) scanning system, dimensionally inspected, neutron radiographed, and then shipped to ANL in September along with other capsule components for sectioning and detailed examinations.

Gamma scanning of the fuel pin was done as soon as possible to retrieve as much information as possible on the short-lived isotopes. The gamma scans showed that the short-lived iodine fission products concentrated at the upper fuel-blanket interface, and the cesium fission products concentrated at both fuel-blanket interfaces and in the charcoal trap. High concentrations of ruthenium isotopes were observed in the same positions at which neutron radiographs showed inclusions in the central void.

Two neutron radiographs were taken of the fuel rod after its removal from the capsule. Positive prints of these radiographs, taken at orientation angles  $90^\circ$  apart, are shown in Fig. 78. After its removal from the capsule, the fuel rod could be placed closer to the film package in the radiography rig, and clearer radiographs were obtained without interference from other capsule components and instrument leads. The end of the BB line, in particular, could be seen much better in these radiographs than in the capsule radiographs. There appeared to be a small amount of material in the end of the BB line.

Detailed results of the ORNL portion of the GB-10 examination studies are presented in a separate report.<sup>28</sup>



Fig. 78. Postirradiation neutron radiographs, 90° apart, showing the condition of the GB-10 fuel rod after its removal from the capsule.

### 13. DISCUSSION OF UNCERTAINTIES IN GB-9 AND GB-10 DATA

Funding and manpower limitations did not permit a detailed analysis of uncertainties in the GB-9 and GB-10 data. However, in this section the authors' general appraisal of known uncertainties in the important measured and calculated quantities is given in the hope that this discussion might serve as a guide for those who may want to apply the data in their work. Included at the end of this section is a description of abnormal occurrences that took place during the irradiations.

#### 13.1 Measured Quantities

Uncertainties in measurements of capsule temperatures, pressures, flow rates, and fission-gas release rates are discussed below. In general, the recorders used in the GB-9 and GB-10 experiments were calibrated once every 2 months, which was standard procedure for all except special measuring instruments.

##### 13.1.1 Temperatures

The capsule temperatures were measured with 1.6-mm-diam (1/16-in.) type 347 stainless-steel-sheathed Chromel-Alumel grounded-junction thermocouples from a thermocouple lot purchased to specifications that required  $\pm 3/8\%$  accuracy, or about  $2^\circ\text{C}$  under the service conditions. Our experience with these thermocouples has been good. At the time of the evaluation of the GB-10 thermal operating data (Sect. 11.2), the possibility of decalibration of the thermocouples was considered. An evaluation to determine if postirradiation calibration of the thermocouples would be justified was made by ORNL, GAC, and ANL. The general findings were that the uncertainty associated with decalibration was small compared to the overall uncertainty in fuel-rod cladding operating temperatures and that significant decalibration under the service conditions was very unlikely. We do not expect that a drift exceeding  $10^\circ\text{C}$  would have occurred under the exposure conditions. The same comments apply to the GB-9 thermocouples.

### 13.1.2 Pressures

The magnitude of uncertainty in pressure measurements is estimated to be about  $\pm 5\%$  and in the fuel-rod  $\Delta P$  measurements about  $\pm 34$  kPa ( $\pm 5$  psi), since the agreement of the recorders used was checked before each  $\Delta P$  measurement. In general, there was redundancy in pressure-measuring elements (pressure transducers and gages) in most sections of the gas systems, which reduced the need for frequent calibrations. Also, at normal operating pressures, the fission-gas venting rates from the fuel rod were not very sensitive to pressure level, although they were quite sensitive to pressure fluctuations, as would be expected. Thus, the pressure elements were calibrated on a need basis rather than a routine basis. For example, the pressure elements were calibrated just prior to the GB-10 reduced-pressure operation, since accurate pressure measurements were more important in this special test than during operation at normal pressure.

### 13.1.3 Flow rates

Uncertainty in the flow-rate measurements was kept within  $\pm 10\%$  during operation of both GB-9 and GB-10. Flow rate was recognized as one of the most important parameters in these experiments, and the required effort was made to ensure that the measurements were accurate. This was done by using more than one measuring element and by performing calibrations as judged necessary.

### 13.1.4 Fission-gas release rates

The determination of fission-gas release rates (R) involved counting the effluent sweep gas (either on-line or in a sample bottle) with a gamma-ray detector, analyzing the spectrum to identify and obtain disintegration rates of the various gamma-emitting isotopes found to be present, and then reducing the data first to isotopic concentrations in the gas and finally to release rates from the fuel rod. The data-reduction step to obtain isotopic concentrations requires sample volume calculation from

sample dimensions and pressures, while the final data-reduction step to release rates requires flow rates and travel times (for decay corrections) as input. Thus, sources of uncertainty in the determination of release rates may be either in the counting and analysis of the spectrum or in the input data used in the data reduction to release rates. The uncertainties in the input data (sample dimensions, pressures, times, etc.) are relatively easy to evaluate, and we believe the uncertainty in release rates due only to the uncertainties in these input data is generally less than about  $\pm 20\%$ . The evaluation of uncertainties in the counting and analyzing of the spectrum is more difficult, dependent upon the isotope (isotopic data for the very short-lived isotopes are generally less well known than for the longer-lived isotopes), and further involved because three different detector systems were used in the GB-9 and GB-10 experiments (see notes on Fig. 68 for a brief description of the three detector systems).

When the gas samples were counted with the Ge(Li) detector system or when the GB-10 on-line Ge(Li) detector system was used, the counting and analyzing of spectra were done by well-qualified personnel of the Analytical Chemistry Division of ORNL. The output from the Ge(Li) detector in either case was transmitted to a Nuclear Data 50/50 Data Acquisition System interfaced to a PDP-15 located in the reactor building. The gamma-ray spectral data acquired were then stored on Dectapes. Reduction of the spectral data to isotopic concentrations was accomplished using the computer program MONSTR. The MONSTR program is a gamma-ray spectral resolution and isotope identification program written for the PDP-15 system. Photopeaks are located by a 5-point first derivative cubic equation function. Each peak is fitted by least squares to a Gaussian function.

The on-line Ge(Li) detector system was calibrated prior to its installation using an exact mock-up of the actual experimental setup. Separate calibrations were made for each collimator. Gamma-ray source solutions of known disintegration rates used in the calibration were calibrated on a Ge(Li) system previously calibrated with National Bureau of Standards (NBS) and International Atomic Energy Agency (IAEA) standards. The isotopes and gamma energies used in the calibrations are listed in

Table 16. The Ge(Li) detector system used to count the gas samples was routinely calibrated with NBS and IAEA standards.

Table 16. Calibration sources used in calibrating the GB-10 on-line Ge(Li) detector system

Gamma energy, $E_{\gamma}$ (keV)			
$^{160}\text{Tb}$	$^{82}\text{Br}$	$^{56}\text{Co}$	$^{24}\text{Na}$
86.79	554.34	846.75	1368.55
298.58	619.12	1238.3	2754.00
879.33	698.37	1771.43	
962.08	776.70	2598.57	
966.10	827.80	3202.19	
1178.12	1044.00	3253.64	
1271.87	1317.40	3273.19	
	1474.90	3451.40	

We believe the counting and analyses methods that were used with the two Ge(Li) detector systems compared well with the state of the art of gamma-ray spectrometry at the times of the measurements. This does not mean, however, that we did not run into any problems. The spectra were complex and required careful interpretation.

One of the larger uncertainties associated with the Ge(Li) detector systems that we could readily identify was in the results from the on-line system using different collimators. There were small differences in the results depending on the collimator selections, the largest difference being about 20% between two of the collimators. We had hoped to pursue this further by performing some postexperiment calibrations, but funding and manpower limitations did not permit this to be done.

When the gas samples were analyzed with the NaI detector system, much less sophisticated analysis methods were employed. Photopeaks were identified visually on the analyzer scope, and the end channels for each photopeaks were selected. Total counts in all the channels associated with each photopeak and the counts in the end channels were output from

the analyzer. Net counts for each photopeak were estimated by subtracting from the total counts the average of the counts in the end channels multiplied by the total number of channels. Count rates for each photopeak were then calculated by dividing the net counts by the live counting time. Detector efficiency factors and isotope data were then included in the calculations of isotopic concentrations. Since the resolution of the NaI detector system was much less than that of the Ge(Li) detector systems, only certain of the more pronounced photopeaks were selected for analysis using these methods, and then only under the guidance of experienced personnel. Use of the NaI detector system in this way was justified, in part, by the fact that we compared the results with those from the Ge(Li) detector systems by taking duplicate samples and analyzing one with each system and by analyzing the same sample with both systems in some cases.

Duplicate gas samples were taken under the TT-BT flow mode early in the GB-10 irradiation (at a fuel burnup of  $\sim 1.35$  MWd/kg heavy metal) to compare the results obtained from the two gas-sample detector systems. One sample was counted using the Ge(Li) detector system, and the other was counted using the NaI detector system. The good agreement between these results (see Fig. 65), as well as the fair agreement obtained in several similar duplicate analyses made during the GB-9 irradiation, indicated that the NaI system could be used satisfactorily to augment the less-frequent data being obtained with the Ge(Li) system. However, later on in the irradiation (at a fuel burnup of  $\sim 23.8$  MWd/kg heavy metal), duplicate counting of several samples indicated that the NaI system results for  $^{85}\text{mKr}$  were a factor of 1.5 lower than the results from the Ge(Li) system and for  $^{87}\text{Kr}$ ,  $^{88}\text{Kr}$ , and  $^{135}\text{Xe}$ , the NaI system results were a factor of 2 to 3 lower. The results of duplicate samples counted on the same detector system [either the NaI or Ge(Li)] showed good agreement.

We were unable to resolve the discrepancies between the two gamma-ray spectrometer systems by counting known sources and reviewing the data-reduction techniques used with each system. We elected to use the Ge(Li) detector system more and the NaI detector system less after the discrepancies appeared.

The results from the on-line Ge(Li) detector system and the gas-sample Ge(Li) system did not agree as well as anticipated either (see Figs. 68 and 69); however, they were in much better agreement than the results from the NaI system and the gas-sample Ge(Li) system.

With all of the above taken into account, the fission-gas release rates that were obtained for the two experiments cannot be expected to have much less uncertainty than about  $\pm 50\%$  for most of the isotopes and perhaps higher uncertainty for some of the very short-lived isotopes such as  $^{137}\text{Xe}$ ,  $^{139}\text{Xe}$ , and  $^{140}\text{Xe}$ .

## 13.2 Calculated Quantities

Uncertainties in the calculations of fuel-rod linear power and cladding temperature, fuel burnup, fission-gas birth rates, and fission-gas release-rate-to-birth-rate ratios (R/B) are discussed below.

### 13.2.1 Fuel-rod power levels and cladding temperatures

The problems and uncertainties in determining the power and cladding temperatures of the GB-10 fuel rod during its irradiation were described in detail in Sect. 11.2. In that evaluation of the GB-10 thermal operating data, Fig. 60 was cited as our current best estimate of the GB-10 fuel-rod peak linear power history and peak cladding-OD temperature history. We believe the uncertainties in the data of Fig. 60 are about  $\pm 5\%$  for both peak power and peak cladding-OD temperature.

There were similar difficulties and uncertainties in determining the power and cladding temperatures of the GB-9 fuel rod, but a detailed evaluation of the GB-9 thermal operating data has not been made. The results of such an evaluation, however, would be much different from the results of the GB-10 evaluation. The GB-9 thermocouple TE-402, and occasionally TE-403, indicated the location of the peak power along the rod and thus controlled the GB-9 operating power level. The orientations of these thermocouples (see Table 2) were such that TE-403 at  $180^\circ$  was on the hot side of the rod and TE-402 at  $120^\circ$  was much closer to the hot side than was the controlling thermocouple in GB-10 (TE-704 on the cold side). GB-9 did not have two thermocouples at the expected peak-power elevation

as did GB-10. If GB-10 had been operated based on the power indicated by TE-703 (located at about the same axial position and orientation in GB-10 as was TE-403 in GB-9) instead of the highest-power-indicating thermocouple, TE-704, and if the same evaluation of GB-10 thermal operating data had been made, then the peak-power history of Fig. 60 would be about 8% higher at the start of the irradiation, would have increased between the step increases in power rather than decreased, and would be about 18% higher at a fuel burnup level of  $\sim 60$  MWd/kg heavy metal (about equal to the burnup level reached in GB-9). In this hypothetical situation, the same evaluation of GB-10 data would have indicated the GB-10 fuel-rod power to be about 4% higher than the nominal value of 39.4 kW/m (12 kW/ft) at the start of the irradiation and about 9% higher than the nominal value of 44.3 kW/m (13.5 kW/ft) at the burnup level of  $\sim 60$  MWd/kg heavy metal. The reason this hypothetical situation is considered is that one might expect the thermal behavior of the GB-9 and GB-10 fuel rods to be somewhat similar, since the fuel rod and capsule designs were similar.

Based on the above considerations, all we can say about the GB-9 fuel-rod peak-power history and peak cladding-OD temperature history is that we believe the peak power and peak cladding-OD temperature at the beginning of the irradiation was probably within about  $\pm 10\%$  of the nominal values [48.6 kW/m  $\pm 10\%$  (14.8 kW/ft  $\pm 10\%$ ), 685°C  $\pm 10\%$ ] and that during the irradiation we expect there was little change from the initial values (or perhaps an increase to slightly above the nominal values).

### 13.2.2 Fuel burnup

Our current best estimate of the GB-10 fuel burnup at the peak-power axial position at any given time during the irradiation was given in Fig. 61, Sect. 11.2. We believe the uncertainty in the Fig. 61 burnup data is about  $\pm 5\%$ , the same as for the peak-power history (Fig. 60) upon which it was based.

An estimate of the GB-9 fuel burnup at the peak-power axial position based on assuming the peak power was 48.6 kW/m  $\pm 10\%$  (14.8 kW/ft  $\pm 10\%$ ) throughout the irradiation is 65 MWd/kg heavy metal  $\pm 10\%$ . Postirradiation burnup data indicated about 62 MWd/kg heavy metal.

### 13.2.3 Fission-gas birth rates

The fission-gas release data obtained during steady-state operation of the GB-9 and GB-10 fuel rods were normally reduced to ratios of release rate to birth rate (R/B), or fractional release values. In the birth rate calculations, the birth rate (B) of each isotope of interest was assumed to be at its equilibrium level corresponding to the fuel-rod total power at the time of the measurement. Inspection of the fission-product chains involved indicated that this assumption was a good one for  $^{85m}\text{Kr}$ ,  $^{87}\text{Kr}$ ,  $^{88}\text{Kr}$ ,  $^{89}\text{Kr}$ ,  $^{90}\text{Kr}$ ,  $^{91}\text{Kr}$ ,  $^{135m}\text{Xe}$ ,  $^{135}\text{Xe}$ ,  $^{137}\text{Xe}$ ,  $^{138}\text{Xe}$ ,  $^{139}\text{Xe}$ , and  $^{140}\text{Xe}$  any time the fuel rod had been at steady power for one day or longer, which was the case for the data presented, but that  $^{133m}\text{Xe}$  and  $^{133}\text{Xe}$  may take several days to reach equilibrium birth rates because of the 21-hr  $^{133}\text{I}$  in its chain and  $^{131m}\text{Xe}$  may take several weeks because of the 8-day  $^{131}\text{I}$  in its chain.

In calculating the fuel-rod total power used in the birth rate calculations, Eq. (1) in the case of GB-9 and Eq. (4) in the case of GB-10 were used to calculate the local fuel-rod linear power at each thermocouple axial position. As indicated in Sect. 5 for GB-9 and in Sect. 10 for GB-10, the effect of fuel burnup was not taken into account in the calculations; that is, the calculations were based entirely on the BOL thermal analyses of the capsules. Total fuel-rod power was then obtained by associating a segment of the fuel region with each thermocouple position and summing the indicated power of all the segments. It should be noted that in the birth rate calculations for GB-10, the power in the segment with the two thermocouples at the same axial position (TE-703 and TE-704) was taken to be the average of the two indications of local power. We believe the uncertainty in calculating the fuel-rod total power in this way was less than  $\pm 10\%$  for both experiments.

One other uncertainty in the birth rate calculations that should be discussed is that all the calculations for both experiments were made on the basis of the initial loading of fissile atoms. Initially, the principal fissile atoms were  $^{239}\text{Pu}$  and  $^{235}\text{U}$ , and the fraction of fissions due to each was calculated to be 0.664 and 0.336, respectively, for both experiments. These values were used in all the calculations. Thus, we

did not take into account the changes that occurred in the fraction of fissions due to  $^{239}\text{Pu}$  and  $^{235}\text{U}$ , nor the buildup of  $^{241}\text{Pu}$ . The changes in the relative isotopic fission rates should be considered, since the yields per fission (Y) from  $^{239}\text{Pu}$ ,  $^{241}\text{Pu}$ , and  $^{235}\text{U}$  are not the same for many of the fission-product isotopes, as can be seen by the comparison of fission-product yield data given in Table 17. The fission-product decay constants and yield values actually used in the GB-9 and GB-10 calculations are listed in Table 18.

Table 17. A comparison of fission-product yields from thermal fission of  $^{235}\text{U}$ ,  $^{239}\text{Pu}$ , and  $^{241}\text{Pu}$ <sup>a</sup>

Fission-product isotope	Yield per fission (%)		
	$^{235}\text{U}$	$^{239}\text{Pu}$	$^{241}\text{Pu}$
$^{85\text{m}}\text{Kr}$	1.33	0.598	0.376
$^{86}\text{Kr}$	1.94	0.743	0.584
$^{87}\text{Kr}$	2.37	0.949	0.720
$^{88}\text{Kr}$	3.64	1.34	0.927
$^{89}\text{Kr}$	4.64	1.44	0.747
$^{131\text{m}}\text{Xe}$	0.0167	0.0233	0.0186
$^{131}\text{Xe}$	2.77	3.89	3.09
$^{132}\text{Xe}$	4.13	5.16	4.59
$^{133\text{m}}\text{Xe}$	0.189	0.193	0.185
$^{133}\text{Xe}$	6.77	6.84	6.61
$^{134}\text{Xe}$	7.19	7.22	7.99
$^{135\text{m}}\text{Xe}$	1.05	1.06	1.07
$^{135}\text{Xe}$	6.72	7.22	7.29
$^{136}\text{Xe}$	6.12	6.55	7.21
$^{137}\text{Xe}$	5.94	6.05	6.55
$^{133}\text{I}$	6.76	6.83	6.61
$^{135}\text{I}$	6.39	6.04	7.05

<sup>a</sup>See Table 18 for yield values actually used in the GB-9 and GB-10 calculations.

At one point during the GB-10 irradiation, a fuel-depletion calculation was made to estimate the neutron flux requirements for the remainder of the irradiation and to ensure that the desired fuel-rod power levels could be maintained. From those results, relative fission rates for  $^{239}\text{Pu}$ ,

Table 18. Fission-product decay constants and yield (Y) values used in GB-9 and GB-10 calculations<sup>a</sup>

Fission-product isotope	Half-life	Decay constant (sec <sup>-1</sup> )	Yield per fission (%)		
			Y <sup>239</sup>	Y <sup>235</sup>	(0.664 Y <sup>239</sup> + 0.336 Y <sup>235</sup> )
<sup>85m</sup> Kr	4.40 hr	4.37 × 10 <sup>-5</sup>	0.536	1.30	0.794
<sup>87</sup> Kr	1.30 hr	1.48 × 10 <sup>-4</sup>	0.880	2.42	1.40
<sup>88</sup> Kr	2.80 hr	6.87 × 10 <sup>-5</sup>	1.27	3.29	1.95
<sup>89</sup> Kr	3.20 min	3.61 × 10 <sup>-3</sup>	1.41	3.94	2.26
<sup>90</sup> Kr	33.0 sec	2.10 × 10 <sup>-2</sup>	1.71	4.73	2.72
<sup>91</sup> Kr	10.0 sec	6.93 × 10 <sup>-2</sup>	1.67	3.85	2.40
<sup>131m</sup> Xe	12.0 days	6.68 × 10 <sup>-7</sup>	0.0302	0.0235	0.0279
<sup>133m</sup> Xe	2.30 days	3.49 × 10 <sup>-6</sup>	0.171	0.158	0.167
<sup>133</sup> Xe	5.27 days	1.52 × 10 <sup>-6</sup>	6.87	6.58	6.77
<sup>135m</sup> Xe	15.3 min	7.55 × 10 <sup>-4</sup>	2.39	2.13	2.30
<sup>135</sup> Xe	9.13 hr	2.11 × 10 <sup>-5</sup>	7.05	6.47	6.85
<sup>137</sup> Xe	3.90 min	2.96 × 10 <sup>-3</sup>	5.32	5.21	5.28
<sup>138</sup> Xe	17.0 min	6.79 × 10 <sup>-4</sup>	4.02	4.16	4.07
<sup>139</sup> Xe	41.0 sec	1.69 × 10 <sup>-2</sup>	2.78	3.53	3.03
<sup>140</sup> Xe	16.0 sec	4.33 × 10 <sup>-2</sup>	1.62	2.31	1.85
<sup>133</sup> I	20.9 hr	9.21 × 10 <sup>-6</sup>	6.85	6.58	6.76
<sup>135</sup> I	6.75 hr	2.85 × 10 <sup>-5</sup>	5.70	5.54	5.65

<sup>a</sup>The values under the heading (0.664 Y<sup>239</sup> + 0.336 Y<sup>235</sup>) were the yield-per-fission values used in the GB-9 and GB-10 calculations.

<sup>241</sup>Pu, and <sup>235</sup>U were calculated at several different irradiation times. The results of these calculations are given in Table 19.

As indicated in Table 19, the relative isotopic fission rates in the GB-10 fuel rod changed appreciably by the end of its 972-day irradiation. Based on the yield data of Table 17 and the relative fission rates of Table 19, the calculated change in the relative fission-rate-weighted yields for the krypton isotopes from the start of irradiation to an accumulated irradiation time of 879 days was an increase of ~5%. The changes in relative fission-rate-weighted yields for the xenons and iodines would be less than 5%.

There are significant differences between the yield values listed in Table 17 for <sup>235</sup>U and <sup>239</sup>Pu and those listed in Table 18. These differences are generally less than 20%, except for <sup>131m</sup>Xe and <sup>135m</sup>Xe. The

Table 19. Calculated isotopic fission-rate distributions in capsule GB-10

Accumulated irradiation time (days)	Relative isotopic fission rates		
	$^{239}\text{Pu}$	$^{241}\text{Pu}$	$^{235}\text{U}$
0	0.668	Negligible	0.332
600	0.555	0.046	0.399
879	0.436	0.152	0.412

Table 18 values, which were used in all the GB-9 and GB-10 calculations, were those in use at GAC in 1970 (Subroutine BLAST, Library No. 254 for fission-product data for radioisotopes generated by the fission of  $^{235}\text{U}$  and  $^{239}\text{Pu}$  in the neutron spectrum of a thermal reactor).

The overall uncertainty in the GB-9 and GB-10 birth rate calculations is estimated to be less than  $\pm 20\%$ , excluding any uncertainties in the yield data shown in Table 18.

#### 13.2.4 Fission-gas release-rate-to-birth-rate ratios

An uncertainty in the GB-9 and GB-10 fission-gas release-rate-to-birth-rate data (R/B), or fractional release values, of about  $\pm 70\%$  is indicated for most of the isotopes of interest from the discussion of uncertainties in the measured release rates R ( $\pm 50\%$  from Sect. 13.1.4) and in the calculated birth rates B ( $\pm 20\%$ , excluding uncertainties in Table 18 yield data, from Sect. 13.2.3). Additional uncertainty was indicated in the measured release rates of the very short-lived isotopes, in the calculated birth rates of several isotopes such as  $^{131\text{m}}\text{Xe}$  that are produced in a chain with a long half-life member where the assumption that the isotopes are at equilibrium is questionable, and in the Table 18 yield data used in the calculations.

Because of the above considerations and because, in general, the fission-gas release rates from the GB-9 and GB-10 fuel rods were very sensitive to cladding temperature changes and temperature profile changes

over the fuel region, we recommend that a factor of 2 uncertainty in the GB-9 and GB-10 R/B data be used in most applications.

### 13.3 Abnormal Occurrences

Three abnormal occurrences took place during operation of the GB-10 fuel rod, none of which are thought to have affected the experimental results. No such significant abnormal occurrences occurred during the operation of the GB-9 fuel rod.

Two of the GB-10 abnormal occurrences were short-duration (spike) increases in fuel-rod power to above the normal operating level caused by an unplanned increase in reactor power in each case. The first spike in power occurred on Dec. 23, 1972 (after 97 days of irradiation) when the ORR reactor power increased to  $\sim 120\%$  of normal full power (30 MW). Abnormal operation of the servocontrol system caused one of the shim rods to withdraw slowly until an automatic reverse in power at 120% of full level took place. The GB-10 fuel rod received the same percentage increase in power [from  $\sim 39.4$  to  $\sim 47.2$  kW/m ( $\sim 12$  to  $\sim 14.4$  kW/ft)]. The duration of the power increase was very short, and we believe the actual time at increased power was much too short to have had any effect on the GB-10 fuel structure at that time (thermocouple readings spiked only about  $25^\circ\text{C}$  above  $\sim 430^\circ\text{C}$ ). The second spike in power occurred on Apr. 7, 1976 (after 898 days of irradiation) while the GB-10 fuel rod was operating at the nominal power level of 48.6 kW/m (14.8 kW/ft). On this second occasion, thermocouple TE-704 spiked from 524 to  $545^\circ\text{C}$ . The operating point at this time for TE-704, which was the thermocouple that controlled the operating power of the rod, was  $526 \pm 10^\circ\text{C}$ . Again, we believe this short-duration spike did not affect the GB-10 fuel structure.

The third GB-10 abnormal occurrence, also of little significance in the authors' opinions, was a small leak that developed in the sweep-gas system. The leak was detected during a periodic leak check made in November 1973. It could not be readily located in the valve box piping. We suspected the leak was at one of the sweep line mechanical couplings inside a junction box in the reactor pool rather than inside the capsule, since a sweep-gas leak of its size inside the capsule would be detected

by an increase in the static cladding external gas system pressure. The leak was not readily found, and it was decided to monitor it for change during the remainder of the irradiation rather than pursue it further. Periodic leak checks showed no change in the leakage rate, which was  $0.53 \text{ cm}^3 \text{ STP/min}$  at 6.9-MPa gage (1000-psig) pressure. The leak could not be detected at low pressure such as during long shutdown periods when the system was usually depressurized and left static under  $\sim 0.52 \text{ MPa}$  gage ( $\sim 75 \text{ psig}$ ) pressure. Late in the irradiation when the BF-TT flow path became constricted to the point of no measurable flow under a pressure differential of 1.72 MPa (250 psi), we observed that the leak was downstream of the BF-TT flow constriction.

## 14. STORAGE OF GB-9 AND GB-10 RECORDS

Records of the design, construction, and operation of the GB-9 and GB-10 capsules are being collected and identified for storage in accordance with applicable quality assurance procedures. Present GCFR guidelines indicate that the GB-9 and GB-10 records will be kept in storage for at least 10 years.

## 15. CONCLUSIONS

The irradiation testing of the GCFR vented fuel rods in the GB-9 and GB-10 capsule experiments has led us to the following conclusions:

1. The first-of-a-kind GB-9 experiment and the follow-up GB-10 experiment yielded a very substantial amount of information on the performance to be expected from the GCFR vented-and-pressure-equalized fuel rod. We believe that both experiments were extremely cost-effective.
2. Essentially all of the objectives of the GB-9 experiment and most of the objectives of the GB-10 experiment were realized. The originally planned GB-10 measurements of direct fission-product release from the fuel and transport through the main regions of the rod (fuel, upper blanket, and charcoal trap) were made as well as additional measurements on internal gas-flow conductances and tritium transport behavior. Many of them were first-of-a-kind measurements. The planned GB-10 power cycling tests and final tritium experiments were not made because of the risk of losing valuable postirradiation information, especially on the location and nature of the fuel-rod flow constriction. Some measurements, such as the measurement of stable noble gas release, could not be brought to successful completion because of inadequate funding.
3. Fission-gas release rates under the normal venting conditions were found to be very sensitive to cladding temperature changes and temperature profile changes over the fuel region, but no significant burst-type release of the radioactive fission gases was detected upon startups or shutdowns in either experiment.
4. The GB-9 and GB-10 measurements indicate that the fuel rods retained volatile fission products well and that the daughter products of the released noble gases were the principal source of plateout activity in the effluent sweep system under normal venting conditions.
5. We believe that the flow constriction at power that developed in the GB-10 fuel rod requires careful analysis and interpretation, which should await results from the GB-10 postirradiation examination at ANL and possibly further investigations. The constriction did not occur until

late in the irradiation and even then was relieved upon a shutdown or large reduction in power.

6. We believe that the results from the GB-9 and GB-10 experiments indicate that the vented-and-pressure-equalized fuel rod should remain a primary candidate fuel-rod design for the GCFR.

7. We believe that one or more additional experiments of the GB-10 type are needed to observe the vented-rod performance under conditions very closely matching those expected in the GCFR, especially with respect to coolant impurities ( $H_2$  and  $H_2O$  levels and  $H_2/H_2O$  ratio), and to obtain additional design data that was not, or could not, be obtained from the GB-9 and GB-10 experiments. Rod performance under power cycling should be observed, for example. If future tests are conducted, it might be cost-effective to operate more than one rod at a time, using one as a control under normal conditions and the other one or more for off-normal and special test conditions.

8. We believe the results from the GB-9 and GB-10 experiments may be applied in the design of the fuel elements and the pressure-equalization system for the GCFR and in the development of computer codes for predicting fast breeder reactor fuel-rod performance, but attention should be given to the discussion of uncertainties in Sect. 13.

## REFERENCES

1. T. N. Washburn, R. B. Fitts, and J. A. Conlin, *Fuel Element Development for the Gas-Cooled Fast Breeder Reactor: Part 1 - Sealed Fuel Rod Design*, ORNL/TM-3427 (June 1971).
2. R. J. Campana, "Pressure Equalization System for Gas-Cooled Fast Breeder Reactor Fuel Elements," *Nucl. Technol.* 12, 185 (October 1971).
3. A. W. Longest et al., "Irradiation of GCBR-ORR Capsule 04-P9," *GCR-TU Programs Semiannu. Prog. Rep. Sept. 30, 1970*, ORNL-4637, pp. 40-47.
4. A. W. Longest et al., "Fission-Gas Release Measurements from Fast Breeder (U,Pu)O<sub>2</sub> Fuel," *Trans. Am. Nucl. Soc.* 13, 604 (1970).
5. A. W. Longest et al., "Irradiation of GCFR-ORR Capsule GB-9," *GCR-TU Programs Annu. Prog. Rep. Sept. 30, 1971*, ORNL-4760, pp. 149-63.
6. A. W. Longest et al., "Irradiation of GCFR-ORR Capsule GB-9," *GCR-TU Programs Annu. Prog. Rep. Dec. 31, 1972*, ORNL-4911, pp. 213-15.
7. A. W. Longest, R. B. Fitts, and J. A. Conlin, "Fission Gas Release Behavior in a Vented (U,Pu)O<sub>2</sub> GCFR Fuel Pin," *Trans. Am. Nucl. Soc.* 15, 197 (1972).
8. R. B. Fitts and E. L. Long, Jr., "Postirradiation Examination of GCFR-ORR Capsule GB-9," *GCR Programs Annu. Prog. Rep. Dec. 31, 1972*, ORNL-4911, pp. 215-20.
9. S. Langer et al., "Volatile Fission Product Migration and Plateout in GCFR Rod Irradiations," *Trans. Am. Nucl. Soc.* 15, 850 (1972).
10. A. W. Longest and J. A. Conlin, "Design and Operation of GCFR-ORR Capsule GB-10," *GCR Programs Annu. Prog. Rep. Dec. 31, 1972*, ORNL-4911, pp. 220-33.
11. R. J. Campana et al., "The Effect of Irradiation Results on the GCFR Pressure Equalization System (Venting) Design," *Trans. Am. Nucl. Soc.* 16, 109 (1973).

12. J. R. Lindgren et al., *Irradiation Testing in the Development of Gas-Cooled Fast Breeder Fuel Elements*, GA-A12657 (1973).
13. A. W. Longest and J. A. Conlin, "Results from Irradiation Testing of Capsule GB-10," *GCR Programs Annu. Prog. Rep. Dec. 31, 1973*, ORNL-4975, pp. 297-303.
14. S. Langer, G. Buzzelli, and P. W. Flynn, *Postirradiation Examination of Charcoal Trap in Irradiation Capsule GB-9*, GA-A13298 (1975).
15. R. V. Strain, C. W. Renfro, and L. A. Neimark, *Postirradiation Examinations of the GB-9 Element*, ANL-8067 (1976).
16. A. W. Longest, U. Gat, J. A. Conlin, and R. J. Campana, "Measured Internal Gas-Flow Conductance of an Operating GCFR Fuel Rod," *Trans. Am. Nucl. Soc.* 23, 148 (1976).
17. A. W. Longest, U. Gat, J. A. Conlin, and R. J. Campana, "Vented Fuel Experiment for Gas-Cooled Fast Reactor Application," *Gas-Cooled Reactors with Emphasis on Advanced Systems, Vol. II*, IAEA-SM-200/47 (1976), pp. 417-27.
18. J. A. Conlin and A. W. Longest, "Results from Irradiation Testing of Capsule GB-10," *GCFR Program Prog. Rep. for Jan. 1, 1974 through June 30, 1975*, ORNL-5119, pp. 62-72.
19. D. B. Trauger, *Some Major Fuel-Irradiation Test Facilities of the Oak Ridge National Laboratory*, ORNL-3574 (1964).
20. J. R. Lindgren et al., *Planned Thermal Irradiation of Manifolded-Vented, (U,Pu)O<sub>2</sub>-Fueled Rod in ORR Capsule P-9*, GA-9896 (1970).
21. R. R. Liguori and J. W. Stephenson, *The HEATING Program (Heat Engineering and Transfer in Nine Geometries)*, ASTRA-417-5.0 (January 1961).
22. J. R. Lindgren et al., *Planned Thermal Irradiation of Manifolded-Vented (U,Pu)O<sub>2</sub>-Fueled Rod in ORR Capsule GB-10*, GA-A12123 (1972).
23. W. D. Turner and M. Siman-Tov, *HEATING3 - An IBM 360 Heat Conduction Program*, ORNL/TM-3208 (1971).

24. J. R. Findley et al., "The Emission of Fission Products from Uranium-Plutonium Dioxide During Irradiation to High Burnup," *J. Nucl. Mat.* 35, 24-34 (1970).
25. M. E. Pruitt and A. W. Longest, *In-Line Tritium Monitoring in the GCFR Vented Irradiation Capsule GB-10*, ORNL/TM-6387 (to be published).
26. B. D. Epstein, *A Review of the Literature Pertinent to Fission-Product Migration and Interaction in Fuel Rods*, GA-A13423 (1975).
27. C. E. Johnson and I. Johnson, "Transport and Reaction of Volatile Fission Products in Gas-Cooled Fast Reactors," *Trans. Am. Nucl. Soc.* 23, 149 (1976).
28. T. N. Tiegs, *Postirradiation Gamma Scanning of GCFR Capsule GB-10*, ORNL/TM-5975 (November 1977).

## Appendix A

SUMMARY OF DATA FOR AS-BUILT FUEL ROD IN  
ORR IRRADIATION CAPSULE GB-10<sup>a</sup>

Fuel-rod designation . . . . .	GA-21
Rod type . . . . .	Vented with integral charcoal trap
Cladding data	
Material . . . . .	316 stainless steel
Surface-roughening rib dimensions	
Height, in. . . . .	0.004
Width, in. . . . .	0.006
Pitch, in. . . . .	0.048
OD (root diameter), in. . . . .	0.3535
ID, in. . . . .	0.305
Wall (root thickness), in. . . . .	0.02425
OD/ID ratio . . . . .	1.16
Length, in. . . . .	14.18
Fuel data	
Pellet dimensions, solid pellets (U,Pu)O <sub>2</sub>	
OD, in. . . . .	0.301
Length (U,Pu)O <sub>2</sub> , in. . . . .	0.270-0.313
End-dish depth, in. . . . .	0.006
Test fuel stack height, <sup>b</sup> in. . . . .	8.876
(U,Pu)O <sub>2</sub> pellets	
Material . . . . .	(U,Pu)O <sub>2</sub> , solgel-derived
Number of (U,Pu)O <sub>2</sub> pellets . . . . .	30
Composition	
UO <sub>2</sub> , % . . . . .	87.75
U enrichment, <sup>235</sup> U, % . . . . .	8.97
PuO <sub>2</sub> , <sup>c</sup> % . . . . .	12.25
Oxygen/metal ratio . . . . .	1.977-1.986
Density, % theoretical . . . . .	86.7-88.4

Stack smear density of (U,Pu)O <sub>2</sub> pellets, % theoretical . . . . .	84.2	
UO <sub>2</sub> power-peak-reducing half-pellets		
Material . . . . .	UO <sub>2</sub>	
Number of pellets . . . . .	2 at each end of fuel stack	
Pellets adjacent to fuel stack		
Enrichment, % <sup>235</sup> U . . . . .	14.9	
Length, in. . . . .	Upper - 0.159 Lower - 0.145	
Oxygen-to-uranium ratio . . . . .	2.004	
Density, % theoretical . . . . .	91-92	
Outer pellets		
Enrichment, % <sup>235</sup> U . . . . .	8.3	
Length, in. . . . .	Upper - 0.154 Lower - 0.161	
Oxygen-to-uranium ratio . . . . .	2.005	
Density, % theoretical . . . . .	90	
5% enriched UO <sub>2</sub> pellet near bottom of rod		
Material . . . . .	UO <sub>2</sub>	
Number of pellets . . . . .	1 at bottom sand- wiched between blanket pellets	
Enrichment, % <sup>235</sup> U . . . . .	5	
Length, in. . . . .	0.1564	
Oxygen-to-uranium ratio . . . . .	2.003	
Density, % theoretical . . . . .	91.7	
Blanket-pellet data		
	<u>Upper</u>	<u>Lower</u>
Pellet material . . . . .	UO <sub>2</sub>	UO <sub>2</sub>
Enrichment, % <sup>235</sup> U . . . . .	0.22 (depleted)	Normal
Number of pellets . . . . .	7	3
OD, in. . . . .	0.3015	0.301
Length, in. . . . .	0.295	0.157, 0.156, 0.1172





## Appendix B

## EVALUATION OF GB-10 THERMAL OPERATING DATA

An evaluation of the GB-10 thermal operating data from startup through Feb. 20, 1976, was made to estimate, as best we could within funding limitations, the GB-10 fuel-rod power history, cladding temperature history, and fuel burnup history up to this point in the irradiation. This evaluation was needed to point out some of the problems involved in determining the GB-10 fuel-rod temperature and power and to resolve some of the uncertainties known to be present in the "nominal values" of temperature and power listed in Table 10.

Operating criteria for the experiment required control on the basis of the hottest cladding temperature indication, whereas final interpretation of the experimental data should be done on the basis of all the indications of temperature and power along the rod. These considerations are discussed in the following paragraphs, and then results of the subject evaluation of GB-10 thermal operating data are given.

In operating the capsule, small position adjustments were made as required to maintain the indicated peak cladding-OD temperature within  $\pm 15^{\circ}\text{C}$  of the desired value at each power level of operation. The peak cladding-OD temperature was taken to be the highest indication obtained when the readings of the six fuel-region thermocouples [located  $\sim 1.8$  mm (0.071 in.) away from the cladding near the ID of a Zircaloy sleeve and at various axial and angular positions] were corrected to cladding-OD-hot-side temperatures. These corrections to the thermocouple readings were based on a beginning-of-life (BOL) thermal analysis of the capsule. No further calculations have been made to account for the expected effect of fuel burnup on the relative temperature distributions.

The BOL two-dimensional R- $\theta$  power and temperature calculations reflected a strong depression of the thermal flux by the fuel and an angular ( $\theta$ ) variation resulting from the capsule being in a rather steep flux gradient. The calculated angular variation of the cladding-OD temperature corresponding to a power level of 48.6 kW/m (14.8 kW/ft) at BOL was about  $63^{\circ}\text{C}$ . The total BOL full-power thermocouple-to-cladding-hot-side temperature corrections (radial component plus circumferential

component) for the six fuel-region thermocouples ranged from 115 to 159°C. Of course, the fuel rod was operated at reduced power levels at first, and the temperature corrections were adjusted accordingly. Uncertainty in the BOL full-power temperature corrections was estimated to be  $\pm 25^\circ\text{C}$ , due mainly to uncertainty in the exact radial positions of the thermocouple junctions in the fairly steep temperature gradients. This uncertainty estimate did not include the effect of fuel burnup with time, nor the possibility that significant bowing of the rod might occur.

From the BOL R- $\theta$  power and temperature distribution calculations, the BOL thermocouple-to-cladding-OD temperature relationships were established as described in Sect. 9.4, and it was found that the BOL fuel-rod linear heat rates of 39.4, 44.3, and 48.6 kW/m (12, 13.5, and 14.8 kW/ft) produced cladding-OD hot-side temperatures of 565, 630, and 685°C, respectively.

In the BOL R-Z temperature distribution calculations that were made in support of the overall capsule design (see Sect. 9.2), it was found that, in this case of an assumed uniform angular power distribution, a fuel-rod peak power of 51 kW/m (15.5 kW/ft) was required to produce a uniform cladding-OD peak temperature of 685°C. The full-power (685°C cladding-OD temperature) thermocouple-to-cladding-OD temperature correction, in this case, was 109°C for the six fuel-region thermocouples. This case was of interest in the present evaluation of GB-10 thermal operating data, because preferential depletion of fuel on the high neutron-flux side of the rod results in an actual trend toward the uniform angular power case with increasing irradiation exposure. Also, the power distribution flattens and approaches that for a rod in a fast neutron spectrum at high burnup.

At the beginning of the GB-10 irradiation, we had planned to make some calculations of the R- $\theta$  power- and temperature-distribution behavior to be expected as a function of fuel burnup, so that this information could be applied to the operation of the capsule. This would have provided information for developing burnup-dependent thermocouple-to-hot-side-cladding-OD temperature corrections. However, these calculations were not made, because funding levels for the GB-10 capsule did not

permit the rather large effort that would have been required. These calculations, which would also aid in detailed interpretation of fission-gas release data, could still be made to better define actual operating conditions of the rod if the potential information to be gained justifies the cost.

In the present evaluation, typical randomly selected sets of GB-10 thermal operating data from startup through Feb. 20, 1976, were examined by estimating the hot-side-cladding-OD temperatures using two methods. The first method, which was used in operation of the capsule, involved using the BOL thermocouple-to-hot-side-cladding-OD temperature corrections. The second method involved an approximation that provided for burnup-dependent temperature corrections. In the second method, it was assumed that the full-power thermocouple-to-cladding-OD-hot-side temperature correction for each of the six fuel-region thermocouples should decrease at a linear rate with increasing fuel burnup from its calculated angular-dependent BOL value to an angular-independent value of  $109^{\circ}\text{C}$  at  $\sim 100$  MWd/kg heavy metal fuel burnup. The fuel-rod linear power required to produce the full-power condition of a cladding-OD-hot-side temperature of  $685^{\circ}\text{C}$  was likewise assumed to increase at a linear rate from 48.6 kW/m (14.8 kW/ft) at BOL for the angular-dependent case to 51 kW/m (15.5 kW/ft) at  $\sim 100$  MWd/kg burnup for the uniform angular power case. These assumptions, which are made only because more detailed calculations are unavailable, are considered reasonable, since at 100 MWd/kg heavy metal burnup about half of the original fissile material has been burned up and the power across the fuel rod should be reasonably flat by this time.

Figures B.1, B.2, and B.3 show sets of GB-10 thermocouple readings, indicated cladding temperatures, and indicated linear heat rates along the fuel rod after 2, 333, and 868 days at power, respectively, for the case in which the indicated cladding temperatures and heat rates were calculated on the basis of the BOL thermal calculations (first method). Similar plots, after 333 and 868 days at power, are shown in Figs. B.4 and B.5 for the case in which the indicated cladding temperatures and heat rates were calculated on the basis of the burnup-dependent approximations described above (second method). It can be seen in Figs. B.1,

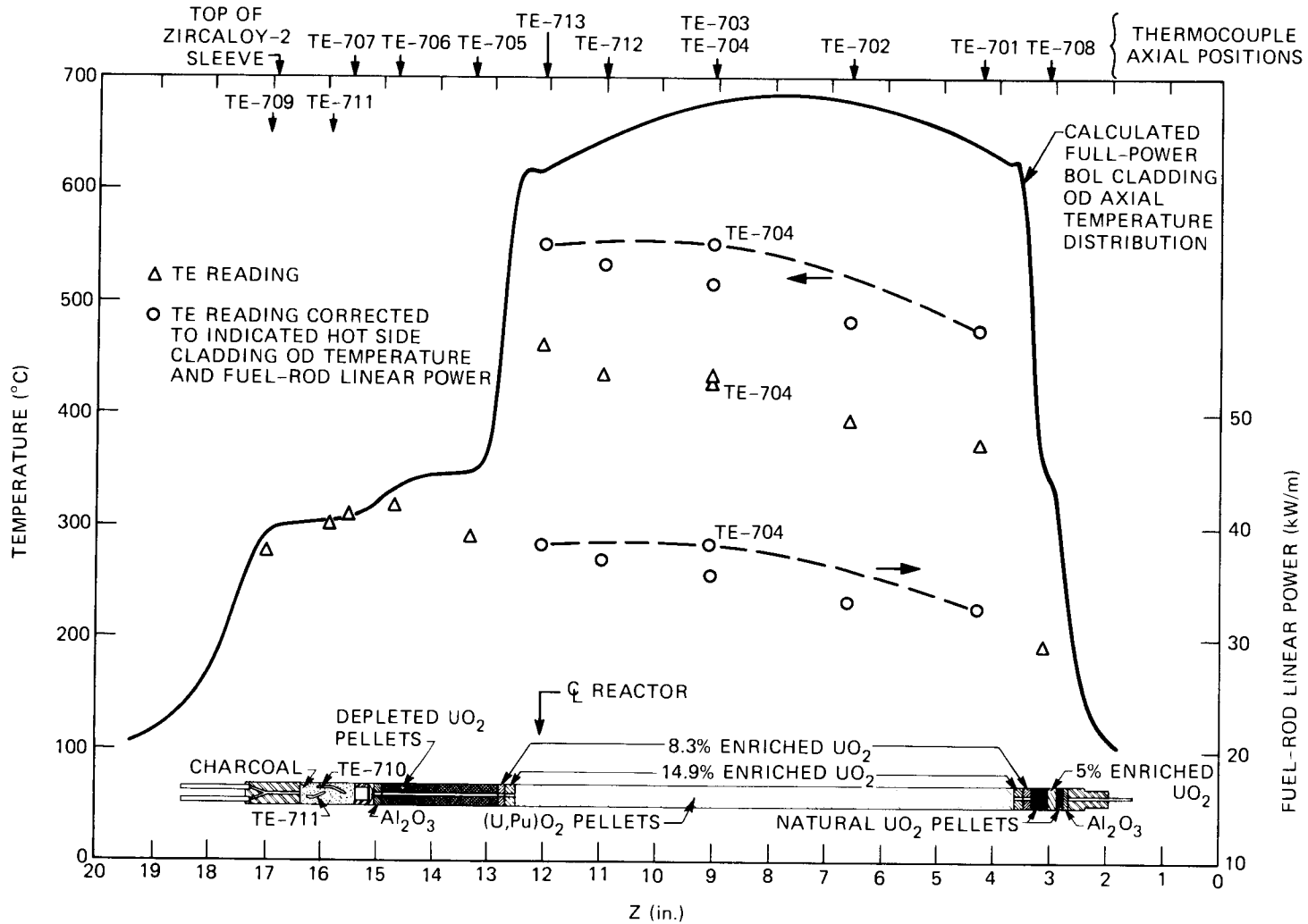


Fig. B.1. Indicated GB-10 cladding temperature and power distributions on Mar. 31, 1972 (after 2 days at power) based on beginning-of-life (BOL) thermal calculations (1 in. = 2.54 cm; 1 m = 3.28 ft).





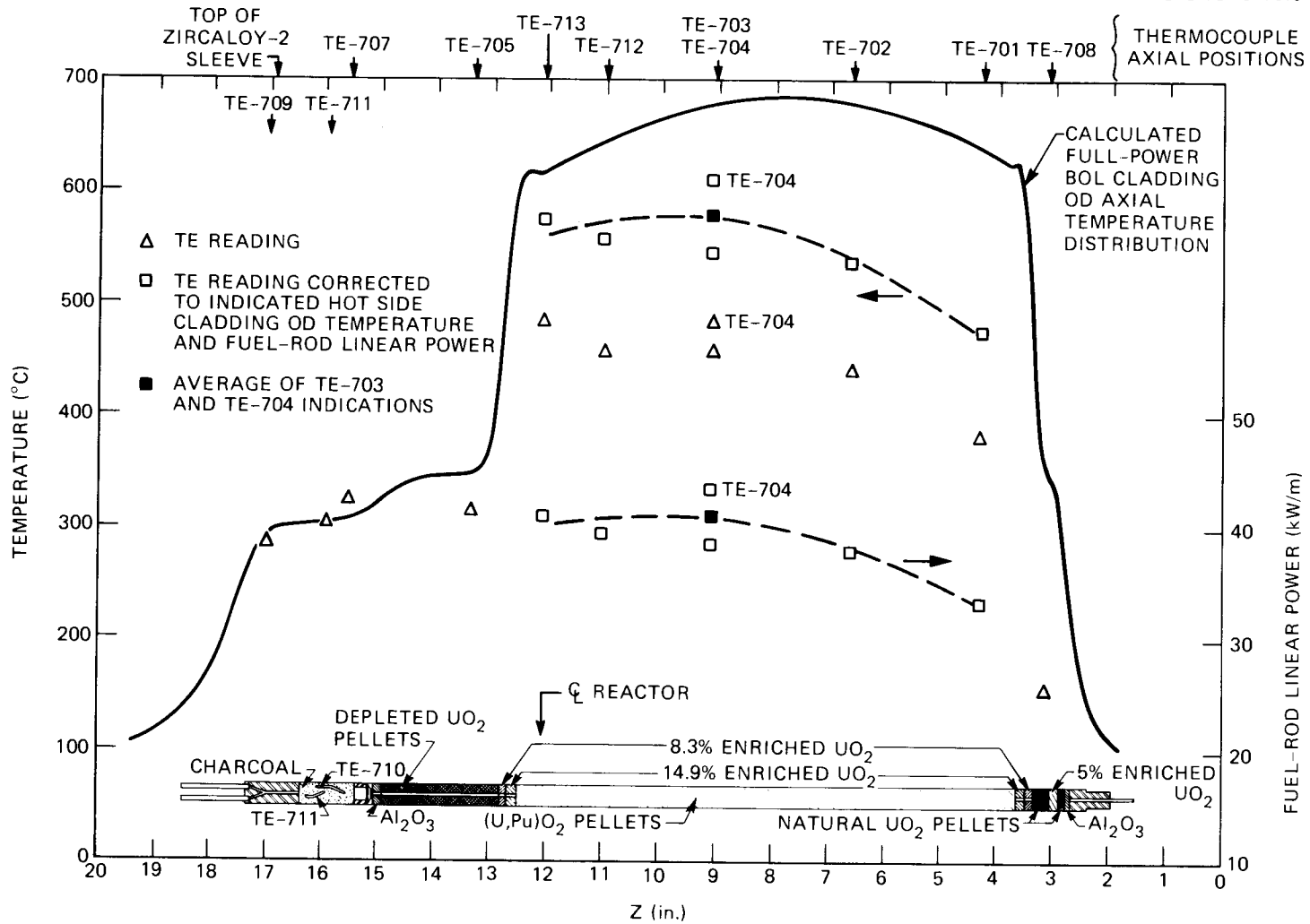


Fig. B.4. Indicated GB-10 cladding temperature and power distributions on Nov. 26, 1973 (after 333 days at power) based on burnup-dependent thermal approximations (1 in. = 2.54 cm; 1 m = 3.28 ft).

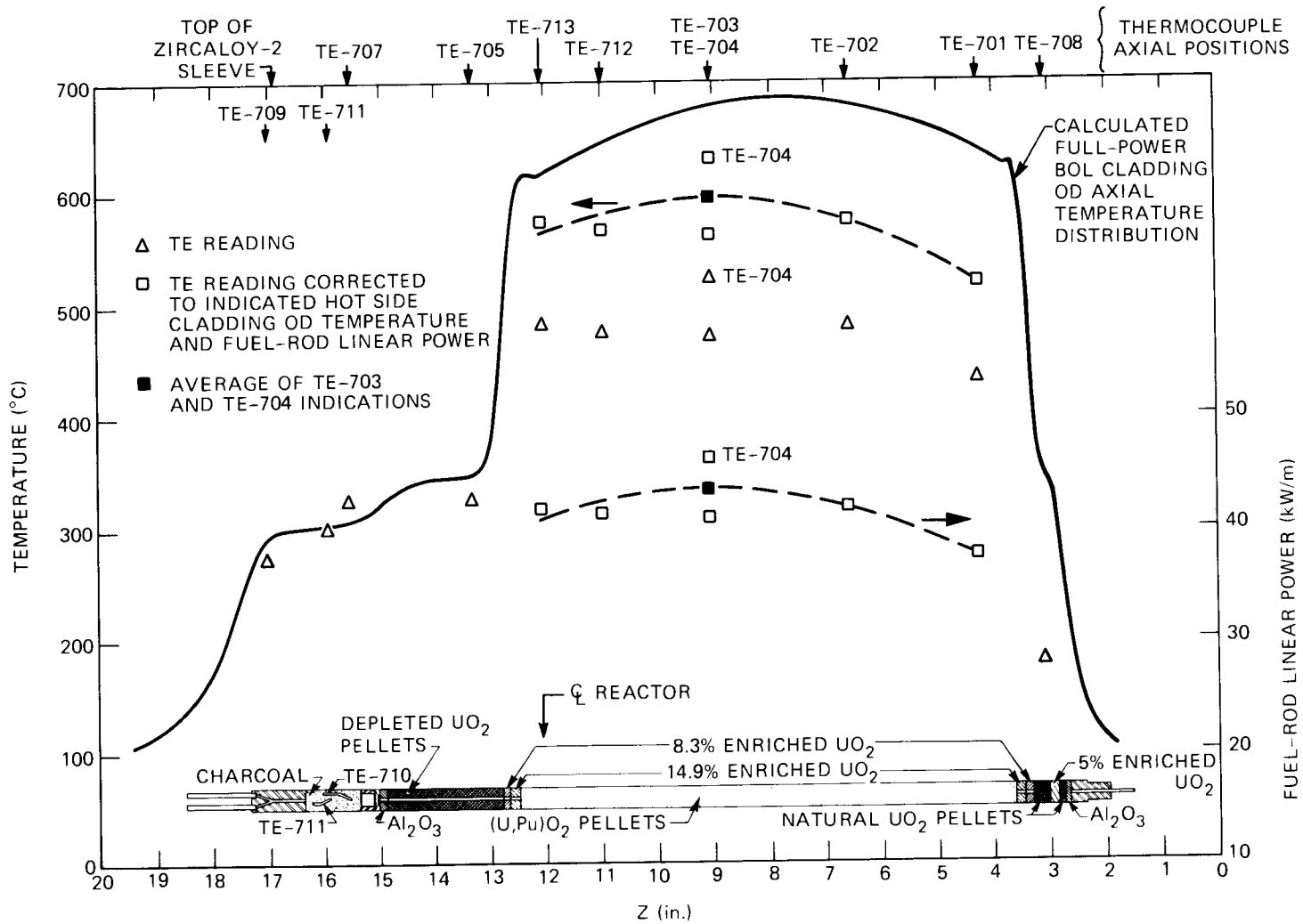


Fig. B.5. Indicated GB-10 cladding temperature and power distributions on Feb. 20, 1976 (after 868 days at power) based on burnup-dependent thermal approximations (1 in. = 2.54 cm; 1 m = 3.28 ft).

B.2, and B.3 that the initial scatter in the indicated values of cladding temperature and power (Fig. B.1) was not too unreasonable considering the uncertainties involved, but that the scatter became much worse with increasing burnup (Figs. B.2 and B.3), even after allowance is made for the different power levels of operation. Applying the burnup-dependent approximations improved the looks of the cladding temperature and power indications significantly (Figs. B.4 and B.5), especially by using the average indications of TE-703 and TE-704 to draw in the curves. TE-703 was located on the hot side of the fuel rod, and TE-704 was located on the cold side of the fuel rod; both were at the same axial position.

Based on Figs. B.1 through B.5 and similar plots of the GB-10 data at other burnup levels, it appears that using the burnup-dependent thermal approximations (second method) is more reasonable than using the BOL thermal calculations (first method) and that the best estimate of the fuel-rod peak cladding-OD temperature and peak power might be the average indications of TE-703 and TE-704. Figure B.6 was prepared using the burnup-dependent thermal approximations and the average indications of TE-703 and TE-704 and shows what we believe at this time to be the most probable GB-10 peak cladding-OD temperature history and peak-power history through Feb. 20, 1976. The burnup scale at the top of Fig. B.6 was calculated on the basis of the fission-rate history that corresponds to the peak-power history of Fig. B.6.

Shown in Fig. B.7 is a plot of the difference between the readings of TE-703 and TE-704 as a function of estimated fuel burnup, along with the predicted behavior of the temperature difference based on the calculated BOL angular temperature distribution and on the burnup-dependent thermal approximations. It should be mentioned that much of the scatter in the temperature difference data in this figure is probably due to the fact that the temperatures could not be read from the recorders to much better than about  $\pm 2^\circ\text{C}$ . Also, the burnup scale in this figure was based on the conservative equation used for estimating and reporting burnup levels during operation and does not correspond exactly to the burnup scale of Fig. B.6.

The long-term trend in the temperature differences plotted in Fig. B.7 shows good agreement with the trend predicted on the basis of

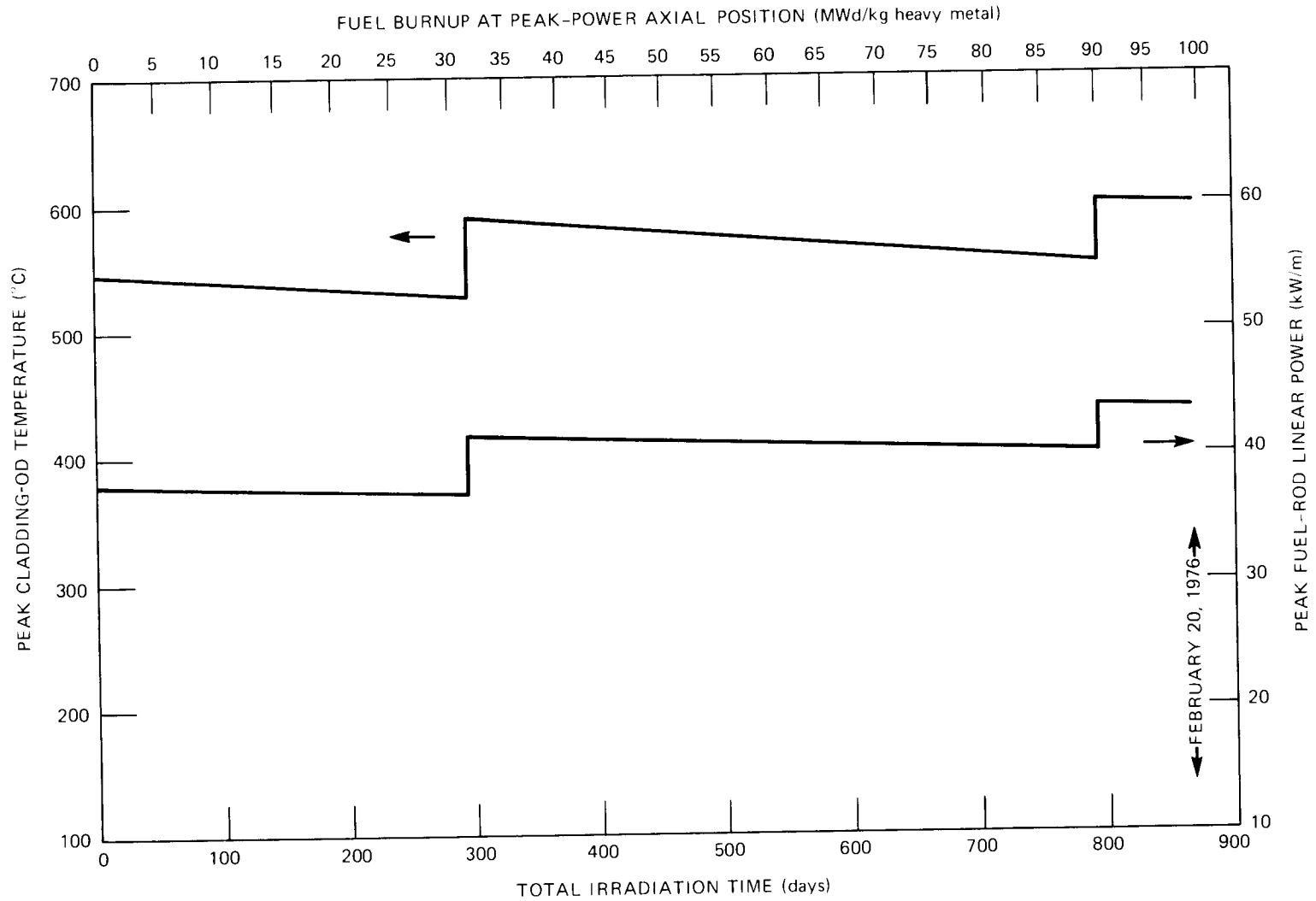


Fig. B.6. Most probable values of GB-10 fuel-rod peak power, cladding temperature, and fuel burnup as a function of irradiation time based on an evaluation of GB-10 thermal operating data (1 m = 3.28 ft).

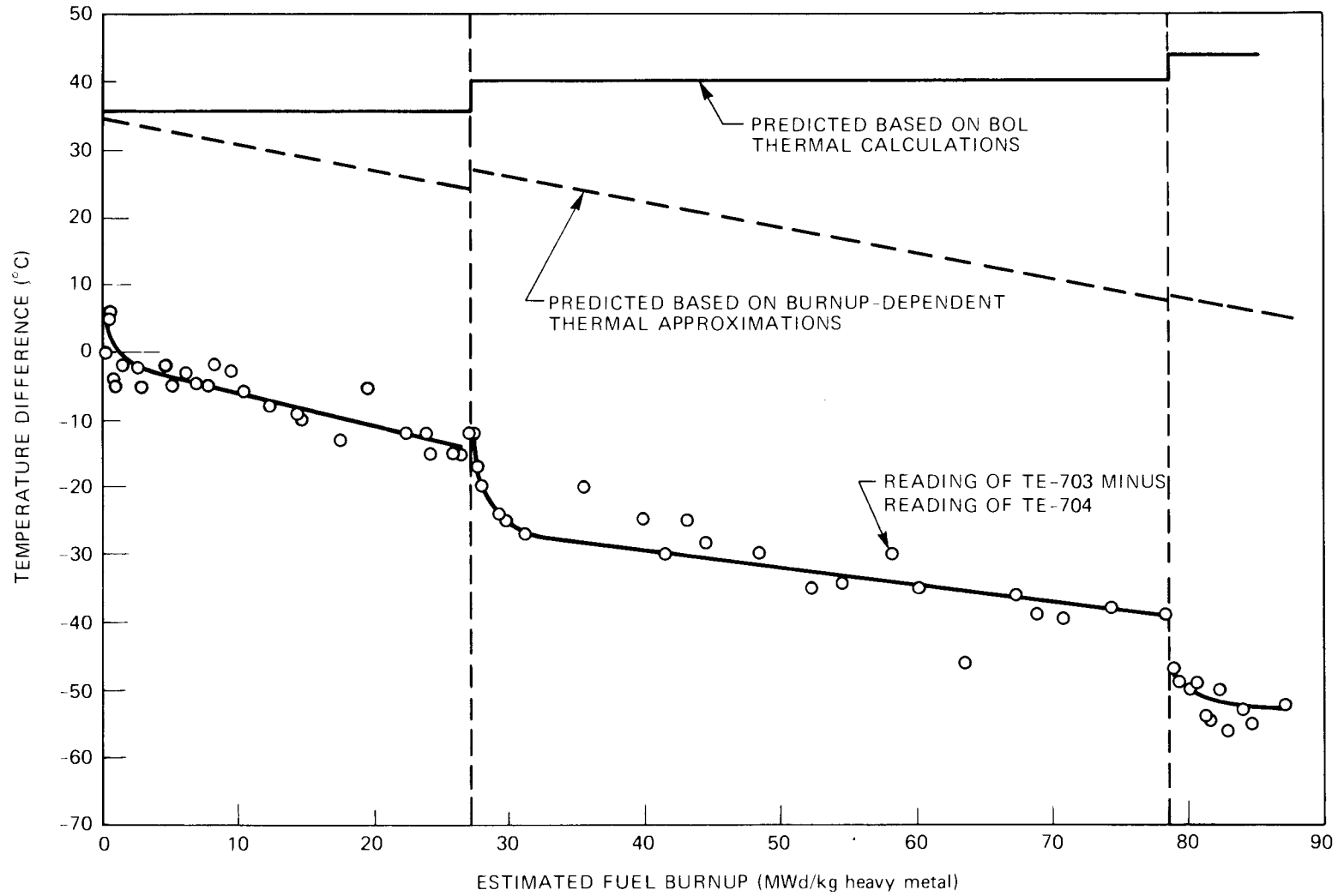


Fig. B.7. Difference between readings of GB-10 thermocouples TE-703 (hot side) and TE-704 (cold side at same elevation as TE-703) as a function of estimated fuel burnup.

the burnup-dependent thermal approximations; however, the short-term trend following each step increase in power is unaccounted for. The data seem to indicate that something else was going on following each step increase in power, such as movement of one of the thermocouple junctions, bowing of the rod, or changes in the outward heat flow patterns in the fuel.

## INTERNAL DISTRIBUTION

- |        |                  |        |                               |
|--------|------------------|--------|-------------------------------|
| 1.     | E. D. Clemmer    | 44.    | F. R. Mynatt                  |
| 2-6.   | J. A. Conlin     | 45.    | F. H. Neill                   |
| 7.     | J. H. Coobs      | 46.    | H. Postma                     |
| 8.     | D. A. Costanzo   | 47.    | M. E. Pruitt                  |
| 9.     | J. F. Emery      | 48.    | R. L. Senn                    |
| 10-19. | Uri Gat          | 49.    | K. R. Thoms                   |
| 20.    | A. G. Grindell   | 50.    | T. N. Tiegs                   |
| 21.    | R. F. Hibbs      | 51.    | H. E. Trammell                |
| 22.    | F. J. Homan      | 52.    | D. B. Trauger                 |
| 23-28. | P. R. Kasten     | 53.    | J. R. Weir                    |
| 29-38. | A. W. Longest    | 54.    | ORNL Patent Office            |
| 39.    | A. L. Lotts      | 55-57. | Central Research Library      |
| 40.    | R. E. MacPherson | 58.    | Document Reference Section    |
| 41.    | H. J. Metz       | 59-64. | Laboratory Records Department |
| 42.    | C. A. Mills      | 65.    | Laboratory Records (RC)       |
| 43.    | R. L. Moore      |        |                               |

## EXTERNAL DISTRIBUTION

66. S. Greenberg, Argonne National Laboratory, 9700 South Cass Avenue, Argonne, IL 60439
67. C. Johnson, Argonne National Laboratory, 9700 South Cass Avenue, Argonne, IL 60439
68. J. T. Madell, Argonne National Laboratory, 9700 South Cass Avenue, Argonne, IL 60439
69. L. A. Neimark, Argonne National Laboratory, 9700 South Cass Avenue, Argonne, IL 60439
70. R. J. Campana, General Atomic Company, P.O. Box 81608, San Diego, CA 92138
71. B. Epstein, General Atomic Company, P.O. Box 81608, San Diego, CA 92138
72. S. Langer, General Atomic Company, P.O. Box 81608, San Diego, CA 92138
73. J. R. Lindgren, General Atomic Company, P.O. Box 81608, San Diego, CA 92138
74. H. J. Snyder, General Atomic Company, P.O. Box 81608, San Diego, CA 92138
- 75-76. DOE Division of Nuclear Research and Applications, Washington, D.C. 20545, Director
77. Director, Reactor Division, DOE, ORO
78. Director, Research and Technical Support Division, DOE, ORO
- 79-255. Given distribution as shown in TID-4500 under category UC-77